

# Using *Xenopus laevis* to investigate developmental mechanisms underlying human neurodevelopmental disorders and intellectual disabilities:

Author: Micaela Cari Lasser

Persistent link: <http://hdl.handle.net/2345/bc-ir:108957>

This work is posted on [eScholarship@BC](#),  
Boston College University Libraries.

---

Boston College Electronic Thesis or Dissertation, 2020

Copyright is held by the author. This work is licensed under a Creative Commons Attribution-NonCommercial-NoDerivatives 4.0 International License (<http://creativecommons.org/licenses/by-nc-nd/4.0>).

**Using *Xenopus laevis* to investigate  
developmental mechanisms underlying  
human neurodevelopmental disorders  
and intellectual disabilities**

Micaela Lasser

A dissertation submitted to the  
Faculty of the Biology Department  
in partial fulfillment of the requirements for the  
degree of Doctor of Philosophy

Boston College  
Morrissey College of Arts and Sciences  
Graduate School

July 2020



**USING *XENOPUS LAEVIS* TO INVESTIGATE  
DEVELOPMENTAL MECHANISMS UNDERLYING  
HUMAN NEURODEVELOPMENTAL DISORDERS  
AND INTELLECTUAL DISABILITIES**

Micaela Lasser

Advisor: Dr. Laura Anne Lowery, PhD

**Abstract**

Development of the central nervous system (CNS) is a complex process that requires the proper function of many genes in order for neurons to proliferate and divide, differentiate, and subsequently migrate long distances to form connections with one another. Abnormalities in any one of these cellular processes can lead to detrimental developmental defects. Growing evidence suggests that genetic mutations caused by rare copy number variants (CNVs) are associated with neurodevelopmental disorders including intellectual disabilities (ID), Autism spectrum disorder (ASD), and schizophrenia. Additionally, these pathogenic CNVs are characterized by extensive phenotypic heterogeneity, as affected individuals often present with microcephaly, craniofacial and heart defects, growth retardation, and seizures. Despite their strong association as risk factors towards neurodevelopmental disorders, the developmental role of individual CNV-affected genes and disrupted cellular mechanisms underlying these mutations remain poorly understood. Moreover, it is unclear as to how the affected genes both individually and combinatorially contribute to the phenotypes associated with pathogenic CNVs. Thus, in this thesis, I explore the functional basis of phenotypic variability of pathogenic CNVs linked to neurodevelopmental disorders. In particular, I focus on the 3q29 deletion and 16p12.1 deletion, to provide insight towards the

convergent cellular, molecular, and developmental mechanisms associated with decreased dosage of the affected gene homologs using two complementary model systems, *Xenopus laevis* and *Drosophila melanogaster*.

First, I examine the role of individual homologs of several CNV-affected genes at chromosome 3q29 and their interactions towards cellular processes underlying the deletion. We find that multiple 3q29-affected genes, including *NCBP2*, *DLG1*, *PAK2* and *FBXO45*, contribute to disruptions in apoptosis and cell cycle pathways, leading to neuronal and developmental defects. I then expand further upon this work by discerning the individual contribution of four CNV-affected genes at chromosome 16p12.1, *POLR3E*, *MOSMO*, *UQCRC2*, and *CDR2*, towards neurodevelopment and craniofacial morphogenesis. We demonstrate that several of these genes affect multiple phenotypic domains during neurodevelopment leading to brain size alterations, abnormal neuronal morphology, and cellular proliferation defects. I then explore their functions during vertebrate craniofacial morphogenesis and demonstrate that some of the 16p12.1-affected genes are enriched in migratory neural crest, and they contribute to early craniofacial patterning and formation of cartilaginous tissue structures. Together, these data are the first to suggest that signature neurodevelopmental phenotypes demonstrated in the 3q29 and 16p12.1 deletions may stem from convergent cellular mechanisms including aberrations in neuronal proliferation, apoptosis and cell cycle regulation, and neural crest cell development.

## ACKNOWLEDGEMENTS

This thesis and my growth as a scientist would not have been possible without the support of many incredible individuals that I have had the privilege to have in my life. I would like to thank everyone who has helped me along the way.

I would first like to thank the entire BC Biology department for fostering a collaborative and supportive environment in which to complete my PhD training in. It has been a pleasure to work with you all and be part of this dynamic community full of passionate people striving to make sure everyone succeeds.

Thank you to the administrative staff in the Biology office, Dina Goodfriend, Colette McLaughlin, and Diane Butera. You have all been a tremendous help in keeping our labs afloat and organizing the business side of things so that we can focus on our research. Thank you Dina for answering my questions and never letting up on keeping track of my conference reimbursements. Thank you Colette for always having the biggest smile on your face when anyone enters the office, chatting about life in the coffee room, and making sure I had all of the tech gadgets that I needed. Thank you Diane for being one of the kindest and warmest individuals and making sure events were organized perfectly.

Thank you to the Higgins Hall staff, Walter Carberry, John O' Grady, Kiel Smith, and Chris Cardoso. You are all amazing and deserve so many thanks for keeping things running in our building, delivering our packages, answering our incessant IT questions, and for saving the day countless times when chaotic things inevitably happen.

Thank you to all of the animal care facility staff, especially Nancy McGilloway and Todd Gaines, for your excellent frog husbandry. Without you, I would not have been

able to focus on my research as much as I have. Your time and energy devoted to taking care of our frog colony will not be forgotten.

Thank you to my thesis committee members, Sarah McMenamin, Eric Folker, Vicki Losick, and my outside reader, Isabel Dominguez, for your never ending support, especially during this last year. I am so grateful for all of your advice, insight, and scientific discussions throughout my years at BC. I would not have grown as much as I have, both scientifically and personally, without your guidance.

Now, I would like to give a very special thanks to the legendary past and present members of the Lowery lab for being amazing colleagues and friends. I woke up every morning excited to see all of your faces and am so lucky to have been able to work alongside you these past four years. Through all of the failures, successes, dead embryos, dance parties, karaoke nights, epic lab parties at my apartment, you have all made such a significant impact on my life that means more to me than you know. Never forget, we can't stop and we won't stop.

In particular, I would like to thank our superhero Sangmook for saving the day more times than I can count. I have learned so much from you and will take that knowledge with me throughout every stage of my career and life.

To my incredible undergrad army (A.K.A. team ID) – Connor, Jess Tiber, Jess Bolduc, Luke, Caroline, Sydney, and Ashley; thank you for giving me the privilege of being your mentor and for all of your insane dedication to learning and getting experiments done. It was a pleasure to have you all work with me and watch your growth as scientists and as individuals. Thank you for trusting me to guide you and asking for my

advice when you needed it. I love you all dearly and will always be here for you no matter what.

I would also like to thank Lowery lab undergrad alumni, Jackson Bowers, Ali Mills, and Fred Kim. You three made a huge impact on my time in lab because of your love, support, and friendship. I am so thrilled to see what you have accomplished since graduating from BC and cannot wait to see what you will achieve going forward. You all mean so much to me and I thank you for all of your conversations in and out of lab.

To the last Lowery lab BC undergrads – Eric Snow, Kathy, David, Liane, and Nick, I thank you for all of your hard work this past year. I could not have done this without you. Seeing your smiles, hearing you laugh, telling jokes, watching silly videos, complaining about frogs, and your endless support got me through the toughest of times. You all have a special place in my heart.

To my dearest GrossCon – Burcu, Beth, and Garrett, thank you for your friendship. I love you all so very much. Words really cannot do justice to describe how grateful I am to have you three in my life. Burcu, you are the kindest human being I have ever met. You never let anything get you down and always have such positive advice to give, no matter what. You see the good in every person and always treat others with the utmost respect. Your passion to learn and try new things is something that I will always admire. You are an incredible person and our friendship will last a lifetime, no matter where we are in the world. Beth, thank you for helping me and answering my questions, no matter how silly they were. Your determination and courage to be yourself will always inspire me. Garrett, thank you for giving me a shoulder to lean on this past year. You are my rock. Thank you for helping me with my experiments, taking care of the frogs,

organizing the lab, and just being there for me whenever I needed a laugh. Thank you for those long walks home, having beers at Harry's, and being ridiculous at the perfect moments. We finally did it dude!

I would also like to thank my friends, Kevin White, Jaclyn Mallard, Julie Valdes, and Claire Meurice. Kevin, my partner in crime, your friendship got me through the best and worst of graduate school. All of the craziest moments of my life these last four years happened with you and I will never forget them. Jaclyn, my fellow Michigan State Spartan, thank you for being my first friend in Boston and welcoming me into your home. Thank you for all of the wine nights at Harry's, dancing at Alibi, football Sunday's, and joining me for game watches at the Baseball Tavern. Julie and Claire, even though we are separated by distance, our friendships will last forever. I love all of you endlessly.

To my burrito, Charlie, thank you for being my biggest champion. You pushed me to persevere through the hardest times this past year and reminded me that I could succeed, even when I felt like the world was crashing down on me. You were my light at the end of the tunnel, my happy place when I was feeling blue. Thank you for listening to me complain, cry, yell, and scream. Thank you for telling me everything would work out like it was meant to. Thank you for telling me it was okay to be afraid, to never let me forget my dreams, and reminding me what my purpose in life is. Thank you for making me laugh uncontrollably until I tear up, for going on spontaneous adventures with me, and talking to me about everything under the sun over endless cups of coffee and chess. Thank you for always being honest with me, even when it might hurt. And most of all,

thank you for never judging me, loving me as I am, and being unapologetically yourself. You are my other half, my person, and I love you always.

To all of my family members – thank you for your immeasurable love and support. Thank you for believing in me and that one day, I would finally be done with school. Mom, thank you for always checking in to make sure I was okay and for all that you've done for me throughout my life. Dad, thank you for always being there to pick me up when I fall, for all of your advice, and for being my hero. I love you both more than you will ever know and hope to become an amazing parent to my children, as you both are to me.

And finally, I save the most important thank you for last, to my advisor and my friend, Laura Anne. I cannot convey how grateful I am to have been part of your life and a member of your lab. Your strength and courage inspired me, and will continue to inspire me, every single day. Thank you for creating and fostering the most amazing environment in which to work, fail, succeed, laugh, and cry in. The lengths you went through in order to make sure everyone felt safe, happy, and supported is incredible. You endlessly fought for what you believed in and for your students success. Your students well-being was always your number one priority. You knew that in order for productivity in lab to happen, the lab culture and your students mental health had to be in the forefront, and that is something I will always value. I will never forget what you've done for me both for my career as a scientist, and personally as an individual trying to figure out her way in this world. Thank you for your unconditional love and advice, your motivational messages, and for ALWAYS believing in me. I doubted myself so many times and thought I wasn't good enough to be a scientist, but you NEVER allowed those

feelings to deter me from my goals. You constantly pushed me out of my comfort zone, dared me to become more than I ever thought I could be, and helped me grow into the person that I am today because you knew I could do it. Thank you for putting your trust in me and knowing that I would be able to succeed, even in the darkest of times. I will take everything you've taught me and the lessons I have learned from you with me throughout my entire life. I will always cherish our friendship and be here for you, no matter what.

## TABLE OF CONTENTS

<b>Abstract</b>	
<b>Acknowledgements</b>	<b>i</b>
<b>Table of Contents</b>	<b>vii</b>
<b>List of Figures and Tables</b>	<b>xi</b>
<b>List of Symbols and Abbreviations</b>	<b>xiv</b>
<b>1 Introduction</b>	<b>1</b>
1.1 Copy number variants (CNVs) in neurodevelopmental disorders	<b>2</b>
1.1.1 Differential pathogenicity of rare CNVs towards neurodevelopmental disorders	<b>3</b>
1.1.2 The 3q29 microdeletion is associated with developmental defects and increased risk of psychiatric disorders	<b>8</b>
1.1.3 The 16p12.1 microdeletion is associated with developmental defects and intellectual disabilities	<b>11</b>
1.1.3.1 Known functions of affected genes within 16p12.1 region	<b>12</b>
1.1.3.2 The 16p12.1 microdeletion supports a “two-hit” model for disease	<b>14</b>
1.2 Using <i>Xenopus laevis</i> as a model system to investigate neurodevelopmental disorders	<b>16</b>
1.2.1 Advantages of <i>X. laevis</i> as a model organism	<b>17</b>
1.2.2 <i>X. laevis</i> as a model for studying the development of tissue and organ systems affected by pathogenic CNVs	<b>21</b>
1.3 Remaining questions	<b>27</b>

<b>2</b>	<b><i>NCBP2</i> modulates neurodevelopmental defects of the 3q29 deletion in <i>Drosophila</i> and <i>Xenopus laevis</i> models</b>	<b>29</b>
2.1	Introduction	30
2.2	Results	33
2.2.1	Reduced expression of individual homologs of 3q29 genes causes global developmental defects in <i>Drosophila</i>	33
2.2.2	Reduced expression of individual homologs of 3q29 genes causes brain size defects in <i>Xenopus laevis</i>	36
2.2.3	<i>Drosophila</i> and <i>Xenopus</i> eye models for genes within 3q29 region show cellular and developmental defects	39
2.2.4	Interactions between fly and <i>Xenopus</i> homologs of 3q29 genes enhance neuronal phenotypes	42
2.2.5	Interactions between <i>Cbp20</i> in flies and <i>ncbp2</i> in <i>Xenopus</i> with other homologs of 3q29 genes enhance apoptosis defects	45
2.3	Discussion	49
2.4	Materials and Methods	54
<b>3</b>	<b>Functional assessment of the “two-hit” model for neurodevelopmental defects in <i>Drosophila</i> and <i>X. laevis</i> models of 16p12.1 deletion</b>	<b>66</b>
3.1	Introduction	67
3.2	Results	70
3.2.1	Multiple homologs of 16p12.1 genes contribute to <i>Drosophila</i> and <i>X. laevis</i> development	70

3.2.2	Homologs of 16p12.1 genes independently contribute to neurodevelopmental defects	80
3.2.3	Homologs of patient-specific “second-hit” genes modulate phenotypes of 16p12.1 homologs	84
3.3	Discussion	88
3.4	Materials and Methods	94
<b>4</b>	<b>16p12.1 deletion homologs are enriched in motile neural crest cells and are important for regulating processes during their development in <i>Xenopus laevis</i></b>	<b>108</b>
4.1	Introduction	109
4.2	Results	111
4.2.1	16p12.1-affected genes display enriched expression in the developing nervous system, pharyngeal arches, and craniofacial structures	111
4.2.2	16p12.1-affected genes are important for maintaining cartilage size and scaling	114
4.2.3	Numerous 16p12.1-affected genes are critical for normal pharyngeal arch migration and NCC motility	116
4.2.4	16p12.1-affected genes do not directly impact NCC proliferation	120
4.2.5	Several 16p12.1-affected genes are critical for NCC induction and specification	122
4.3	Discussion	124
4.4	Materials and Methods	132

<b>5 Discussion</b>	<b>138</b>
5.1 Contributions to the Literature	139
5.1.1 Interactions between pairs of genes within the 3q29 region underlie the potential for highly complex models of CNV pathogenicity	139
5.1.2 16p12.1 deletion homologs independently contribute to neurodevelopmental phenotypes and are modulated by complex interactions with “second-hit” genes	141
5.1.3 16p12.1 deletion homologs contribute to craniofacial and cartilage phenotypes through aberrant neural crest cell development	144
5.2 Future Directions	146
5.2.1 Dissecting the convergent biological mechanisms underlying CNVs associated with neurodevelopmental disorders	147
5.2.2 A multigenic model for CNV pathogenicity	149
5.3 Concluding remarks	151
<b>References</b>	<b>153</b>

## LIST OF FIGURES AND TABLES

<b>Figure 1.1-</b> Genes affected by CNVs lead to phenotypes in different ways	<b>3</b>
<b>Figure 1.2-</b> Chromosome 4 and WHS-associated genes	<b>4</b>
<b>Figure 1.3-</b> 16p12.1 microdeletion is associated with intellectual disabilities	<b>12</b>
<b>Figure 1.4-</b> Excessive rare variants in genetic background contribute to phenotypic severity and diversity of 16p12.1 microdeletion	<b>15</b>
<b>Figure 1.5-</b> <i>X. laevis</i> unilateral injections allow for side-by-side comparison to wild-type gene expression following genetic manipulation	<b>19</b>
<b>Figure 1.6-</b> <i>X. laevis</i> neural tube dissection and axon outgrowth imaging	<b>22</b>
<b>Figure 1.7-</b> Measurements of <i>X. laevis</i> craniofacial features	<b>23</b>
<b>Figure 1.8-</b> Measurements of <i>X. laevis</i> cartilage elements	<b>24</b>
<b>Figure 1.9-</b> Analysis of <i>in vivo</i> NCC migration using whole-mount <i>in situ</i> hybridization	<b>25</b>
<b>Figure 2.1-</b> Strategy for identifying cellular phenotypes and genetic interactions of 3q29 gene homologs	<b>34</b>
<b>Figure 2.2-</b> Neurodevelopmental defects in flies with knockdown of individual homologs of 3q29 genes	<b>36</b>
<b>Figure 2.3-</b> Quantification of 3q29 morpholino knockdown levels in <i>X. laevis</i>	<b>37</b>
<b>Figure 2.4-</b> Brain size phenotypes observed with knockdown of 3q29 gene homologs in <i>X. laevis</i>	<b>39</b>
<b>Figure 2.5-</b> Eye phenotypes for flies with eye-specific knockdown of individual 3q29 gene homologs	<b>40</b>
<b>Figure 2.6-</b> Eye phenotypes observed with knockdown of 3q29 gene homologs in <i>X. laevis</i>	<b>41</b>
<b>Figure 2.7-</b> Pairwise interactions of fly and <i>Xenopus</i> 3q29 gene homologs	<b>43</b>
<b>Figure 2.8-</b> Transcriptome analysis of flies with knockdown of select 3q29 gene homologs	<b>45</b>
<b>Figure 2.9-</b> Cellular phenotypes with pairwise knockdown of fly 3q29 gene homologs	<b>46</b>

<b>Figure 2.10-</b> Rescue of phenotypes due to knockdown of fly and <i>Xenopus</i> 3q29 gene homologs with overexpression of apoptosis inhibitors	<b>48</b>
<b>Figure 3.1-</b> Strategy to evaluate the contributions of 16p12.1 gene homologs and interactions with “second-hit” genes towards neurodevelopmental phenotypes	<b>71</b>
<b>Figure 3.2-</b> Multiple homologs of 16p12.1 genes contribute to neurodevelopmental defects in <i>Drosophila</i> and <i>X. laevis</i>	<b>74</b>
<b>Figure 3.3-</b> Enriched GO terms observed with knockdown of 16p12.1 fly homologs in the nervous system	<b>75</b>
<b>Figure 3.4-</b> Expression levels of 16p12.1 homologs in <i>Drosophila</i> and <i>X. laevis</i>	<b>76</b>
<b>Figure 3.5-</b> Decreased dosage of 16p12.1 homologs leads to multiple neurodevelopmental phenotypes in <i>X. laevis</i>	<b>78</b>
<b>Figure 3.6-</b> Western blot for phosphorylated histone-3 in <i>X. laevis</i> embryos with knockdown of <i>polr3e</i> , <i>mosmo</i> , and <i>setd5</i>	<b>79</b>
<b>Figure 3.7-</b> Knockdown of <i>Sin</i> and <i>CG14182</i> lead to disruption of the fly eye	<b>81</b>
<b>Figure 3.8-</b> Homologs of 16p12.1 genes independently contribute towards neurodevelopmental defects	<b>83</b>
<b>Figure 3.9-</b> Fly homologs of 16p12.1 genes show complex interactions with homologs of patient-specific “second-hit” and neurodevelopmental genes	<b>86</b>
<b>Figure 3.10-</b> <i>setd5</i> establishes additive interactions with <i>polr3e</i> in <i>X. laevis</i>	<b>87</b>
<b>Figure 3.11-</b> <i>setd5</i> establishes synergistic interactions with <i>mosmo</i> in <i>X. laevis</i>	<b>88</b>
<b>Figure 4.1-</b> Expression patterns for 16p12.1-affected genes across early development	<b>113</b>
<b>Figure 4.2-</b> 16p12.1-affected genes are expressed in migrating neural crest cells during embryonic development	<b>114</b>
<b>Figure 4.3-</b> <i>In situ</i> hybridization probes generated against sense strands of 16p12.1-affected gene mRNAs	<b>114</b>
<b>Figure 4.4-</b> Knockdown of <i>Polr3e</i> , <i>Mosmo</i> , and <i>Uqcrc2</i> impact cartilage morphology	<b>116</b>
<b>Figure 4.5-</b> Knockdown of <i>Polr3e</i> , <i>Mosmo</i> , and <i>Uqcrc2</i> affect NCC migration <i>in vivo</i>	<b>118</b>

<b>Figure 4.6-</b> Manipulation of <i>Polr3e</i> , <i>Uqcrc2</i> , and <i>Cdr2</i> impacts NCC migration speeds <i>in vitro</i>	<b>120</b>
<b>Figure 4.7-</b> Manipulation of 16p12.1-affected genes does not impact NCC proliferation <i>in vitro</i>	<b>122</b>
<b>Figure 4.8-</b> Manipulation of <i>Polr3e</i> and <i>Mosmo</i> affects NCC specification	<b>124</b>
<b>Table 1-</b> Summary of major experiments for knockdown of 3q29 gene homologs in <i>Drosophila</i> and <i>Xenopus laevis</i> show widespread cellular and neuronal defects	<b>49</b>
<b>Table 2-</b> Phenotypes observed for individual 16p12.1 gene homologs in <i>Drosophila</i> and <i>X. laevis</i>	<b>93</b>
<b>Table 3-</b> Summary of 16p12.1-affected gene craniofacial, cartilage, and NCC phenotypes	<b>132</b>

**LIST OF SYMBOLS AND ABBREVIATIONS**

**CNV** – copy number variant

**ID** – intellectual disability

**ASD** – Autism spectrum disorder

**NCC** – neural crest cell

**WHS** – Wolf-Hirschhorn Syndrome

**WHSCR** – Wolf-Hirschhorn Syndrome critical region

**PA** – pharyngeal arch

**MO** – antisense morpholino oligonucleotide

**OE** – overexpression

**KD** – knockdown

**TF** – transcription factor

**Shh** – Sonic hedgehog signaling

## CHAPTER 1

### Introduction

Some material in this chapter was adapted from:

**Lasser, M.\*, Pratt, B.\***, Monahan, C., Kim, S.W., Lowery, L.A. The Many Faces of *Xenopus*: *Xenopus laevis* as a Model System to Study Wolf-Hirschhorn Syndrome. *Front Physiol.* 2019; 10:817. doi: 10.3389/fphys.2019.00817. eCollection 2019.

\*authors contributed equally to work

## 1.1 Copy number variants (CNVs) in neurodevelopmental disorders

Nervous system development and wiring of the brain encompasses a vast array of cellular processes that are orchestrated by proper gene and protein function. However, during embryonic development, problems may emerge due to mutations in genes that are critical for regulating processes such as neuronal cell division and proliferation, differentiation, migration, or synapse formation. These mutations may then have downstream impacts on neural connectivity, and can ultimately result in neurodevelopmental disorders or neurological diseases (Girirajan et al., 2011; Vicari et al., 2019; Wilfert et al., 2017). While the pathogenesis of neurodevelopmental disorders is still not fully understood, significant advances in high-throughput genomic sequencing technologies have helped identify hundreds of genes as risk factors for neurodevelopmental and neuropsychiatric disorders. For example, recent studies suggest that rare recurrent copy number variants (CNVs) account for about 15% of individuals with neurodevelopmental disorders including intellectual disabilities (ID), Autism spectrum disorder (ASD), schizophrenia, and epilepsy (Ashitha and Ramachandra, 2020; Coe et al., 2019; Jensen and Girirajan, 2017, 2019; Wilfert et al., 2017).

CNVs are large deletions or duplications of regions >1 kb in the genome, and can either be inherited or occur *de novo* (**Fig. 1.1.A**) (Nowakowska, 2017). Most CNVs present in individual genomes are relatively common, playing an important role in terms of biodiversity and they do not have harmful effects (Lauer and Gresham, 2019). However, recurrent CNVs that arise by nonallelic homologous recombination events with breakpoints typically mapping within segmental duplications are enriched in neuropsychiatric disorders, and often encompass genes that are dosage-sensitive

(Deshpande and Weiss, 2018; Vicari et al., 2019; Wilfert et al., 2017). As

neurodevelopment involves nearly 70% of all expressed genes, it is not surprising that the deleterious effects of rare pathogenic CNVs manifest in brain and behavioral phenotypes (Deshpande and Weiss, 2018). Therefore, determining the functional significance of critical genes affected by CNVs is essential in order to gain a deeper comprehension of the convergent cellular and developmental mechanisms underlying the pathogenesis of complex neurodevelopmental disorders.

### 1.1.1. Differential pathogenicity of rare CNVs towards neurodevelopmental disorders

Recurrent CNVs have increasingly become a strong risk factor for neurodevelopmental disorders; however, they most often are characterized by phenotypic heterogeneity, as the genes within CNVs can lead to developmental defects in different ways (**Fig. 1.1.B**).

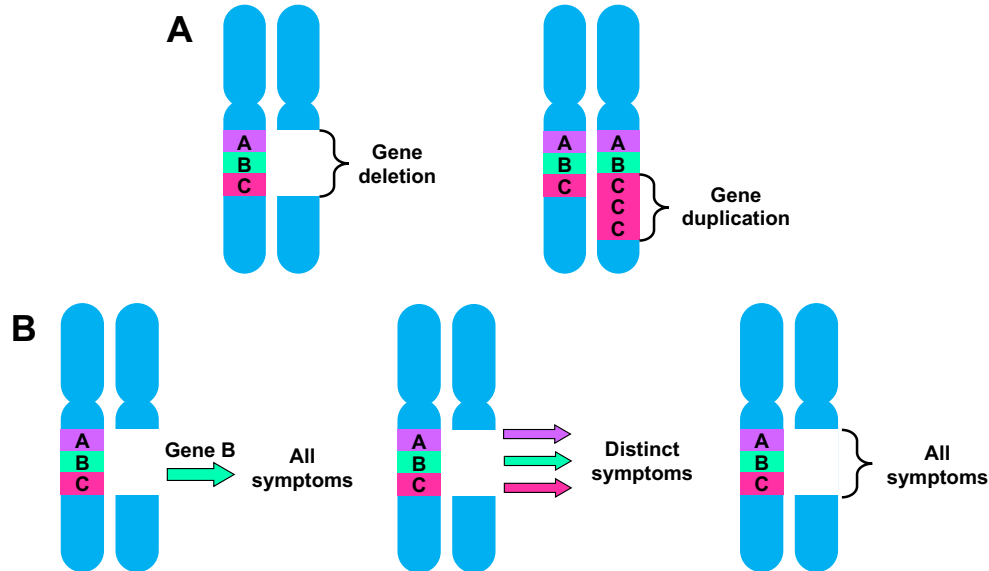


**Figure 1.1** Genes affected by CNVs lead to phenotypes in different ways

**(A)** CNVs are typically large deletions or duplications of multiple genes within a region of the genome. **(B)** Pathogenic CNVs associated with neurodevelopmental disorders can lead to phenotypes of the disease in different ways. 1) It is possible that a singular gene within a CNV is sufficient to cause all symptoms of a disease; 2) it could be that each individual CNV-affected gene contributes to one distinct phenotype of a disease; 3) or it may be more complex, in which phenotypes result through interactions between all CNV-affected genes.

Traditionally, gene discovery within rare syndromic CNVs has involved identifying a single causative gene that explains all of the distinct phenotypes associated with the CNV, followed by detailed functional evaluation of that gene using animal model systems. For example, in the 17p11.2 deletion that leads to Smith-Magenis Syndrome (SMS), haploinsufficiency of *RAI1* is considered the primary cause for most SMS features (Falco et al., 2017; Huang et al., 2016). Likewise, in Wolf-Hirschhorn Syndrome (WHS), heterozygous deletion of genes within the WHS critical region (WHSCR) at chromosome 4p16.3, encompassing *WHSC1*, *WHSC2*, and *LETM1*, was originally thought to be sufficient to cause all core WHS phenotypes (Fig. 1.2) (Battaglia et al., 2015; Rutherford and Lowery, 2016).

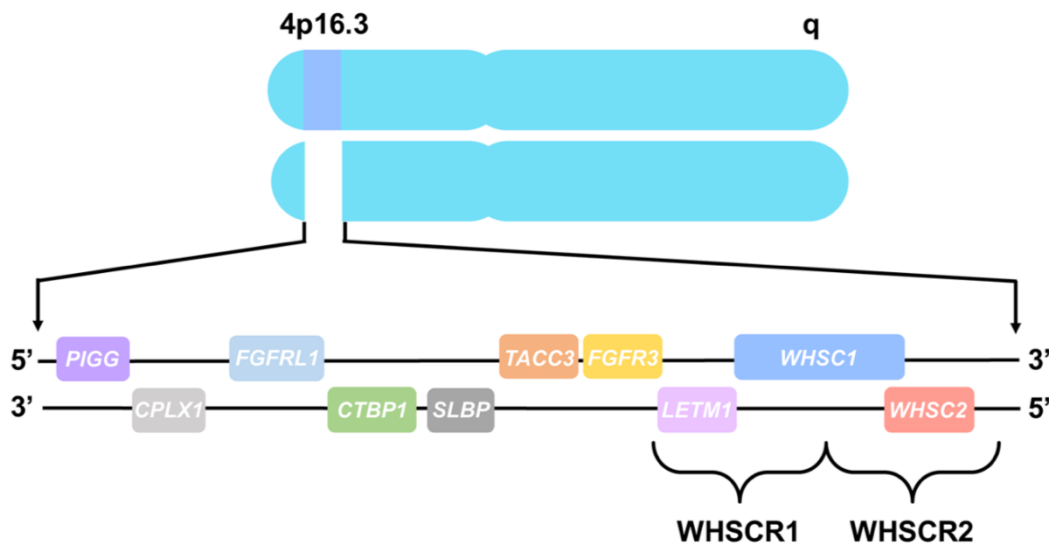


**Figure 1.2 Chromosome 4 and WHS-associated genes**

All WHS-associated genes are represented in their order from left to right, telomeric to centromeric orientation, located on the distal arm of chromosome 4p16.3. Brackets delineate WHS critical regions (WHSCR), comprised of *LETM1*, *WHSC1*, and *WHSC2*.

Although some variability in phenotypic expression of these disorders has been documented, SMS and WHS usually occur *de novo* and are characterized by high penetrance for the disease-associated phenotypes. In these cases, individuals manifesting

strong characteristic features of the syndrome were used to identify singular causative genes for the major phenotypes. However, further investigations have revealed that this approach has, in fact, been largely unsuccessful in accounting for the variable expressivity of neurodevelopmental phenotypes among affected patients with a majority of other pathogenic CNVs. Thus, several themes have emerged from more recent studies that describe the etiology underlying neurodevelopmental diseases associated with CNVs. First, extensive heterogeneity and incomplete penetrance of associated neurodevelopmental phenotypes adds challenges to genetic mapping strategies in identifying a singular gene as causative for these diseases on their own. Second, growing evidence suggests that the range of neurodevelopmental defects are likely not caused by haploinsufficiency of one individual gene, but rather are modulated by dosage alterations of multiple closely-linked genes, and that phenotypes could result from the interaction between these CNV-affected genes (Jensen and Girirajan, 2019; Lauer and Gresham, 2019; Nowakowska, 2017; Zarrei et al., 2015).

For instance, in a contiguous gene model, multiple individual genes within an affected region contribute to distinct phenotypes as opposed to a singular gene being causative for all disease phenotypes (**Fig. 1.1.B**). In Williams-Beuren syndrome, disruption of individual genes at chromosome 7q11.23 are linked to specific phenotypes of the disease, such as *ELN* for cardiovascular features (Ghaffari et al., 2018; Schubert, 2009). Similarly, *TBX1* was identified as the candidate gene responsible for aortic arch defects in individuals with the 22q11.2 deletion/DiGeorge syndrome (Lindsay et al., 2001). Furthermore, the etiology underlying WHS has recently expanded beyond the haploinsufficiency of genes residing in the WHSCR, and is now considered a true

contiguous gene syndrome. While loss-of-function of genes within the WHSCR were originally believed to be sufficient to cause all WHS features, the discovery of additional mutations in genes distal to this region are now associated with distinct phenotypes (Battaglia et al., 2015; Rutherford and Lowery, 2016). For example, *CPLX1* and *CTBPI* are likely candidate genes for epilepsy, whereas *FGFR3* and *FGFRL1* are candidate genes for skeletal defects observed in WHS (Battaglia et al., 2015).

Additionally, neurodevelopmental defects associated with another category of syndromic CNVs are thought to be modulated by multiple dosage-sensitive genes through combinatorial mechanisms within pathways related to neurodevelopmental processes (Iyer et al., 2018; Mulle, 2015; Rutkowski et al., 2019; Singh et al., 2020; Weiss et al., 2008). For instance, the 16p11.2 deletion has been implicated in 1% of individuals with ASD, but only 25% of individuals with the deletion exhibit an autism phenotype, whereas others may manifest intellectual disability, obesity, or epilepsy (Iyer et al., 2018; Pizzo et al., 2019). Several individual genes affected within this region have been associated with specific congenital features of the disorder, such as *TBX6* for scoliosis and kidney defects, but recent functional studies have uncovered a more complex model of genetic interactions in this region (Iyer et al., 2018; Ren et al., 2020; Yang et al., 2020). Studies using cellular, mouse, zebrafish, and *Drosophila* models have implicated several different genes within the 16p11.2 region to be responsible for the neurodevelopmental phenotypes associated with the deletion (Blaker-Lee et al., 2012; Blumenthal et al., 2014; Iyer et al., 2018; Pucilowska et al., 2015). Moreover, interactions between pairs of 16p11.2 gene homologs were found to enhance or suppress cellular phenotypes observed for individual gene depletion models in *Drosophila*, suggesting that

interactions between genes within the deletion may act through common pathways to determine the phenotypic severity of the disease (Iyer et al., 2018). This further illustrates the importance of genetic interactions towards causation and modulation of neurodevelopmental disease, and emphasizes the need for a more detailed function-based analysis, in addition to sequencing studies, towards discovery of gene function in the context of pathogenic CNVs.

In a similar fashion, despite years of research following their discovery as risk factors for neurodevelopmental and neuropsychiatric disease, very little remains known about the effect of individual and combinatorial dosage alterations of genes within the 3q29 and 16p12.1 regions on behavioral and developmental phenotypes. Moreover, the potential genetic interactions and disrupted biological mechanisms underlying these deletions have still not been thoroughly characterized. Originally, the 3q29 deletion was implicated as a significant risk factor for schizophrenia and the 16p12.1 deletion was identified as a risk factor for intellectual disabilities and mild cognitive impairment (Antonacci et al., 2010; Girirajan et al., 2010b; Mulle, 2015). Although these CNVs are enriched in affected individuals compared to population controls, patients display variable degrees of penetrance and expressivity of clinical features. Individuals manifest a range of neuropsychiatric and neurodevelopmental features including ASD, attention-deficit/hyperactivity disorder, bipolar disorder, microcephaly, craniofacial defects, and speech delay (Girirajan et al., 2010b; Pizzo et al., 2019; Rutkowski et al., 2019; Singh et al., 2020). While these two pathogenic CNVs encompass distinct sets of genes, it is clear they share commonalities in observed clinical symptoms, making the specific gene-to-phenotype mapping challenging. Therefore, studies aimed at developing a clearer and

more comprehensive understanding of the complex disease-causative mechanisms associated with these two CNV-affected genomic regions are necessary. To this aim, this thesis focuses on approaches that combine a functional evaluation of each gene within the CNV-affected 3q29 and 16p12.1 regions, and their genetic interactions, to identify key neurodevelopmental pathways and molecular mechanisms of the phenotypes associated with these pathogenic CNVs.

### ***1.1.2 The 3q29 microdeletion is associated with developmental defects and increased risk of psychiatric disorders***

Since the advent of large-scale sequencing studies, the number of pathogenic CNVs associated with neurodevelopmental disorders, such as ASD, intellectual disabilities, and schizophrenia has increased dramatically (Ashitha and Ramachandra, 2020; Girirajan et al., 2011; Jensen and Girirajan, 2019; Lauer and Gresham, 2019; Wilfert et al., 2017; Zarrei et al., 2015). However, as previously mentioned, while many syndromic CNVs have been identified as risk factors for disease, their probable mechanisms of action towards neurodevelopmental pathologies remains to be elucidated. One of these syndromic CNVs is the 3q29 deletion. This CNV results in a heterozygous deletion of a 1.6 Mb interval containing 21 protein coding genes and is characterized by variable clinical presentation (Mulle, 2015). Individuals display a range of neurodevelopmental features including mild to moderate intellectual disability, gait ataxia, microcephaly, and craniofacial defects (Mulle, 2015; Rutkowski et al., 2019). Affected patients also show psychiatric disturbances including aggression, anxiety,

hyperactivity, and bipolar disorder. Moreover, this deletion confers a >40-fold increase in risk for schizophrenia and a >20-fold risk for autism (Mulle, 2015).

Of the 21 genes within the interval, several have been shown to play important roles in brain and neurocognitive development. In particular, *DLG1*, *PAK2*, and *FBXO45* have received attention as likely candidate genes for causing intellectual disability and neuropsychiatric phenotypes (Chirita Emandi et al., 2019; Pollak et al., 2019; Rutkowski et al., 2019; Willatt et al., 2005). *DLG1* is a scaffolding protein that interacts with N-methyl-D-aspartate (NMDA) and AMPA type glutamate receptors and organizes the synaptic structure at neuromuscular junctions, affecting synaptic plasticity during development (Budnik et al., 1996; Li et al., 2018; Walch, 2013). Previous functional studies of *DLG1* demonstrate that both *Dlg1*-null and *Dlg1*<sup>+/-</sup> mice display cartilage and bone malformations, as well as subtle cognitive and motor deficits (Li et al., 2018; Rutkowski et al., 2019). However, they did not recapitulate the severity of major developmental and behavioral features observed in mouse models of the entire 3q29 deletion, suggesting that haploinsufficiency of *Dlg1* alone is not sufficient to explain the phenotypes associated with the deletion (Rutkowski et al., 2019).

One potential modifier of *DLG1* is *PAK2*, which is a serine/threonine protein kinase that functions as a regulator of Rho GTPases, resulting in downstream effects on cytoskeletal dynamics, cell motility, cell cycle progression, proliferation, and apoptosis (Marlin et al., 2011; Wang et al., 2018). Specifically, *PAK2* is thought to be a key mediator of the ERK signaling pathway, critical for neuronal extension and is activated by caspases during apoptosis (Shin et al., 2002; Wang et al., 2018). *Pak2*<sup>+/-</sup> mouse models display some mild autism-related behaviors and neuronal deficits, though in *drosophila*,

single *dlg*<sup>+/-</sup> or *pak*<sup>+/-</sup> mutants do not show any phenotypes (Grice et al., 2015; Wang et al., 2018). However, when *dlg* and *pak* are simultaneously reduced in flies, various behavioral and molecular phenotypes arise, such as decreased number of neuromuscular boutons (Grice et al., 2015). These results indicate a potential genetic interaction between *DLG1* and *PAK2*, and that their combined depletion, along with other genes in this region, are necessary to drive neurodevelopmental defects.

*FBXO45* is a component of the E3 ubiquitin ligase complex and is required for normal synaptogenesis, axon pathfinding, and neuronal migration in developing central and peripheral neurons through the ubiquitin proteasome system (Saiga et al., 2009; Tada et al., 2010). Mice deficient in *Fbxo45* show abnormal synapse formation at neuromuscular junctions and aberrant development of axon fiber tracts in the brain (Saiga et al., 2009). Moreover, this gene is considered to be a prominent candidate that may contribute to schizophrenia susceptibility associated with the 3q29 deletion (Wang et al., 2014). The correlation between schizophrenia and dysregulation of the ubiquitin proteasome system has been implicated by a variety of gene expression analyses in post-mortem brain tissue (Altar et al., 2005; Middleton et al., 2002; Vawter et al., 2002). Thus, as the *FBXO45* protein plays a critical role in synaptic development and transmission via the ubiquitin proteasome system, the link between *FBXO45* as a candidate gene for schizophrenia is strong. However, further studies must be done to address this potential association and whether the neuronal phenotypes that arise due to partial depletion of *FBXO45* may be modified by haploinsufficiency of other genes affected within the 3q29 region.

Though the role of some individual 3q29-affected genes have been examined in relation to neurodevelopment, many remain understudied and their genetic interactions, as well as the disrupted biological mechanisms underlying the deletion have not been thoroughly characterized. As stated, it is likely that haploinsufficiency of singular 3q29-affected genes alone is not sufficient to cause the range of neurodevelopmental phenotypes associated with the deletion, and that these phenotypes likely arise due to interactions between multiple dosage-imbalanced genes through shared cellular pathways. Therefore, identifying the conserved molecular mechanisms linking individual genes or combinations of genes within the 3q29 region to neurodevelopmental phenotypes observed in patients with the entire deletion is necessary.

### ***1.1.3 The 16p12.1 microdeletion is associated with developmental defects and intellectual disabilities***

As stated, a majority of known recurrent genomic disorders result from nonallelic homologous recombination events between large, highly identical segmental duplications (Ashitha and Ramachandra, 2020; Coe et al., 2019; Deshpande and Weiss, 2018; Wilfert et al., 2017). Specific human chromosomes (e.g. 7, 15, 16, 17, and 22) are enriched for segmental duplications and as a result, multiple genomic disorders have already been associated with these regions of the genome (Girirajan et al., 2011; Jensen and Girirajan, 2017; Pizzo et al., 2019; Vicari et al., 2019; Zarrei et al., 2015). In particular, at least three microdeletion/microduplication syndromes have been linked to the short arm of chromosome 16, including the 520-kb heterozygous microdeletion at 16p12.1, recently identified by our collaborators (Antonacci et al., 2010). This CNV affects several genes,

including *POLR3E*, *MOSMO*, *UQCRC2*, and *CDR2*, and it has been significantly associated with intellectual disabilities and developmental delay (**Figure 1.3.A**) (Girirajan et al., 2010b). In addition to intellectual disabilities, individuals with this deletion display a variety of symptoms including microcephaly, craniofacial abnormalities, seizures, cardiac defects, and growth retardation (**Figure 1.3.B**).

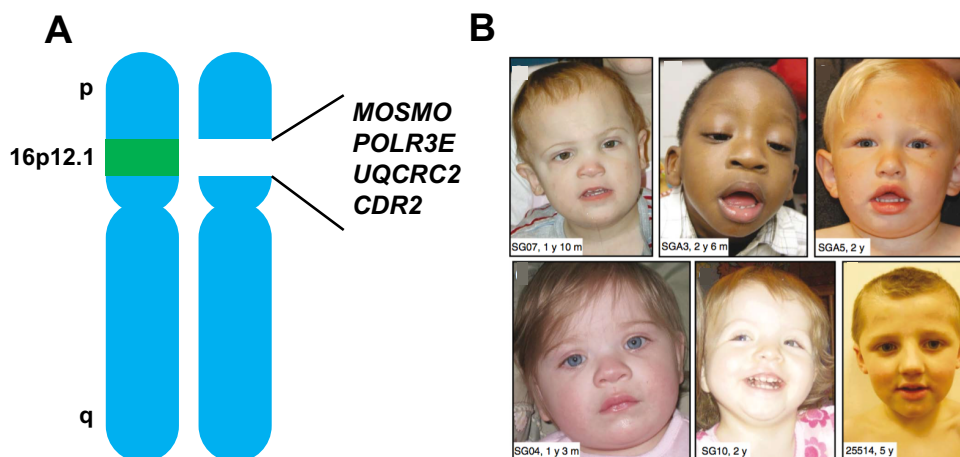


**Figure 1.3 16p12.1 microdeletion is associated with intellectual disabilities**

**(A)** The CNV located at chromosome 16p12.1 results in a 520-kb heterozygous microdeletion of several genes including *MOSMO*, *POLR3E*, *UQCRC2*, and *CDR2*. **(B)** Children patients harboring the 16p12.1 deletion display phenotypic heterogeneity, presenting with intellectual disabilities, microcephaly, craniofacial abnormalities, heart defects, growth retardation, and seizures (image, Girirajan *et al.*, 2010).

### ***1.1.3.1 Known functions of affected genes within the 16p12.1 region***

As stated, the 16p12.1 deletion impacts several genes, including *POLR3E*, *MOSMO*, *UQCRC2*, and *CDR2*. The multigenic nature of this deletion adds complexity to our understanding regarding the etiology of the mutation, due in part to the functional diversity of the affected genes. Below, we summarize the currently-known core biological functions of the 16p12.1-affected genes.

RNA polymerase III subunit E (*POLR3E*) encodes a subunit of RNA polymerase III, which primarily synthesizes small RNAs, such as 5S rRNA and tRNAs; however, the precise role of *POLR3E* in relation to RNA polymerase III activity is still unclear (Hu et

al., 2002). While mutations in this particular subunit have not previously been linked to neurodevelopmental disorders, mutations in other subunits of RNA polymerase III, *POLRIC* and *POLRID* have been associated with leukodystrophy, ataxia, and the congenital craniofacial disorder, Treacher Collins syndrome (Ghesh et al., 2019; Noack Watt et al., 2016; Sanchez et al., 2020). It is known that cell growth and differentiation are tightly dependent on the proper function of RNA polymerase III, supporting the idea that alteration of *POLR3E* could lead to deficits in these processes during embryonic development (Dumay-Odelot et al., 2010).

Recent work has identified Modulator of Smoothed (*MOSMO*) as a negative regulator of sonic hedgehog (Shh) signaling by participating in the degradation of the Frizzled class receptor, Smoothed (Pusapati et al., 2018a). The Shh pathway coordinates the downstream intracellular regulation of transcription factors that are known to be critical during many aspects of embryonic development including cell fate determination and patterning, neural progenitor proliferation and differentiation, axon guidance, and neural crest cell specification and migration (Dworkin et al., 2016; Tickle and Towers, 2017; Yam and Charron, 2013). As dysregulation of the Shh pathway is associated with an array of developmental defects including holoprosencephaly, it is plausible that dosage changes of *MOSMO* may impact one or more of these cellular processes (Sasai et al., 2019).

Ubiquinol-cytochrome C reductase core protein 2 (*UQCRC2*) encodes a component of the mitochondrial respiratory chain complex and is essential for the production of ATP (Gaignard et al., 2017; Shan et al., 2019). Mitochondrial complex III deficiency caused by *UQCRC2* mutations can lead to neonatal onset recurrent

hepatocellular insufficiency, lactic acidosis, hypoglycemia, ketosis, and hyperammonemia (Gaignard et al., 2017; Miyake et al., 2013). Moreover, it has been shown that reduced expression of *UQCRC2* induces an increase in reactive oxygen species (ROS) production and overexpression is correlated with tumor progression through increased cellular proliferation (Shang et al., 2018). However, functional information about the involvement of *UQCRC2* during embryonic development has not been examined.

*CDR2* is an oncogenic protein that is strongly expressed in Purkinje neurons of the cerebellum and is ectopically expressed in tumor cells, particularly in ovarian and breast malignancies (Schubert et al., 2014). It is thought that loss of immune tolerance towards this protein triggers the synthesis of an autoantibody, leading to immune-mediated paraneoplastic neurologic degeneration (Hwang et al., 2016; Schubert et al., 2014). Although the regulation of *CDR2* is not well-understood, some studies suggest that it acts during mitosis in cycling cells, in part through interactions with c-myc, to regulate a cascade of downstream cellular activities (O'Donovan et al., 2010).

Despite there being some information known about the cellular functions of these genes, they still have never been carefully investigated in the context of embryonic development, nor has any study determined whether their depletion contributes to phenotypes associated with the 16p12.1 deletion. Therefore, a mechanistic approach to understand the role of individual homologs of 16p12.1 genes and their interactions towards the developmental processes that underly the deletion is warranted.

### ***1.1.3.2. The 16p12.1 deletion supports a “two-hit” model for disease***

While the 16p12.1 CNV is linked to damaging neurodevelopmental features, in 96% of the cases, the deletion is inherited from a parent who presents only mild neuropsychiatric disease or does not exhibit any overt features (**Figure 1.4.A**) (Girirajan et al., 2010b; Pizzo et al., 2019). Moreover, severely affected probands with the deletion carry an excess of rare pathogenic mutations, or ‘second-hits’, in known neurodevelopmental genes elsewhere in the genome, compared to their mildly-affected carrier parents (**Figure 1.4.B**).

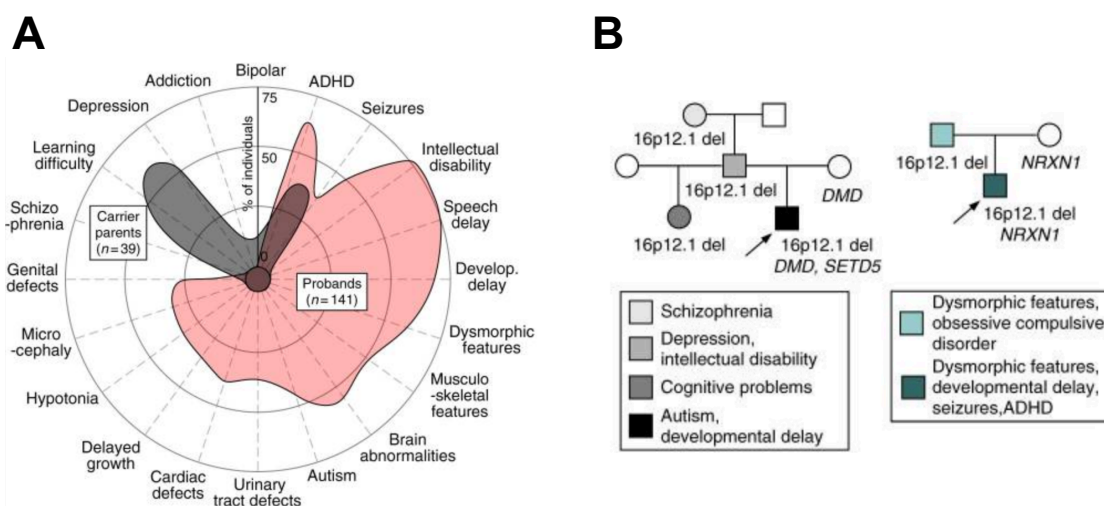


**Figure 1.4 Excessive rare variants in genetic background contribute to phenotypic severity and diversity of 16p12.1 microdeletion**

(A) Spectrum of phenotypes associated with 16p12.1 probands (red) and carrier parents (gray). Probands display a spectrum of developmental defects compared with the mild cognitive and psychiatric features observed in carrier parents. (B) Example of families with inherited 16p12.1 deletion. Family 1 (left) shows three generations carrying 16p12.1 deletion, with the proband carrying *de novo* loss-of-function variants in second-hit genes, *DMD* and *SETD5*. Family 2 (right) shows a proband with 16p12.1 deletion and a deletion of the second-hit gene, *NRXN1*. In both cases, carrier parents present with mild neuropsychiatric symptoms, while probands present with more severe neurodevelopmental features (images, Pizzo et al., 2019).

In contrast, other rare CNVs associated with neurodevelopmental disease, such as the 16p11.2 deletion, occur mostly *de novo* and less frequently in combination with another large chromosomal alteration (Iyer et al., 2018; Jensen and Girirajan, 2019; Pizzo et al., 2019). Therefore, this supports a “two-hit” model for disease, whereby the 16p12.1 deletion sensitizes the genome for disease, but other hits in the genetic background may

modulate the severity and diversity of phenotypic outcomes (Girirajan et al., 2010b). Thus, exploring these findings, by delineating the functional role of genes within the 16p12.1 region, along with ‘second-hit’ genes, in vertebrate models, and integrating them with human functional data is critical. Together, this analysis will aid in discovering a conserved mechanism of the pathogenicity associated with the 16p12.1 deletion, to further delineate global models of the molecular etiology associated with neurodevelopmental disorders.

## **1.2 Using *Xenopus laevis* as a model system to study neurodevelopmental disorders**

The model organism *Xenopus laevis* has been used extensively in the research community for many decades to examine fundamental developmental and cellular biological processes, making it an ideal system for investigating human genetic disorders. Every model system has its benefits and limitations; however, *X. laevis* offers a number of advantages, as they are inexpensive and easy to culture, maintain, manipulate, and image, compared to other vertebrate model systems (Bolus et al., 2020; Erdogan et al., 2016; Rosch et al., 2019; Slater et al., 2017; Ugur et al., 2016). With the *X. laevis* genome sequenced, genetic manipulation strategies can be readily designed in order to alter the dosage of CNV-affected candidate genes. Moreover, a variety of assays exist in order to examine how manipulation of these genes lead to changes in the development of tissue and organ systems affected in neurodevelopmental and neurological disorders.

Systematic functional testing of genes within the 3q29 and 16p12.1 regions requires model systems that are amenable for rapid phenotypic evaluation during embryonic development and allows for testing interactions between multiple dosage-

imbalanced genes without affecting the viability of the organism. While mouse models are an excellent mammalian system due to the similarity between the mouse and human genomes and the large genetic toolkit available, they are very costly to house and maintain. Moreover, litter sizes are small, embryonic development occurs *in utero*, and creating genetic lines that harbor mutant alleles is time-consuming. Though zebrafish produce many offspring and have well-developed genetic manipulation strategies, their genome has lost a great deal of synteny with mammals and many relevant disease-related genes do not perform the same function (Garcia de la Serrana et al., 2014). Zebrafish also lack certain organ systems, such as limbs, digits, and lungs, that are involved in many human congenital syndromes. Additionally, the zebrafish heart only has one atrium and one ventricle, and cannot fully model developmental heart abnormalities. However, using *X. laevis* to investigate human genetic diseases of development has enormous potential and can complement other model systems, like mouse or zebrafish. Moreover, by using this vertebrate model organism, we can enhance our knowledge regarding the conserved function of understudied genes and the underlying mechanisms by which developmental abnormalities arise due to pathogenic CNVs. In the sections below, we provide a detailed description of why *X. laevis* is an advantageous model to choose for investigating neurodevelopmental disorders.

### ***1.2.1 Advantages of X. laevis as a model organism***

*Xenopus laevis* is an excellent system for moderate-throughput analysis of how genetic manipulation affects various processes that are critical during vertebrate embryonic development. *X. laevis* shares a high degree of synteny with humans and a

majority of disease-associated genes are conserved between these species (Hellsten et al., 2010; Session et al., 2016). The *X. laevis* genome is widely-available to the research community through the efforts of NIH-funded *Xenbase*, an online resource that has organized current annotated genetic information, protocols, *X. laevis* anatomy and development, scientific literature, and provides useful sequencing tools, such as the genome browser and *Xenopus*-specific BLAST (James-Zorn et al., 2018; Karimi et al., 2018).

A key characteristic of *X. laevis* is the ease of acquiring large amounts of high-quality embryos, by inducing females to lay eggs via hormone priming (Erdogan et al., 2016; Sive et al., 2007a, b; Slater et al., 2017). Hundreds of embryos (or more) can be obtained in a single clutch, enabling numerous embryos to be manipulated and observed in a single experiment. *X. laevis* development occurs rapidly and externally, with gastrulation and neurulation occurring between 9-26 hours post fertilization, and organogenesis almost complete by 5 days post fertilization (Zahn et al., 2017). *X. laevis* organ development has been well-characterized and is comparable to those of mammalian systems, including orofacial (Dickinson, 2016), heart (Hempel and Kuhl, 2016), kidney (Getwan and Lienkamp, 2017), and nervous system development (Lee-Liu et al., 2017; Pratt and Khakhlin, 2013). Moreover, *X. laevis* is now being used extensively as a model to understand a number of different human genetic diseases that lead to defects in these systems, such as congenital heart disorders (Boskovski et al., 2013; Deniz et al., 2017; Duncan and Khokha, 2016; Sojka et al., 2014), kidney disease (Blackburn et al., 2019; Getwan and Lienkamp, 2017), ciliopathies (Brooks and Wallingford, 2015; Huizar et al., 2018; Wallmeier et al., 2016), orofacial defects

(Dickinson, 2016; Tahir et al., 2014), and neurodevelopmental disorders (Lichtig et al., 2020; Ott et al., 2019; Willsey et al., 2018).

In order to characterize CNV-affected gene functions in relation to development and disease, *X. laevis* embryos can be injected with a variety of materials to manipulate gene expression. These include CRISPR/cas9 or morpholino oligonucleotides (MOs), in either the whole embryo or selected blastomeres (up to the 64-cell stage) (Bestman and Cline, 2020; Bhattacharya et al., 2015; DeLay et al., 2016; Moody, 2018a, b; Tandon et al., 2017). As the lineage of individual cells has been well-documented, injections can be precisely targeted to specific tissues and organs that are affected by pathogenic CNVs, such as the heart, kidney, or brain. A unique feature of *Xenopus* compared to other models is the ability to perform unilateral embryo injections, wherein only one hemisphere of the embryo is experimentally manipulated and the opposite side serves as an internal control (**Figure 1.5.A**) (Lasser et al., 2019; Mills et al., 2019; Willsey et al., 2018). Thus, assessing phenotypic consequences that arise as a result of genetic manipulation can be compared side-by-side to wild-type gene expression within the same embryo.

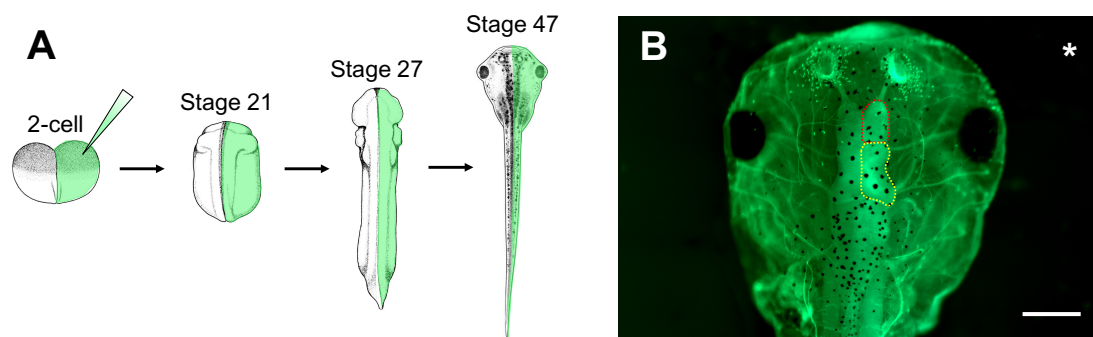


**Figure 1.5** *X. laevis* unilateral injections allow for side-by-side comparison to wild-type gene expression following genetic manipulation

**(A)** *X. laevis* embryos can be unilaterally injected in one hemisphere at the 2-cell stage with genetic manipulation macromolecules and fluorescent mRNA. Embryos can be sorted based on side that was injected (left vs. right) and used for various assays throughout development. **(B)** Representative image of stage 47 *X.*

*laevis* tadpole immunolabeled for acetylated tubulin. Asterisk represents side that was injected with genetic manipulation macromolecule and fluorescent mRNA. Brain morphology, such as forebrain size (red outline), and midbrain size (yellow outline) of the manipulated side can be measured and compared to the unaltered, wild-type side to be used as a straightforward readout of brain development. Scale bar: 500 $\mu$ m.

MOs are particularly useful in modeling genetic diseases, as they can be easily titrated to reduce gene dosage levels, similar to those in human patients (Bestman and Cline, 2020; Lichtig et al., 2020; McCammon and Sive, 2015; Ott et al., 2019; Schwenty-Lara et al., 2019; Willsey et al., 2018). Because many CNV-associated mutations result in haploinsufficiency, a full knockout of the candidate genes would not appropriately model the disease. Additionally, simultaneous knockdown of genes can be achieved by injecting multiple MOs at once, allowing for concurrent knockdown of genes that are often deleted together (Blum et al., 2015). While it is certainly possible to produce mouse lines with mutations in multiple genes (Simon and Bergemann, 2008), this is a costlier and more time-consuming process than the equivalent in *X. laevis*. As with all manipulation strategies, the appropriate controls must be used to account for off-target effects, such as generating more than one MO towards the target gene, testing for dose dependency, and rescuing phenotypes by co-injecting mRNA that is not targeted by the MO (Blum et al., 2015; Simon and Bergemann, 2008).

The CRISPR/cas9 system has also been used as an extremely effective method to knock out target genes in *X. laevis* (Bhattacharya et al., 2015; Tandon et al., 2017; Wang et al., 2015). While the off-target effects of CRISPR/cas9 are thought to be minimal, the use of proper controls is critical by carefully designing multiple sgRNAs and performing rescue experiments to confirm that any phenotypes observed are due to the knockout of a particular gene (Wang et al., 2015). The CRISPR/cas9 system can be employed to validate phenotypes that arise as a result of MO-mediated gene knockdown by comparing

phenotypes generated by both methods (Bharathan and Dickinson, 2019; Willsey et al., 2018). Thus, *X. laevis* is well-suited for using these genetic manipulation strategies to elucidate the mechanisms by which manipulation of CNV-associated genes alters proper embryonic development.

### ***1.2.2. X. laevis as a model for studying the development of tissue and organ systems affected by pathogenic CNVs***

Understanding the pathogenesis of CNVs associated with neurodevelopmental disorders is contingent upon uncovering the convergent cellular pathways and molecular mechanisms linking individual genes, or combinations of genes within affected regions, to the developmental phenotypes observed in individuals with the mutation. As previously stated, patients with either the 3q29 deletion or 16p12.1 deletion oftentimes display a variety of symptoms in addition to ID, ASD, or schizophrenia, such as microcephaly, craniofacial defects, heart defects, and renal defects. Whether the affected genes in these regions are required for proper development of these organ and tissue systems in relation to disease pathology still remains unclear. However, many techniques exist in *X. laevis* to study brain, craniofacial, heart, and kidney development.

*X. laevis* neurodevelopment has been explored extensively using both *in vitro* and *in vivo* methods (Erdogan et al., 2016; Slater et al., 2017). For example, due to the large size of its embryonic neuronal growth cones, *X. laevis* is an excellent model to study cytoskeletal dynamics in axon outgrowth and guidance during early development (**Figure 1.6**). Moreover, live imaging can be done on both retinal and spinal axonal tracts *in vivo* (Erdogan et al., 2016; Slater et al., 2017). Additionally, changes in brain morphology can

be quantified simply by measuring the area of the forebrain, midbrain, and hindbrain (**Figure 1.5.B**), and this is also used as a technique to reflect the microcephaly phenotype (Mills et al., 2019; Singh et al., 2020; Willsey et al., 2018).

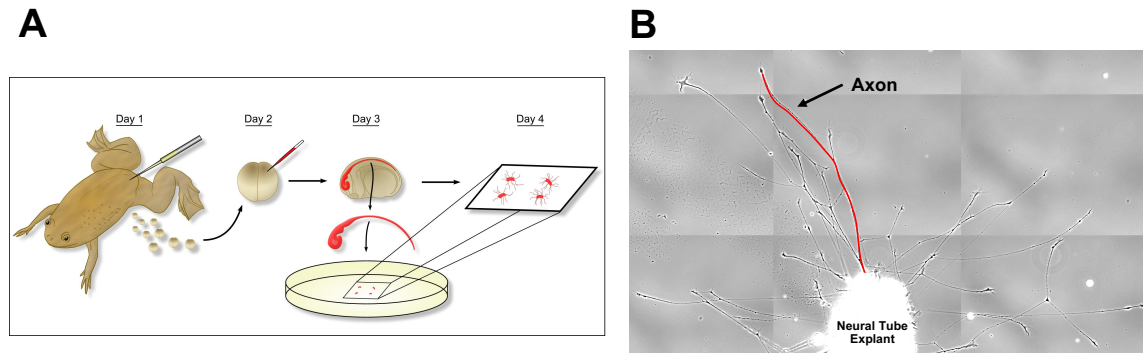


**Figure 1.6** *Xenopus laevis* neural tube dissection and axon outgrowth imaging

**(A)** (Day 1) Female frogs are injected with chorionic gonadotropin hormone (hCG) 12-18hr before egg collection. (Day 2) Eggs are collected and maintained in a salt solution and fertilized with minced testes. As development occurs *ex utero*, developmental stages can be tracked at room temperature and injection of genetic manipulation strategies can be performed at desired stages. (Day 3) Neural tube can be dissected at stage 20. Cultured explants can be kept at room temperature on bench overnight. **(B)** (Day 4) Explants can be imaged using various microscopy techniques to measure axon outgrowth parameters (length, velocity, directionality, and retraction rates) or cytoskeletal dynamics in the growth cone (adapted from Lowery et al., 2012).

Craniofacial abnormalities are a common phenotype that often accompany neurodevelopmental disorders, and *X. laevis* has emerged as an excellent system for determining whether CNV-affected genes are important for craniofacial morphogenesis. As orofacial development is highly conserved between *X. laevis* and other mammalian species, craniofacial abnormalities in *X. laevis* can resemble phenotypes present in human patients (Dickinson and Sive, 2007; Dickinson and Sive, 2006; Dubey and Saint-Jeannet, 2017; Mills et al., 2019; Tahir et al., 2014).

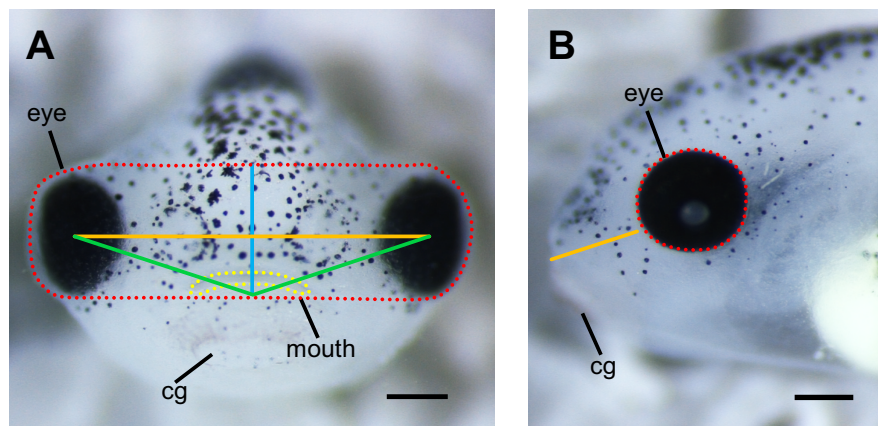


**Figure 1.7** Measurements of *X. laevis* craniofacial features

(A) Representative frontal view image of stage 42 *X. laevis* tadpole. Measurements of facial features include facial height (blue line), facial width (orange line), facial area (red dotted line), facial angle (green line), and mouth roundness (yellow dotted line). (B) Representative lateral view image of stage 42 *X. laevis* tadpole. Measurements of facial features include eye area (red dotted line) and snout length (orange line). All measurements can be performed using ImageJ. cg, cement gland. Scale bar: 100 $\mu$ m.

Various techniques to assess changes in *X. laevis* orofacial development have already been developed and used to study craniofacial defects associated with human genetic disorders. Measurements of craniofacial features such as facial width, height, angle, and area can be done on embryos at different developmental stages using ImageJ (Figure 1.7) (Dickinson, 2016; Kennedy and Dickinson, 2014a; Mills et al., 2019). These measurements can be combined with geometric morphometrics in order to detect subtle differences in face shape and size throughout development. Furthermore, techniques for visualizing cartilaginous tissue, such as Alcian blue staining, can be used to determine whether craniofacial abnormalities arise as a result of defects in cartilage development (Figure 1.8) (Devotta et al., 2016; Tahir et al., 2014).

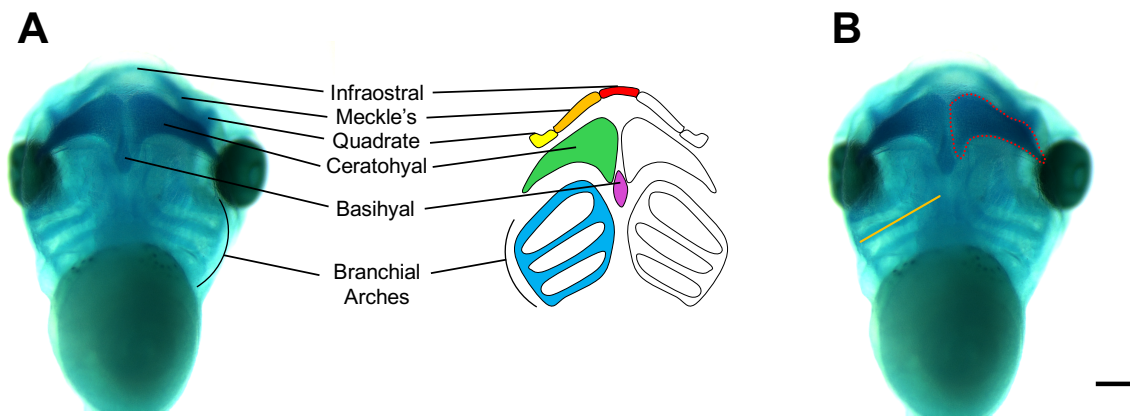


**Figure 1.8 Measurements of *X. laevis* cartilage elements**

(A) *Xenopus* cartilage anatomy with all major cartilage elements labeled in various colors. (B) Representative ventral view image of stage 42 *X. laevis* tadpole stained for Alcian blue. Measurements of cartilage elements include branchial arch length (orange line) and ceratohyal area (red dotted line), which can be performed using ImageJ. Scale bar: 300 $\mu$ m.

Another particularly promising avenue of research in regards to craniofacial morphogenesis is the investigation of the formation and migration of the neural crest cell (NCC) population in the developing embryo (Rutherford and Lowery, 2016). NCCs are a multipotent stem cell population that originate along the neural tube, delaminate, and migrate throughout the developing embryo to reach their final destinations. Once at their proper locations, NCCs differentiate and contribute to various tissues and organ systems, including craniofacial cartilage and bone, smooth muscle of the heart, peripheral and enteric neurons, melanocytes, and glia (Bronner and LeDouarin, 2012). Considering craniofacial defects are often observed in patients with the 3q29 and 16p12.1 deletions, it is possible that aberrations during NCC developmental processes may be the cellular mechanism underlying the craniofacial phenotypes.

*X. laevis* serves as an ideal model organism for studying processes during NCC development, as both *in vivo* and *in vitro* NCC specification, proliferation, and migration can be tracked through multiple methods. NCC migration can be observed *in vivo* by performing transplantation assays, whereby NCCs are dissected from GFP-injected *X.*

*laevis* embryos and transplanted to wild-type host embryos (Cousin, 2018). These embryos can then be imaged using time-lapse confocal microscopy, and NCC migration can be analyzed by measuring the number, width, and migration distance of the GFP-marked cranial segments. *In vivo* NCC specification and migration can also be analyzed through whole-mount *in situ* hybridization by observing the expression patterns of NCC specification markers, such as *twist* or *sox9* (Figure 1.9) (Corsinovi et al., 2019; Devotta et al., 2016; Mills et al., 2019; Szabo et al., 2016).

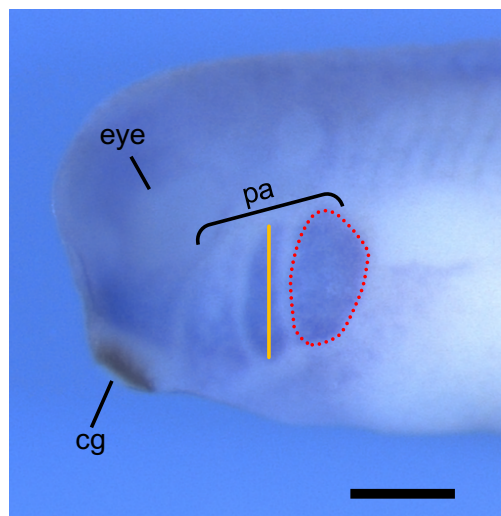


**Figure 1.9 Analysis of *in vivo* NCC migration using whole-mount *in situ* hybridization**

Representative image of stage 28 *X. laevis* embryo labeled for *twist*, a transcription factor that is critical for NCC specification and enriched in the pharyngeal arches. Measurements of the length (orange line) and area (red dotted line) of each individual pharyngeal arch can be done using ImageJ. cg, cement gland; pa, pharyngeal arch. Scale bar: 500 $\mu$ m.

NCC motility can be examined *in vitro* by dissecting NCCs from stage 16 *X. laevis* embryos and culturing explants on fibronectin-coated coverslips (Cousin and Alfandari, 2018). Migratory behavior of NCC explants can be observed using time-lapse confocal microscopy and multiple parameters of migration can be measured including velocity and dispersion (Cousin and Alfandari, 2018; DeSimone et al., 2005; Milet and Monsoro-Burq, 2014). Moreover, chemotaxis assays can be performed *in vitro* to assess

the directional migration of NCCs towards an external, soluble factor by coating beads with a chemoattractant cue, such as SDF-1 (Chow et al., 2019; Mayor and Theveneau, 2013; Szabo et al., 2016; Theveneau and Mayor, 2011). Altogether, these assays demonstrate how *X. laevis* can provide a unique and varied approach to study how alterations in NCC migratory behavior may contribute to phenotypes of neurodevelopmental disease.

Congenital heart defects (CHD) have emerged as the most life-threatening birth defect in newborn patients across different developmental disorders (Duncan and Khokha, 2016; Sojka et al., 2014). Early heart development is highly conserved between *X. laevis* and mammalian systems, and assays to analyze CHD candidate genes have been created for use in *X. laevis* (Deniz et al., 2017; Duncan and Khokha, 2016; Garfinkel and Khokha, 2017; Hempel and Kuhl, 2016; Sojka et al., 2014; Tandon et al., 2017). The effect of genetic manipulation on heart development can be explored at early tadpole stages using whole-mount *in situ* hybridization, immunohistochemistry with anti-tropomyosin (Tmy) antibody, scanning electron microscopy (SEM), transmission electron microscopy (TEM), or optical coherence tomography (OCT) (Deniz et al., 2017; Hempel and Kuhl, 2016; Sojka et al., 2014). These assays help to visualize and detect improperly-looped hearts, failed chamber formation, and abnormal structure of the adjacent connective tissue, and can be used to elucidate how mutations of CNV-affected genes lead to CHD (Duncan and Khokha, 2016; Sojka et al., 2014).

*In vitro* explant, transplant, and ablation techniques can be used to derive insight into how mutations of genes associated with renal disease affect the progression of kidney development in *X. laevis* (Getwan and Lienkamp, 2017). *In vivo* experiments of

kidney development range from optogenetic manipulations of physiological parameters (calcium, pH) to characterizations of electrophysiological recordings (Getwan and Lienkamp, 2017; Lienkamp, 2016). Together, *X. laevis* can be used as a powerful system to study how mutations of pathogenic CNV-associated genes affect the development of multiple tissue and organ systems.

### 1.3 Remaining questions

Although CNVs are prevalent in the normal healthy population, they are implicated in numerous neurodevelopmental diseases, as they encompass multiple genes of vital functions and disrupt gene dosage or large DNA segments (Deshpande and Weiss, 2018; Girirajan et al., 2011; Wilfert et al., 2017). However, the pathogenesis underlying syndromic CNVs and specific gene-to-phenotype associations have been challenging to determine. Moreover, we still lack a fundamental understanding of the basic biological functions and interactions between CNV-affected genes towards neurodevelopmental processes. Thus, studying such prominent genomic structural changes is central to our efforts in comprehending the genetic basis of heterogeneous developmental disorders such as ASD, intellectual disabilities, and schizophrenia.

To this aim, in collaboration with my colleagues in the Girirajan lab at Pennsylvania State University, I explore the functional basis of the phenotypic variability associated with the 3q29 and 16p12.1 deletions using both *Xenopus laevis* and *Drosophila melanogaster* model systems. This thesis starts with the functional characterization of genes within the 3q29 region (Chapter 2), followed by functional characterization of genes within the 16p12.1 region (Chapters 3 and 4), by examining the

molecular, cellular, and developmental phenotypes associated with decreased dosage of 3q29 and 16p12.1 gene homologs. Additionally, I investigate potential interactions between genes in these regions to determine the convergent cellular mechanisms that underly defects associated with these deletions. Finally, I conclude in Chapter 5 by summarizing how my thesis work has moved the field forward and discuss future directions. Together, this work aims to address the unexplored pathogenesis of the 3q29 and 16p12.1 deletions in order to gain a deeper understanding of the biological underpinnings of syndromic CNVs linked to neurodevelopmental disorders.

## CHAPTER 2

### ***NCBP2* modulates neurodevelopmental defects of the 3q29 deletion**

#### **in *Drosophila* and *Xenopus laevis* models**

The material in this chapter was adapted from:

**Dhruba Singh\***, M., Jensen, M\*., Lasser, M., Huber, E., Yusuff, T., Pizzo, L., Lifschutz, B., Desai, I., Kubina, A., Yennawar, S., Kim, S., Iyer, J., Rincon-Limas, D.E., Lowery, L.A., Girirajan, S. *NCBP2* modulates neurodevelopmental defects of the 3q29 deletion in *Drosophila* and *Xenopus laevis* models. *PLoS Genet*, 2020; 16(2):e1008590. doi: 10.1371/journal.pgen.1008590

\*authors contributed equally to work

## 2.1 Introduction

Rare copy number variants (CNVs), including deletions and duplications in the human genome, significantly contribute to complex neurodevelopmental disorders such as schizophrenia, intellectual disability/developmental delay, autism, and epilepsy (Girirajan et al., 2011; Malhotra and Sebat, 2012). Despite extensive phenotypic heterogeneity associated with recently described CNVs (Girirajan and Eichler, 2010a), certain rare CNVs have been linked to specific neuropsychiatric diagnoses. For example, the 22q11.2 deletion (DiGeorge/velocardiofacial syndrome), the most frequently occurring pathogenic CNV, is found in about 1–2% of individuals with schizophrenia (Karayiorgou et al., 1995; Karayiorgou et al., 2010), and animal models of several genes within the region show neuronal and behavioral phenotypes on their own (Fenelon et al., 2011; Mukai et al., 2015). Similarly, the 1.6 Mbp recurrent deletion on chromosome 3q29, encompassing 21 genes, was initially identified in individuals with a range of neurodevelopmental features, including intellectual disability, microcephaly, craniofacial features, and speech delay (Ballif et al., 2008; Mulle et al., 2010). Further studies have implicated this deletion as a major risk factor for multiple disorders (Glassford et al., 2016). In fact, the deletion confers a >40-fold increase in risk for schizophrenia (Kirov et al., 2012; Mulle, 2015), as well as a >20-fold increase in risk for autism (Pollak et al., 2020). More recently, two studies have reported decreases in body and brain sizes as well as a range of behavioral and social defects in mouse models of the entire deletion, mimicking the human developmental phenotypes associated with the deletion (Baba et al., 2019; Rutkowski et al., 2019).

Identifying the biological underpinnings of the 3q29 deletion is contingent upon uncovering the conserved molecular mechanisms linking individual genes or combinations of genes within the 3q29 region to the neurodevelopmental phenotypes observed in individuals with the entire deletion. Recent studies have suggested a subset of genes in the 3q29 region as potential candidates for these phenotypes based on their established roles in neuronal development (Quintero-Rivera et al., 2010; Rutkowski et al., 2017). For example, *DLGI* is a scaffolding protein that organizes the synaptic structure at neuromuscular junctions (Budnik et al., 1996), affecting both synaptic density and plasticity during development (Walch, 2013). However, mouse models of *Dlgl*<sup>+/-</sup> did not recapitulate the behavioral and developmental phenotypes observed in mice with the entire deletion (Rutkowski et al., 2019), suggesting that haploinsufficiency of *DLGI* by itself does not account for the wide range of phenotypes associated with the deletion. Given that genes within rare pathogenic CNV regions tend to share similar biological functions (Andrews et al., 2015b) and interact with each other to contribute towards developmental phenotypes (Iyer et al., 2018; Jensen and Girirajan, 2019), it is likely that multiple genes within 3q29 jointly contribute to these phenotypes through shared cellular pathways. Therefore, an approach that integrates functional analysis of individual genes within the 3q29 deletion and their combinatorial effects on neuronal and cellular phenotypes is necessary to understand the pathways and mechanisms underlying the deletion.

Systematic testing of genes within 3q29 towards developmental and cellular phenotypes requires model systems that are amenable for rapid phenotypic evaluation and allow for testing interactions between multiple dosage-imbalanced genes without

affecting the viability of the organism. *Drosophila melanogaster* and *Xenopus laevis* provide such powerful genetic models for studying conserved mechanisms that are altered in neurodevelopmental disorders, with the ability to manipulate gene expression in a tissue-specific manner in *Drosophila* (Wangler et al., 2015) and examine developmental defects in *X. laevis* (Pratt and Khakhalin, 2013). Both model systems contain homologs for a majority of disease-causing genes in humans, and show a high degree of conservation in key developmental pathways (Gatto and Broadie, 2011; Harland and Grainger, 2011; Reiter et al., 2001; Wangler et al., 2015). For example, *Drosophila* knockdown models of the candidate schizophrenia gene *DTNBPI* showed dysregulation of synaptic homeostasis and altered glutamatergic and dopaminergic neuron function (Dickman and Davis, 2009; Shao et al., 2011), and fly models for *UBE3A*, the gene associated with Angelman syndrome, showed sleep, memory and locomotor defects (Wu et al., 2008). Furthermore, *X. laevis* models have been widely used to identify morphological and neuronal defects associated with developmental disorders (Pratt and Khakhalin, 2013), such as dendritic connectivity defects with overexpression of *MECP2*, the causative gene for Rett syndrome (Marshak et al., 2012). Thus, *Drosophila* and *X. laevis* models of individual CNV homologs and their interactions would allow for a deeper dissection of the molecular mechanisms disrupted by the deletion, complementing the phenotypes documented in mouse models of the entire deletion (Baba et al., 2019; Rutkowski et al., 2019).

Here, I used a mechanistic approach to understand the role of individual homologs of 3q29 genes and their interactions towards the cellular processes underlying the deletion. First, my collaborators systematically characterized developmental, cellular,

and nervous system phenotypes for 14 conserved homologs of human 3q29 genes and 314 pairwise interactions using *Drosophila*, and I then validated these phenotypes using *X. laevis*. Together, we found that multiple homologs of genes within the 3q29 region, including *NCBP2*, *DLG1*, *FBXO45*, *PIGZ*, and *BDH1*, contribute to disruptions in apoptosis and cell cycle pathways, leading to neuronal and developmental defects in both model systems. These defects were further enhanced when each of the homologs were concomitantly knocked down with homologs of *NCBP2* in *Drosophila* (*Cbp20*) and *X. laevis* (*ncbp2*), resulting in increased apoptosis and dysregulation of cell cycle genes. Our results support an oligogenic model for the 3q29 deletion, and implicate specific cellular mechanisms disrupted by genes in the deletion region.

## 2.2 Results

### 2.2.1. Reduced expression of individual homologs of 3q29 genes causes global developmental defects in *Drosophila*

My collaborators first used reciprocal BLAST and orthology prediction tools to identify fly homologs for 15 of the 21 genes within the 3q29 deletion region (**Fig 2.1**), and found that the biological functions of these 15 genes were highly conserved (~88.4%) between *Drosophila* and humans. For example, *dlg1* (*DLG1*) and *Cbp20* (*NCBP2*) share the same roles in both flies and vertebrates, as a scaffolding protein at the synaptic junction (Muller et al., 1995) and a member of the RNA cap binding complex (Sabin et al., 2009), respectively. I note that the genes and crosses tested in this study are represented as fly gene names along with the human counterparts at first mention in the text, i.e. *Cbp20* (*NCBP2*), and fly genes with allele names in the figures, i.e. *Cbp20*<sup>KK109448</sup>. RNA interference (RNAi) and the *UAS-GAL4* system was used to

knockdown expression levels of fly homologs of genes within the 3q29 region ubiquitously and in neuronal, wing and eye tissues (**Fig 2.1**), and quantitative PCR (qPCR) confirmed partial knockdown of gene expression for each of the tested homologs.

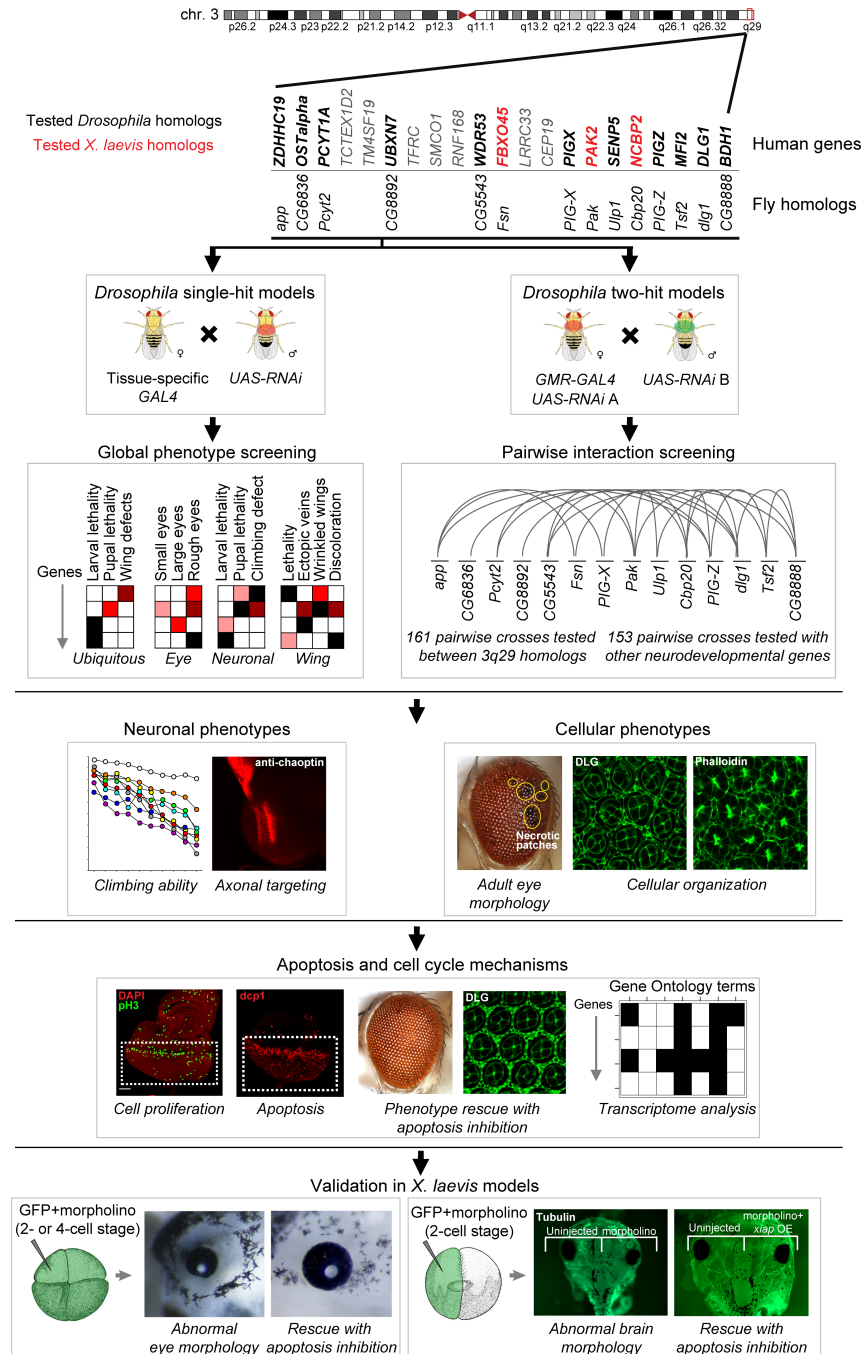


**Figure 2.1 Strategy for identifying cellular phenotypes and genetic interactions of 3q29 gene homologs**

First, individual or pairs of 14 *Drosophila* homologs in the 3q29 region were knocked down using tissue-specific RNAi. After screening for global phenotypes for individual 3q29 homologs, 314 pairwise gene interactions were tested using the fly eye. Deeper cellular and neuronal phenotypes of individual and pairwise 3q29 gene knockdowns were assayed in flies and disruptions in apoptosis and cell cycle mechanisms were observed. To further validate the conserved cellular functions of these genes towards disease pathogenesis, we tested three 3q29 gene homologs in *X. laevis*. We used morpholinos (MOs) to reduce expression of these genes and observed similar developmental defects as seen in *Drosophila*, such as abnormal brain morphology, eye morphology, and increased apoptosis.

To identify genes essential for organism survival and neurodevelopment, my collaborators first assessed the effect of ubiquitous knockdown of homologs of 3q29 genes (**Fig 2.2.A**). Seven of the 14 homologs, including *dlg1*, *Cbp20*, and *Tsf2* (*MFI2*), showed lethality and severe developmental and wing defects with ubiquitous knockdown or wing-specific knockdown, suggesting that multiple homologs of 3q29 genes are essential for viability during early development.

Several fly homologs for genes within the 3q29 region have previously been associated with a range of neuronal defects during fly development. For example, loss of *dlg1* contributed to morphological and physiological defects at the neuromuscular junction (NMJ), as well as increased brain size, abnormal courtship behavior, and loss of gravitaxis response (Armstrong et al., 2006; Mendoza-Topaz et al., 2008; Thomas et al., 1997). Similarly, *Pak* mutant flies exhibited extensive defects in the axonal targeting of sensory and motor neurons (Hing et al., 1999; Kim et al., 2003), in addition to abnormal NMJ and mushroom body development (Ng and Luo, 2004; Parnas et al., 2001). Thus, to determine whether fly homologs for other genes in the 3q29 region also contribute to defects in neuronal function, climbing assays to assess motor defects and staining of larval brains for axonal targeting with pan-neuronal knockdown of fly homologs were performed. Interestingly, pan-neuronal knockdown caused larval or pupal lethality in *dlg1*, *Tsf2*, and *CG5543* (*WDR53*) flies (**Fig 2.2.A**), and about 30% of adult flies with knockdown of *dlg1* did not survive beyond day 5, indicating an essential role for these

genes in neuronal development. Furthermore, flies with pan-neuronal knockdown of several 3q29 homologs, including *dlg1* and *Cbp20*, exhibited a strong reduction in climbing ability over ten days (**Fig 2.2.B**), suggesting that these genes could contribute to abnormalities in synaptic and motor functions.

Next, the axonal projections of photoreceptor cells into the optic lobe were examined by staining third instar larval brains with anti-chaoptin. Eye-specific knockdown of *Cbp20*, *dlg1*, *Pak* and *Fsn* (*FBXO45*) showed several axonal targeting defects (**Fig 2.2.C**). Specifically, these defects were similar to targeting defects observed in models of other candidate neurodevelopmental genes, including *Drosophila* homologs for human *DISC1* and *FMRI* (Chen et al., 2011; Morales et al., 2002). Overall, my collaborators' data shows that multiple conserved homologs of genes in the 3q29 region beyond just *dlg1* or *Pak* are important for *Drosophila* neurodevelopment.

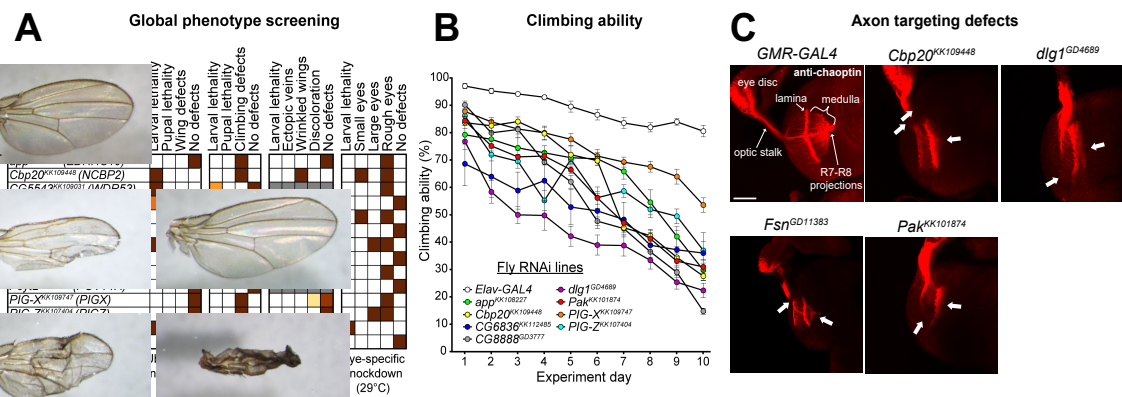


**Figure 2.2 Neurodevelopmental defects in flies with knockdown of individual homologs of 3q29 genes**

(A) Percentage of flies with tissue-specific RNAi knockdown of 3q29 gene homologs (listed with their human counterparts) that manifest lethality or developmental phenotypes. (B) Eight 3q29 gene homologs with pan-neuronal RNAi knockdown showed defects in climbing ability over ten days. Data represented show mean  $\pm$  standard deviation of 10 independent groups of 10 flies for each homolog. (C) Representative confocal images of larval eye discs stained with anti-chaoptin illustrate defects in axon targeting (white arrows) from the retina to the optic lobes of the brain upon eye-specific knockdown of 3q29 gene homologs. n = 8-20 larval eye discs; Scale bar = 30 $\mu$ m.

## 2.2.2. Reduced expression of individual homologs of 3q29 genes causes brain size

### defects in *Xenopus laevis*

After identifying a wide range of neurodevelopmental defects due to knockdown of fly homologs of 3q29 genes, I sought to gain further insight into the conserved functions of these genes in vertebrate embryonic brain development using *Xenopus laevis* as a model system. I examined the effect of targeted knockdown of *ncbp2*, *fbxo45*, and *pak2*, as homologs of these genes displayed multiple severe phenotypes with reduced gene expression in flies. Knockdown of *X. laevis* homologs for each 3q29 gene was accomplished using antisense morpholino oligonucleotides (MOs) targeted to early splice sites of each homolog (Fig 2.1). *X. laevis* embryos were injected unilaterally at either the two- or four-cell stage with various concentrations of MO for each homolog or a standard control, and knockdown of each homolog was validated using qPCR (Fig 2.3.A-B).

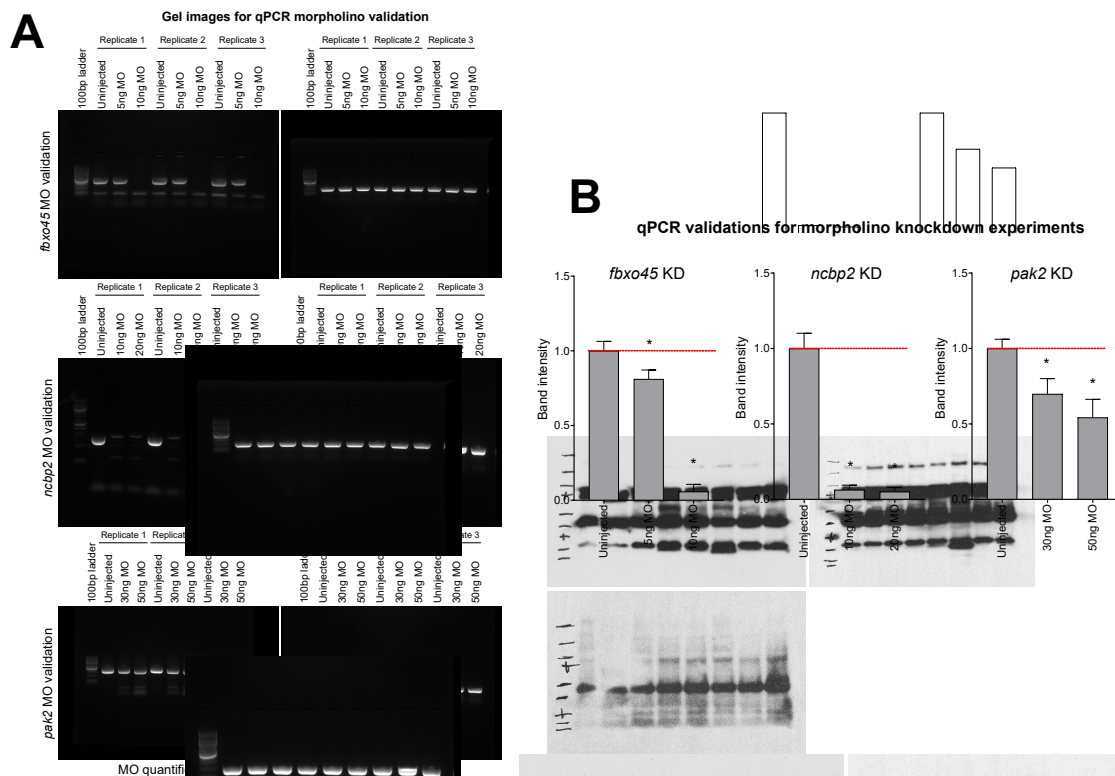


**Figure 2.3 Quantification of 3q29 morpholino knockdown levels in *X. laevis***

(A) Electrophoretic gels show decreased expression of 3q29 gene homologs due to morpholino (MO) knockdown at various concentrations in *X. laevis* embryos. Three replicates (uninjected and two MO concentrations) were performed for each MO, and band intensities were compared with expression of *ODC1* controls taken from the same cDNA samples and run on gels processed in parallel. (B) Quantification of

expression for 3q29 gene homologs at different MO concentrations, as measured by band intensity ratio to *ODC1* controls.

As knockdown of *Cbp20*, *Fsn*, and *Pak* each resulted in neuronal defects in *Drosophila*, I examined the effects of knockdown of these homologs on *X. laevis* brain development at stage 47. To test this, I knocked down each gene in one hemisphere of the embryo at the two-cell stage, and left the other hemisphere uninjected to create a side-by-side comparison of brain size (**Fig 2.4.A**). I performed whole-mount immunostaining with anti-alpha tubulin and found that reduced expression of *ncbp2*, *fbxo45*, or *pak2* each resulted in smaller forebrain and midbrain size compared with controls (**Fig 2.4.B**). Interestingly, the reduced brain volumes that I observed with knockdown of homologs of 3q29 genes in *X. laevis* recapitulate the reduced brain volume observed in 3q29 deletion mice (Baba et al., 2019; Rutkowski et al., 2019), suggesting that multiple genes in the 3q29 region contribute to this phenotype. Together, our results support a conserved developmental role for *NCBP2*, *FBXO45*, and *PAK2* in both an invertebrate and vertebrate model system, and that they are critical for various processes during neurodevelopment.

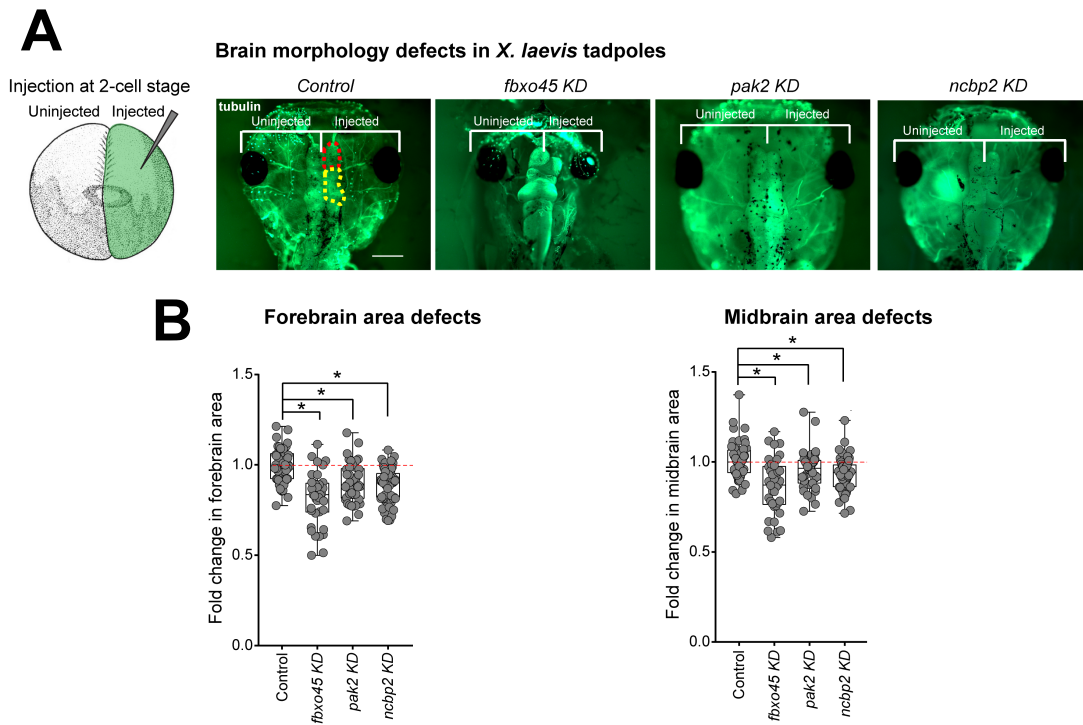


**Figure 2.4 Brain size phenotypes observed with knockdown of 3q29 gene homologs in *X. laevis***

(A) To study brain morphology upon knockdown of *X. laevis* 3q29 gene homologs, one cell in a two-cell embryo was injected with 3q29 gene-specific MO while the other cell remained uninjected. Representative images of stage 47 tadpoles with MO knockdown of *ncbp2*, *fbxo45*, and *pak2* show brain morphological defects and decreased size, including decreased forebrain (highlighted in red on control image) and midbrain (highlighted in yellow on control image) area. (B) Box plot of forebrain area and midbrain area shows that knockdown of *fbxo45*, *pak2*, and *ncbp2* all reduce brain size of these lobes compared to controls.  $n = 30-63$ ;  $*p < 0.05$ , two-tailed Welch's T-test; Scale bar =  $500\mu\text{m}$ .

### 2.2.3. *Drosophila* and *Xenopus* eye models for genes within the 3q29 region show

#### cellular and developmental defects

The study of *Drosophila* and *X. laevis* eye development has been classically used to perform high-throughput genetic screens and quantitative assays of cellular and neurodevelopmental defects (Ritter et al., 2020; Shin et al., 2019; Thomas and Wassarman, 1999). For instance, the *Drosophila* eye model was recently used to screen a large set of intellectual disability genes (Oortveld et al., 2013), and *Xenopus* eye development has been used to study ocular lens disease, neurodevelopmental diseases, and retinal ganglion cell axon outgrowth (Flach et al., 2018; Rahman et al., 2020; Viet et al., 2020). Thus, we used the developing fly and *Xenopus* eyes as *in vivo* systems to

quantify the effect of gene knockdown on various aspects of eye development in both model systems (**Fig 2.1**).

First, eye-specific RNAi knockdown of fly homologs of genes in the 3q29 region was performed, and the rough eye phenotype of each knockdown line was measured using *Flynotyper*, a quantitative tool that calculates a phenotypic score based on defects in ommatidial arrangement (Iyer et al., 2016). Eye-specific knockdown of 8/13 homologs of 3q29 genes showed significant external eye phenotypes compared with control flies (**Fig 2.5.A**). To examine the cellular mechanisms underlying the rough eye phenotypes observed with knockdown of fly homologs of 3q29 genes, changes in area and ommatidial size of the adult eyes were measured. Knockdown of *CG8888* and *Cbp20* caused a significant reduction in eye size, while the eyes of flies with knockdown of *dlg1* were significantly larger than controls (**Fig 2.5.B**). Similarly, decreases in ommatidial diameter with knockdown of *Cbp20* and *CG8888* were observed, suggesting that these genes may also contribute to abnormal cell growth phenotypes (**Fig 2.5.C**)

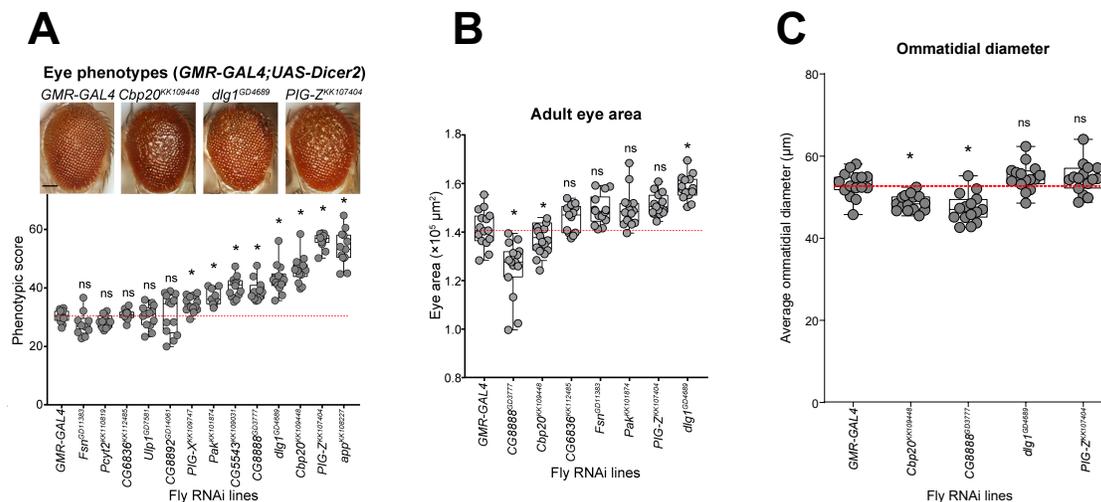


**Figure 2.5** Eye phenotypes for flies with eye-specific knockdown of individual 3q29 gene homologs

(**A**) Representative brightfield adult eye images of flies with eye-specific RNAi knockdown of individual 3q29 gene homologs show rough eye phenotypes. The boxplot shows *Flynotyper*-derived phenotypic scores ( $n = 10-14$ ; \* $p < 0.05$ , one-tailed Mann-Whitney test). (**B**) Boxplot of adult eye area in flies with RNAi

knockdown of 3q29 gene homologs (n = 13-16; \*p < 0.05, two-tailed Mann-Whitney test). (C) Boxplot of average ommatidial diameter in flies with knockdown of select 3q29 gene homologs (n = 15; \*p < 0.05, two-tailed Mann-Whitney test).

I further examined the effect of knocking down 3q29 homologs of *ncbp2*, *fbxo45*, and *pak2* on *X. laevis* eye development at stage 42, and found that knockdown of these genes caused irregular shapes and decreased eye size compared with controls (Fig 2.6.A and Fig 2.6.C). The reductions in eye size were rescued to control levels when mRNA was co-injected along with a MO for each homolog, indicating that these phenotypes are specific to depletion of each individual gene (Fig 2.6.B and Fig 2.6.D). Together, these data show that individual knockdown of homologs of 3q29 genes in *X. laevis* leads to both abnormal brain and eye morphology, confirming the conserved role of these genes during vertebrate development.

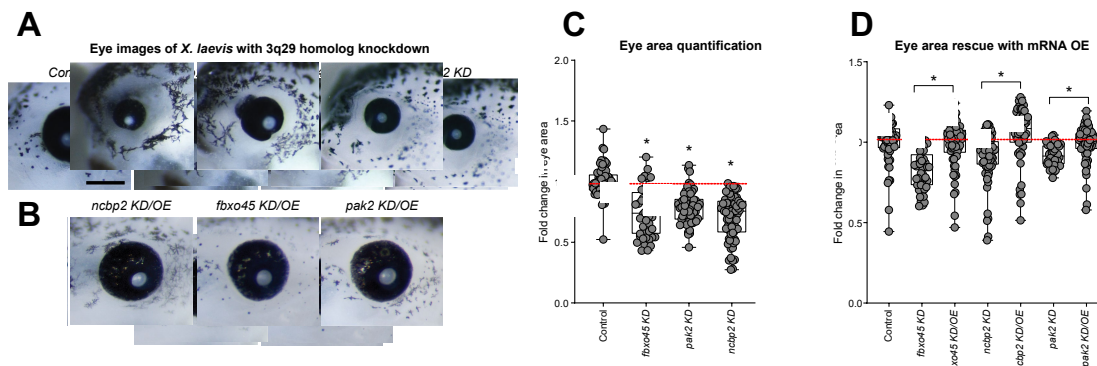


**Figure 2.6** Eye phenotypes observed with knockdown of 3q29 gene homologs in *X. laevis*

(A-B) Representative lateral view eye images of stage 42 *X. laevis* tadpoles with MO knockdown of individual 3q29 gene homologs show defects in eye size and morphology compared to the control (top). These defects were rescued with co-injection and overexpression of mRNA for each 3q29 gene homolog, respectively (bottom) (Scale bar = 500 $\mu$ m). (C) Boxplots of eye area with knockdown of individual 3q29 gene homologs, normalized to controls (n = 48-71; \*p < 0.05, two-tailed Welch's t-test). (D) Boxplot of eye area with knockdown and overexpression of mRNA of individual 3q29 gene homologs, normalized to controls (n = 56-63; \*p < 0.05, two-tailed Welch's t-test). All boxplots indicate mean (center line), 25<sup>th</sup> and 75<sup>th</sup> percentiles (bounds of box), and minimum and maximum (whiskers), with red dotted lines representing the control median.

#### 2.2.4. Interactions between fly and *Xenopus* homologs of 3q29 genes enhance neuronal phenotypes

As knockdown fly and *Xenopus* models for homologs of multiple 3q29 genes showed a variety of neuronal, developmental, and cellular defects, we hypothesized that these genes could interact with each other to further disrupt cellular processes during development. To test this, recombined lines for nine fly homologs of 3q29 genes were generated, and these lines were crossed with multiple RNAi or mutant lines for other homologs to generate 161 two-hit crosses for testing 94 pairwise gene interactions (**Fig 2.1**). In *Xenopus*, pairwise knockdown of 3q29 gene homologs was achieved by co-injecting multiple gene-specific MOs simultaneously (**Fig 2.1**).

Interestingly, a significant enhancement in fly eye phenotypic severity was observed, measured using *Flynotyper*, for 19 out of 21 pairwise interactions involving *Cbp20* as either a first or second-hit gene, suggesting that reduced expression of *Cbp20* drastically modifies the morphological phenotypes of other homologs of 3q29 genes (**Fig 2.7.A-B**). Moreover, simultaneous knockdown of *Cbp20* with either *dlg1* or *Fsn* led to an increase in severity of axon targeting defects (**Fig 2.7.C**). Overall, these data show that *Cbp20* interacts with other homologs of genes in the 3q29 region to enhance the observed cellular and neuronal defects in *Drosophila* (**Table 1**).

As simultaneous depletion of *Cbp20* with other 3q29 gene homologs resulted in a significant enhancement of both eye and neuronal defects in flies, I wondered whether these genetic interactions would lead to an enhancement of neurodevelopmental phenotypes in a vertebrate model system. Thus, I examined the effects of simultaneous knockdown of *ncbp2* with either *fbxo45* or *pak2* on *Xenopus laevis* brain development. I

found that simultaneous knockdown of *ncbp2* with *fbxo45* caused a significant decrease in forebrain size and a trend towards decreased midbrain size ( $p = 0.093$ ) compared with *ncbp2* knockdown alone (Fig 2.7.D-E). I also observed that knockdown of *pak2* with *ncbp2* showed a similar trend towards decreased forebrain size ( $p = 0.051$ ). Together, these data show that pairwise knockdown of *ncbp2* with several homologs of 3q29 genes in *X. laevis* leads to an enhancement of abnormal brain size, confirming the conserved role of this genetic interaction towards neurodevelopment between an invertebrate and vertebrate model system.

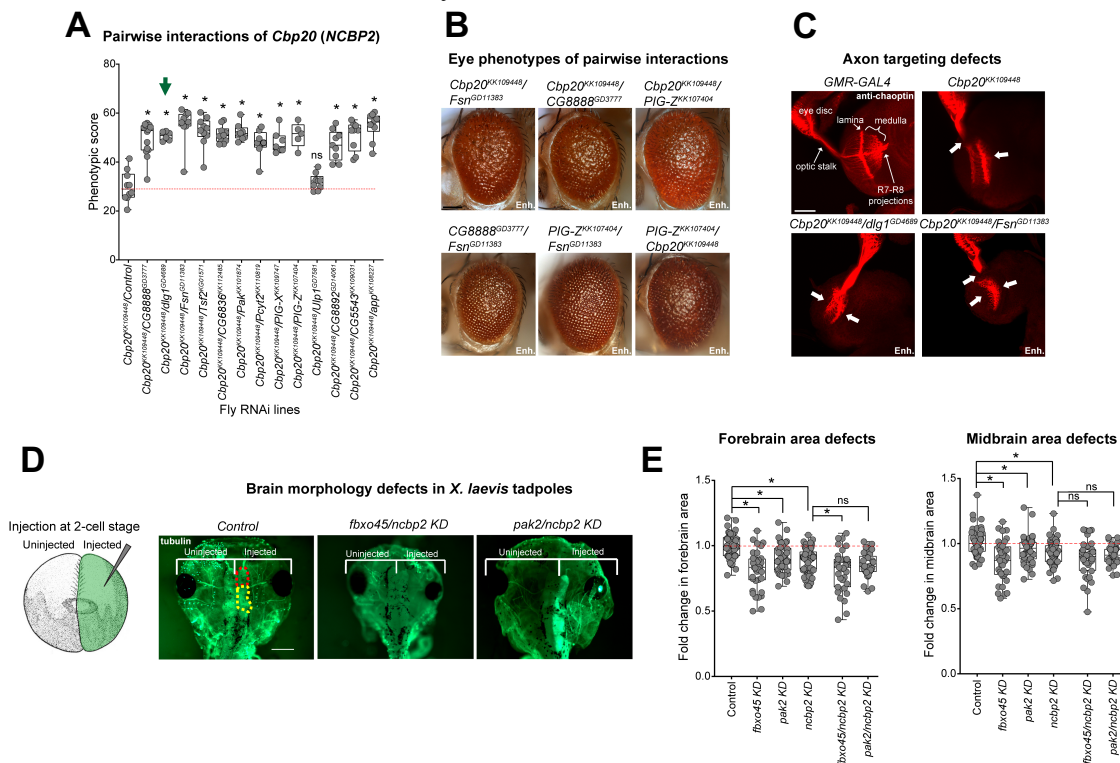


**Figure 2.7** Pairwise interactions of fly and *Xenopus* 3q29 gene homologs

(A) Boxplot of phenotypic scores for pairwise RNAi knockdown of *Cbp20* with other fly homologs of 3q29 genes in the adult eye, compared with recombined lines for individual 3q29 gene homologs crossed with controls. Green arrow indicates an example pair of reciprocal lines showing enhanced phenotypes compared with their respective single-hit recombined controls ( $n = 5-14$ ;  $*p < 0.05$ , two-tailed Mann-Whitney test). (B) Representative brightfield adult eye images of flies with pairwise knockdown of 3q29 gene homologs show enhancement of rough eye phenotypes compared with recombined lines for individual homologs of 3q29 genes cross with controls (Scale bar =  $100\mu\text{m}$ ). (C) Representative confocal images of larval eye discs stained with anti-chaoptin illustrate enhanced defects in axon targeting (white arrows) from the retina to the optic lobes of the brain with eye-specific knockdown of *Cbp20/dlg1* and *Cbp20/Fsn* compared with *Cbp20* knockdown ( $n = 9-17$ ; Scale bar =  $30\mu\text{m}$ ). (D) Representative dorsal view images of stage 47 *X. laevis* tadpoles with pairwise MO knockdown of *ncbp2* with either *fbxo45* or *pak2* show enhanced morphological

defects and decreased brain size, including decreased forebrain and midbrain (Scale bar = 500 $\mu$ m). **(E)** Boxplots of forebrain area and midbrain area with knockdown of 3q29 gene homologs, normalized to controls (n = 30-63; \*p < 0.05, two-tailed Welch's t-test).

Finally, to further characterize the functional effects of interactions between homologs of 3q29 genes, my collaborators analyzed changes in gene expression by performing RNA-sequencing of heads from flies with select pan-neuronal knockdown of individual (*Cbp20*, *dlg1*, *Fsn*, and *Pak*) and pairs (*Cbp20/dlg1* and *Cbp20/Fsn*) of homologs of 3q29 genes. Flies with knockdown of *dlg1* and *Cbp20* showed enrichment for dysregulation of homologs for human synaptic transmission genes, such as *Glt* (*NLGN1*) and *nAChR $\beta$ 3* (*HTR3A*) (**Fig 2.8.A**). While dysregulated genes in *Cbp20/dlg1* knockdown flies showed enrichments for protein folding and sensory perception, *Cbp20/Fsn* knockdown flies were uniquely enriched for dysregulated homologs of cell cycle genes, including *Aura* (*AURKA*), *Cdk1* (*CDK1*), *lok* (*CHEK2*), and *CycE* (*CCNE1*) (**Fig 2.8.B**). Similarly, 17 differentially-expressed homologs corresponding to human apoptosis genes were observed in *Cbp20/Fsn* knockdown flies, including the DNA fragmentation gene *Sid* (*ENDOG*) and the apoptosis signaling genes *tor* (*RET*) and *Hsp70Bb* (*HSPA1A*) (**Fig 2.8.B**). Together, these data suggest that *Cbp20* interacts with other homologs of genes in the 3q29 region to disrupt a variety of key biological functions, including apoptosis and cell cycle pathways as well as synaptic transmission and metabolic pathways (**Table 1**).

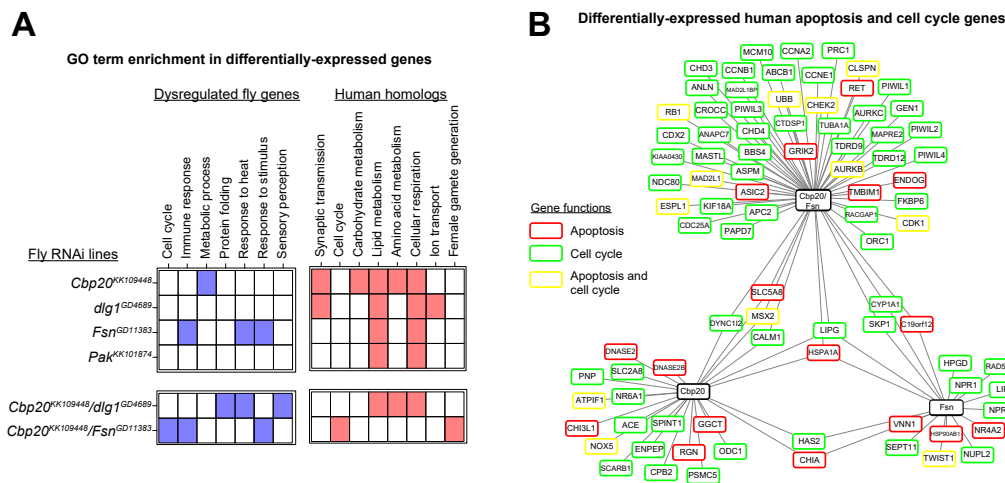


**Figure 2.8** Transcriptome analysis of flies with knockdown of select 3q29 gene homologs

(A) Clusters of Gene Ontology terms enriched among differentially-expressed fly genes (blue) and their corresponding human homologs (red) with individual and pairwise RNAi knockdown of fly 3q29 gene homologs. (B) Diagram showing human cell cycle and apoptosis genes whose fly homologs are differentially expressed with knockdown of *Cbp20* and *Fsn*, as well as concomitant knockdown of *Cbp20/Fsn*. Red boxed indicate apoptosis genes, green boxes indicate cell cycle genes, and yellow boxes indicate genes associated with both functions.

### 2.2.5. Interactions between *Cbp20* in flies and *ncbp2* in *Xenopus* with other homologs of 3q29 genes enhance apoptosis defects

Cell death and proliferation are two antagonistic forces that maintain an appropriate number of neurons during development (Yamaguchi and Miura, 2015). In fact, both processes have been previously identified as candidate mechanisms for several neurodevelopmental disorders (Ernst, 2016; Glantz et al., 2006; Pinto et al., 2010). While knockdown of *Cbp20/ncbp2* with other homologs of 3q29 genes likely disrupts multiple cellular processes that contribute towards the enhanced cellular defects, we next specifically investigated the role of apoptosis towards these defects in both flies and *Xenopus*, as our RNA-sequencing data showed a strong association between knockdown of *Cbp20* and increases in apoptosis pathways.

To test this in flies, black necrotic patches on the ommatidia in adult eyes were observed with knockdown of *Cbp20/dlg1* and *Cbp20/Fsn*, indicating that an increase in cell death occurs with these interactions (Fig 2.9.A). Concomitant knockdown

of *Cbp20* with *dlg1*, *Fsn* or *CG8888* also enhanced disruption of ommatidial cell organization and loss of photoreceptors in pupal flies, emphasizing the role of these genes in maintaining cell count and organization (**Fig 2.9.B-C**). Furthermore, a significant increase in the number of apoptotic cells in larval eye discs of flies was observed, as measured by *dcp1* staining (**Fig 2.9.D-E**) when *Cbp20* was knocked down along with *CG8888*, *dlg1*, or *Fsn*.

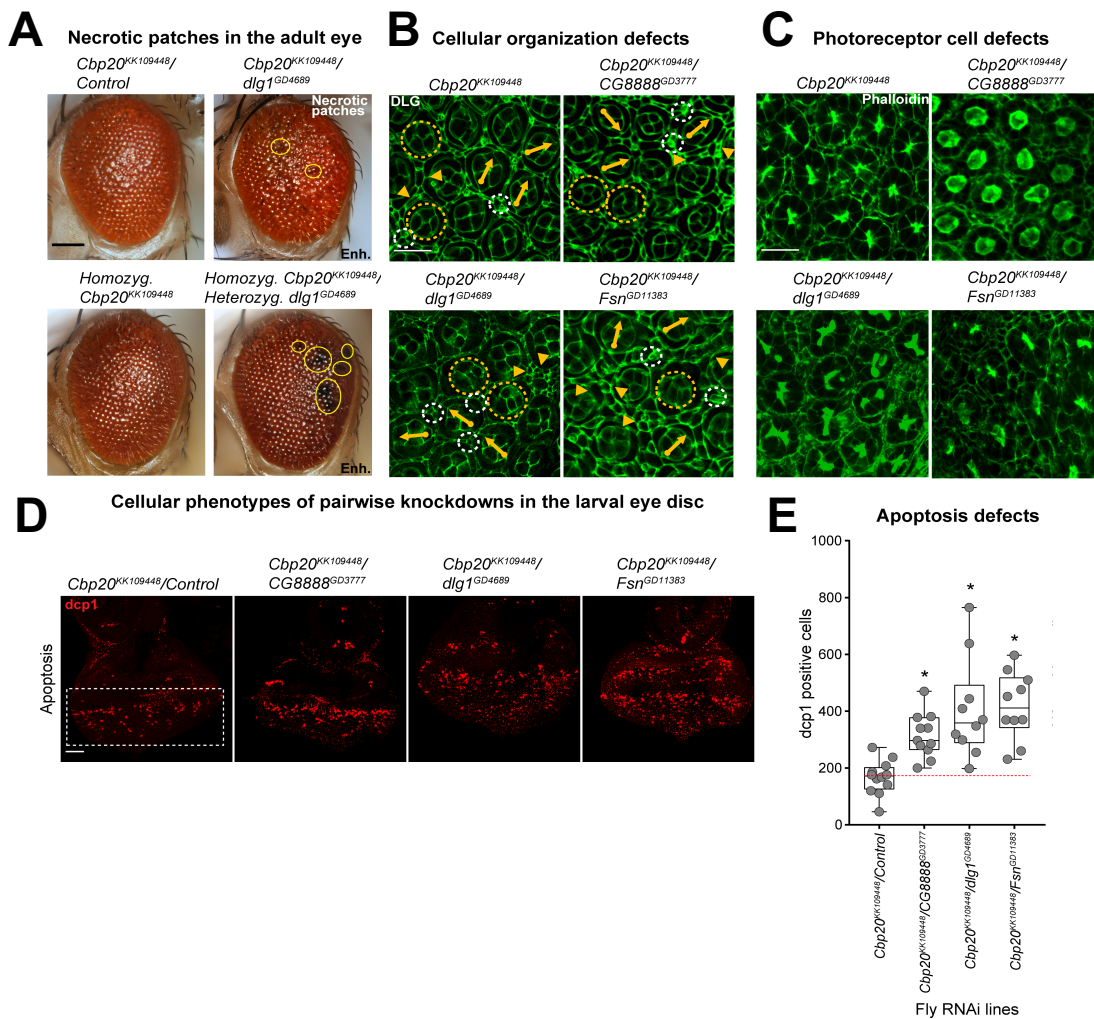


**Figure 2.9 Cellular phenotypes with pairwise knockdown of fly 3q29 gene homologs**

(A) Representative brightfield adult eye images show that heterozygous RNAi knockdown of *dlg1* enhanced the rough eye phenotype and necrotic patches (yellow circles) of flies heterozygous or homozygous for *Cbp20* RNAi (Scale bar = 100 $\mu$ m). (B) Representative confocal images of pupal eyes stained with anti-DLG illustrate enhanced defects in ommatidial organization upon simultaneous knockdown of *Cbp20* with other 3q29 fly homologs compared with *Cbp20* knockdown alone. Yellow circles in DLG images indicate cone cell defects, white circles indicate bristle cell defects, yellow arrows indicate rotation defects, and yellow arrowheads indicate secondary cell defects (Scale bar = 5 $\mu$ m). (C) Representative confocal images of pupal

eyes stained with Phalloidin illustrate enhanced defects in photoreceptor cell count and organization upon simultaneous knockdown of *Cpb20* and other fly 3q29 homologs compared with *Cbp20* knockdown alone (Scale bar = 5 $\mu$ m). **(D)** Representative confocal images of larval eye discs stained with anti-dcp1 show enhanced defects in apoptosis with pairwise knockdown of *Cbp20* and other fly 3q29 homologs compared with recombined *Cbp20* knockdown crossed with controls (Scale bar = 30 $\mu$ m). **(E)** Boxplot of dcp1-positive cells in the larval eye discs of flies with pairwise knockdown of 3q29 gene homologs (n = 10-11; \*p < 0.05, two-tailed Mann-Whitney t-test).

To validate apoptosis as a candidate mechanism for the cellular defects of flies with knockdown of homologs of 3q29 genes, recombined fly lines for *Cbp20* and *dlg1* were crossed with flies overexpressing *Diap1* (death-associated inhibitor of apoptosis). Overexpression of *Diap1* rescued the adult rough eye phenotypes (**Fig 2.10.A**) and led to significant reductions in the number of dcp1-positive cells in the larval eye discs of flies with knockdown of *Cbp20* and *dlg1*, confirming the rescue of apoptosis defects in these flies (**Fig 2.10.B**). Together, these results suggest that apoptosis mediates the cellular defects observed in flies with knockdown of *Cbp20* and *dlg1*.

To determine if the knockdown of homologs of 3q29 genes also disrupted apoptotic processes in *X. laevis*, I tested whether overexpression of the X-linked inhibitor of apoptosis gene (*xiap*) could rescue the observed eye and brain developmental defects. I found that overexpression of *xiap* rescued the midbrain and forebrain size deficits observed with *ncbp2* knockdown to control levels (**Fig 2.10.C**). Similarly, I found that the decreased eye sizes and morphological defects observed with knockdown of *ncbp2* were rescued with *xiap* overexpression (data not shown). To further validate these findings, I performed a Western blot following knockdown of *fbxo45* and *ncbp2* using anti-cleaved caspase-3 (Asp175) as a marker for apoptosis (**Fig 2.10.D**). I found that reduction of *fbxo45* and *ncbp2* expression each led to an increase in cleaved caspase-3 levels compared with controls, which were restored to control levels with concomitant overexpression of *xiap* (**Fig 2.10.D**). Caspase-3 levels

were also enhanced when *fbxo45* and *ncbp2* were knocked down together, suggesting that these two homologs interact with each other and contribute towards developmental phenotypes through increased apoptosis. Overall, these results suggest involvement of apoptotic processes towards the developmental phenotypes observed with knockdown of homologs of 3q29 genes in a vertebrate model (Table 1).

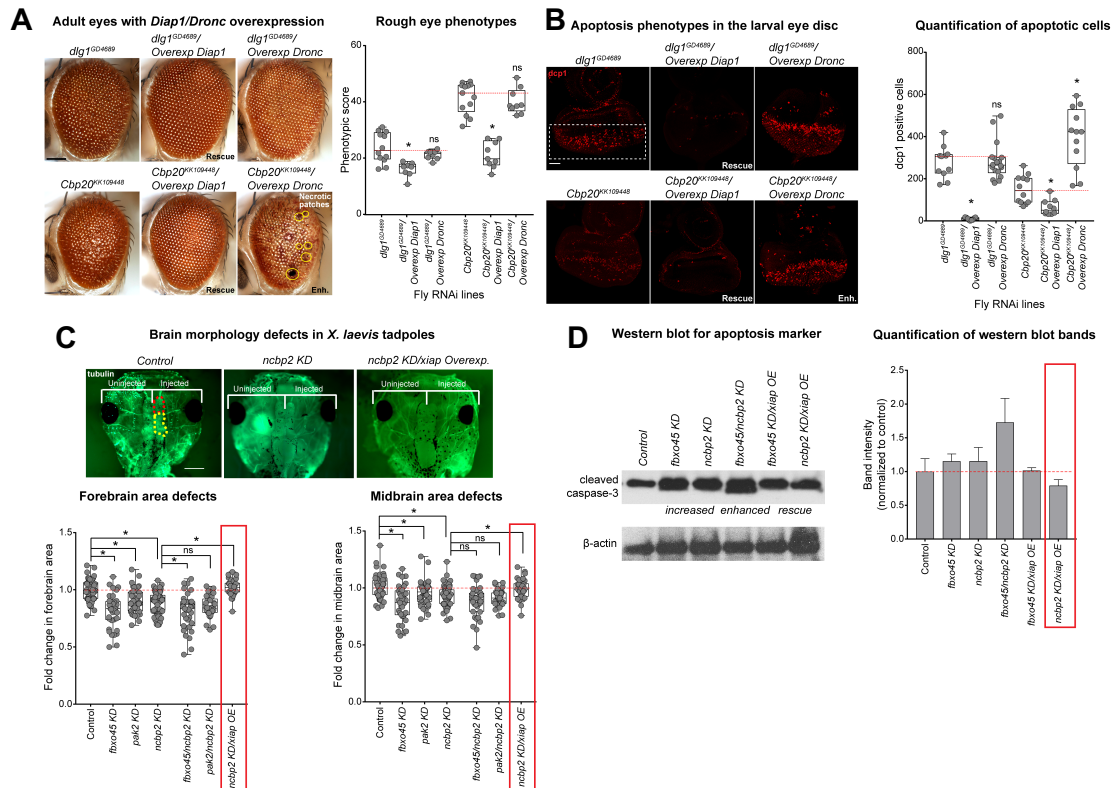


**Figure 2.10 Rescue of phenotypes due to knockdown of fly and *Xenopus* 3q29 gene homologs with overexpression of apoptosis inhibitors**

(A) Representative brightfield adult eye images and boxplot of phenotypic scores show rescue of rough eye phenotypes for flies with concomitant RNAi knockdown of *Cbp20* or *dlg1* and overexpression of *Diap1*, as well as enhanced phenotypes with overexpression of caspase-9 homolog, *Dronc* (n = 8-9; \*p < 0.05, two-tailed Mann-Whitney test; Scale bar = 100µm). (B) Larval eye discs stained with anti-dcp1 and boxplot of dcp1-positive cells in the larval eye discs of flies with knockdown of *Cbp20* or *dlg1* show rescue of apoptosis phenotypes upon *Diap1* overexpression and enhanced phenotypes upon *Dronc* overexpression (n = 9-18; \*p < 0.05, two-tailed Mann-Whitney test; Scale bar = 30µm). (C) Representative dorsal view images of stage 47 *X. laevis* tadpoles with simultaneous MO knockdown of *ncbp2* and overexpression of the apoptosis inhibitor, *xiap*, show rescue of brain size phenotypes caused by *ncbp2* knockdown alone (n = 30-63, \*p < 0.05, two-tailed Welch's T-test; Scale bar = 500µm). (D) Western blot analysis and quantification of *X. laevis* whole embryo lysates show increased intensity of cleaved caspase-3 bands at 19kD and 17kD with knockdown of 3q29 gene homologs and rescued levels with overexpression of *xiap*. β-actin was used as a loading control on the same blot. Quantification of western blot band intensities are normalized to the loading control. Red box indicates rescue of increased caspase-3 levels with overexpression of *xiap*.

Experiment		RNAi knockdown of <i>Drosophila</i> homologs of 3q29 genes						
Phenotype	Assay	<i>Cbp20</i>	<i>dlg1</i>	<i>Cbp20/dlg1</i>	<i>Cbp20/Fsn</i>	<i>Cbp20/CG8888</i>	<i>Cbp20/Diap1</i>	<i>dlg1/Diap1</i>
Adult eye morphology	Rough eye phenotype	Rough eye	Rough eye	Enhanced rough eye	Enhanced rough eye	Enhanced rough eye	Rescue	Rescue
	Necrotic patches	None (Present in homozygous KD)	None	Yes (more severe in homozygous KD)	Yes	None	None	None
	Eye area	Decreased area	Increased area	NA	NA	NA	Rescue	Rescue
Neuronal phenotypes	Climbing ability	Climbing defects	Climbing defects	Enhanced climbing defects	Enhanced climbing defects	NA	NA	NA
	Axonal targeting	Axon targeting defects	Axon targeting defects	Enhanced targeting defects	Enhanced targeting defects	NA	Rescue	Rescue
Cell organization (pupal eye)	DLG staining	Cellular defects	Cellular defects	Enhanced cellular defects	Enhanced cellular defects	Enhanced cellular defects	Rescue	Rescue
	Phalloidin staining	Loss of photoreceptors	Loss of photoreceptors	No change	Enhanced photoreceptor loss	Enhanced photoreceptor loss	Rescue	Rescue
Cell cycle (larval eye disc)	pH3 staining	No change	No change	No change	No change	Decreased proliferation	NA	NA
	BrdU staining	No change	Increased proliferation	NA	NA	NA	NA	NA
Apoptosis (larval eye disc)	dcp1 staining	Increased apoptosis	Increased apoptosis	Increased apoptosis	Increased apoptosis	Increased apoptosis	Rescue	Rescue
	TUNEL assay	Increased apoptosis	Increased apoptosis	Increased apoptosis	Increased apoptosis	Increased apoptosis	Rescue	Rescue
Cellular phenotypes (larval wing disc)	pH3 staining	Decreased proliferation	Increased proliferation	NA	NA	NA	NA	NA
	dcp1 staining	Increased apoptosis	Increased apoptosis	NA	NA	NA	NA	NA
RNA sequencing (adult heads)	Differential gene expression	Synaptic transmission, metabolism	Synaptic transmission, ion transport	Cellular respiration, protein folding	Cell cycle, response to stimulus	NA	NA	NA
Experiment		Morpholino knockdown of <i>X. laevis</i> homologs of 3q29 genes						
Phenotype	Assay	<i>nbp2</i>	<i>fbxo45</i>	<i>pak2</i>	<i>nbp2/fbxo45</i>	<i>nbp2/pak2</i>	<i>nbp2/xiap</i>	<i>fbxo45/xiap</i>
Craniofacial morphology	Eye area	Decreased area	Decreased area	Decreased area	NA	NA	Rescue	NA
	Midbrain area	Decreased area	Decreased area	Decreased area	No change	No change	Rescue	NA
	Forebrain area	Decreased area	Decreased area	Decreased area	Decreased area	No change	Rescue	NA
Apoptosis	Cleaved caspase-3 levels	Increased caspase-3	Increased caspase-3	NA	Increased caspase-3	NA	Rescue	Rescue

**Table 1 Summary of major experiments for knockdown of 3q29 gene homologs in *Drosophila* and *Xenopus laevis* show widespread cellular and neuronal defects**

### 2.3. Discussion

Using complementary *Drosophila* and *X. laevis* models, we interrogated developmental effects, cellular mechanisms, and genetic interactions of individual homologs of genes within the 3q29 region. Our major findings were recapitulated across both model systems (**Table 1**) and could also potentially account for the developmental phenotypes reported in mouse models of the entire deletion. Several themes have emerged from our study that exemplify the genetic and mechanistic complexity of the 3q29 deletion region.

First, our analysis of developmental phenotypes with knockdown of homologs for individual 3q29 genes showed that a single gene within the region may not be solely

responsible for the effects of the deletion. In fact, we found that knockdown of 12 out of 14 fly homologs showed developmental defects in *Drosophila*, while every fly homolog showed an enhanced rough eye phenotype when knocked down along with at least one other homolog. Although our study is limited to examining conserved cellular phenotypes of homologs of 3q29 genes in *Drosophila* and *X. laevis*, evidence from other model organisms also supports an oligogenic model for the deletion. In fact, knockout mouse models for several 3q29 genes have been reported to exhibit severe developmental phenotypes, including axonal and synaptic defects in *Fbxo45*<sup>-/-</sup> and embryonic lethality in *Pak2*<sup>-/-</sup> and *Pcyt1a*<sup>-/-</sup> knockout mice (Marlin et al., 2011; Saiga et al., 2009; Wang et al., 2005). Notably, although *Dlg1*<sup>+/-</sup> or *Pak2*<sup>+/-</sup> mice showed a range of neuronal phenotypes compared with control mice, they did not recapitulate the major developmental and behavioral features observed in mouse models of the entire deletion (Baba et al., 2019; Rutkowski et al., 2019; Wang et al., 2018), suggesting that the deletion phenotypes are contingent upon haploinsufficiency of multiple genes in the region. While no common variants associated with neurodevelopmental traits have been observed in the 3q29 region (Eicher et al., 2015), rare variants of varying effects in 9/21 genes have been identified among patients with different developmental disorders (Abrahams et al., 2013; Purcell et al., 2014; Turner et al., 2017). These data, combined with our findings in *Drosophila* and *X. laevis*, implicate multiple genes within the 3q29 region as potential candidates for neurodevelopmental defects.

Second, our screening of 161 crosses between pairs of fly homologs of 3q29 genes identified 44 interactions that showed enhanced rough eye phenotypes, suggesting that complex interactions among genes in the 3q29 region could contribute towards

developmental defects. While we only tested a subset of all possible interactions among the non-syntenic homologs of 3q29 genes in *Drosophila*, our results highlight conserved mechanistic relationships between “parts”, or the individual genes, towards understanding the effects of the “whole” deletion. For example, knockdown of *Cbp20* enhanced the phenotypes of 11 out of 12 other fly homologs, and concomitant knockdown of *ncbp2* with *fbxo45* or *pak2* in *Xenopus* enhanced brain and eye developmental phenotypes, suggesting that *NCBP2* could be a key modulator of other genes within the region. *NCBP2* encodes a subunit of the nuclear cap-binding complex (CBC), which binds to the 5' end of mRNA and microRNA in the nucleus (Pabis et al., 2010). Given the role of the CBC in post-transcriptional regulatory mechanisms such as nonsense-mediated decay, alternative splicing and mRNA transport (Gonatopoulos-Pournatzis and Cowling, 2014; Maquat, 2004), it is possible that disruption of this complex could result in changes to a broad set of genes and biological processes. In fact, our analysis of differentially-expressed genes in *Cbp20* knockdown flies showed disruption of synaptic transmission, cellular respiration, and several metabolic pathways. In contrast to other proposed candidate genes in the 3q29 region, *NCBP2* is not predicted to be pathogenic on its own in humans and does not have identified deleterious mutations in sequencing studies of neurodevelopmental disease cohorts so far, indicating its potential role as a modifier of the other candidate genes in the region. Our results also complement previous reports of synergistic interactions among fly homologs of 3q29 genes in the nervous system (Grice et al., 2015), representing another hallmark of an oligogenic model for the deletion. As these genetic interactions may vary across different

species, developmental timepoints, and tissues, the role of these interactions should be more deeply explored using mouse and human cell culture models.

Third, we identified disruptions to several cellular processes due to both single and pairwise knockdown of homologs in *Drosophila* and *X. laevis* models (**Table 1**). For example, simultaneous knockdown of *NCBP2* and *FBXO45* homologs in *Drosophila* led to enhanced cellular disorganization and altered expression of cell cycle and apoptosis genes, as well as enhanced morphological defects and increased caspase-3 levels in *X. laevis*. We further found that overexpression of the apoptosis inhibitors *Diap1* and *xiap* rescued the cellular and neuronal phenotypes observed with knockdown of homologs of 3q29 genes, providing important validations for the potential involvement of apoptosis in the deletion (**Table 1**). We propose that *NCBP2* could modify several cellular and molecular processes that may not be directly related to apoptosis, but could instead lead to a cascade of biological events that ultimately result in apoptosis. Apoptosis mechanisms are well-conserved between *Drosophila*, *X. laevis*, and humans, with key genes such as *XIAP* (*Diap1*), *CASP2* (*Dronc*), *CASP3* (*DrICE*), and *CASP7* (*Dcp-1*) sharing the same roles in programmed cell death across the three organisms (Kornbluth and White, 2005; Tittel and Steller, 2000; Xu et al., 2009). Although we focused on testing apoptosis phenotypes with knockdown of homologs of 3q29 genes, we note that apoptosis is potentially one of many cellular pathways disrupted by the 3q29 deletion. For example, *DLG1* is a tumor suppressor gene whose knockdown in *Drosophila* leads to neoplasms in the developing brain and eye disc (Bilder et al., 2000; Humbert et al., 2003), while *PAK2* is a key downstream mediator of the ERK signaling pathway for neuronal extension and is activated by caspases during apoptosis

(Luo and Rubinsztein, 2009; Marlin et al., 2011; Shin et al., 2002). Our results recapitulate the role of *DLG1* towards cell cycle regulation, and also implicate *NCBP2* and its interactions towards multiple cellular and developmental phenotypes.

More broadly, genes involved with apoptosis and cell proliferation have been implicated in several neurodevelopmental disorders. For example, disrupted cell proliferation was observed upon knockdown of *Drosophila* homologs of genes in the 16p11.2 deletion region, as well as an enrichment of cell cycle function among connector genes between pairs of 16p11.2 genes in a human brain-specific network (Iyer et al., 2018). Furthermore, abnormal apoptosis in the early developing brain has been suggested as a possible mechanism for the decreased number of neurons observed in individuals with autism and schizophrenia (Courchesne et al., 2011; Kreczmanski et al., 2007). For example, increased apoptosis was observed in both postmortem brain tissue from autism patients (Dong et al., 2018) and primary fibroblasts from schizophrenia patients (Batalla et al., 2015; Gasso et al., 2014). Further, growing evidence supports the role of apoptosis in these disorders as significant enrichments for genes associated with apoptotic processes among candidate genes for autism (Abrahams et al., 2013), intellectual disability (Thormann et al., 2019), and schizophrenia (Purcell et al., 2014) have been identified. In addition to neuropsychiatric disorders, apoptosis has also been implicated in syndromic forms of microcephaly in humans (Poulton et al., 2011) as well as decreased brain size in animal models of microcephaly genes (Faheem et al., 2015; Silver et al., 2010). Overall, these findings highlight the importance of cell cycle-related processes,

particularly apoptosis and proliferation, towards modulating neuronal phenotypes that could be responsible for developmental disorders.

In this study, the use of *Drosophila* and *X. laevis* models, both of which are amenable to high-throughput screening of developmental phenotypes, allowed us to systematically examine the conserved cellular and mechanistic roles of homologs of 3q29 genes and their interactions. Follow-up studies in more evolutionarily-advanced systems, such as mouse or human cell lines, will be useful to overcome limitations of *Drosophila* and *X. laevis* models, including testing the neurodevelopmental phenotypes and interactions of 3q29 genes without fly or *Xenopus* homologs. Collectively, these results emphasize the utility of quantitative functional assays for identifying conserved pathways associated with neurodevelopmental disorders, which will hopefully allow for future discoveries of treatments for these disorders.

## **2.4. Materials and Methods**

### **2.4.1. Ethics statement**

All *X. laevis* experiments were approved by the Boston College Institutional Animal Care and Use Committee (Protocol #2016–012) and were performed according to national regulatory standards.

### **2.4.2. Fly stocks and genetics**

Using reciprocal BLAST searches and orthology predictions from the DRSC Integrative Ortholog Prediction Tool (*DIOPT*) v.7.1 (Hu et al., 2011), 15 fly homologs were identified for the 21 human genes within the chromosome 3q29 region. No fly homologs were present for six genes, including *LRRC33*, *CEP19*, *RNF168*, *SMCO1*, *TFRC*,

and *TM4SF19*. A similar strategy was used to identify homologs for other neurodevelopmental genes tested for interactions in this study. Gene Ontology-Slim (GO-Slim) terms for each human gene and fly homolog were obtained from PantherDB (Mi et al., 2017). RNAi lines for fly homologs were obtained from the Vienna Drosophila Resource Centre (VDRC) (Dietzl et al., 2007), including both KK and GD lines, and the Bloomington *Drosophila* Stock Center (BDSC) (NIH P40OD018537). Fly RNAi lines for homologs of 3q29 genes were tested for gene knockdown using quantitative PCR. Microarray data and modENCODE Anatomy RNA-Seq from FlyBase (Chintapalli et al., 2007; Graveley et al., 2011) showed that all of the 14 tested homologs were expressed in the fly central nervous system and eye tissues. All fly stocks and crosses were cultured on conventional cornmeal-sucrose-dextrose-yeast medium at 25°C, unless otherwise indicated. RNAi lines were crossed with a series of *GAL4* driver lines to achieve tissue-specific knockdown of genes, including *w<sup>1118</sup>;da-GAL4* (Scott Selleck, Penn State) for ubiquitous, *w<sup>1118</sup>;dCad-GFP,GMR-GAL4/CyO* (Zhi-Chun Lai, Penn State) and *w<sup>1118</sup>;GMR-GAL4;UAS-Dicer2* (Claire Thomas, Penn State) for eye-specific, *w<sup>1118</sup>,bx<sup>MS1096</sup>-GAL4;;UAS-Dicer2* (Zhi-Chun Lai, Penn State) for wing-specific, and *w<sup>1118</sup>,Elav-GAL4* (Mike Grotewiel, VCU) and *w<sup>1118</sup>,Elav-GAL4;;UAS-Dicer2* (Scott Selleck, Penn State) for pan-neuronal knockdown of gene expression. To perform interaction studies, recombined stock lines of *GMR-GAL4* were generated with reduced expression of nine select homologs of 3q29 genes. Females from these stocks with constitutively reduced gene expression for each of these genes were crossed with RNAi lines of other homologs to achieve simultaneous knockdown of two genes (**Fig 2.1**). All

unique biological materials described in the manuscript, such as recombined fly stocks, are readily available from the authors upon request.

#### **2.4.3. Quantitative polymerase chain reaction for *Drosophila* RNAi knockdowns**

Levels of gene expression knockdown were confirmed using quantitative reverse-transcriptase PCR (qPCR) on RNA isolated from pooled groups of 35 fly heads per line tested. Briefly, RNAi lines were crossed with *Elav-GAL4* (to test RNAi line efficacy) or *Elav-GAL4;;UAS-Dicer2* (to test for *tiptop* overexpression) at 25°C to achieve pan-neuronal knockdown of the fly homolog. Adult fly heads at day 3 were separated by vortexing, and total RNA was isolated using TRIzol (Invitrogen, Carlsbad, CA, USA). cDNA was prepared using the qScript cDNA synthesis kit (Quantabio, Beverly, MA, USA). Quantitative PCR was performed using an Applied Biosystems Fast 7500 system with SYBR Green PCR master mix (Quantabio) to estimate the level of gene expression. All experiments were performed using three biological replicates of 35 fly heads each. Primers were designed using NCBI Primer-BLAST, with primer pairs separated by an intron in the corresponding genomic DNA.

#### **2.4.4. Climbing assay**

Fly crosses were set at 25°C with *Elav-GAL4* to obtain pan-neuronal knockdown for select homologs of 3q29 genes. For each RNAi line tested, groups of ten female flies were first allowed to adjust at room temperature for 30 minutes and then transferred to a climbing apparatus, made by joining two vials, and allowed to adjust for 5 minutes. The flies were tapped down to the bottom, and the number of flies climbing past the 8 cm mark measured from the bottom of the apparatus in 10 seconds was then counted. This assay was repeated nine additional times for each group, with a one-minute rest between

trials. The sets of 10 trials for each group were repeated daily for ten days, capturing data for 100 replicates from day 1 until day 10, starting the experiments with 1-2-day old flies. All experiments were performed during the same time of the day for consistency of results.

#### **2.4.5. Imaging of adult fly eyes and wings**

RNAi lines were crossed with *GMR-GAL4* and reared at 29°C for eye-specific knockdown and *bx<sup>MS1096</sup>-GAL4* at 25°C for wing-specific knockdown. For eye imaging, adult 2-3-day old female progenies from the crosses were collected, immobilized by freezing at -80°C, mounted on Blu-tac (Bostik Inc, Wauwatosa, WI, USA), and imaged with an Olympus BX53 compound microscope with LMPLan N 20X air objective using a DP73 c-mount camera at 0.5X magnification and a z-step size of 12.1µm. (Olympus Corporation, Tokyo, Japan). CellSens Dimension software (Olympus Corporation, Tokyo, Japan) was used to capture the images, and stacked the image slices using Zereine Stacker (Zerene Systems LLC, Richland, WA, USA). All eye images presented in this study are maximum projections of 20 consecutive optical z-sections. Adult wings were plucked from 2–5 day old female flies, mounted on a glass slide, covered with a coverslip and sealed with clear nail polish. The wings were imaged using a Zeiss Discovery V20 stereoscope (Zeiss, Thornwood, NY, USA) with ProgRes Speed XT Core 3 camera (Jenoptik AG, Jena, Germany) using a 40X objective, and wing images were captured with ProgRes CapturePro v.2.8.8 software.

#### **2.4.6. Quantitative phenotyping of fly eyes using *Flynolyper***

A computational method called *Flynolyper* (<http://flynolyper.sourceforge.net>) was used to measure the degree of roughness of the adult eyes with knockdown of individual or pairs of homologs. The software uses an algorithm to detect the center of each

ommatidium, and calculates a phenotypic score based on the number of ommatidia detected, the lengths of six local vectors with direction pointing from each ommatidium to the neighboring ommatidia, and the angle between these six local vectors. Eye areas, ommatidial diameter, and areas of necrotic patches, which may not be reflected in the *Flynotyper* scores, were measured using ImageJ. Significant pairwise interactions were reported as “validated” when multiple RNAi or mutant lines, if available, showed the same phenotype.

#### **2.4.7. Immunohistochemistry of eye and wing discs**

Third instar larval and 44-hour-old pupal eye discs, reared at 29°C, and third instar larval wing discs, reared at 25°C, were dissected in 1X phosphate-buffered saline (PBS) and fixed in 4% paraformaldehyde for 20 minutes. The eye and wing discs were then washed thrice in PBT (PBS with 0.1% Triton-X) for 10 minutes each, treated with blocking solution (PBS with 1% normal goat serum (NGS) for eye discs, or 1% bovine serum albumin (BSA) for wing discs) for 30 minutes, and then incubated overnight with primary antibodies at 4°C. Rabbit anti-cleaved *Drosophila* dcp1 (Asp216) (1:100; 9578S, Cell Signaling Technology, Danvers, MA, USA), a marker for cells undergoing apoptosis, and Mouse anti-phospho-Histone H3 (S10) antibody (1:100; 9706L, Cell Signaling Technology), a mitotic marker for measuring proliferating cells, were used to assay cell proliferation and apoptosis defects in larval eye and wing discs. Mouse anti-DLG (1:200; 4F3, DSHB, Iowa City, Iowa, USA), a septate junction marker, and Rhodamine Phalloidin (1:200; R415, Invitrogen Molecular Probes, Carlsbad, CA, USA), an F-actin marker, were used to visualize and count ommatidial cells and photoreceptor cells in pupal eyes. Mouse anti-chaoptin (1:200; 24B10, DSHB) was used to visualize

retinal axon projections. Preparations were then washed thrice with PBT for 10 minutes, and incubated for two hours with fluorophore-conjugated secondary antibodies (Alexa fluor 568 goat anti-mouse (1:200) (A11031), Alexa fluor 488 goat anti-mouse (1:200) (A11029), Alexa fluor 647 goat anti-rabbit (1:200) (A21245), and Alexa fluor 647 goat anti-mouse (1:200) (A21236), Invitrogen Molecular Probes, Carlsbad, CA, USA)) with gentle shaking. Preparations were washed thrice in PBT for 10 minutes, and the tissues were then mounted in Prolong Gold antifade mounting media with DAPI (P36930, Thermo Fisher Scientific, Waltham, MA, USA) or Vectashield hard set mounting media with DAPI (H-1500, Vector Laboratories, Burlingame, CA, USA) for imaging.

#### **2.4.8. Confocal imaging and analysis**

Confocal images of larval and pupal eye and wing discs were captured using an Olympus Fluoview FV1000 laser scanning confocal microscope (Olympus America, Lake Success, NY). Maximum projections of all optical sections were generated for display. As DLG staining was only used to visualize cell boundaries in the pupal eye and not for any expression or quantitative analysis, the laser intensity was increased from 400-490V in control flies to 530-570V in flies with knockdown of *dlg1* to account for decreased DLG expression. Acquisition and processing of images was performed using the Fluoview FV10-ASW 2.1 software (Olympus Corporation, Tokyo, Japan), and the z-stacks of images were merged using ImageJ. The number of *dcpl*-positive cells from larval eye discs were counted using two ImageJ plugins, AnalyzeParticles and Image-based Tool for Counting Nuclei (ITCN). Apoptotic cells in wing discs stained with *dcpl* were analyzed using manual counting. Images stained with anti-chaoptin were manually scored as having either “mild” (minor axon disorganization compared with control), “moderate”

(partial loss of axon projection. i.e. loss of R7-R8 projection into the medulla), or “severe” (loss of projections for most axons at the lamina) axon targeting defects.

#### **2.4.9. Differential expression analysis of transcriptome data**

RNA sequencing (RNA-Seq) was performed with samples isolated from three biological replicates of 35 fly heads each for individual (*Cbp20*, *dlg1*, *Fsn*, *Pak*) and pairwise (*Cbp20/dlg1*, *Cbp20/Fsn*) *Elav-GAL4* mediated knockdowns of homologs of 3q29 genes. Gene expression levels were compared of each cross to VDRC control flies carrying the same genetic background (GD or KK control lines crossed with *Elav-GAL4*). cDNA libraries were prepared for the three biological replicates per genotype using TruSeq Stranded mRNA LT Sample Prep Kit (Illumina, San Diego, CA), and single-end sequencing using Illumina HiSeq 2000 was performed at the Penn State Genomics Core Facility to obtain 100 bp reads at an average coverage of 36.0 million aligned reads/sample. Trimmomatic v.0.36 was used for quality control assessment, TopHat2 v.2.1.1 to align the raw sequencing data to the reference fly genome and transcriptome (build 6.08), and HTSeq-Count v.0.6.1 to calculate raw read counts for each gene. edgeR v.3.20.1 (generalized linear model option) was used to perform differential expression analysis, and genes with  $\log_2$ -fold changes  $>1$  or  $<-1$  and false-discovery rates  $<0.05$  (Benjamini-Hochberg correction) were considered to be differentially expressed. Human homologs of differentially-expressed fly genes (top matches for each fly gene, excluding matches with “low” rank) were identified using DIOPT. Enrichment analysis of Panther GO-Slim Biological Process terms among the differentially-expressed fly genes and their human homologs was performed using the PantherDB Gene List Analysis tool. Enrichments for genes preferentially expressed in the developing brain were calculated

using the Cell-type Specific Expression Analysis tool based on expression data from the BrainSpan Atlas.

#### **2.4.10. *X. laevis* embryos**

Eggs collected from female *X. laevis* frogs were fertilized *in vitro*, dejellied, and cultured following standard methods (Lowery et al., 2012; Sive et al., 2010). Embryos were staged according to Nieuwkoop and Faber (Zahn et al., 2017).

#### **2.4.11. Morpholino and RNA constructs**

Morpholinos (MOs) were targeted to early splice sites of *X. laevis ncbp2*, *fbxo45*, *pak2*, or standard control MO, purchased from Gene Tools LLC (Philomath, OR, USA). For knockdown experiments, all MOs were injected at either the 2-cell or 4-cell stage, with embryos receiving injections two or four times total in 0.1X MMR media containing 5% Ficoll. Control and *fbxo45* MOs were injected at 10ng/embryo, *ncbp2* and control MOs were injected at 20ng/embryo, and *pak2* and control MOs were injected at 50ng/embryo. For rescue experiments, the same amounts of MOs used in the KD experiments were injected along with gene-specific mRNA tagged with GFP (800pg/embryo for *xiap*-GFP; 1000pg/embryo for *ncbp2*-GFP and *fbxo45*-GFP, and 300pg/embryo for *pak2*-GFP) in the same injection solution. Capped mRNAs were transcribed *in vitro* using SP6 or T7 mMessage mMachine Kit (Thermo Fisher Scientific, Waltham, MA, USA). RNA was purified with LiCl precipitation. *X. laevis ncbp2*, *fbxo45*, *pak2*, and *xiap* ORFs obtained from the European *Xenopus* Resource Center (EXRC, Portsmouth, UK) were gateway-cloned into pCSf107mT-GATEWAY-3'GFP destination vectors. Constructs used included *ncbp2*-GFP, *fbxo45*-GFP, *pak2*-GFP, *xiap*-GFP, and GFP in pCS2+. Embryos either at the 2-cell or 4-cell stage received four injections in 0.1X MMR containing 5%

Ficoll with the following total mRNA amount per embryo: 300pg of GFP, 800pg of *xiap*-GFP, 1000pg of *ncbp2*-GFP, 1000pg of *fbxo45*-GFP, and 300pg of *pak2*-GFP.

#### **2.4.12. qPCR for *X. laevis* morpholino knockdown**

Morpholino validation and knockdown was assessed using qPCR. Total RNA was extracted using TRIzol reagent (Life Technologies, Grand Island, NY, USA), followed by chloroform extraction and ethanol precipitation from 2-day old embryos injected with increasing concentrations of MO targeted to each homolog of the tested 3q29 gene.

cDNA synthesis was performed with SuperScript II Reverse Transcriptase (Life Technologies, Grand Island, NY, USA) and random hexamers. qPCR was performed in triplicate, with band intensities quantified by densitometry in ImageJ and normalized to the uninjected control mean relative to *ODCI*, which was used as a housekeeping control.

#### **2.4.13. Brain and eye morphology assays**

In brain morphology experiments, all embryos received two injections at the 2-cell stage in 0.1X MMR containing 5% Ficoll. One cell was left uninjected and the other cell was injected with either control MO or MO targeted to the tested 3q29 gene, along with 300pg of GFP mRNA in the same injection solution. Stage 47 tadpoles were fixed in 4% PFA diluted in PBS for one hour, rinsed in PBS and gutted to reduce autofluorescence. Embryos were incubated in 3% bovine serum albumin and 1% Triton-X 100 in PBS for two hours, and then incubated in anti-acetylated tubulin primary antibody (1:500, monoclonal, clone 6-11B-1, AB24610, Abcam, Cambridge, UK) and goat anti-mouse Alexa fluor 488 conjugate secondary antibody (1:1000, polyclonal, A11029, Invitrogen Life Technologies, Carlsbad, CA). Embryos were then rinsed in 1% PBS-Tween and imaged in PBS. Skin dorsal to the brain was removed if the brain was not clearly visible due to pigment. For eye phenotype experiments, all embryos received four injections at

the 2-cell or 4-cell stage in 0.1X MMR containing 5% Ficoll with either the control MO or MOs targeted to each 3q29 gene. Stage 42 tadpoles were fixed in 4% PFA diluted in PBS. Tadpoles were washed three times in 1% PBS-Tween for one hour at room temperature before imaging.

#### **2.4.14. *X. laevis* image acquisition and analysis**

Lateral view images of stage 42 tadpoles for eye experiments and dorsal view images of stage 47 tadpoles for brain experiments were each collected on a SteREO Discovery.V8 microscope using a Zeiss 5X objective and AxioCam 512 color camera (Zeiss, Thornwood, NY, USA). Areas of the left and right eye, forebrain, and midbrain were determined from raw images using the polygon area function in ImageJ. Eye size was quantified by taking the average area of both the left and right eye, while forebrain and midbrain area were quantified by taking the ratio between the injected and uninjected sides for each sample.

#### **2.4.15. Western blot for apoptosis**

Two replicate Western blot experiments were performed to test for apoptosis markers in *X. laevis* with 3q29 gene knockdown. Embryos at stages 20–22 were lysed in buffer (50mM Tris pH 7.5, 1% NP40, 150mM NaCl, 1mM PMSF, 0.5 mM EDTA) supplemented with cOmplete Mini EDTA-free Protease Inhibitor Cocktail (Sigma-Aldrich, Basel, Switzerland). Blotting was carried out using rabbit polyclonal antibody to cleaved caspase-3 (1:500, 9661S, Cell Signaling Technology, Danvers, MA, USA), with mouse anti-beta actin (1:2500, AB8224, Abcam, Cambridge, UK) as a loading control on a Mini-PROTEAN TGX precast 4–15% gradient gel (Bio-Rad, Hercules, CA, USA). Chemiluminescence detection was performed using Amersham ECL Western blot reagent (GE Healthcare Bio-Sciences, Pittsburgh, PA, USA). Band intensities were

quantified by densitometry in ImageJ and normalized to the control mean relative to beta-actin. Due to the low number of replicates, we did not perform any statistical tests on data derived from these experiments.

#### **2.4.16. Statistical analysis**

All statistical analyses of functional data were performed using R v.3.4.2 (R Foundation for Statistical Computing, Vienna, Austria). Non-parametric one-tailed and two-tailed Mann-Whitney tests were used to analyze *Drosophila* functional data and human network data, as several datasets were not normally distributed ( $p < 0.05$ , Shapiro-Wilk tests for normality). Climbing ability and survival data for each fly RNAi line across each experiment day were analyzed using two-way and one-way repeated values ANOVA tests with post-hoc pairwise t-tests. We also used parametric t-tests to analyze *Drosophila* qPCR data and all *X. laevis* data, as these data were either normally distributed ( $p > 0.05$ , Shapiro-Wilk tests for normality) or had a robust sample size ( $n > 30$ ) for non-normality. All p-values from statistical tests derived from similar sets of experiments (i.e. *Flynotyper* scores for pairwise interactions, *dcp1* rescue experiments with *Diap1*) were corrected using Benjamini-Hochberg correction.

#### **2.4.17. Reproducibility**

*Drosophila* eye area staining experiments for select individual knockdown lines, as well as climbing ability experiments for a subset of individual and pairwise knockdown lines, were performed on two independent occasions with similar sample sizes. *X. laevis* brain and eye area experiments were performed on three independent occasions, with the data shown in the figures representing pooled results of each of the three experimental batches (normalized to the respective controls from each batch). *X. laevis* qPCR experiments were performed three times and western blot experiments were performed twice. Sample

sizes for each experiment were determined by testing all available organisms; no prior power calculations for sample size estimation were performed. No data points or outliers were excluded from the experiments presented in the manuscript.

#### **2.4.18. Code availability**

All source code and datasets for generating genomic data (RNA-Seq, network analysis, and neurodevelopment/apoptosis gene overlap) are available on the Girirajan lab GitHub page at [https://github.com/girirajanlab/3q29\\_project](https://github.com/girirajanlab/3q29_project).

### CHAPTER 3

#### Functional assessment of the “two-hit” model for neurodevelopmental defects

#### in *Drosophila* and *X. laevis* models of 16p12.1 deletion

The material in this chapter was adapted from the following manuscript in review:

**Pizzo, L.\***, **Lasser, M.\***, Yusuff, T., Jensen, M., Ingraham, P., Huber, E., Dhruva Singh, M., Iyer, J., Desai, I., Karthikeyan, S., Weiner, A., Krishnan, A., Monahan, C., Rolls, M., Lowery, L.A., Girirajan, S. Functional assessment of the “two-hit” model for neurodevelopmental defects in *Drosophila* and *X. laevis* models of 16p12.1 deletion. *Genome Research* (2020) (in review)

\* authors contributed equally to work

### 3.1 Introduction

Rare recurrent copy-number variants (CNVs) account for about 15% of individuals with neurodevelopmental disorders, such as autism, intellectual disability, and schizophrenia (Girirajan et al., 2011; Wilfert et al., 2017). While certain CNVs were initially associated with specific neuropsychiatric diagnoses, such as the 16p11.2 deletion and autism (Weiss et al., 2008; Zufferey et al., 2012), 3q29 deletion and schizophrenia (Mulle, 2015), and 15q13.3 deletion and epilepsy (Helbig et al., 2009), variable expressivity of phenotypes seems to be the norm rather than the exception for these CNVs (Girirajan and Eichler, 2010b). A prominent example of this is the 520 kbp deletion encompassing seven genes on chromosome 16p12.1, which is associated with multiple neuropsychiatric disorders, including intellectual disability/ developmental delay (ID/DD), schizophrenia, and epilepsy (Girirajan et al., 2010a; Pizzo et al., 2018). Furthermore, a large-scale study on a control population reported cognitive defects in seemingly-unaffected individuals with the 16p12.1 deletion (Stefansson et al., 2014), suggesting that the deletion is sufficient to cause neuropsychiatric features on its own. In contrast to other pathogenic CNVs that occur mostly *de novo*, the 16p12.1 deletion is inherited in more than 95% of individuals from a mildly-affected or unaffected carrier parent (Girirajan et al., 2012; Girirajan et al., 2010a; Pizzo et al., 2018). In fact, affected children with the deletion were more likely to carry another large CNV or deleterious mutation elsewhere in the genome (“second hit”) compared to their carrier parents (Girirajan et al., 2010a; Pizzo et al., 2018), providing evidence that additional rare variants in the genetic background could modulate the effect of the deletion. These results suggest that the 16p12.1 deletion confers significant risk for disease and sensitizes the

genome for a range of neuropsychiatric outcomes, while additional rare variants in the genetic background determine the phenotypic trajectory of the deletion.

The extensive phenotypic variability and lack of chromosomal events such as translocations and atypical deletions has made causal gene discovery for variably-expressive CNVs such as the 16p12.1 deletion challenging. In particular, the molecular mechanisms that are affected by individual 16p12.1 genes and the interaction models that explain how “second-hit” genes modulate the associated phenotypes have not been assessed. Therefore, evaluation of developmental, neuronal, and cellular defects caused by reduced expression of individual 16p12.1 genes, as well as their interactions with each other and with “second-hit” genes from patients with the deletion, would allow us to understand the pathogenesis of the variable phenotypes associated with the deletion. As stated previously, *Drosophila melanogaster* and *Xenopus laevis* serve as excellent models for systematic evaluation of developmental and tissue-specific effects of multiple genes and their genetic interactions, as they are amenable for rapid genetic manipulation and high-throughput evaluation. In fact, *Drosophila* has been classically used to study the role of genes and genetic interactions towards developmental and neurological phenotypes (Gatto et al., 2014; Jumbo-Lucioni et al., 2016; Sears and Broadie, 2017). For example, Grossman and colleagues overexpressed human transgenes from chromosome 21 in flies and identified synergistic interactions between *DSCAM* and *COL6A2*, which potentially contribute to the heart defects observed in individuals with Down syndrome (Grossman et al., 2011). Furthermore, functional assays using *X. laevis* have uncovered developmental defects, behaviors, and molecular mechanisms for several homologs of genes associated

with neurodevelopmental disorders, such as *NLGN* (Chen et al., 2010), *CACNA1C* (Lewis et al., 2009), *GRIK2* (Ishimaru et al., 1996) and *PTEN* (Ueno et al., 2006).

In chapter 2, using *Drosophila* and *X. laevis* models, we showed that multiple genes within the variably-expressive 3q29 deletion region individually contribute to neurodevelopmental defects (Iyer et al., 2018; Singh et al., 2020), suggesting that no single gene could be solely causative for the wide range of defects observed with deletion of an entire region. Moreover, we identified complex genetic interactions within conserved biological pathways among homologs of genes affected by these CNVs. For example, fly and *X. laevis* homologs of *NCBP2* enhanced the neuronal and cellular phenotypes of each of the other 3q29 deletion homologs (Singh et al., 2020). In fact, several aspects of the interactions observed in our studies were also functionally or thematically validated in vertebrate model systems, providing further evidence for the utility of these models to study complex genetic interactions (McCammon et al., 2017; Qiu et al., 2019). While our previous work showed pervasive interactions of homologs within regions associated with neurodevelopmental disease, the deletions within these regions occur primarily *de novo* (Girirajan et al., 2012), indicating a strong phenotypic impact associated with these CNVs. In contrast, the 16p12.1 deletion is mostly inherited and frequently co-occurs with “second-hit” variants in affected individuals, suggesting that interactions involving “second-hit” genes confer a higher impact towards variable neurodevelopmental phenotypes compared with those caused by gene interactions within the CNV region.

Here, using *Drosophila melanogaster* and *X. laevis* as two complementary model systems of development, we present the first systematic assessment of genes within the

16p12.1 deletion towards developmental, neuronal, and cellular phenotypes in functional models. We found that knockdown of each individual 16p12.1 homolog affects phenotypic domains of neurodevelopment, leading to developmental delay and seizure susceptibility, brain size alterations, neuronal morphology abnormalities, and cellular proliferation defects. In contrast to genes within other CNVs such as the 16p11.2 deletion, homologs of 16p12.1 genes independently contribute towards specific developmental and neuronal domains, and show phenotypic variability within different genetic backgrounds. Simultaneous knockdown of homologs of genes carrying “second-hits” in affected children with the deletion modulated the defects observed with knockdown of 16p12.1 homologs through additive, suppressive or synergistic interactions. In fact, we observed that knockdown of both fly and *X. laevis* homologs of the intellectual disability-associated gene *SETD5* synergistically enhanced neurodevelopmental and cellular phenotypes due to knockdown of homologs of the 16p12.1 gene *MOSMO*. Our results suggest a model where reduced expression of each individual gene within 16p12.1 is sufficient to sensitize the genome towards distinct neurodevelopmental defects, which are modulated by complex interactions with “second-hit” genes.

## **3.2 Results**

### **3.2.1 Multiple homologs of 16p12.1 genes contribute to *Drosophila* and *X. laevis* development**

My collaborators first identified four conserved fly homologs out of the seven 16p12.1 genes using reciprocal BLAST and orthology prediction tools (Hu et al., 2011).

Using RNA interference (RNAi) and the *UAS-GAL4* system (Brand and Perrimon, 1993), the expression of the four fly homologs was reduced in a tissue-specific manner, and their individual contributions towards developmental, neuronal, and cellular defects were observed (**Fig. 3.1**). 40-60% expression of the four homologs was confirmed using RT-qPCR (**Fig. 3.4.A**). I note that the genes are represented with fly gene names along with human counterparts at first mention in the text, and as fly genes with allele names in the figures.

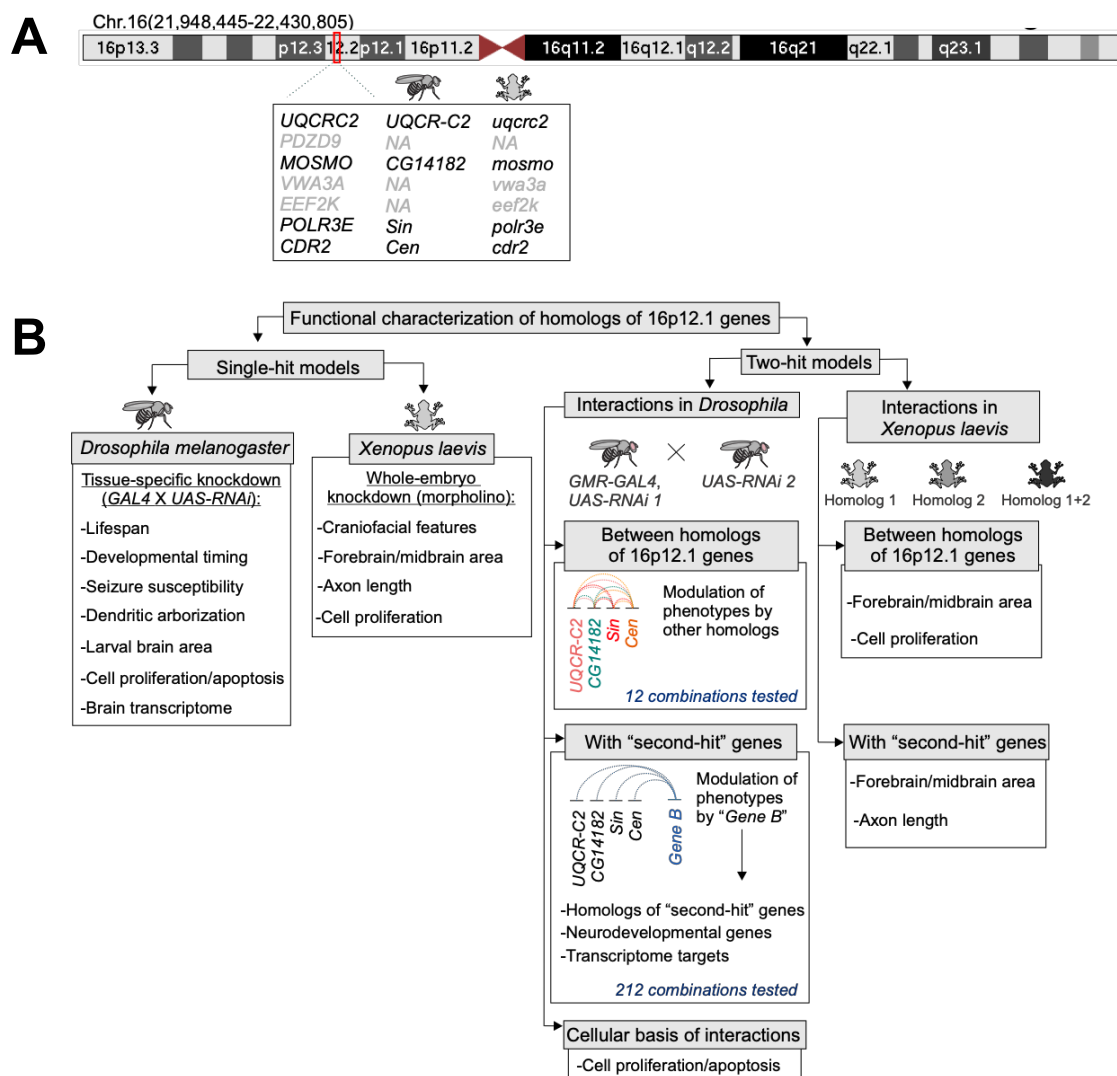


**Figure 3.1 Strategy to evaluate the contributions of 16p12.1 gene homologs and interactions with "second-hit" genes towards neurodevelopmental phenotypes**

**(A)** Diagram of human chromosome 16 indicating the region hg19(chr16:21,948,445-22,430,408) deleted in the 16p12.1 deletion. Seven protein coding genes are deleted in the 16p12.1 deletion, including *POLR3E*, *MOSMO*, *UQCRC2*, *CDR2*, *EEF2K*, *VWA3A*, and *PDZD9*. Four out of the seven genes are conserved in both *Drosophila* and *X. laevis*. **(B)** We followed a global phenotypic screening strategy using RNAi lines and tissue-specific knockdown in *Drosophila*, and morpholino-mediated whole embryo knockdown in *X. laevis*, to identify individual contributions of the homologs towards multiple developmental and neuronal features. We also evaluated pairwise interactions among the 16p12.1 homologs towards eye phenotypes in *Drosophila*, and brain size and cellular proliferation defects in *X. laevis*. We next characterized 212 pairwise interactions between the 16p12.1 homologs with homologs of genes identified in children with 16p12.1 deletion (“second-hits”), genes within conserved neurodevelopmental pathways, and transcriptome targets. We found that homologs of “second-hit” genes can establish complex genetic interactions with 16p12.1 homologs towards neurodevelopmental and cellular phenotypes. We assessed specific interaction pairs towards brain size and axon length in *X. laevis*, and observed a domain-specific behavior of the interactions.

First, the global role of the 16p12.1 homologs during development was assessed by decreasing their expression in a ubiquitous manner, and larval lethality was detected with knockdown of *Sin* (*POLR3E*) and *UQCR-C2* (*UQCRC2*) (**Fig. 3.2.A**). The *Drosophila* wing serves as a relevant model to rapidly assess early developmental defects, as multiple conserved signaling pathways, including Notch, Hedgehog, and Wnt pathways, are required for wing development (Strigini and Cohen, 1997; Yan et al., 2004; Yusuff et al., 2020). Wing-specific knockdown led to severe phenotypes for *Sin* and severe defects and lethality for *UQCR-C2* fly models, mirroring the observations made with ubiquitous knockdown (**Fig. 3.2.A**) and suggesting a role of these homologs in global development.

Next, we evaluated whether decreased expression of the homologs leads to neuronal phenotypes frequently observed in animal models of neurodevelopmental disease, including altered lifespan, susceptibility to seizures, delayed developmental timing, changes in brain size, and dendritic arbor defects (Callan et al., 2010; Kishi and Macklis, 2004; Kwon et al., 2006; Lee et al., 2003; Parker et al., 2011; Rujano et al., 2013; Stuss et al., 2012). Pan-neuronal knockdown led to early lethality in adult flies with knockdown of *Sin* and *CG14182* (*MOSMO*) (**Fig. 3.2.B**). As previously reported for genes associated with aging, such as *Hsp26*, *Hsp27* (Wang et al., 2004) and *SOD3* (Orr

and Sohal, 1994), extended lifespan was observed with knockdown of *UQCR-C2* compared to controls (**Fig. 3.2.B**). Furthermore, measurements of developmental transitions revealed delayed pupariation with knockdown of *Sin* and *CG14182*, indicating a possible role for these genes in developmental timing (**Fig. 3.2.C**). Alterations in dendritic morphology in *Drosophila* have been observed in genes associated with neurodevelopmental disorders, such as *Fmr1* (Lee et al., 2003), *kismet* (Melicharek et al., 2010), and *Dscam* (Matthews et al., 2007; Soba et al., 2007; Wang et al., 2004). Thus, dendritic arbors were measured in *Drosophila* class IV sensory neurons and reduced complexity of dendritic branching for *CG14182* was observed (**Fig. 3.2.D**). Next, the total area of the developing third instar larval brain was measured, and reduced brain sizes were observed with knockdown of *CG14182* and *Sin* (**Fig. 3.2.E**). This reduction corresponded with a decreased number of cells in the brain lobe stained with anti-phosphorylated-Histone 3 (pH3), a marker for proliferating cells (**Fig. 3.2.F**).

To identify transcriptional changes and disruption of pathways associated with knockdown of 16p12.1 homologs, RNA-sequencing of fly heads with pan-neuronal knockdown of the homologs was performed. Gene Ontology analysis of differentially-expressed genes identified enrichments for multiple cellular and neuronal processes that were dysregulated by knockdown of each homolog (**Fig 3.3**). For example, knockdown of *CG14182* altered the expression of fly homologs of human genes involved in synapse assembly and transmission, as well as histone methyltransferase binding function. Similarly, knockdown of *Sin* showed enrichment for both fly genes and human homologs involved in muscle contraction, as well as human homologs of fly genes involved in neuronal projection, neurotransmitter release and GABA pathways. Human homologs of

genes differentially expressed with knockdown of *Sin* were also enriched for genes involved in development of several non-neuronal organ systems, including cardiac, kidney, lung, and muscle, further indicating the importance of *Sin* towards global development. Interestingly, each homolog disrupted unique sets of biological functions, suggesting they act in independent pathways.

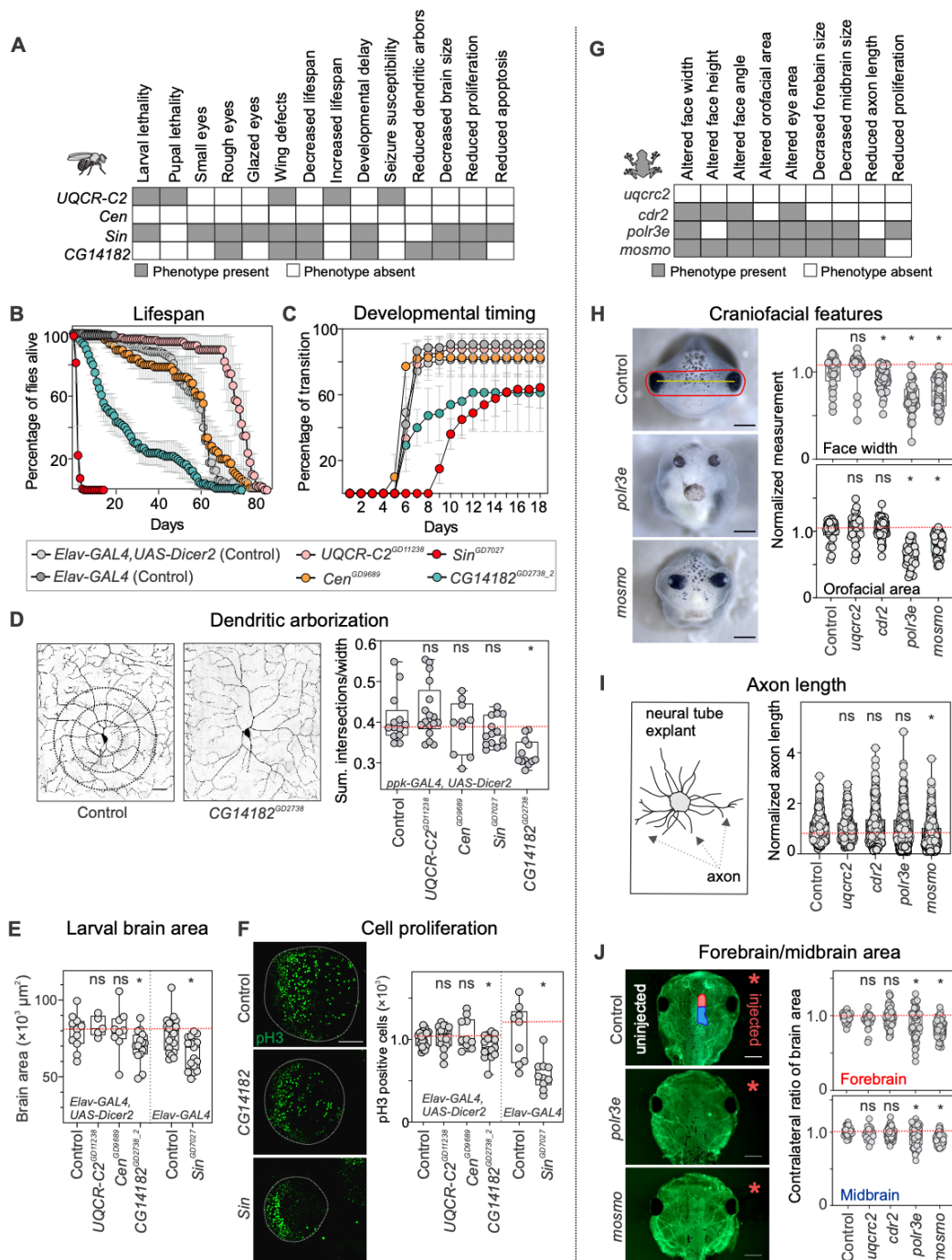


**Figure 3.2 Multiple homologs of 16p12.1 genes contribute to neurodevelopmental defects in *Drosophila* and *X. laevis***

(A) Schematic showing multiple phenotypes affected by knockdown of individual 16p12.1 homologs in *Drosophila*. (B) Nervous system mediated knockdown led to reduced lifespan with knockdown of *CG14182<sup>GD2738\_2</sup>* (n=100, one-way repeat measures ANOVA with post-hoc pairwise t-test, days 6-61, p<0.05) and *Sin<sup>GD7027</sup>* (n=160, day 1-6, p<0.05). Increased lifespan was observed with knockdown of *UQCR-C2<sup>GD11238</sup>* (n=120, days 51-81, p<0.05). Data represented show mean  $\pm$  standard deviation of 4-8 independent groups of 20 flies for each line tested. (C) Nervous-system mediated knockdown led to delayed pupariation time for *CG14182<sup>GD2738\_2</sup>* (n=150, one-way repeat measures ANOVA with post-hoc pairwise t-test, days 7-18, p<0.05) and *Sin<sup>GD7027</sup>* (n=180, days 6-18, p<0.05). Data represented show mean  $\pm$  standard deviation of 5-9 independent groups of 30 larvae for each line tested. (D) Specific knockdown of the homologs in sensory class IV dendritic arborization neurons showed reduced complexity of dendritic arbors (measured as sum of intersections normalized to width) for *CG14182<sup>GD2738</sup>* (n=12, two-tailed Mann-Whitney, \*p=5.35  $\times 10^{-5}$ ; Scale bar = 25  $\mu$ m). (E) Third instar larvae with nervous system-specific knockdown of the homologs showed reduced brain area for *CG14182<sup>GD2738\_2</sup>* (n=15, two-tailed Mann-Whitney, \*p=0.047) and *Sin<sup>GD7027</sup>* (n=17, \*p= 0.001). (F) Developing third instar larvae with knockdown of *CG14182<sup>GD2738\_2</sup>* (n=15, two-tailed Mann-Whitney, \*p=0.0255) and *Sin<sup>GD7027</sup>* (n=10, \*p= 9.74 $\times 10^{-4}$ ) showed reduced number of phosphorylated Histone-3 (pH3) positive cells in the brain lobe (green) (Scale bar = 50  $\mu$ m). (G) Schematic showing the phenotypes observed with knockdown of 16p12.1 homologs in *X. laevis*. “Phenotype present” represent phenotypes observed with stronger knockdown of the homologs. (H) Representative images of tadpoles injected with control morpholino, indicating facial landmarks for face width (yellow) and orofacial area (red), and tadpoles with knockdown of *polr3e* and *mosmo*. Knockdown of *cdr2* (n=54, two-tailed student’s t-test, \*p=7.75  $\times 10^{-4}$ ), *polr3e* (n=37, \*p=1.97  $\times 10^{-13}$ ) and *mosmo* (n=50, \*p=1.36  $\times 10^{-11}$ ) led to decreased face width, while knockdown of *polr3e* (\*p=3.29  $\times 10^{-16}$ ) and *mosmo* (\*p=1.47  $\times 10^{-8}$ ) led to decreased orofacial area. All measures were normalized to their respective control injected with the same morpholino amount. (Scale bar = 500  $\mu$ m). (I) Strong knockdown of *mosmo* led to decreased axon length in neural tube explants (n=566, two-tailed student’s t-test, \*p=7.40  $\times 10^{-12}$ ). All measures were normalized to their respective control injected with the same morpholino amount. Representative schematic for axon length measurements is shown on the left. (J) Representative images show forebrain (red on control image) and midbrain (blue) areas of the side injected with morpholino (right, red asterisk), which were normalized to the uninjected side (left). Strong knockdown of *mosmo* (n=67, two-tailed student’s t-test, \*p<4  $\times 10^{-13}$ ) and *polr3e* (n=48, \*p<8  $\times 10^{-4}$ ) led to decreased midbrain and forebrain area of *X. laevis* tadpoles (stained with tubulin) (Scale bar = 500  $\mu$ m). In all cases, *X. laevis* data represents strong knockdown of the 16p12.1 homologs, except for *cdr2*, which showed lethality and is represented with partial knockdown. Controls used for *Drosophila* experiments match the genetic background of the RNAi lines used. All control data for *X. laevis* represents control injected with highest amount of morpholino (50ng). Boxplots represent all data points with median, 25th and 75th percentiles, and red dotted lines indicate the control median.

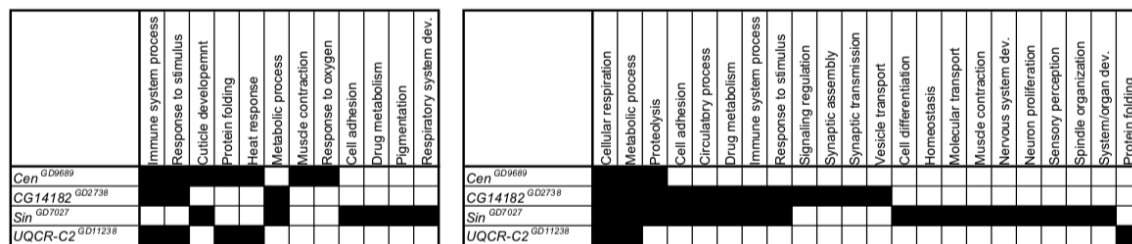


**Figure 3.3 Enriched GO terms observed with knockdown of 16p12.1 fly homologs in the nervous system**

Clusters of enriched GO biological process terms for differentially expressed fly genes observed with nervous system-specific knockdown of 16p12.1 homologs (left) and their human homologs (right). While some terms overlap, genes dysregulated with knockdown of several 16p12.1 homologs exhibit unique enrichments for GO terms, suggesting their independent action towards neuronal development.

Next, I examined developmental phenotypes associated with decreased dosage of homologs of 16p12.1 genes in *X. laevis*, a complementary vertebrate model system (**Fig 3.1** and **Fig 3.2.G**). I injected homolog-specific morpholinos at two- or four-cell stage embryos to reduce the expression of each homolog to approximately 50%, and further reduced expression with higher morpholino concentrations to increase our sensitivity to detect more specific phenotypes (**Fig 3.4.B**).

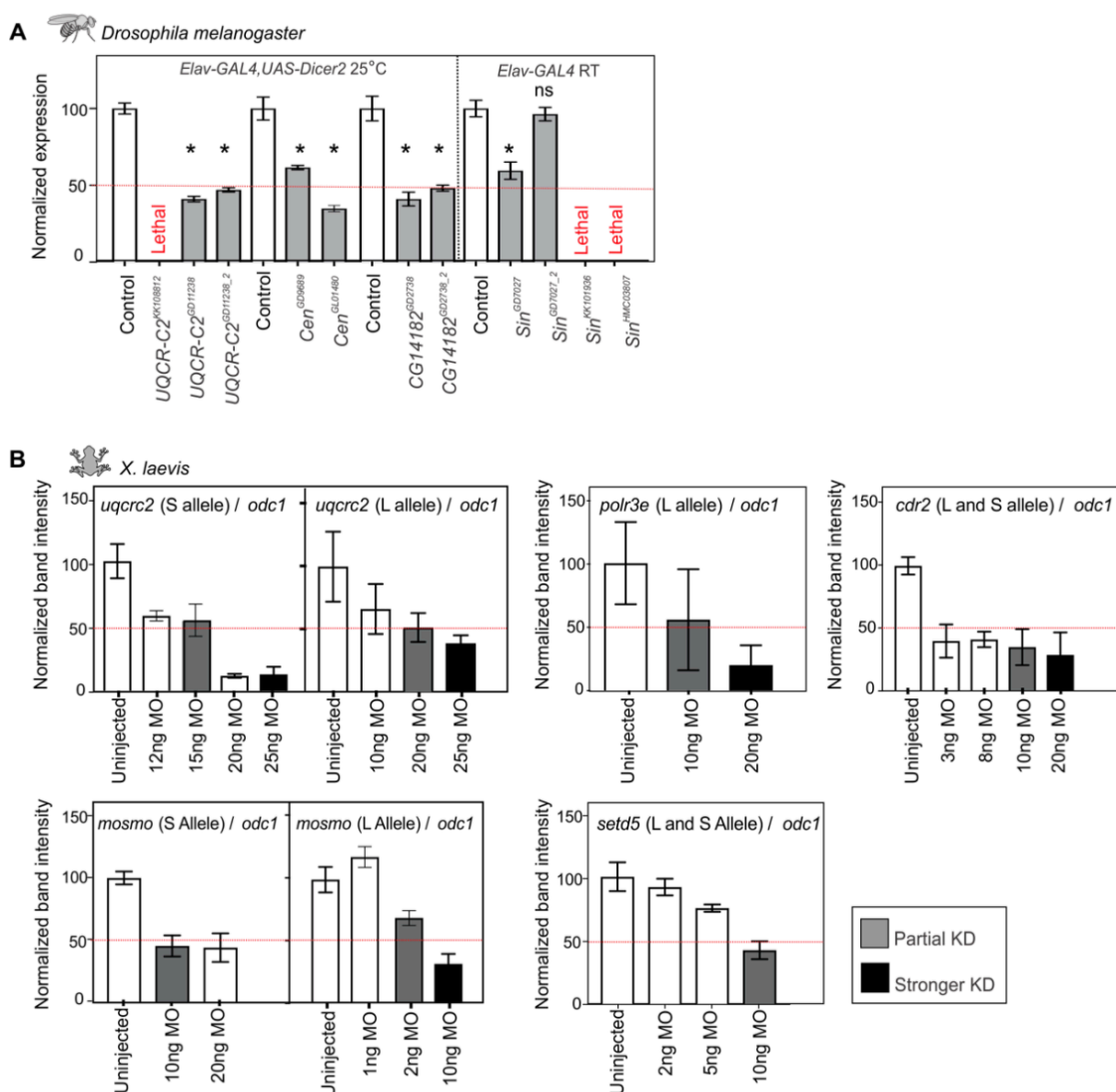


**Figure 3.4** Expression levels of 16p12.1 homologs in *Drosophila* and *X. laevis*

(A) *Drosophila* homologs of 16p12.1 genes were knocked down using nervous system-specific Elav-GAL4 driver with overexpression of *Dicer2* at 25°C. RT-qPCR confirmed 40-60% knockdown of the 16p12.1 homologs (two-tailed student's t-test, \* $p < 0.05$ ). As knockdown of *Sin* caused embryonic lethality in these conditions, all experiments in the nervous system and RT-qPCR were performed without overexpression of *Dicer2* and reared at RT. (B) Normalized band intensity of RT-PCR of *X. laevis* embryos injected with

different morpholino (MO) concentrations of the 16p12.1 homologs compared to uninjected controls. Different MO sequences were used for the L and S alleles for *uqcrc2* and *mosmo*, while unique sequences were used for both L and S alleles for *cdr2* and *setd5*. As the S allele for *polr3e* has not been annotated, only the L allele was targeted. Colored bars represent the dosages for MOs used, with grey bars indicating amounts for “partial knockdown” (approximately 50% of expression) and black bars indicating amounts for “stronger knockdown”. Bar plots represent mean  $\pm$  SD, and red dotted lines indicate 50% expression.

I first examined the craniofacial features of stage 42 tadpoles following partial depletion of individual 16p12.1 gene homologs by measuring specific facial landmarks, including face width, height and angle, and orofacial and eye area. I observed that reduced expression of either *mosmo* or *polr3e* lead to severe craniofacial defects, while milder defects were observed for *cdr2*. This suggests a role for these homologs in key developmental processes involved in craniofacial morphogenesis, such as neural crest cell formation and migration (**Fig 3.2.H** and **Fig 3.5.A**)(Hunt et al., 1991a; Hunt et al., 1991b; Lasser et al., 2019; Le Lievre and Le Douarin, 1975; Lumsden et al., 1991; Mills et al., 2019).

I next examined axon outgrowth phenotypes in neural tube explants from stage 20-22 *X. laevis* embryos following partial depletion of 16p12.1 gene homologs. I found that stronger knockdown of *mosmo* (at 20ng of morpholino) led to a significant reduction in axon length (**Fig 3.2.I** and **Fig 3.5.B**), suggesting that decreased expression of the homolog may affect the cytoskeletal signaling processes involved in axon outgrowth (Goldberg, 2003). Furthermore, stronger knockdown of *mosmo* (with 20 ng of morpholino) and *polr3e* (with 20 ng of morpholino) resulted in decreased forebrain and midbrain area (**Fig 3.2.J** and **Fig 3.5.C**), mirroring the brain size defects observed in *Drosophila* models. Interestingly, I also observed that partial knockdown of *mosmo* (with 12 ng of morpholino) led to a severe reduction in forebrain and midbrain area (**Fig 3.5.C**).

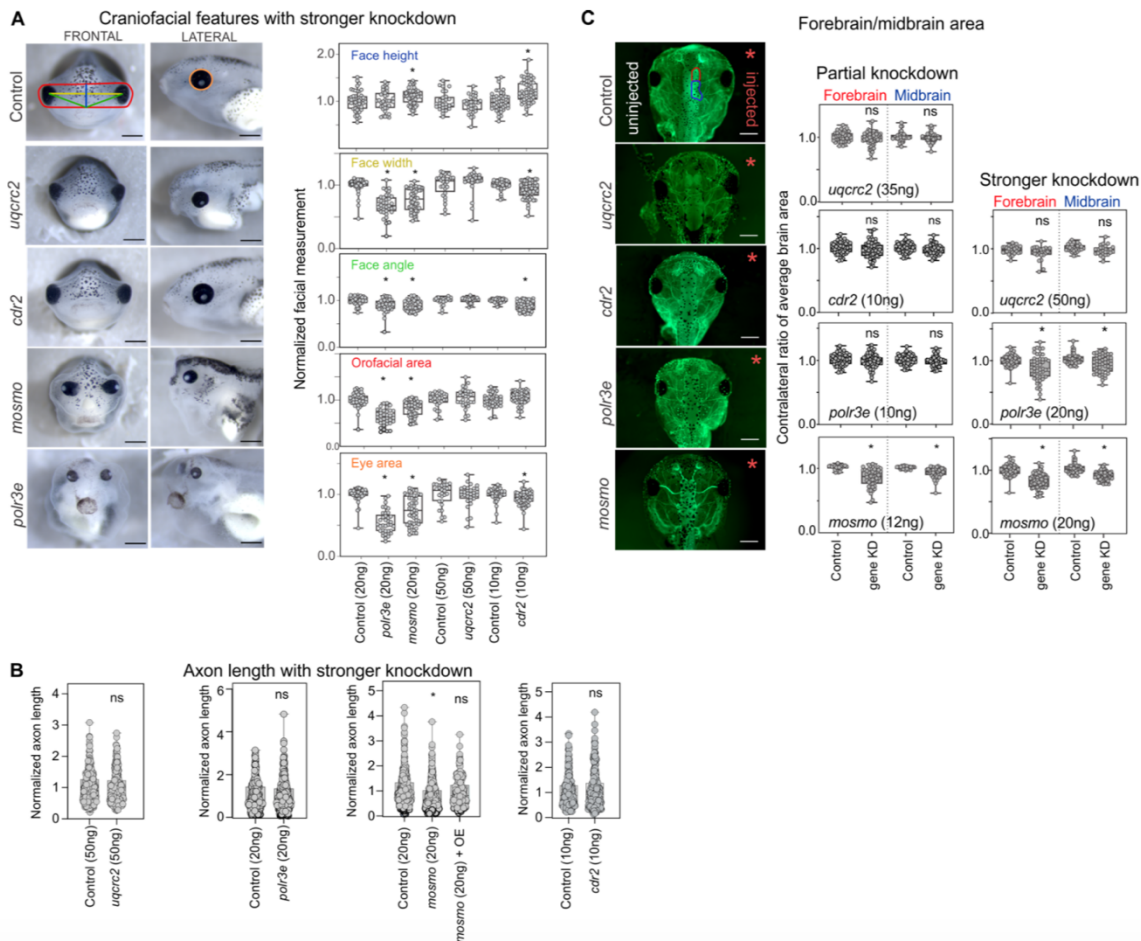


**Figure 3.5 Decreased dosage of 16p12.1 homologs leads to multiple neurodevelopmental phenotypes in *X. laevis***

(A) Representative images of tadpoles injected with control morpholino or morpholinos for 16p12.1 homologs, indicating facial landmarks for face width (yellow), height (blue), angle (green), and orofacial (red) and eye (orange) area. Boxplots showing face height, width, angle, and orofacial and eye area of each knockdown compared to its own control. Knockdown of *mosmo* ( $n=50$ , two-tailed student's t-test,  $*p=0.0102$ ) and *cdr2* ( $n=54$ ,  $*p=3.68 \times 10^{-6}$ ) led to decreased face height. Knockdown of *cdr2* ( $*p=7.75 \times 10^{-4}$ ), *polr3e* ( $n=37$ ,  $*p=1.97 \times 10^{-13}$ ) and *mosmo* ( $*p=1.36 \times 10^{-11}$ ) led to decreased face width, while knockdown of *cdr2* ( $*p=1.03 \times 10^{-8}$ ), *polr3e* ( $*p=2.73 \times 10^{-4}$ ) and *mosmo* ( $*p=3.50 \times 10^{-7}$ ) led to decreased face angle. Knockdown of *polr3e* ( $*p=3.29 \times 10^{-16}$ ) and *mosmo* ( $*p=1.47 \times 10^{-8}$ ) led to decreased orofacial area, and knockdown of *polr3e* ( $*p=1.01 \times 10^{-18}$ ), *mosmo* ( $*p=7.23 \times 10^{-10}$ ) and *cdr2* ( $*p=0.0092$ ) led to decreased eye area. Data represents strong knockdown of the 16p12.1 homologs, except for *cdr2*, which showed lethality and is represented with partial knockdown. All measures were normalized to their respective control injected with the same morpholino amount (Scale bars = 500 $\mu$ m). (B) Boxplots showing axon length of each knockdown compared to its own control. Strong knockdown of *mosmo* led to decreased axon length in neural tube explants ( $n=566$ , two-tailed student's t-test,  $*p=7.40 \times 10^{-12}$ ), which was rescued by co-injection with overexpressed (OE) mRNA of the gene ( $*p=4.06 \times 10^{-5}$ ). All measures were normalized to their respective control injected with the same morpholino amount. (C) Representative images stained with anti-tubulin show forebrain (red on control image) and midbrain (blue) areas of the side injected with morpholino (right, red asterisk), which were normalized to the uninjected side (left). Partial knockdown of *mosmo* led to decreased forebrain ( $n=47$ , two-tailed student's t-test,  $*p=1.18 \times 10^{-9}$ ) and midbrain ( $*p=1.45 \times 10^{-7}$ ) area. Graphs represent contralateral ratio of brain area compared to uninjected side of the embryo. Scale bars represent 500 $\mu$ m. All boxplots represent all data points with median, 25th and 75th

percentiles. In each case, measurements for each knockdown were compared to controls injected with equal amounts of morpholino.

To assess whether the cellular proliferation defects observed with *Drosophila* models of *MOSMO* and *POLR3E* were also present in *X. laevis* models, I performed Western blot analysis with whole embryo lysates following partial knockdown of either *mosmo* or *polr3e*, using anti-pH3 antibody as a marker for cell proliferation. I observed that knockdown of *polr3e* led to decreased cellular proliferation, validating our observations in flies (**Fig 3.6**). However, knockdown of *mosmo* did not lead to any significant changes in proliferation, potentially due to species-specific differences in sensitivity to dosage reduction, tissue and developmental stage, or inherent limitations specific to the assays. Overall, these results suggest that multiple homologs of 16p12.1 genes contribute to *Drosophila* and *X. laevis* development.

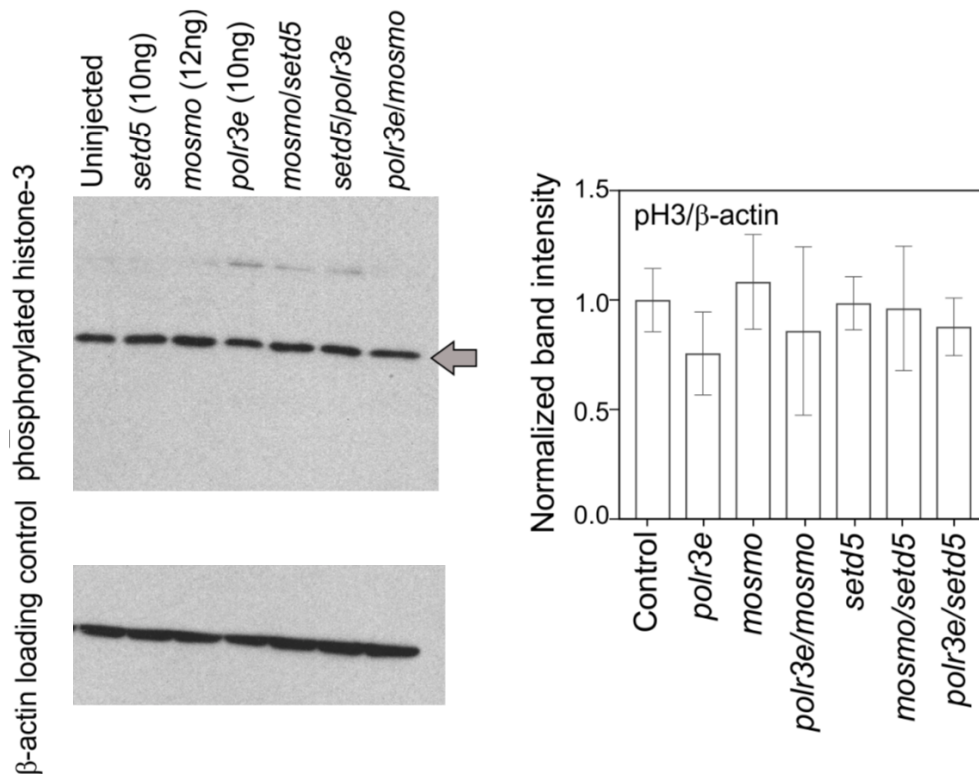


**Figure 3.6** Western blot for phosphorylated histone-3 in *X. laevis* embryos with knockdown of *polr3e*, *mosmo*, and *setd5*

Three replicate Western blot experiments were performed. The intensity of bands at 17 kDa, corresponding with pH3 (top, indicated with arrow), were normalized to the  $\beta$ -actin loading control (bottom). Partial knockdown of *polr3e* shows reduced band intensity with anti-pH3 antibody compared to  $\beta$ -actin loading control. Bar plot represents mean  $\pm$  SD.

### **3.2.2 Homologs of 16p12.1 genes independently contribute to neurodevelopmental defects**

Our collaborators previous functional studies of genes within CNV regions identified several potential models for how genes within CNVs interact with each other to influence neurodevelopmental phenotypes (Jensen and Girirajan, 2019). For example, they found that genes within the 16p11.2 region interact with each other to both enhance and suppress cellular phenotypes (Iyer et al., 2018). Moreover, my recent work shows that neuronal and cellular phenotypes of genes within the 3q29 deletion region were each enhanced with simultaneous knockdown of *Cbp20/ncbp2*, the fly and *Xenopus* homolog of *NCBP2* (Singh et al., 2020).

As multiple homologs of 16p12.1 genes contribute towards developmental, neuronal, and cellular phenotypes, my collaborators first used the sensitive fly eye system to assess for genetic interactions among the 16p12.1 fly homologs. Approximately two-thirds of *Drosophila* vital genes are expressed in the fly eye, making it a strong model to identify genetic interactions that disrupt ommatidial organization during development (Thaker and Kankel, 1992). In fact, modifier genes for homologs of several human diseases, including Spinocerebellar Ataxia type 1, Huntington's disease (Branco et al., 2008), and Fragile X syndrome (Cziko et al., 2009), have been studied in flies. Eye-specific knockdown of individual homologs was performed and the severity of eye roughness was measured using *Flynotyper*, a tool that quantifies the levels of disorderliness of ommatidia in the adult fly eye (Iyer et al., 2016). Knockdown of *Sin* and

*CG14182* led to severe eye phenotypes, including subtle disruption of ommatidial organization compared to the control, while no phenotypes were observed with knockdown of the other homologs (Fig 3.7).

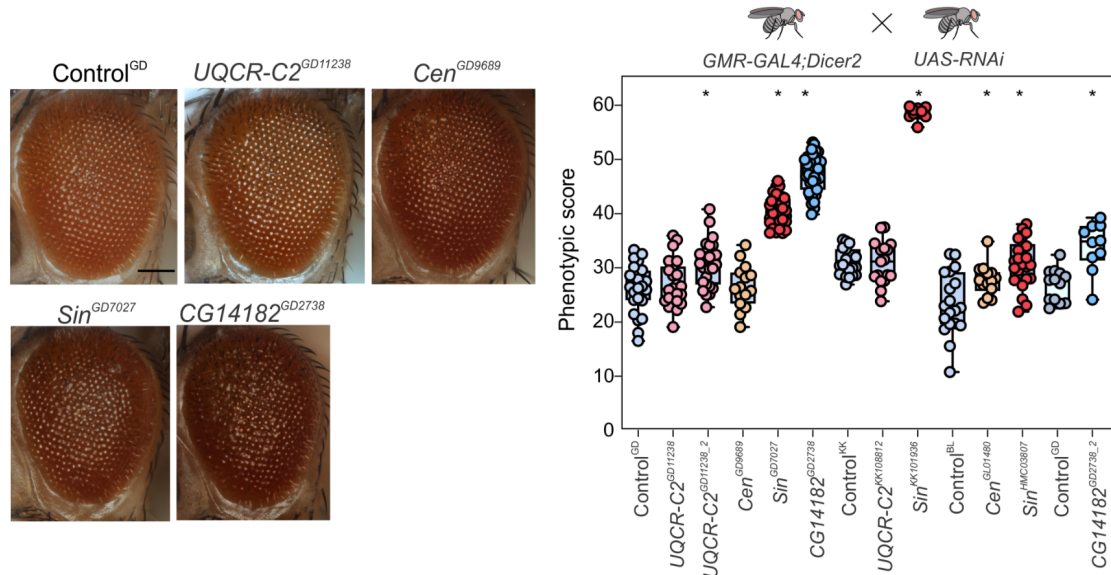


**Figure 3.7** Knockdown of *Sin* and *CG14182* lead to disruption of the fly eye

Representative images of *Flyncpter* scores of eye-specific knockdown of 16p12.1 fly homologs. Severe eye phenotypes were observed for all tested RNAi lines of *Sin* ( $*p < 2.0 \times 10^{-4}$ ) and *CG14182* ( $*p < 5.0 \times 10^{-4}$ ) (Scale bar = 100 $\mu$ m). Boxplots represent all data points with median, 25<sup>th</sup> and 75<sup>th</sup> percentiles.

Next, eye-specific recombinant lines for each homolog were generated and crossed with RNAi lines for other 16p12.1 homologs, to test a total of 30 two-hit crosses for 12 pairwise gene interactions (Fig 3.8.A). Significant changes in eye severity for four pairwise interactions were observed, validated by multiple RNAi lines, and further tested for the nature of enhancer interactions using two-way ANOVA analysis (Mackay et al., 2009) (Fig 3.8.B-C). For example, simultaneous knockdown of *UQCR-C2* with *Sin* or *CG14182* led to an increase in eye phenotype compared to knockdown of *UQCR-C2* crossed with control (Fig 3.8.D). Similarly, decreased expression of *Sin* led to an enhancement of the *CG14182* eye phenotype. Two-way ANOVA analyses indicated that

all validated enhancers among the 16p12.1 homologs were additive in nature (Mackay et al., 2009) (**Fig 3.8.D**).

As homologs of *MOSMO* and *POLR3E* individually contributed to multiple defects in both fly and *X. laevis* models, I further investigated the effect of their combined knockdown towards *X. laevis* development (**Fig 3.8.E**). Pairwise interactions in *X. laevis* models were tested using partial knockdown of the homologs to avoid potential lethality with stronger knockdown. Partial pairwise knockdown of *polr3e* (with 10ng of morpholino) and *mosmo* (with 12ng of morpholino) showed significantly reduced forebrain and midbrain area when compared to knockdown of *polr3e* alone (**Fig 3.8.F**), but not when compared to knockdown of *mosmo* alone. Similarly, I assessed whether *mosmo* and *polr3e* interact to modulate cellular proliferation processes during *X. laevis* development by evaluating the intensity of anti-pH3 signals in Western blots of the double knockdown. As with my other experiments, I did not observe any changes in anti-pH3 signals with combined knockdown of *polr3e* and *mosmo* compared with knockdown of *polr3e* alone (**Fig 3.8.G**). Overall, our analysis in *Drosophila* and *X. laevis* suggests that homologs of the 16p12.1 genes do not participate in complex interactions with each other, but individually contribute towards the tested neurodevelopmental phenotypes.

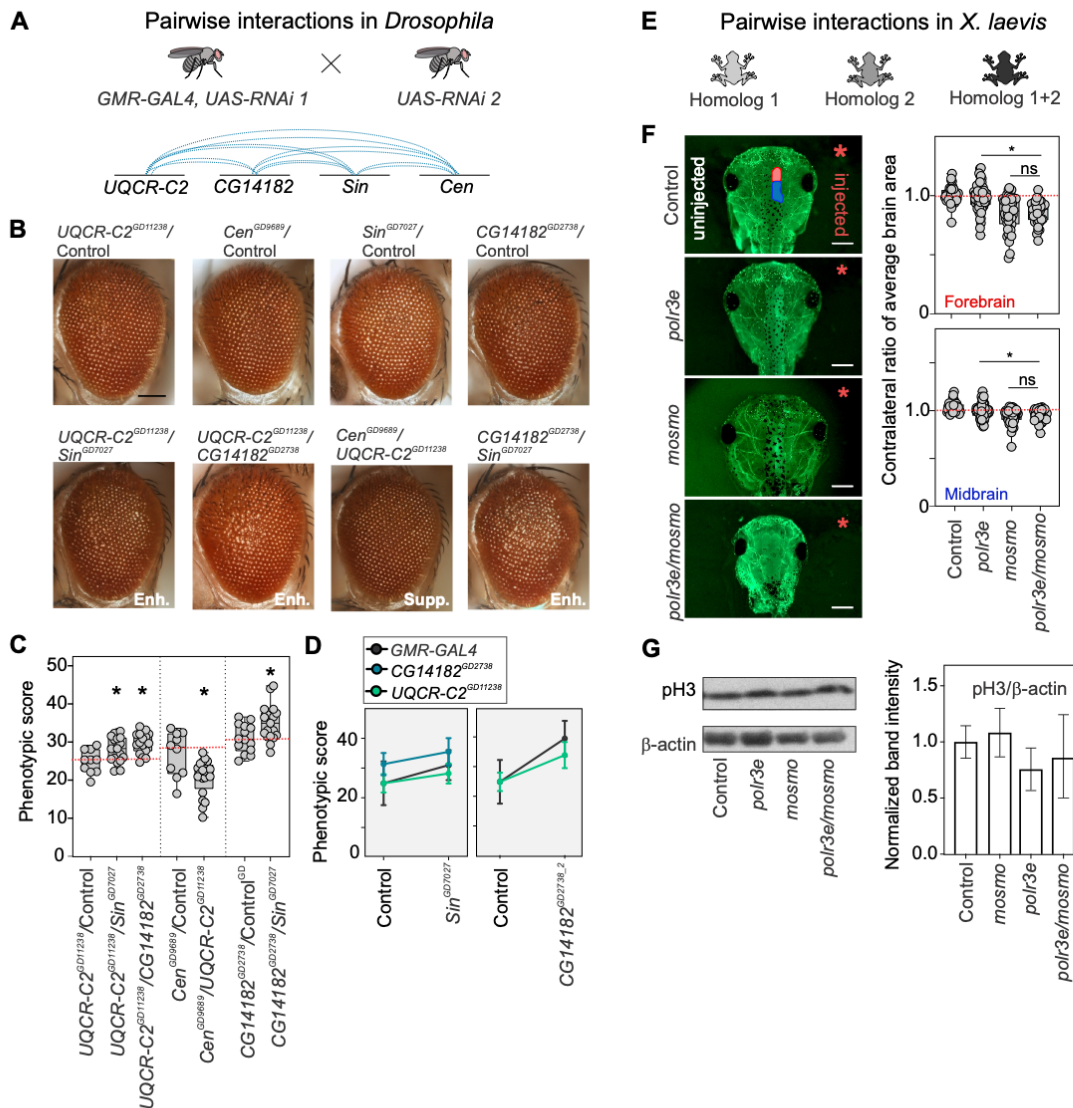


**Figure 3.8 Homologs of 16p12.1 genes independently contribute towards neurodevelopmental defects**

(A) Eye-specific recombinant lines for the four 16p12.1 homologs were generated to test a total of twelve pairwise interactions towards eye defects. (B) Representative brightfield images of *Drosophila* adult eyes for recombinant lines of 16p12.1 homologs crossed with RNAi lines for the other homologs, which show enhancement (Enh.) or suppression (Supp.) of the phenotypes compared with crosses with control background (Scale bar = 100  $\mu$ m). (C) Simultaneous knockdown of *UQCR-C2*<sup>GD11238</sup> with *CG14182*<sup>GD2738</sup> (n=18, two-tailed Mann-Whitney with Benjamini-Hochberg correction, \*p=0.002) or *Sin*<sup>GD7027</sup> (n=19, \*p=0.023) led to a significant enhancement in the eye phenotype (measured using *Flyntyper* scores) compared to single knockdown of *UQCR-C2*<sup>GD11238</sup>. Similarly, simultaneous knockdown of *CG14182*<sup>GD2738</sup> with *Sin*<sup>GD7027</sup> (n=19, \*p=0.021) enhanced the eye phenotype observed for *CG14182*<sup>GD2738</sup>. Simultaneous knockdown of *Cen*<sup>GD9689</sup> with *UQCR-C2*<sup>GD11238</sup> (n=20, \*p=0.023) led to a milder suppression of the eye phenotype compared to single knockdown of *Cen*<sup>GD9689</sup>. Double knockdowns were compared to the recombinant lines of the 16p12.1 homologs crossed with wild-type controls matching the genetic background of the second 16p12.1 homolog. (D) Interaction plots for *Flyntyper* scores of pairwise knockdowns that led to a significant enhancement of the eye phenotype of individual 16p12.1 homologs. The interaction plots show the changes in *Flyntyper* scores (mean  $\pm$  s.d.) for control (grey) or *CG14182*<sup>GD2738</sup> (blue) and *UQCR-C2*<sup>GD11238</sup> (green) recombinant lines crossed with either wild-type control background (left) or with *Sin*<sup>GD7027</sup> and *CG14182*<sup>GD2738\_2</sup> as second-hits (right). Two-way ANOVA tests showed no epistatic effects for the interactions, suggesting additive effects of the homologs towards eye phenotypes. (E) Double knockdowns

of 16p12.1 homologs were generated in *X. laevis* models by co-injecting embryos with morpholinos of two homologs. All double knockdown experiments were performed with partial knockdown of the genes, to avoid potential lethality with stronger knockdown. (F) Representative images of tadpoles stained with anti-tubulin show forebrain (red on control image) and midbrain (blue) areas of the side injected with morpholino (right, red asterisk), which were normalized to the uninjected side (left). Simultaneous knockdown of *polr3e* and *mosmo* led to decreased forebrain ( $n=36$ , two-tailed student's t-test,  $*p=1.1\times 10^{-9}$ ) and midbrain area ( $*p=1.98\times 10^{-7}$ ), which were not different than the partial knockdown of *mosmo* alone. Control data represents control injected with highest amount of morpholino (22ng) (Scale bar = 500  $\mu\text{m}$ ). (G) Representative western blots show bands for phosphorylated histone-3 (pH3) and  $\beta$ -actin for the uninjected control, knockdown of *polr3e*, knockdown of *mosmo*, and pairwise knockdown of *polr3e* and *mosmo*. Bar plot shows intensity of pH3 band normalized to  $\beta$ -actin. Simultaneous knockdown of *polr3e* and *mosmo* does not lead to changes in the proliferation defects observed with knockdown with *polr3e* alone. Boxplots represent all data points with median, 25th and 75th percentiles, and red dotted lines indicate the control median.

### 3.2.3. Homologs of patient-specific “second-hit” genes modulate phenotypes of

#### 16p12.1 homologs

My collaborators recently identified that an increased burden of rare variants (or “second hits”) outside of disease-associated CNVs, such as 16p11.2 deletion, 15q13.3 deletion, and 16p12.1 deletion, contributed to the variability of cognitive and developmental phenotypes among affected children with these CNVs (Girirajan et al., 2012; Girirajan et al., 2010a; Pizzo et al., 2018). In fact, they found that severely affected children with the 16p12.1 deletion had additional loss-of-function or severe missense variants within functionally-intolerant genes compared to their mildly-affected carrier parents (Girirajan et al., 2012; Girirajan et al., 2010a; Pizzo et al., 2018). Therefore, we hypothesized that homologs of genes carrying patient-specific “second hits” modulate the effects of individual 16p12.1 homologs not only additively but also in an epistatic manner.

To test this, my collaborators first performed 227 crosses to study 96 pairwise interactions between eye-specific recombinant fly lines for each of the four 16p12.1 homologs and 46 RNAi or mutant lines for 24 homologs of patient-specific “second-hit” genes identified in 15 families with 16p12.1 deletion (Pizzo et al., 2018). Out of the 24

“second-hit” homologs tested, 12 enhanced and 3 suppressed one or more 16p12.1 homologs, with a total of 11 out of 15 families with interacting “second-hit” genes (**Fig 3.9.A**). Interestingly, different “second-hit” homologs showed differential patterns of interactions with homologs of 16p12.1 genes (**Fig 3.9.A**). For example, the affected child in family GL\_11 carried “second-hit” pathogenic mutations in *NRXN1* and *CEP135*. Knockdown of the fly homolog *Nrx-1* enhanced the eye phenotype caused by knockdown of *Sin* and *UQCR-C2*, while knockdown of *Cep135* suppressed the eye phenotype caused by knockdown of *UQCR-C2* (**Fig 3.9.A**). Likewise, the affected child in family GL\_01 carried an inherited “second-hit” variant in *LAMC3*, as well as a *de novo* loss-of-function mutation in the intellectual disability-associated and chromatin regulator gene *SETD5* (Grozeva et al., 2014) (**Fig 3.9.A**). Knockdown of *Lanb2*, homolog of *LAMC3*, and *upSET*, homolog of *SETD5*, led to additive enhancements of the phenotypes caused by knockdown of *UQCR-C2* and *Sin*, respectively (**Fig 3.9.A**). However, knockdown of *upSET* synergistically enhanced the eye phenotype observed with knockdown of *CG14182*.

To assess the cellular processes affected by these interactions, apoptosis and proliferation processes in the third instar larval eye discs were observed, and simultaneous knockdown of *CG14182* and *upSET* led to an increase in the number of cells undergoing cellular proliferation and apoptosis compared to knockdown of *CG14182* alone (**Fig 3.9.B**). Interestingly, epistatic interactions between *CG14182* and other chromatin modifier genes were identified, including *Nipped-A*, a transcriptional target of *Sin*, and *Osa*, homolog of the “second-hit” gene *ARID1B*, identified in family

GL\_13. These interactions also modulated cellular proliferation and apoptosis processes in the developing eye discs with knockdown of *CG14182* (data not shown).

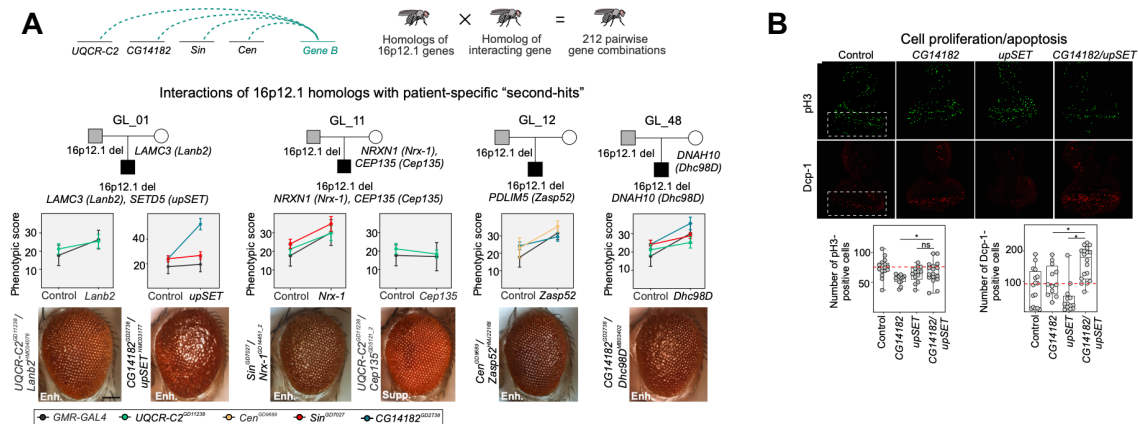


**Figure 3.9 Fly homologs of 16p12.1 genes show complex interactions with homologs of patient-specific “second-hit” and neurodevelopmental genes**

(A) Eye-specific recombinant lines for each homolog with a total of 124 RNAi, mutant, or overexpression lines for 76 interacting genes were generated to test a total of 212 pairwise gene combinations. Evaluation of how homologs of genes outside of the CNV region (Gene B) affect phenotypes observed for 16p12.1 gene homologs was performed, including genes carrying “second-hit” variants in children with the 16p12.1 deletion, genes within conserved neurodevelopmental pathways, and transcriptome targets. Representative pedigrees of families with 16p12.1 deletion (affected child in black, carrier parent in grey) that were selected to study the effect of homologs (represented within parenthesis) of genes carrying “second-hits” towards phenotypes of homologs of 16p12.1 genes. Interaction plots and representative brightfield adult eye images for validated enhancers (Enh.) or suppressors (Supp.) are shown below each pedigree. Interaction plots show the changes in Flyopter scores (mean  $\pm$  S.D.) for control (grey) or recombinant lines of 16p12.1 homologs crossed with either wild-type control background line (left) or with “second-hit” homologs (right). Two-way ANOVA analyses showed epistatic enhancements for *CG14182<sup>GD2738</sup>/upSET<sup>HMC03177</sup>*, *Sin<sup>GD7027</sup>/Dhc98D<sup>MB03402</sup>*, and *UQCR-C2<sup>GD11238</sup>/Dhc98D<sup>MB03402</sup>* ( $p < 0.05$  with Benjamini-Hochberg correction), while *Cep135<sup>GD5121-2</sup>* suppressed *UQCR-C2<sup>GD11238</sup>* (Scale bar = 100  $\mu$ m). (B) Representative confocal images of third instar larval eye discs stained with anti-phosphorylated histone-3 (pH3, green) or anti-Dcp-1 (red), markers of cellular proliferation and apoptosis, respectively. Positive pH3 or Dcp-1 cells were quantified posterior to the morphogenetic furrow, indicated by white boxes in left panels. Double knockdown of *CG14182<sup>GD2738</sup>/upSET<sup>HMC03177</sup>* led to increased pH3 ( $n=17$ , two-tailed Mann-Whitney,  $*p=0.0458$ ) and Dcp-1 ( $n=19$ ,  $*p=0.0055$ ) positive cells compared to knockdown of *CG14182<sup>GD2738</sup>* alone. The double knockdown also led to increased Dcp-1 positive cells compared to knockdown of *upSET<sup>HMC03177</sup>* alone ( $*p=2.19 \times 10^{-5}$ ) (Scale bar = 50  $\mu$ m).

I further evaluated whether interactions between the fly homologs of *POLR3E* and *MOSMO* with *SETD5* were also conserved during vertebrate development, and studied brain and axon outgrowth phenotypes of homologs of these genes in *X. laevis*. I observed that simultaneous knockdown of *polr3e* and *setd5* led to smaller forebrain and midbrain areas compared with *polr3e* knockdown alone (Fig 3.10.A). Similarly,

simultaneous knockdown of *mosmo* and *setd5* led to a significant reduction in midbrain area compared to knockdown of *mosmo* alone (**Fig 3.11.A**). Furthermore, analysis of axon outgrowth in developing *X. laevis* embryos showed that simultaneous knockdown of *mosmo* and *setd5* led to a significantly reduced axon length compared to the individual knockdowns of both *mosmo* or *setd5*, while no changes were observed for knockdown of *polr3e* and *setd5* (**Fig 3.10.B** and **Fig 3.11.B**). This result mirrors the interactions observed in *Drosophila* eye development, and suggests a synergistic interaction between *mosmo* and *setd5* during nervous system development. Overall, our results show that both additive and epistatic interactions with “second-hit” genes modulate neurodevelopmental and cellular phenotypes associated with homologs of the 16p12.1 genes.

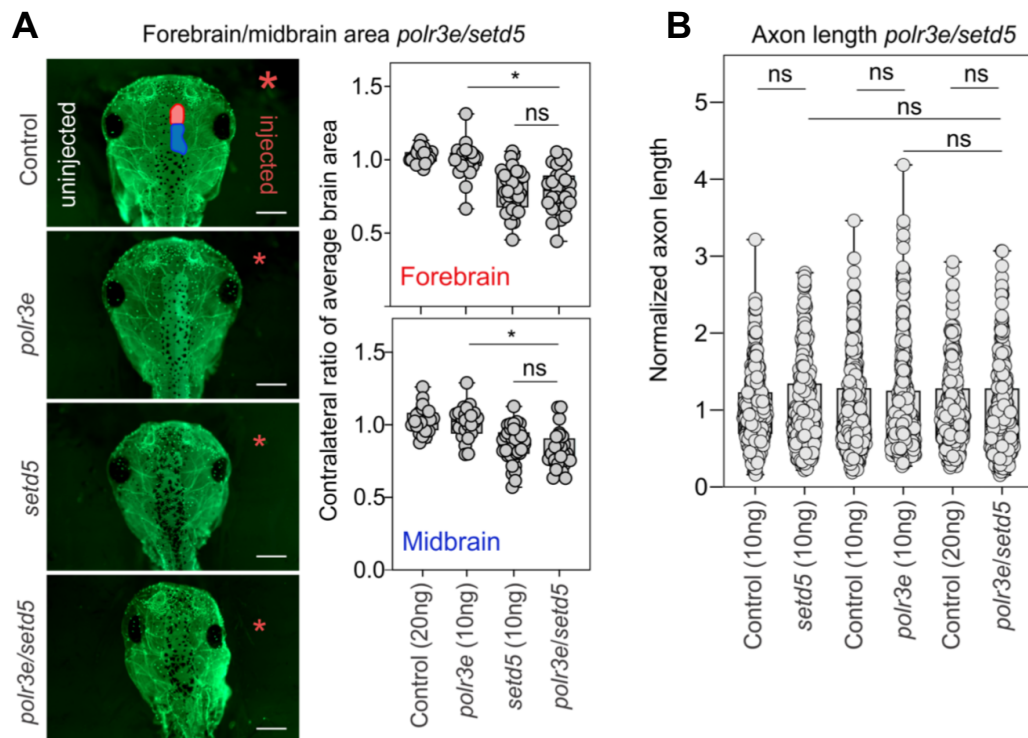


**Figure 3.10** *setd5* establishes additive interactions with *polr3e* in *X. laevis*

(A) Representative images stained with anti-tubulin show forebrain (red on control image) and midbrain (blue) areas of the side injected with morpholino (right, red asterisk), normalized to the uninjected side (left). Simultaneous knockdown of *polr3e* and *setd5* in *X. laevis* led to decreased forebrain ( $n=28$ , two-tailed student's t-test,  $*p=6.01 \times 10^{-7}$ ) and midbrain area ( $*p=1.67 \times 10^{-7}$ ) compared to knockdown of *polr3e* alone, which were not different to the partial knockdown of *setd5* alone (two-tailed student's t-test,  $p>0.05$ ) (Scale bar = 500  $\mu\text{m}$ ). (B) Normalized axon length of *X. laevis* embryos with simultaneous knockdown of *polr3e*

and *setd5* showed no change in axon length two-tailed student's t-test,  $p > 0.05$ ). In each case, the individual knockdown was normalized and compared to the control injected with the same amount of morpholino. Boxplots represent all data points with median, 25th and 75th percentiles.

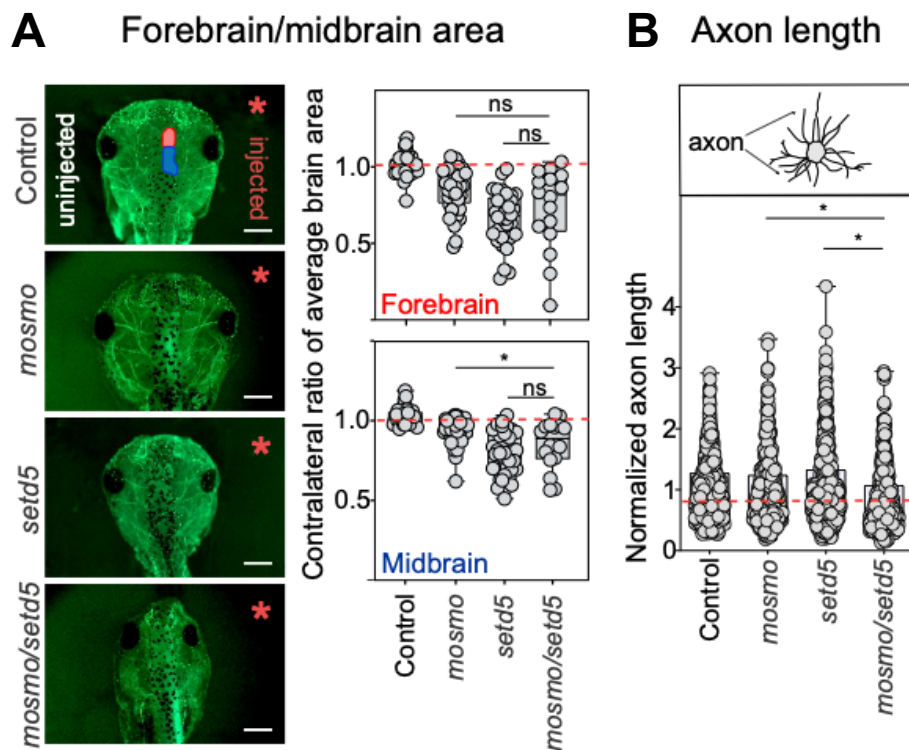


**Figure 3.11** *setd5* establishes synergistic interactions with *mosmo* in *X. laevis*

(A) Representative images of tadpoles stained with anti-tubulin show forebrain (red on control image) and midbrain (blue) areas of the side injected with morpholino (right, red asterisk), which were normalized to the uninjected side (left). Partial knockdown of *mosmo* with *setd5* led to a reduction in the midbrain area compared to the knockdown of *mosmo* alone ( $n=16$ , two-tailed student's t-test,  $*p=0.0472$ ). Control data represents control injected with highest amount of morpholino (22ng) (Scale bar = 500  $\mu\text{m}$ ). (B) Normalized axon length of *X. laevis* embryos with simultaneous knockdown of *mosmo* and *setd5* led to a significant reduction in axon length that was not observed for the single knockdown of *mosmo* ( $n=438$ , two-tailed student's t-test,  $*p=3.34 \times 10^{-6}$ ) or *setd5* ( $*p=1.86 \times 10^{-9}$ ). All measures were normalized to their respective control injected with the same morpholino amount. Control data represents control injected with highest amount of morpholino (22ng). All double knockdown experiments were performed with partial knockdown of the genes, to avoid potential lethality with stronger knockdown. Boxplots represent all data points with median, 25th and 75th percentiles, and red dotted lines indicate the control median.

### 3.3 Discussion

We previously described multiple models for how genes within CNVs contribute towards neurodevelopmental phenotypes (Iyer et al., 2018; Jensen and Girirajan, 2019; Singh et al., 2020). Here, we analyzed the cellular and molecular mechanisms of individual and pairwise knockdown of 16p12.1 homologs in *Drosophila* and *X. laevis* to

understand how genes within the deletion contribute to neurodevelopmental phenotypes. Our results provide multiple conclusions of how homologs of 16p12.1 genes lead to developmental defects. First, in line with our previous findings for other CNV regions, our results show that no single homolog within the region is solely responsible for the observed neurodevelopmental phenotypes. In fact, we observed a global developmental role for multiple 16p12.1 homologs, as well as specific roles of each homolog towards craniofacial and brain development (**Table 2**). These findings are in accordance with the core biological functions described for some of these genes. For example, *POLR3E* encodes a cofactor of the RNA polymerase III, which is involved in the transcription of small RNA, 5S ribosomal RNA and tRNA (Hu et al., 2002), while *MOSMO* is a negative regulator of the hedgehog signaling pathway (Pusapati et al., 2018b). Second, knockdown of individual homologs sensitized both model organisms towards specific phenotypes. For example, knockdown of *CG14182/mosmo* led to neuronal morphology defects and *Sin/polr3e* knockdown led to cellular proliferation defects in both model systems, while knockdown of *UQCR-C2* led to seizure susceptibility in flies. Third, our interaction studies showed that 16p12.1 homologs independently contribute towards specific developmental phenotypes, including eye, brain and cellular proliferation defects. While we only examined cellular phenotypes and interactions of four non-syntenic conserved homologs in *Drosophila*, our analyses of all seven human genes in the context of a brain specific interaction network further supported an additive model for the deletion. Overall, we show that multiple 16p12.1 homologs independently contribute towards a range of developmental features, and that their combined effects sensitize the human genome towards multiple neurodevelopmental outcomes.

We recently showed that additional variants or “second-hits” in the genetic background modulate the manifestation of developmental and cognitive phenotypes associated with disease-causing variants (Girirajan et al., 2012; Girirajan et al., 2010a; Pizzo et al., 2018), including intelligence quotient and head circumference phenotypes. Using the 16p12.1 deletion as a paradigm for complex genetics, we examined how “second-hit” variants of modest and high effect size modulate the phenotypes caused by decreased expression of CNV genes. We observed that 16p12.1 homologs interact with background-specific variants, as they exhibited variable phenotypes in different *Drosophila* strains. Furthermore, knockdown of homologs of genes carrying “second-hits” in severely affected children with 16p12.1 deletion modified the phenotypes associated with the 16p12.1 homologs through complex interactions. In fact, while two-thirds (9/15) of the interacting genes additively modified the phenotypes of the homologs, the remainder of the interactions were epistatic in nature (6/15). For example, homologs of *ARID1B*, *CEP135* and *CACNA1A* suppressed the eye phenotypes of one or multiple 16p12.1 homologs, while *Dhc98D*, homolog of *DNAH10*, epistatically enhanced the eye phenotype of *UQCR-C2* and *CG14182*. Furthermore, we identified a synergistic interaction between *mosmo/CG14182* and *upSET/setd5* which led to highly severe eye phenotypes in *Drosophila* and modulated brain size defects and led to axon outgrowth phenotypes in *X. laevis* not observed with individual knockdown of the homologs. (Greene et al., 2015; Krishnan et al., 2016). Interestingly, mouse embryonic stem cells lacking *Setd5* exhibited dysregulation of genes involved in hedgehog signaling (Osipovich et al., 2016), pathway recently associated with *MOSMO* function (Pusapati et al., 2018b). Additionally, we observed non-additive interactions between *CG14182* and

other genes with chromatin regulating function, such as *Nipped-A (TRRAP)* and *osa (ARID1B)* (data not shown). Therefore, we propose that while genes carrying “second hits” may additively interact with 16p12.1 genes, they may also synergistically enhance or suppress developmental phenotypes. The ultimate nature of these interactions depends on the role of the individual CNV genes towards a specific phenotype and the genetic complexity associated with the phenotypic domain.

The high inheritance rate of the 16p12.1 deletion (Girirajan et al., 2010a; Pizzo et al., 2018) suggests that while it confers risk for multiple phenotypes, the CNV can be transmitted throughout generations until additional variants accumulate and cumulatively surpass the threshold for severe disease. In contrast, the autism-associated 16p11.2 deletion occurs mostly *de novo* and is less likely to co-occur with another “second-hit”, suggesting a higher pathogenicity of the deletion on its own (Girirajan et al., 2012). Several lines of evidence from our functional analyses suggest that the differential pathogenicity of the CNVs could be explained by the differential connectivity of genes within each region. First, we observed more complex genetic interactions among 16p11.2 homologs compared to 16p12.1 homologs. Second, transcriptome analyses showed a higher overlap of differentially expressed genes in 16p11.2 compared to 16p12.1 homologs, further suggesting a higher functional relatedness among the 16p11.2 genes. Third, 16p11.2 genes showed higher connectivity between each other in a human brain network compared to 16p12.1 genes, suggesting that the human 16p11.2 genes could work more closely together in the brain. Furthermore, we observed that the genes connecting pairs of 16p11.2 genes were uniquely enriched for genes intolerant to functional variation, suggesting that the 16p11.2 deletion affects a tight network of genes

in the brain, including other neurodevelopmental genes (Krumm et al., 2015; Petrovski et al., 2013). For example, *ASH1L*, a histone methyltransferase activator and autism candidate gene (Iossifov et al., 2015), and *CAMK2B*, a protein kinase gene causative for intellectual disability (Kury et al., 2017), are connectors of 16p11.2 genes, while the connector genes unique to 16p12.1 genes were not associated with neurodevelopmental disease (data not shown). The high functional connectivity among the 16p11.2 genes may also explain the high phenotypic robustness observed with knockdown of *CG10465*. These observations are in line with the large-scale network studies in yeast, which showed that genes within highly connected networks are more likely to exhibit robust phenotypes and are less likely to be modified by additional genetic variants (Hou et al., 2018). In contrast, 16p12.1 genes are less tightly connected in a human brain network, and thus more easily affected by variants in the genetic background. Furthermore, Andrews and colleagues showed that functionally related genes are clustered within pathogenic *de novo* CNVs compared to benign CNVs (Andrews et al., 2015a). Here, our results provide further functional evidence for diverse mechanisms of action for genes within CNV regions that confer different degrees of pathogenicity.

In this work, we postulate that multiple conserved genes within the 16p12.1 region independently sensitize an individual towards developmental features, and their phenotypes are modulated by complex interactions with genes that carry “second-hit” variants. The individual and combined contribution of these genes towards developmental phenotypes will need to be further examined in higher order model systems, including mouse and human cellular models. Contiguous gene models have been previously proposed for the independent contribution of CNV genes towards

phenotypes, such as those affected by the 7q11.23 deletion in Williams Syndrome (Schubert, 2009). Here, we propose that 16p12.1 genes independently sensitize towards different domains of disease, but the ultimate phenotypic manifestation depends on the effects of other variants in the genetic background. Our results highlight the importance of a thorough functional characterization of both individual CNV genes and their interactions with genes carrying “second-hit” variants towards disease-associated phenotypes.

		Experiment		16p12.1 deletion homolog			
		Phenotype	Assay	<i>UQCR-C2</i>	<i>Cen</i>	<i>Sin</i>	<i>CG14182</i>
<i>Drosophila melanogaster</i>	Adult eye morphology	Eye phenotype (overexpression of <i>Dicer2</i> )		Normal	Normal	Rough eye	Rough eye
		Eye phenotype (no overexpression of <i>Dicer2</i> )		Normal	Normal	Moderate rough eye	Normal
	Role in development	Ubiquitous knockdown		Larval lethal	Normal	Larval lethal	Normal
		Wing development		Lethal	Normal	Severe phenotype	Normal
	Neuronal phenotypes	Lifespan		Increased	Normal	Reduced	Reduced
		Developmental timing		Normal	Normal	Delayed	Delayed
		Seizure susceptibility		Increased	Normal	Normal	Normal
		Complexity of dendritic arbors		Normal	Normal	Normal	Reduced
		Brain size		Normal	Normal	Reduced	Reduced
	Cellular proliferation (developing brain)	pH3 staining		NA	NA	Reduced	Reduced
	Apoptosis (developing brain)	Dcp-1 staining		NA	NA	Reduced	Normal
	RNA sequencing (adult heads)	Differential gene expression (fly homologs)		Protein folding, heat shock	Protein folding, heat shock protein, muscle contraction	Cell adhesion, respiratory system development	No clear relevant functional enrichment
		Differential gene expression (human homologs)		Protein folding	Proteolysis	Muscle contraction, nervous system development, system/organ development	Synapse assembly and transmission, histone methyltransferase function, small nuclear ribonuclear complex

		Experiment		16p12.1 deletion homolog			
		Phenotype	Assay	<i>uqcr2</i>	<i>cdr2</i>	<i>polr3e</i>	<i>mosmo</i>
<i>Xenopus laevis</i>	Craniofacial features	Face width		Normal	Decreased	Decreased	Decreased
		Face height		Normal	Increased	Normal	Increased
		Orofacial area		Normal	Normal	Decreased	Decreased
		Eye area		Normal	Decreased	Decreased	Decreased
		Face angle		Normal	Decreased	Decreased	Decreased
	Brain phenotypes	Forebrain size (partial KD)		Normal	Normal	Normal	Reduced
		Midbrain size (partial KD)		Normal	Normal	Normal	Reduced
		Forebrain size (stronger KD)		Normal	Lethal	Reduced	Reduced
		Midbrain size (stronger KD)		Normal	Lethal	Reduced	Reduced
	Axon outgrowth	Axon length (stronger KD)		Normal	Lethal	Normal	Decreased
	Cellular proliferation (developing embryo)	pH3 staining - western blot		NA	NA	Reduced	Normal

**Table 2 Phenotypes observed for individual 16p12.1 gene homologs in *Drosophila* and *X. laevis***

### 3.4 Materials and Methods

#### 3.4.1. *Drosophila* stocks and genetics

Using *Ensembl* database (Yates et al., 2020), NCBI Protein-Protein BLAST tool (Altschul et al., 1997), and DRSC Integrative Ortholog Prediction Tool (DIOPT) (Hu et al., 2011), four homologs were identified out of the seven genes within the 16p12.1 deletion region in *Drosophila melanogaster*. No fly homologs were present for three genes, including *VWA3A*, *PDZD9* and *EEF2K*. Fly Atlas Anatomy microarray expression data from FlyBase confirmed the expression of the 16p12.1 homologs in the nervous system during *Drosophila* development (Chintapalli et al., 2007). Similar strategies were used to identify fly homologs of conserved neurodevelopmental genes and genes carrying “second hits” in children with the 16p12.1 deletion. RNAi, mutant or overexpression lines for fly homologs were obtained from the Vienna Stock Resource Center (VDRC), Bloomington *Drosophila* Stock Center (BDSC), or Kyoto Stock Center. The following lines used were generated from various research labs: *Drice*<sup>17-1</sup> and *Drice*<sup>17-2</sup> from Bergmann lab (Xu et al., 2006), *GluRIIB*<sup>Overexp EGFP</sup> from Sigrist lab (Schmid et al., 2008), *Hsp26*<sup>Overexp Hsp26</sup> from Benzer lab (Wang et al., 2004), and *Hsp70Ab*<sup>Overexp Hsp70-9.1</sup> and *Hsp70Ab*<sup>Overexp Hsp70-4.3</sup> from Robertson lab (Xiao et al., 2007). Tissue-specific knockdown of homologs of 16p12.1 genes was achieved using the *UAS-GAL4* system, with specific lines including *w*<sup>1118</sup>; *dCad-GFP*, *GMR-GAL4/CyO* (Zhi-Chun Lai, Penn State University), *w*<sup>1118</sup>; *GMR-GAL4*; *UAS-Dicer2* (Claire Thomas, Penn State University), *w*<sup>1118</sup>; *mcd8-GFP*, *Elav-GAL4/Fm7c*; *UAS-Dicer2* (Scott Selleck, Penn State University), *w*<sup>1118</sup>; *Elav-GAL4* (Mike Groteweil, VCU), *w*<sup>1118</sup>; *Elav-GAL4*, *UAS-Dicer2* (Scott Selleck, Penn State University), *w*<sup>1118</sup>; *da-GAL4* (Scott Selleck, Penn State

University),  $w^{1118}, bx^{MS1096}-GAL4$ ;  $UAS-Dicer2$  (Zhi-Chun Lai, Penn State University), and  $UAS-Dicer2; ppk-GAL4, UAS-mCD8-GFP$  (Melissa Rolls, Penn State University). Fly crosses were reared on a cornmeal-sucrose-dextrose-yeast medium at room temperature (RT), 25°C or 30°C. In all cases, eye phenotypes were compared to a control with the same genetic background to account for background-specific effects. Three different controls were used:  $w^{1118}$  GD from VDRC (line v60000), in which inverted repeats are inserted by P-element insertion;  $y, w^{1118}$  KK from VDRC (line v60100), where inverted repeats are inserted by site-specific recombination; and  $\{y[1] v[1]; P\{y[+t7.7]=CaryP\}attP2$  from BDSC (line BL36303).

#### 3.4.2. RT-quantitative PCR for *Drosophila* RNAi knockdown of 16p12.1 homologs

Decreased expression of homologs of 16p12.1 genes in the nervous system was confirmed using reverse transcription quantitative PCR (RT-qPCR) for individual *Drosophila* RNAi lines. Decreased expression of the genes was achieved using  $Elav-GAL4; UAS-Dicer2$  lines, reared at 25°C. As nervous system-specific knockdown of *Sin* with  $Elav-GAL4; UAS-Dicer2$  caused developmental lethality in all three RNAi lines studied ( $Sin^{GD7027}$ ,  $Sin^{KK101936}$ ,  $Sin^{HMC03807}$ ), knockdown of *Sin* was confirmed using  $Elav-GAL4$  without overexpression of *Dicer2* and reared at RT. All experiments with nervous system-specific knockdown of *Sin* were performed under these conditions. Briefly, three biological replicates, each containing 35-40 F1 female heads, were collected after being separated by repeated freezing in liquid nitrogen and vortex cycles. Total RNA was extracted from *Drosophila* heads using TRIzol (Invitrogen, Carlsbad, CA, USA), and cDNA was generated using qScript cDNA synthesis kit (Quantabio, Beverly, MA, USA).

Quantitative RT-PCR was performed in an Applied Biosystems Fast 7500 system using SYBR Green PCR master mix (Quantabio), with rp49 as the reference gene. Primers were designed using NCBI Primer-BLAST, with primer pairs separated by an intron in the corresponding genomic DNA, if possible. The delta-delta Ct method was used to calculate the percentage of expression compared to the control (Livak and Schmittgen, 2001), and statistical significance compared to the control was identified using t-tests.

### **3.4.3. Eye imaging**

Eye-specific knockdown of the 16p12.1 homologs was achieved using *GMR-GAL4* driver at 30°C. Female progeny were collected on day 2-3 and imaged using an Olympus BX53 compound microscope with LMPLan N 20X air objective and a DP73 c-mount camera at 0.5X magnification, with a z-step size of 12.1µm (Olympus Corporation, Tokyo, Japan). Individual image slices were captured using the CellSens Dimension software (Olympus Corporation, Tokyo, Japan), and were stacked into their maximum projection using Zerene Stacker (Zerene Systems, Richland, WA, USA). 10-30 eye images were assessed for rough, glazed, eye size, and necrotic patches defects. Quantitative assessment of rough adult eye phenotypes was performed using a software called *Flynotyper* (Iyer et al., 2018; Iyer et al., 2016), which calculates a phenotypic score for each eye image by integrating the distances and angles between neighboring ommatidia. The phenotypic scores generated by *Flynotyper* were compared between RNAi lines and their respective controls using one-tailed Mann-Whitney tests, with Benjamini-Hochberg correction for multiple tests.

### **3.4.4. Lifespan Measurement**

Lifespan assessment of homologs of 16p12.1 genes was performed as previously reported (Sun et al., 2013). Briefly, fly crosses were set up at 25°C with *Elav-GAL4;;UAS-Dicer2* for each of the fly homologs, or *Elav-GAL4* at RT for *Sin<sup>GD7027</sup>*. In all cases, emerged F1 progeny were collected every day for five consecutive days, and the birth date was recorded. F1 flies were let to mate for 24 hrs., and were separated under CO<sub>2</sub> into at least four vials, each containing 20 females. Vials were transferred every 2-3 days, and the age and number of alive flies were registered. One-way repeated measures ANOVA with post-hoc pairwise t-tests were performed to identify changes in lifespan for the individual 16p12.1 homologs.

#### **3.4.5. Assessment of delay in developmental timing**

Pupariation time was assessed in third instar larvae obtained from crosses between RNAi lines and *w<sup>1118</sup>;;Elav-GAL4,UAS-Dicer2* or *w<sup>1118</sup>,Elav-GAL4* flies. Developmentally-synced larvae were obtained from apple juice plates with yeast paste, and were reared for 24 hrs. Thirty newly emerged first instar larvae were transferred to culture vials, for a total of five to ten vials per RNAi line. The number of larvae transitioning to pupae cases in the F1 progeny was counted every 24 hrs. Significant differences in pupariation timing compared with the control across the duration of the experiment was identified with one-way repeated measures ANOVA and post-hoc pairwise t-tests.

#### **3.4.6. Dendritic arborization experiments**

Class IV sensory neuron-specific knockdown was achieved by crossing the RNAi lines to *UAS-Dicer2; ppk-GAL4* driver at 25°C in apple juice plates. First instar larvae were

collected and transferred to cornmeal-based food plates for 48 h. Z-stack images of the dorsal side of third instar larvae were obtained using a Zeiss LSM 800 (Zeiss, Thornwood, NY, USA) confocal microscope. To perform Sholl analyses, the number of intersections of dendrite branches was assessed with four concentric circles starting from the cell body and separated by 25  $\mu\text{m}$ . The total number of intersections was normalized to the width of the larval hemi-segment, and significant changes compared with control were assessed using two-tailed Mann-Whitney tests.

#### **3.4.7. Measurement of larval brain area**

Larval brain area was assessed in third instar larvae obtained from crosses between the RNAi lines with *Elav-GAL4*. Crosses were set up in apple plates containing yeast paste to control for size effects generated by food availability. Fifteen first instar larvae were transferred to culture vials containing a fixed volume (8-10 mL) of cornmeal-based food. Brains were dissected from third instar larva in PBS (13mM NaCl, 0.7mM Na<sub>2</sub>HPO<sub>4</sub>, and 0.3mM NaH<sub>2</sub>PO<sub>4</sub>), fixed in 4% paraformaldehyde in PBS for 20 minutes, washed three times in PBS, and mounted in Prolong Gold antifade reagent with DAPI (Thermo Fisher Scientific, P36930). Z-stacks of *Drosophila* brains were acquired every 10 $\mu\text{m}$  with a 10X air objective with 1.2X magnification using an Olympus Fluoview FV1000 laser scanning confocal microscope (Olympus America, Lake Success, NY). The area of the maximum projection of the Z-stack was measured using Fiji software (Schindelin et al., 2012). Differences in brain area were assessed using two-tailed Mann-Whitney tests.

#### **3.4.8. RNA sequencing and differential expression analysis in *Drosophila melanogaster***

RNA sequencing was performed for three biological replicates of RNA isolated from 35-40 *Drosophila* heads with nervous-system specific knockdown of 16p12.1 homologs as well as controls with matching drivers and rearing temperatures. cDNA libraries were prepared with TruSeq Stranded mRNA LT Sample Prep Kit (Illumina, San Diego, CA). Single-end 100bp sequencing of the cDNA libraries was performed using Illumina HiSeq 2000 at the Pennsylvania State University Genomics Core Facility, at an average coverage of 35.1 million reads/sample. Quality control was performed using Trimmomatic (Bolger et al., 2014), and raw sequencing data was aligned to the fly reference genome and transcriptome build 6.08 using TopHat2 v.2.1.1 (Kim et al., 2013). Total read counts per gene were calculated using HTSeq-Count v.0.6.1 (Anders et al., 2015). Differences in gene expression were identified using a generalized linear model method in edgeR v.3.20.1 (Robinson et al., 2010), with genes showing a  $\log_2$ -fold change  $>1$  or  $<-1$  and with a Benjamini-Hochberg corrected  $FDR < 0.05$  defined as differentially expressed. Human homologs of differentially-expressed genes in flies were identified using DIOPT v8.0. Biological pathways and processes affected by downregulation of homologs of 16p12.1 genes, defined as significant enrichments of Gene Ontology (GO) terms ( $p < 0.05$ , Fisher's exact test with Benjamini-Hochberg multiple testing correction), were identified using PantherDB (Thomas et al., 2003).

#### **3.4.9. Screening of eye phenotypes of 16p12.1 homologs in different background strains**

Recombinant lines for each 16p12.1 homolog was generated by crossing RNAi lines with eye-specific *GMR-GAL4*. Phenotypic robustness of the homologs was assessed by

crossing the recombinant lines to the isogenic host strains v60000, v60100, and BL36303. The recombinant lines were crossed to seven additional *Drosophila* strains derived from natural populations, including *Samarkand*, *KSA\_4*, *Malawi*, *Oregon-R-P2*, *Canton-S*, *Urbana-S*, *Amherst\_3*, and *Berlin-K*. Fly crosses were reared at 30°C, and eye imaging was performed as detailed above for individual 16p12.1 homologs. *Flyntyper* phenotypic scores of the homologs in different genetic backgrounds were compared to the score of the control for each specific strain crossed to *GMR-GAL4* driver using two-tailed Mann-Whitney tests and Benjamini-Hochberg multiple testing correction.

#### **3.4.10 Analysis of genetic interactions in the fly eye**

Genetic interactions between homologs of 16p12.1 genes were assessed with each other as well as with homologs of “second-hits” identified in children with the 16p12.1 deletion, conserved neurodevelopmental genes, and select transcriptional targets. Genes carrying “second-hits” were selected as disease-associated genes carrying rare (ExAC frequency  $\leq 1\%$ ) copy-number variants, loss-of-function (frameshift, stopgain or splicing) mutations, or *de novo* or likely-pathogenic (Phred-like CADD  $\geq 25$ ) missense mutations previously identified from exome sequencing and SNP microarrays in 15 affected children with the 16p12.1 deletion and their family members (Kircher et al., 2014; Lek et al., 2016; Pizzo et al., 2018). Conserved genes were selected based on strong association with neurodevelopmental disorders (Iyer et al., 2018; Iyer et al., 2016) and genes with previously described functional associations with individual 16p12.1 genes, such as mitochondrial genes for *UQCRC2* (Duncan et al., 1993) and *Myc* for *POLR3E* and *CDR2* (Gomez-Roman et al., 2003; O'Donovan et al., 2010).

*GMR-GAL4* recombinant lines for the homologs of 16p12.1 genes were crossed with RNAi or mutant lines for the interacting genes to achieve simultaneous knockdown in the eye. Overexpression lines for specific genes functionally related to 16p12.1 homologs were also tested, including *Myc*, *Hsp23* and *Hsp26*. Previous assessment showed no changes in phenotypic scores for recombinant lines crossed with *UAS-GFP* compared to crosses with controls, demonstrating that the lines have adequate *GAL4* to bind to two independent *UAS-RNAi* constructs (Iyer et al., 2018). *Flynotyper* phenotypic scores of the double knockdowns were compared to phenotypic scores of the knockdown of the 16p12.1 homolog crossed to the control lines for the specific genetic background of the interacting gene. Significant enhancers and suppressors were identified with two-tailed Mann-Whitney tests and Benjamini-Hochberg multiple testing correction. An interaction was considered to be validated when the observed trend was reproduced by multiple RNAi lines when available. Epistatic enhancers were identified as non-additive interactions that showed significant interaction components using two-way ANOVA analysis with multiple testing correction at  $FDR < 0.05$ . When epistatic effects were not confirmed with more than two RNAi lines, if available, the interaction was considered to be additive.

#### **3.4.11 Immunohistochemistry of the developing brain and eye discs in *Drosophila melanogaster***

Third instar larvae brain or eye discs were dissected in PBS and fixed in 4% paraformaldehyde in PBT (0.3% Triton X-100 in PBS), followed by three washes with PBT. Preparations were blocked for one hour in blocking buffer (5% FBS or 1% BSA in

0.3% PBT), followed by incubation overnight at 4°C with the primary antibody. We assessed for markers of proliferation using mouse anti-pH3 (S10) (1:100; 9706, Cell Signaling Technology, Danvers, MA, USA) and apoptosis using rabbit anti-Dcp-1 (Asp216) (1:100, 9578, Cell Signaling). Secondary antibody incubation was performed using Alexa fluor 647 goat anti-mouse (1:100, Invitrogen, Carlsbad, CA, USA) and Alexa fluor 568 goat anti-rabbit (1:100, Invitrogen) for 2 hrs. at 25°C, followed by three washes with PBT. Tissues were mounted in Prolong Gold antifade reagent with DAPI (Thermo Fisher Scientific, P36930) prior to imaging. Z-stacks of brain lobe or eye discs were acquired every 4µm with a 40X air objective with 1.2X magnification using an Olympus Fluoview FV1000 laser scanning confocal microscope (Olympus America, Lake Success, NY). Image analysis was performed using Fiji (Schindelin et al., 2012). The number of cells undergoing proliferation or apoptosis were quantified throughout the brain lobe, or posterior to the morphogenetic furrow in the developing eye discs. The total number of Dcp-1 positive cells in larval brain and eye discs, as well as pH3 cells in the eye discs, were manually counted from the maximum projections. The total number of pH3 positive cells in the larval brain were quantified using the MaxEntropy automated thresholding algorithm per slice, followed by counting the number of particles larger than 1.5 µm. Differences in the number of positive pH3 or Dcp-1 cells were compared with appropriate controls using two-tailed Mann-Whitney tests.

#### **3.4.12 *Xenopus laevis* embryos**

All *X. laevis* experiments were approved by the Boston College Institutional Animal Care and Use Committee (Protocol #2016–012), and were performed according to national

regulatory standards. Eggs collected from female *X. laevis* frogs were fertilized *in vitro*, dejellied, and cultured following standard methods (Chen et al., 2010; Lowery et al., 2012). Embryos received injections of exogenous mRNAs or antisense oligonucleotide strategies at the two- or four-cell stage, using four total injections performed in 0.1X MMR media containing 5% Ficoll. Embryos were staged according to Nieuwkoop and Faber (Nieuwkoop PD, 1994).

### 3.4.13. Depletion and Rescue

Morpholinos (MOs) were targeted to early splice sites of *X. laevis mosmo*, *polr3e*, *uqcrc2*, *cdr2*, and *setd5*, or standard control MO purchased from Gene Tools (Philomath, OR). In knockdown experiments, all MOs were injected at either the 2-cell or 4-cell stage, with embryos receiving injections two or four times total. *mosmo* and control MOs were injected at 12ng/embryo for partial and 20ng/embryo for stronger knockdown; *polr3e* and control MOs were injected at 10ng/embryo for partial and 20ng/embryo for stronger; *uqcrc2* and control MOs were injected at 35ng/embryo for partial and 50ng/embryo for stronger; *cdr2* and control MOs were injected at 10ng/embryo for partial and 20ng for stronger knockdown; and *setd5* and control MOs were injected at 10ng/embryo for partial knockdown. All double knockdown experiments were performed with partial knockdown to avoid potential lethality.

Splice site MOs were validated using Reverse Transcriptase Polymerase Chain Reaction (RT-PCR). Total RNA was extracted using Trizol reagent, followed by chloroform extraction and ethanol precipitation from 2-day old embryos injected with increasing concentrations of MO targeted to each 16p12.1 homolog, respectively. cDNA

was synthesized using SuperScript II Reverse Transcriptase (Invitrogen, Carlsbad, CA, USA). PCR was performed in a Mastercycler using HotStarTaq DNA Polymerase (Qiagen, Germantown, MD, USA) following manufacturer instructions. RT-PCR was performed in triplicate, and band intensity was measured using the densitometry function in ImageJ (Schneider et al., 2012) and normalized to the uninjected control mean relative to the housekeeping control *odc1*. Phenotypes were suppressed or rescued with exogenous mRNAs co-injected with their corresponding MO strategies. *X. laevis* ORFs for *mosmo* and *polr3e* were purchased from the European *Xenopus* Resource Center (EXRC, Portsmouth, UK) and gateway-cloned into pCSF107mT-GATEWAY-3'GFP destination vectors. Constructs used were *mosmo*-GFP, *polr3e*-GFP, and GFP in pCS2+. In rescue experiments, MOs of the same amount used as for the knockdown of each homolog were injected with mRNA (1000pg/embryo for *mosmo*-GFP; 1000pg/embryo for *polr3e*-GFP) in the same injection solution.

#### **3.4.14. Quantifying craniofacial shape and size of *X. laevis* embryos**

The protocol for quantifying craniofacial shape and size was lightly adapted from Kennedy and Dickinson (Kennedy and Dickinson, 2014b). Embryos at stage 42 were fixed overnight in 4% paraformaldehyde in PBS. A razor blade was used to make a cut bisecting the gut to isolate the head. Isolated heads were mounted in small holes in a clay-lined dish containing PBS. Frontal and lateral view images were taken using a Zeiss AxioCam MRc attached to a Zeiss SteREO Discovery.V8 light microscope (Zeiss, Thornwood, NY, USA). ImageJ software was used to perform craniofacial measurements, including: 1) facial width, which is the distance between the eyes, 2) face

height, which is the distance between the top of the eyes and the top of the cement gland at the midline, 3) dorsal mouth angle, which is the angle created by drawing lines from the center of one eye, to the dorsal midline of the mouth, to the center of the opposite eye, and 4) midface area, which is the area measured from the top of the eyes to the cement gland encircling the edges of both eyes. For all facial measurements, two-tailed student's t-tests were performed between knockdown embryos and control MO-injected embryos with the same amount of morpholino.

#### **3.4.15 Neural tube explants, imaging, and analysis**

Embryos were injected with either control MO or 16p12.1 homolog-specific MO at the 2-4 cell stage, and culturing of *Xenopus* embryonic neural tube explants from stage 20-22 embryos were performed as previously described (Lowery et al., 2012). For axon outgrowth analysis, phase contrast images of axons were collected on a Zeiss Axio Observer inverted motorized microscope with a Zeiss 20x/0.5 Plan Apo phase objective (Zeiss, Thornwood, NY, USA). Raw images were analyzed by manually tracing the length of individual axons using the NeuronJ plug-in in ImageJ (Popko et al., 2009). All experiments were performed on multiple independent occasions to ensure reproducibility. Axon outgrowth data were normalized to controls from the same experiment to account for day-to-day fluctuations. Statistical differences were performed between knockdown embryos and control MO-injected embryos with same amount of morpholino using two-tailed student's t-tests.

#### **3.4.16 Immunostaining for brain morphology, imaging, and analysis**

For brain morphology analysis, half embryo KDs were performed at the two-cell stage. *X. laevis* embryos were unilaterally injected two times with either control MO or 16p12.1 homolog-specific MO and a GFP mRNA construct (300pg/embryo). The other blastomere was left uninjected. Embryos were raised in 0.1X MMR through neurulation, and then sorted based on left/right fluorescence. Stage 47 embryos were fixed in 4% paraformaldehyde diluted in PBS for one hour, rinsed in PBS, and gutted to reduce autofluorescence. Embryos were processed for immunoreactivity by incubating in 3% bovine serum albumin and 1% Triton-X 100 in PBS for two hours, and then incubated in anti-acetylated tubulin (1:700, T7451SigmaAldrich, St. Louis MO, USA) and goat anti-mouse Alexa Fluor 488 conjugate secondary antibody (1:1000, Invitrogen, Carlsbad, CA, USA). Embryos were rinsed in 1% Tween-20 in PBS and imaged in PBS. Removal of the skin dorsal to the brain was performed if the brain was not clearly visible due to pigment.

Images were taken at 3.2X magnification using a Zeiss AxioCam MRc attached to a Zeiss SteREO Discovery.V8 light microscope (Zeiss, Thornwood, NY, USA). Images were processed in ImageJ. The areas of the forebrain and midbrain were determined from raw images using the polygon area function in ImageJ. Brain sizes were quantified by taking the ratio of forebrain and midbrain areas between the injected side versus the uninjected side for each sample. All experiments were performed on at least three independent occasions to ensure reproducibility. The data represent findings from these multiple replicates. Statistical differences were identified between knockdown embryos and control MO injected embryos with the same amount of morpholino using two-tailed student's t-tests.

### 3.4.17 Western blot for cell proliferation

Embryos at stage 20 to 22 were lysed in buffer (50mM Tris pH 7.5, 1% NP40, 150mM NaCl, 1mM PMSF, 0.5 mM EDTA), supplemented with cOmplete™ Mini EDTA-free Protease Inhibitor Cocktail (Sigma-Aldrich) and PhosSTOP™ Phosphatase Inhibitor Cocktail (Sigma-Aldrich). Blotting was carried out using rabbit polyclonal antibody to Phospho-Histone H3 (Ser10) (1:500, PA5-17869, Invitrogen), with mouse anti-beta actin (1:2500, ab8224, Abcam, Cambridge, MA, USA) as a loading control. Bands were detected by chemiluminescence using Amersham ECL Western blot reagent (GE Healthcare Bio-Sciences, Pittsburgh, PA). Band intensities were quantified by densitometry in ImageJ and normalized to the control mean relative to  $\beta$ -actin.

## CHAPTER 4

**16p12.1 deletion homologs are enriched in motile neural crest cells and are important for regulating processes during their development in *Xenopus laevis***

The material in this chapter was adapted from the following unpublished manuscript:

**Lasser, M., Bolduc, J., Murphy, L., O'Brien, C., Lee, S., Girirajan, S., Lowery, L.A.**  
16p12.1 deletion homologs are enriched in motile neural crest cells and are important for regulating processes during their development in *Xenopus laevis*. (in preparation)

#### 4.1. Introduction

Embryonic development is extremely complex and requires the proper function of thousands of genes in order for cells to proliferate and divide, differentiate, migrate long distances to their final destination, and communicate with one another appropriately. Disruption of protein function due to mutations of genes that are required for these processes during embryogenesis can lead to severe developmental defects and neurodevelopmental disorders such as intellectual disabilities (ID) or Autism spectrum disorder (ASD) (Alonso-Gonzalez et al., 2018; Chen et al., 2019; Kasherman et al., 2020; Lasser et al., 2018; Sierra-Arregui et al., 2020). As stated in previous chapters, genetic mutations caused by rare copy number variants (CNVs), including deletions and duplications, have been associated with neurodevelopmental disorders to varying degrees (Blazejewski et al., 2018; Deshpande and Weiss, 2018; Jensen et al., 2018; Pizzo et al., 2019; Rylaarsdam and Guemez-Gamboa, 2019; Singh et al., 2020). As described in chapter 3, a pathogenic CNV was recently identified in children diagnosed with ID, that results in a heterozygous deletion of several genes located at chromosome 16p12.1 (Antonacci et al., 2010; Girirajan et al., 2010b). In our previous study, we performed detailed functional analysis of individual genes affected within this region and their interactions with one another, in order to elucidate which genes and cellular mechanisms contributed to the neurodevelopmental phenotypes associated with the deletion. We found that reduced dosage of *polr3e* and *mosmo* severely impact proper brain development in both *Drosophila melanogaster* and *Xenopus laevis*, suggesting that they may contribute to the ID and microcephaly phenotypes observed in patients with the 16p12.1 deletion. However, individuals with this mutation display a wide range of other

developmental defects, in addition to neurodevelopmental-specific symptoms. In particular, patients often manifest severe craniofacial abnormalities including facial asymmetries, micrognathia (undersized jaw), a short philtrum (space between the nose and lip), as well as cartilage malformation of the ears and nose.

Craniofacial defects are one of the most prevalent congenital defects that can severely affect quality of life (Kirby, 2017; Trainor, 2010; Vega-Lopez et al., 2018). As craniofacial patterning relies heavily on the specification, proliferation, and subsequent migration of neural crest cells (NCCs), many craniofacial and cartilage defects arise due to aberrant NCC development (Fish, 2016; Rutherford and Lowery, 2016; Trainor, 2010; Vega-Lopez et al., 2018). Several of the tissue and organ systems affected by the 16p12.1 deletion are derived from NCCs; however, the function of the genes within this region have not been carefully investigated in the context of vertebrate craniofacial development, nor has any study determined whether their depletion might impact NCC behavior. Therefore, the underlying developmental mechanism by which each gene contributes to the craniofacial phenotypes associated with the deletion remains to be elucidated.

Due to the broad range of cellular functions of each 16p12.1-affected gene, it is imperative to determine whether their individual depletion leads to specific craniofacial defects, or whether depletion of multiple genes within this region combinatorially contribute to a collaborative craniofacial phenotype. Thus, I investigated the contributions of *polr3e*, *mosmo*, *uqcrc2*, and *cdr2* to developmental processes that govern early craniofacial patterning in *Xenopus laevis*. First, I examined expression profiles for each transcript across early stages of embryonic development and I observed their

enrichment in motile NCCs residing in the pharyngeal arches (PAs), suggesting that they may influence NCC development and migration. Knockdown (KD) strategies were then utilized to assess the contribution of each 16p12.1-affected gene to facial and cartilage development. I showed in chapter 3 that depletion of *polr3e*, *mosmo*, and *uqcrc2* led to smaller facial features and in the present study, I find that these three genes also severely disrupt cartilage morphology. I then performed both *in vivo* and *in vitro* NCC migration assays showing that some of these genes also directly impact pharyngeal arch migration and NCC motility rates. Finally, I examined NCC specification and proliferation and while I found that reduced dosage of each gene did not have a significant impact on proliferation, I did find that some of these genes are critical for NCC specification. Together, my results support the hypothesis that the craniofacial phenotypes associated with the 16p12.1 deletion are in part due to several genes within this region performing critical functions during NCC development and migration, craniofacial patterning, and cartilaginous tissue formation. Moreover, this work is the first to elucidate the roles of the 16p12.1-affected genes during embryonic craniofacial morphogenesis on a shared, directly-comparable background, providing deeper insight into how diverse genetic mutations lead to distinct developmental phenotypes and disease within the context of a multigenic syndrome.

## **4.2. Results**

### **4.2.1. 16p12.1-affected genes display enriched expression in the developing nervous system, pharyngeal arches, and craniofacial structures**

One of the more prominent symptoms in patients with the 16p12.1 deletion are craniofacial dysmorphisms with varying severity (Girirajan et al., 2010b). Children often present with facial asymmetries, micrognathia, a short philtrum, small and deep-set eyes, hypertelorism, a depressed nasal bridge, and dysplastic ears. Comorbidities commonly include microcephaly, growth retardation, scoliosis, and defects in hand and foot development (Girirajan et al., 2010b). As proper NCC specification, proliferation, and migration are critical for governing embryonic facial patterning in many of these affected tissues, we hypothesized that one or more of the 16p12.1-affected genes are required for NCC development, and that their depletion would result in defects associated with one or more of these NCC-related processes.

First, I investigated the spatiotemporal expression of four 16p12.1-affected gene homologs, *polr3e*, *mosmo*, *uqcrc2*, and *cdr2*, across multiple stages of development in *Xenopus laevis* embryos. To examine this, I performed whole-mount *in situ* hybridization with DIG-labeled antisense RNA probes against these four genes (**Figure 4.1** and **Figure 4.2**; for *in situ* hybridization controls against RNA sense strands, see **Figure 4.3**). I observed ubiquitous expression of all four gene transcripts during early blastula and gastrula stages (st. 10 and 13; data not shown), with no significant enrichment in specified, premigratory neural crest (st. 20; **Figure 4.1.A-B,E-F,I-J,M-N**). However, by stage 25, more defined expression became visible during early craniofacial morphogenesis, with enriched expression of each gene in migratory NCCs that reside in the pharyngeal arches (**Figure 4.2.B-E**), and their expression patterns somewhat resemble the NCC-enriched transcription factor, *twist* (**Figure 4.2.A**). At this stage, expression of both *polr3e* and *mosmo* is particularly strong in the developing brain and

eye, which is consistent with previous data in chapter 3, suggesting that these genes are important for both brain and eye development. All four genes remain enriched in the developing head and facial structures throughout stage 35 (**Figure 4.1.C-D,G-H,K-L,O-P**); *polr3e* expression appears to become more defined in the hindbrain region, whereas *mosmo* expression is stronger in the forebrain region (**Figure 4.1.C,G**), and *uqcrc2* expression is heavily enriched in the developing kidney and somites (**Figure 4.1.K**). By stage 40, *mosmo* expression is also observed in the developing spinal cord (**Figure 4.1.H**). Additionally, the expression patterns of all four genes show potential overlap with cardiac tissue (**Figure 4.1.D,H,L,P**). Thus, my findings demonstrate that the four 16p12.1-gene homologs display enriched expression in the developing nervous system, migratory NCCs in the pharyngeal arches, and later craniofacial structures, among other tissues.

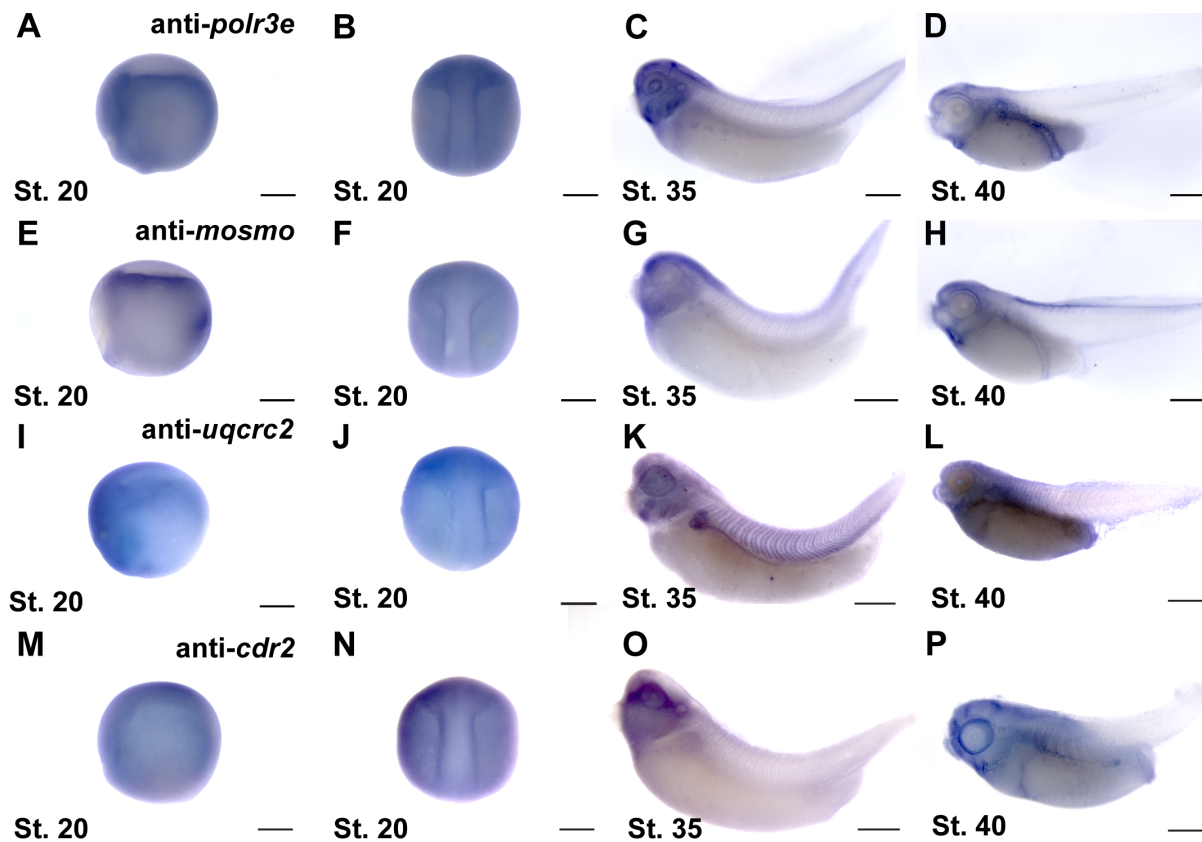


### Figure 4.1 Expression patterns for 16p12.1-affected genes across early development

*In situ* hybridization utilized (A-D) antisense mRNA probe to *polr3e*, (E-H) antisense mRNA probe to *mosmo*, (I-L) antisense mRNA probe to *uqcrc2*, and (M-P) antisense mRNA probe to *cdr2*. Lateral and dorsal view images of embryos shown at stage 20 (A-B, E-F, I-J, M-N), lateral view at stage 35 (C, G, K, O), and lateral view at stage 40 (D, H, L, P) (n = 10 per probe) Scalebar = 300 $\mu$ m.

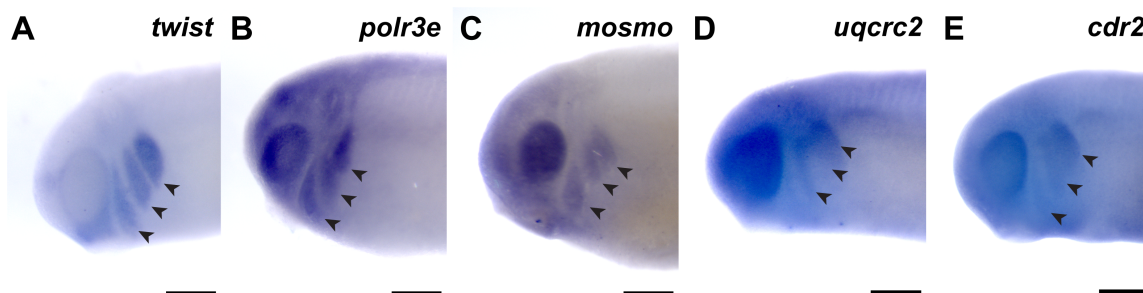


**Figure 4.2** 16p12.1-affected genes are expressed in migrating neural crest cells during embryonic development

(A) Lateral view of whole-mount *in situ* hybridization at stage 25 for *twist*, a NCC-enriched transcription factor. Arrows indicate the pharyngeal arches (PAs). (B-E) *In situ* hybridization at stage 25 for *polr3e*, *mosmo*, *uqcrc2*, and *cdr2* demonstrate enrichment in NCCs that occupy the PAs (n = 10 per probe). Scalebar = 300 $\mu$ m.

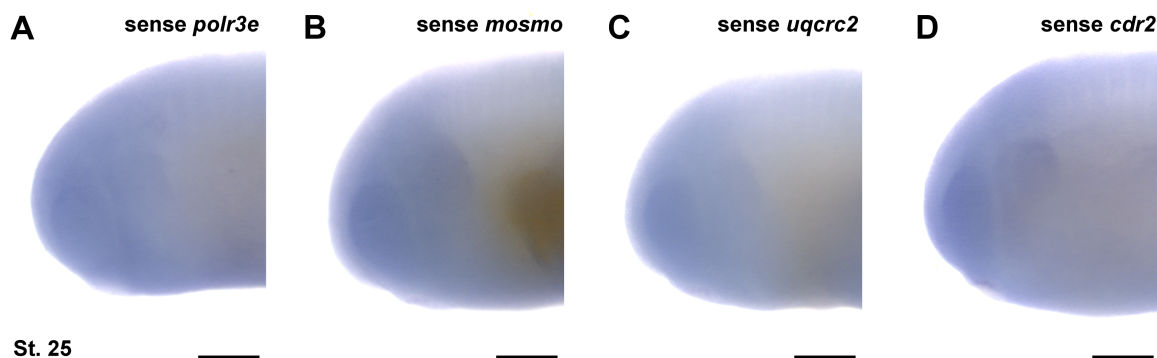


**Figure 4.3** *In situ* hybridization probes generated against sense strands of 16p12.1-affected gene mRNAs

*In situ* hybridization utilized (A) sense mRNA probe against *polr3e*, (B) sense mRNA probe against *mosmo*, (C) sense mRNA probe against *uqcrc2*, and (D) sense mRNA probe against *cdr2*, shown at stage 25. (n = 10 per probe). Scalebar = 300 $\mu$ m.

#### 4.2.2. 16p12.1-affected genes are important for maintaining cartilage size and scaling

Many individuals with the 16p12.1 deletion display defects in cartilage and skeletal development including deformed nose and ears, tooth malformation, short

stature, smaller head size, and delayed growth (Girirajan et al., 2010b). Additionally, patients also have speech, feeding, and swallowing impairments that are linked to abnormal jaw and throat formation (Girirajan et al., 2010b). As these cartilaginous and skeletal tissues are derived from NCCs (Etchevers et al., 2019; Merkuri and Fish, 2019; Szabo and Mayor, 2018; Van Otterloo et al., 2016), I hypothesized that one or more of the 16p12.1-affected genes may play an essential role during embryonic development of craniofacial cartilage and skeletal structures. To examine this, I performed partial depletion of the four 16p12.1 gene homologs to determine their influence on cartilage scaling and morphology in *Xenopus laevis* embryos (**Figure 4.4**).

Reduced dosage of *polr3e*, *mosmo*, and *uqcrc2* was sufficient to severely impact cartilage development of stage 42 embryos. When I knocked down these three genes individually, I observed overt defects of cartilage morphology compared to controls (**Figure 4.4.B-D**), including a decrease in the average ceratohyal area and the width of the first branchial arch (**Figure 4.4.F-G**). Surprisingly, given that I showed that partial depletion of *Cdr2* led to a minor reduction in facial size, this did not cause similar overt cartilage abnormalities (**Figure 4.4.E**), nor was there any obvious effect on the size of individual cartilage elements (**Figure 4.4.F-G**). However, the craniofacial defects associated with reduced dosage of *Cdr2* are quite mild, and thus, this gene may not play a major role during craniofacial and cartilage morphogenesis when partially depleted compared to the other genes affected in the 16p12.1 region. It is also possible that there may be genetic compensation by other closely related genes, such as *cdr1*, *cdr2-like*, and *cdr3*. Overall, these results indicate that *polr3e*, *mosmo*, and *uqcrc2* are essential for early cartilaginous tissue formation and are likely important for later development of head and

facial skeletal structures. Moreover, these results demonstrate that partial depletion of the 16p12.1-associated genes creates persistent defects on craniofacial patterning and cartilage formation that are not ameliorated later in development (stage 42), leading to my hypothesis that these genes may impact processes important for the embryonic progenitors of these tissues.

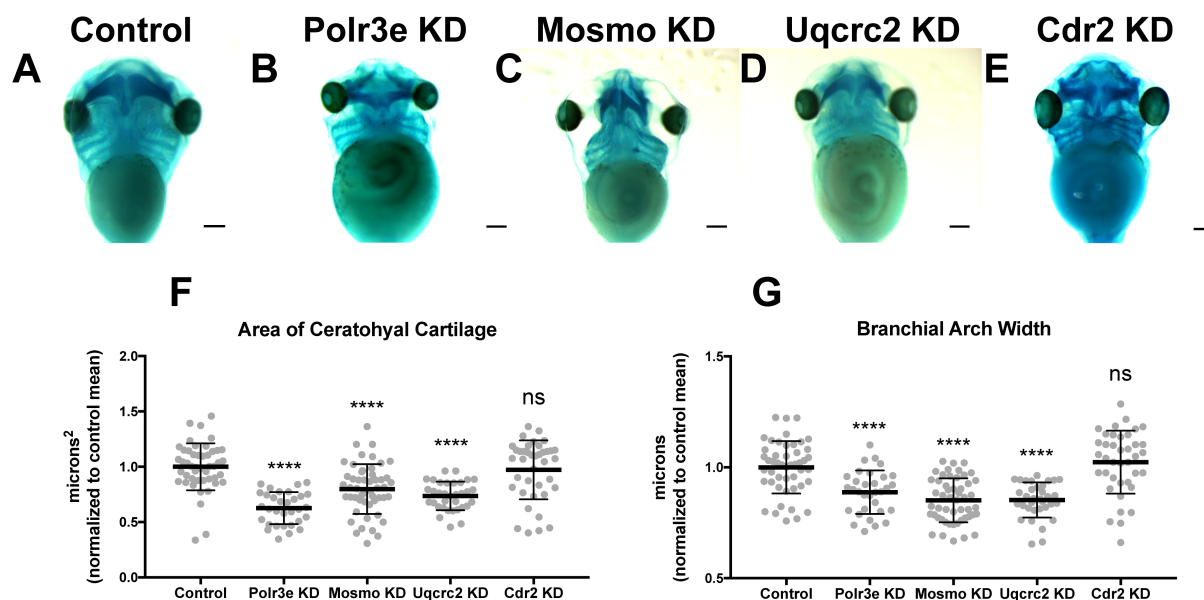


**Figure 4.4** Knockdown of *Polr3e*, *Mosmo*, and *Uqcr2* impact cartilage morphology

(A-E) Ventral view of stage 42 embryos following single 16p12.1-associated gene KD, stained with Alcian blue to label cartilage elements. (F-G) Measurements of the average ceratohyal area and width of the first branchial arch. The data was normalized to the condition with the highest control MO concentration, however, each experimental KD condition was injected alongside a corresponding control MO condition of the same concentration. Partial depletion of *Polr3e*, *Mosmo*, and *Uqcr2* significantly reduced the size of both of these cartilage elements compared to controls, while depletion of *Cdr2* had no effect on cartilage size. Significance determined using a student's unpaired *t*-test. (Embryos quantified: Control = 48, *Polr3e* KD = 32, *Mosmo* KD = 51, *Uqcr2* KD = 34, *Cdr2* KD = 39). \*\*\*\**p* < 0.0001, \*\*\**p* < 0.001, \*\**p* < 0.01, \**p* < 0.05, n.s., not significant. Scalebar = 300μm.

### 4.2.3. Several 16p12.1-affected genes are critical for normal pharyngeal arch

#### migration and NCC motility

Given that the 16p12.1-affected gene transcripts display enriched expression in NCCs residing in the pharyngeal arches during stages that correspond with their migration (st. 25-30), I hypothesized that depletion of one or more of these genes may

disrupt NCC migration and motility. To test this, I utilized single-hemisphere injection strategies to generate left-right chimeric embryos, allowing for a side-by-side comparison of *twist* expression patterns between wild-type or knockdown (KD) sides to track the progress of migratory NCCs (**Figure 4.5**). I note here that rescue experiments for these NCC-related phenotypes have not been performed, and thus, specificity of the NCC phenotypes that arise due to genetic manipulation of individual 16p12.1 genes must still be confirmed. Following single-sided individual depletion of each 16p12.1 gene, embryos were staged to 25-28, fixed, and *in situ* hybridization was performed against *twist*. To quantify NCC migration away from the anterior neural tube, measurements were taken of the total pharyngeal arch area, length of each individual pharyngeal arch, and total migration distance of each individual pharyngeal arch for both the uninjected and control or KD side of each embryo (**Figure 4.5.F-Q**). I found that *Polr3e* and *Mosmo* depletion significantly reduced total area of NCC streams (**Figure 4.5.F-G**). Further, when *Polr3e* levels were reduced, the posterior PA was shorter in length (**Figure 4.5.J**), whereas depletion of *Mosmo* reduced the length of the anterior PA and hyoid PA (**Figure 4.5.L**). Additionally, individual depletion of these genes reduced the ventral migration distance of all three NCC streams compared to controls (**Figure 4.5.K,M**). Interestingly, depletion of *Uqcrc2* resulted in an increase in total PA area (**Figure 4.5.H**) and a slight increase in the length of the anterior and hyoid PAs (**Figure 4.5.N**), though it did not impact PA migration (**Figure 4.5.O**). It is possible that NCC proliferation is upregulated to compensate for reduced *Uqcrc2* levels, leading to an increase in PA area and length. While depletion of *Cdr2* slightly increased hyoid PA length (**Figure 4.5.P**), it did not result in significant changes in PA area or migration (**Figure 4.5.I,Q**). Together, these

results suggest a specific role for *Polr3e*, *Mosmo*, and *Uqcr2* in maintaining NCC migration *in vivo*.

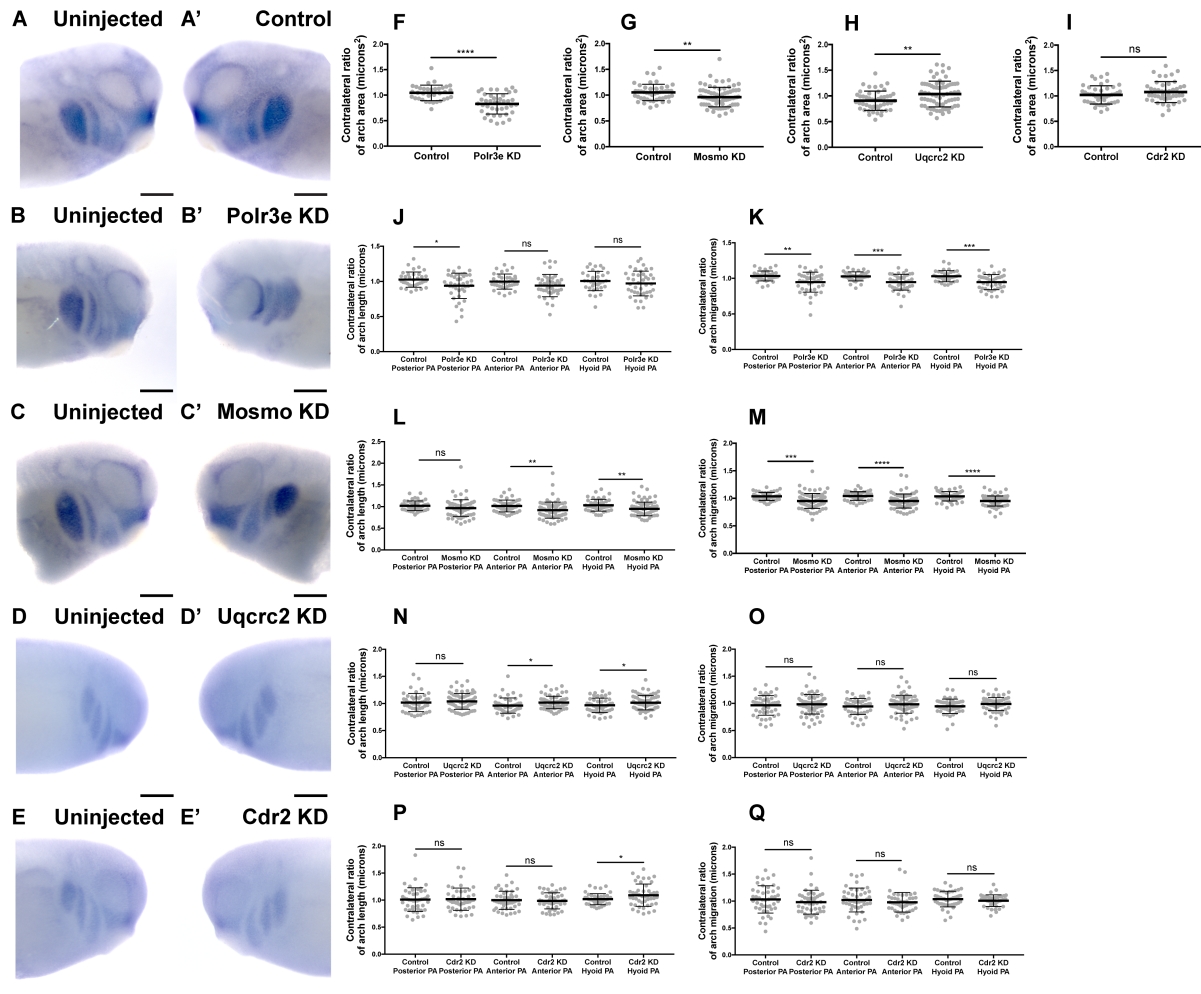


**Figure 4.5** Knockdown of *Polr3e*, *Mosmo*, and *Uqcr2* affect NCC migration *in vivo*

(A-E, A'-E') Anterior lateral views of stage 25 embryos following whole-mount *in situ* hybridization against *twist*. Each column of panels are lateral views of two sides of the same embryo. Embryos were unilaterally injected to KD each individual 16p12.1-affected gene in half of the embryo and the other half was left uninjected. The left panels (A-E) represent the uninjected side and the right panels (A'-E') represent the injected side. (F-Q) Measurements were taken for the total area of the three PAs (posterior PA, anterior PA, and hyoid PA), the length of each individual arch, and the migration distance, as measured from the dorsal most tip of each arch to the neural tube by taking ratios of the injected side versus the uninjected side. Significance was determined using an unpaired students *t*-test with these ratios. (F-H) Partial depletion of both *Polr3e* and *Mosmo* significantly reduced the total area of the three PAs, while partial depletion of *Uqcr2* slightly increased the total area of the three PAs. (J-K) *Polr3e* KD significantly reduced the length of the posterior PA but had no effect on the length of the anterior PA or hyoid PA. However, partial depletion of this gene significantly reduced the total migration distance of all three PAs. (L-M) *Mosmo* KD significantly reduced the length of the anterior PA and hyoid PA but had no effect on the length of the posterior PA. Partial depletion of this gene also significantly reduced the total migration distance of all three PAs. (N-O) *Uqcr2* KD slightly increased the length of the anterior and hyoid PA but had no effect on the length of the posterior PA, nor did it affect the total migration distance of any three PAs. (I, P-Q) *Cdr2* KD had no effect on the total area of the three PAs, nor did it affect the total migration distance of any three PAs. However, partial

depletion of this gene slightly increase the length of the hyoid PA but did not affect the posterior or anterior PAs. (Embryos quantified: Control for *Polr3e* = 35, Control for *Mosmo* = 48, Control for *Uqrc2* = 48, Control for *Cdr2* = 45, *Polr3e* KD = 41, *Mosmo* KD = 75, *Uqrc2* KD = 68, *Cdr2* KD = 45). \*\*\*\* $p < 0.0001$ , \*\*\* $p < 0.001$ , \*\* $p < 0.01$ , \* $p < 0.05$ , n.s., not significant. Scalebar = 300 $\mu$ m.

While the previous experiment suggested a role for these genes in regulating NCC migration, other phenotypes might lead to changes in measured PA area, length, and migration distance. Thus, to investigate whether reduced dosage of any of the 16p12.1-affected genes impacted NCC migration rate itself, I performed *in vitro* migration assays, as previously described (Lasser et al., 2019; Mills et al., 2019). Individual genes were partially depleted in the whole embryo and NCCs were dissected prior to delamination from the neural tube (st. 17) from both KD and control conditions. These tissue explants were cultured on fibronectin-coated coverslips and individual cell migration for each explant was imaged using time-lapse phase-contrast microscopy for six hours (**Figure 4.6.A-E,A'-E'**). I then mapped and measured the trajectories and speed of individual cells that escaped the explant using automated particle tracking (**Figure 4.6.F**) (Schindelin et al., 2012; Tinevez et al., 2017). I found that partial depletion of *Polr3e* and *Uqrc2* resulted in slower individual NCC speed compared to controls (**Figure 4.6.G,I**), while partial depletion of *Mosmo* did not significantly impact NCC speed (**Figure 4.6.H**). As partial depletion of *Cdr2* was not sufficient to significantly alter NCC streaming *in vivo*, nor was it sufficient to cause severe craniofacial or cartilage morphology defects, I hypothesized that NCC motility *in vitro* would not be affected by this depletion. Instead, depletion of *Cdr2* led to a significant increase in the speed of CNCs migrating *in vitro* (**Figure 4.6.J**). I hypothesize that individual cell speed of *Cdr2* KD *in vitro* may not directly correspond to differences in NCC streaming *in vivo* as the boundaries of NCC migration *in vivo* are heavily restricted due to repellent guidance cues within the PAs.

Thus together, I show that depletion of *Polr3e* and *Uqcr2* alters NCC migration into the PAs, and that this defect could be driven by a reduction in individual NCC motility rates.

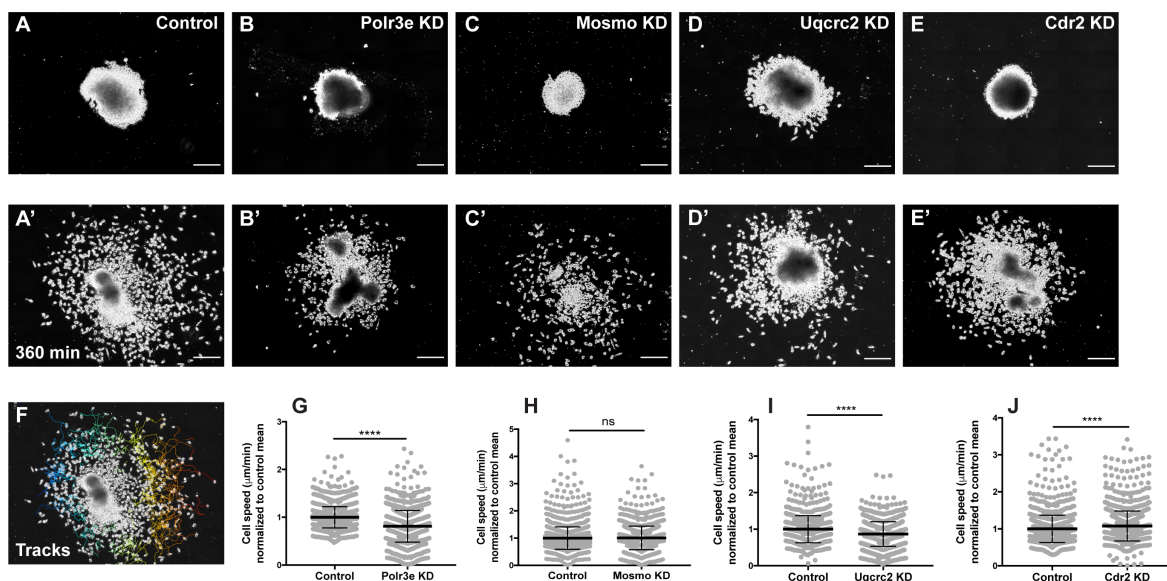


**Figure 4.6 Manipulation of *Polr3e*, *Uqcr2*, and *Cdr2* impacts NCC migration speeds *in vitro***

Dissected NCC explants from control, *Polr3e* KD, *Mosmo* KD, *Uqcr2* KD, or *Cdr2* KD embryos were plated on fibronectin-coated coverslips, allowed to adhere and begin migration, and imaged for 6h using 20x phase microscopy. (A-E) Representative images of explants at initial timepoint (0 min). (A'-E') Representative images of explants after 6h migration (360 min). (F) Representative tracks generated by Fiji Trackmate plugin. (G-J) Mean track speeds of *Polr3e* KD, *Mosmo* KD, *Uqcr2* KD, and *Cdr2* KD explants compared to their controls. Partial depletion of *Polr3e* and *Uqcr2* significantly reduced mean NCC speed, while depletion of *Cdr2* increased mean NCC speed. Partial depletion of *Mosmo* had no effect on mean NCC speed. (Explants quantified: 6-7 explants from control and KD embryos were plated for each experiment. Three separate experiments were performed for each depletion.) \*\*\*\* $p < 0.0001$ , \*\*\* $p < 0.001$ , \*\* $p < 0.01$ , \* $p < 0.05$ , n.s., not significant. Scalebar = 200 $\mu$ m.

#### 4.2.4. 16p12.1-affected genes do not directly impact NCC proliferation

As NCCs exit the dorsal neural tube and undergo directed migration along stereotypical pathways during vertebrate development, they must also balance between cell division and migration (Szabo and Mayor, 2018). Reduced gene dosage could result in smaller areas of *twist* expression due to decreased cellular migration rates, but it is also possible that there are fewer NCCs within the PAs if genetic manipulations affect NCC proliferation rates. To test this, I depleted each 16p12.1 gene individually in the whole

embryo and I dissected NCCs as described in the previous section. These tissue explants were cultured on fibronectin-coated coverslips and NCCs were allowed to migrate away from the explant for four hours before being fixed. Immunocytochemistry was then performed using a phospho-histone H3 (PH3) antibody as a marker for cell proliferation (**Figure 4.7.A-A'**). To measure NCC proliferation, I quantified the number of cells positively labeled for PH3 versus the total number of cells per explant using an automated particle counter after thresholding each image. Interestingly, I found that partial depletion of individual 16p12.1-affected genes had no statistically significant effect on NCC proliferation *in vitro* (**Figure 4.7.B-E**). However, Mosmo KD resulted in a trend towards increased proliferation, and Cdr2 KD resulted in a trend towards decreased proliferation, suggesting a potential role for these genes in regulating this process (**Figure 4.7.C,E**). Division of NCCs occurs over a wide range of times after exiting the neural tube, with mitotic activity significantly increasing as cells enter the pharyngeal arches (Gonsalvez et al., 2015; Rajan et al., 2018). Thus, it is possible that I did not observe a direct effect of genetic manipulation on NCC proliferation due to the absence of *in vivo* microenvironmental signals that are necessary for cell division.

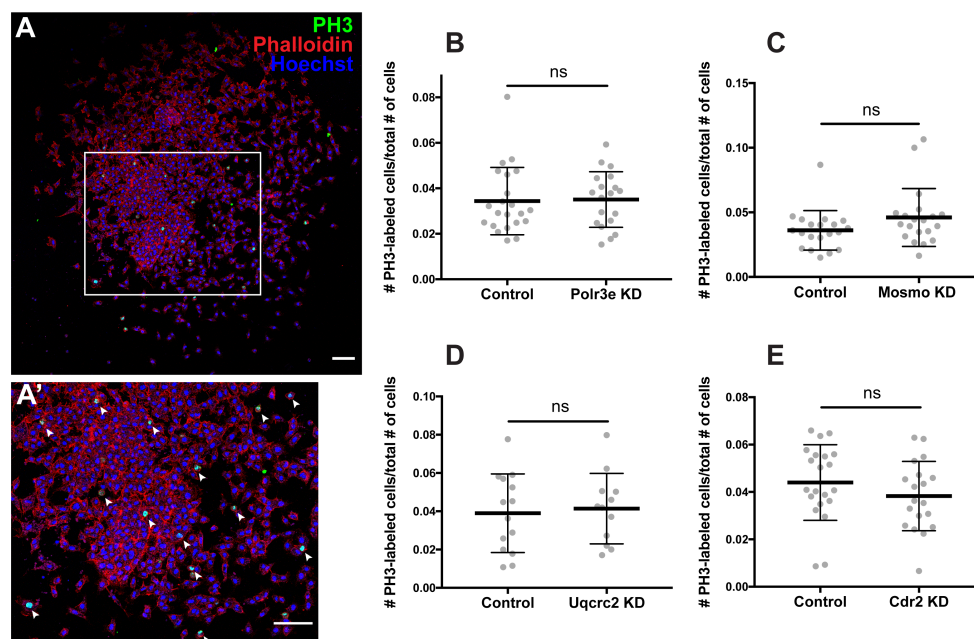


**Figure 4.7 Manipulation of 16p12.1-affected genes does not impact NCC proliferation *in vitro***

Dissected NCC explants from control, Polr3e KD, Mosmo KD, Uqrc2 KD, and Cdr2 KD embryos were plated on fibronectin-coated coverslips, allowed to adhere and begin migration for 4h before being fixed in 4% PFA and immunostained with PH3 antibody as a marker for NCC proliferation, phalloidin to label the actin cytoskeleton, and Hoechst to label nuclei. (A, A') Representative image of control NCC explant immunostained with PH3, phalloidin, and Hoechst. White arrows denote cells positively labeled for PH3. (B-E) Quantification of the number of positively PH3-labeled cells versus the total number of cells per NCC explant for Polr3e KD, Mosmo KD, Uqrc2 KD, and Cdr2 KD compared to controls. Partial depletion of each individual 16p12.1-affected did not have a significant impact on NCC proliferation *in vitro*. (Explants quantified: 6-7 explants from control and KD embryos were plated for each experiment. Three separate experiments were performed for each depletion). \*\*\*\* $p < 0.0001$ , \*\*\* $p < 0.001$ , \*\* $p < 0.01$ , \* $p < 0.05$ , n.s., not significant. Scalebar = 300 $\mu$ m.

#### 4.2.5. Several 16p12.1-affected genes are critical for NCC induction and specification

The process of NCC induction and specification is complex and requires a specific level of signaling by the BMP, Wnt, FGF, RA, Shh, and Notch/Delta pathways to establish a gene regulatory network that is crucial for determining NCC identity (Pla and Monsoro-Burq, 2018; Prasad et al., 2019; Rogers and Nie, 2018; Theveneau and Mayor, 2012). During the early steps of NCC formation, these morphogen pathways work in concert with various NCC transcription factors (TFs) such as *snai1*, *snai2/slug*, *sox9*, and *twist*, to establish the neural plate border, regulate NCC specification, and subsequent NCC migration (Pla and Monsoro-Burq, 2018; Rogers and Nie, 2018). As

shown in the previous sections, I found that partial depletion of several 16p12.1-affected genes significantly impacted *twist* expression patterns and PA migration, and that these defects were not due to changes in NCC proliferation rates. However, it is possible that reduced dosage of these genes causes PA migration defects due to changes in NCC specification, resulting in fewer numbers of cells. Therefore, I tested this by utilizing single-hemisphere injection strategies to generate left-right chimeric embryos, and compared side-by-side expression patterns of TFs required for NCC induction and specification between wild-type or KD sides.

Following single-sided individual depletion of each 16p12.1 gene, embryos were fixed at st. 16 and *in situ* hybridization was performed against *sox9* and *twist* (**Figure 4.8.A-J**). To quantify changes in expression of NCC specification markers, I measured the total area of expression of each marker for both the uninjected and control or KD side of each embryo (**Figure 4.8.K-L**). Although both NCC specification markers were present, there were clear abnormalities including reduced signal and smaller total area of expression following partial depletion of either *Polr3e* or *Mosmo* (**Figure 4.8.C-F,K-L**). In contrast, depletion of *Uqcrc2* or *Cdr2* did not significantly affect the signal or total area of expression for any NCC specification marker (**Figure 4.8.G-J,K-L**). Together, these results suggest that *Polr3e* and *Mosmo* are distinctly required for NCC specification, as reduced levels of these genes alters expression of NCC specification markers, which may result in fewer cells and subsequent PA migration defects.

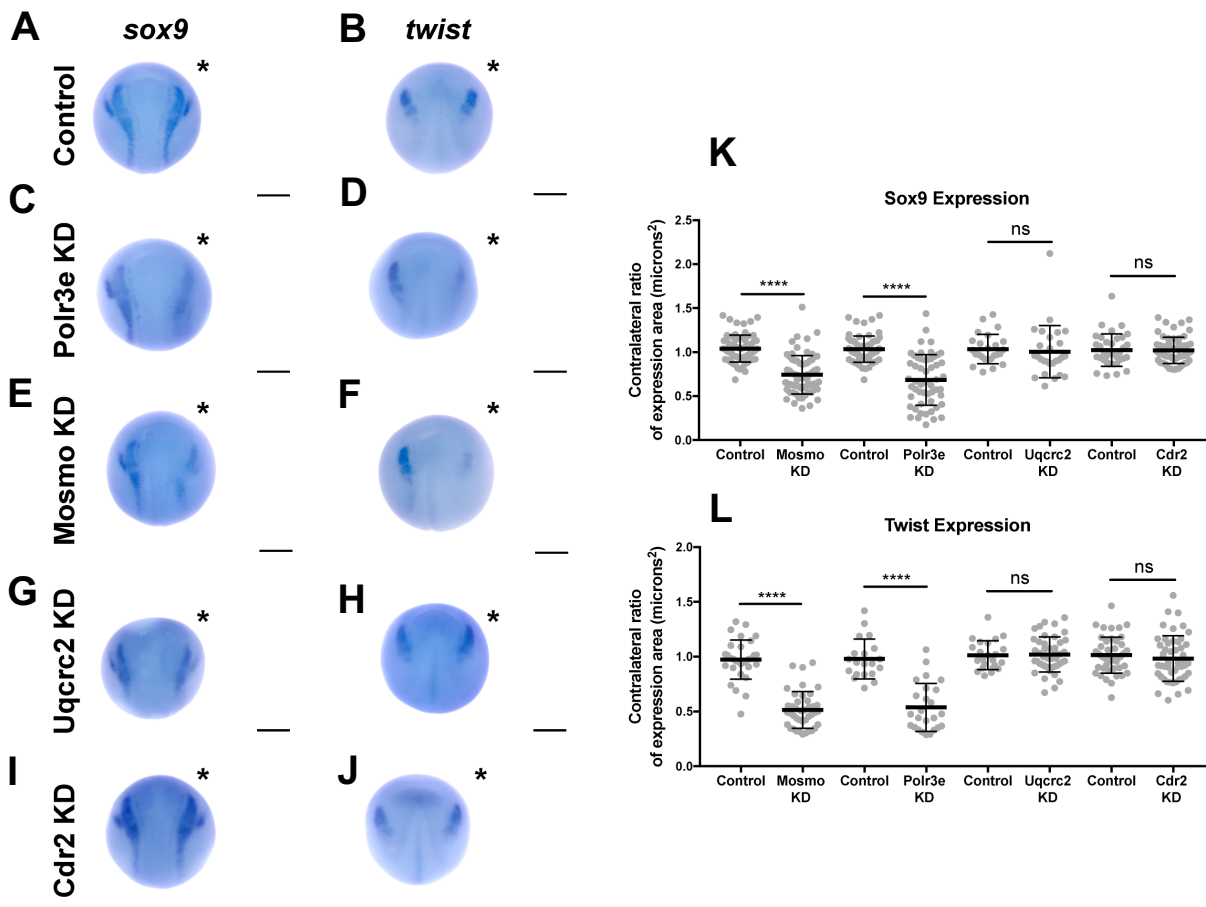


**Figure 4.8 Manipulation of Polr3e and Mosmo affects NCC specification**

*In situ* hybridization utilized (A,C,E,G,I) antisense mRNA probe against *sox9* and (B,D,F,H,J) antisense mRNA probe against *twist*. Each column of panels are dorsal views of two sides of the same embryo. Embryos were unilaterally injected to KD each individual 16p12.1-affected gene in half of the embryo and the other half was left uninjected. The left side represents the uninjected side and the right side, indicated with an asterisk (\*), represents the injected side. (K-L) Measurements were taken for the total area of the expression pattern for either *sox9* (K) or *twist* (L) using the polygon tool in ImageJ by taking ratios of the injected side versus the uninjected side. Significance was determined using an unpaired students *t*-test with these ratios. Partial depletion of either Mosmo or Polr3e significantly reduced the total area of expression for both *sox9* and *twist*, while partial depletion of either Uqrc2 or Cdr2 did not significantly affect the total area of expression for either NCC specification marker. (Embryos quantified with *sox9* probe: Control for Polr3e = 60, Control for Mosmo = 66, Control for Uqrc2 = 25, Control for Cdr2 = 36, Polr3e KD = 55, Mosmo KD = 69, Uqrc2 KD = 27, Cdr2 KD = 59. Embryos quantified with *twist* probe: Control for Polr3e = 20, Control for Mosmo = 33, Control for Uqrc2 = 23, Control for Cdr2 = 46, Polr3e KD = 25, Mosmo KD = 41, Uqrc2 KD = 44, Cdr2 KD = 50). \*\*\*\* $p < 0.0001$ , \*\*\* $p < 0.001$ , \*\* $p < 0.01$ , \* $p < 0.05$ , n.s., not significant. Scalebar = 300 $\mu$ m.

### 4.3. Discussion

To functionally explore the basis of the craniofacial and cartilage defects associated with the 16p12.1 deletion, I analyzed craniofacial phenotypes and cellular mechanisms underlying decreased dosage of four genes affected within this region. My

results show that all four genes impacted by this CNV variably contribute to normal craniofacial morphogenesis in *Xenopus laevis* (**Figure 4.9**), in a model where decreased gene dosage leads to global and specific effects. I also provide evidence that deficits during NCC development may significantly contribute to the craniofacial dysmorphisms associated with the deletion. Specifically, I demonstrate, for the first time, that the 16p12.1-affected genes are enriched in motile NCCs and contribute to normal craniofacial patterning and cartilage formation. Several of these genes also directly impact NCC migration *in vivo* (*Polr3e*, *Mosmo*, and *Uqrc2*), NCC motility (*Polr3e*, *Uqrc2*, and *Cdr2*), and NCC specification (*Polr3e* and *Mosmo*), revealing new basic roles for these genes during embryonic development.

As the 16p12.1 deletion is multigenic in nature, I sought to determine the basis of phenotypic variability associated with craniofacial malformations by investigating whether singular or multiple genes within this region contribute to either a specific craniofacial defect or a collaborative craniofacial phenotype. Although I have narrowed my studies to focus on how each individual 16p12.1-affected gene contributes to facial patterning, my findings align well with the idea that the presentation of symptoms associated with the deletion is a cumulative product of the impacted region. While *Polr3e* and *Mosmo* depletions severely impacted nearly all examined aspects of craniofacial morphogenesis and NCC development across early developmental stages, *Uqrc2* and *Cdr2* depletions produced very minimal or no phenotypes in these areas.

In particular, I observed a global functional role for *Polr3e*, *Mosmo*, and *Uqrc2* in both craniofacial and cartilage development. Individual depletion of these genes narrowed facial width and area, and decreased eye size in a way that appears analogous to

the smaller head and smaller eye size phenotypes observed in children with the 16p12.1 deletion. Moreover, reduced levels of these genes decreased the size of cartilaginous tissue structures important for jaw and mouth formation, which may correlate with the micrognathia phenotype. However, the phenotypes associated with *Uqcrc2* KD were quite mild in comparison to *Polr3e* or *Mosmo* KD, and *Cdr2* KD had little to no effect on craniofacial or cartilage formation. Thus, further investigation into how these gene depletions function combinatorially to generate the full signature of the 16p12.1 deletion craniofacial dysmorphism is necessary.

It is worthwhile to mention that depletion of the 16p12.1-affected genes in *X. laevis* almost certainly diverges from perfect recapitulation of the 16p12.1 deletion symptoms. *Xenopus* has emerged as a powerful model system to study human genetic diseases of craniofacial development as the majority of disease-associated pathways that drive craniofacial morphogenesis are conserved between these species (Devotta et al., 2018; Dickinson, 2016; Dubey and Saint-Jeannet, 2017; Griffin et al., 2018; Lasser et al., 2019; Lichtig et al., 2020; Mills et al., 2019; Schwenty-Lara et al., 2020; Tahir et al., 2014). However, there are some craniofacial and cartilage morphological differences between *Xenopus* and humans that will prevent some direct correlations to disease pathology. For example, NCCs residing in the hyoid PA that give rise to the ceratohyal cartilage in *Xenopus*, will later give rise to anterior portions of the face and combine with contributions from the Meckel's cartilage to form regions of the lower jaw (Gross and Hanken, 2008; Kerney et al., 2012). In humans, Meckel's cartilage will similarly form portions of the lower jaw but will also become part of the middle ear skeletal structures. Therefore, morphological impacts resulting from aberrant development of these tissues

may have more direct correlates to human pathology in the context of PA migration and NCC development.

Within that effort, my work has demonstrated an enrichment of these gene transcripts in NCCs and their necessity during specific NCC-related processes which may be the driving mechanism underlying the observed craniofacial and cartilage defects. Decreased dosage of *Polr3e* or *Mosmo* significantly affected PA migration *in vivo* leading to decreased PA area, length, and migration distance from the neural tube. Although *Uqcrc2* KD led to both craniofacial and cartilage defects, surprisingly, its depletion caused an increase in PA area and length, possibly due to inappropriate proliferation and expansion of NCCs. My data suggests that these PA migration defects are likely due to gene-specific effects during aspects of NCC development, as *Polr3e* KD impacted both NCC motility and specification, *Mosmo* KD impacted NCC specification, and *Uqcrc2* KD impacted NCC motility.

While I show that several 16p12.1-affected genes are important for regulating NCC development and subsequent formation of their tissue derivatives, this largely neglects why any of these genes may be exceptionally critical in these tissues. This question must be left to some speculation, as the cell biological functions of these genes are extremely diverse and warrant further comprehensive investigation in the context of embryonic craniofacial and NCC development. However, a brief summary of the known roles of these genes and how they may mechanistically influence NCC-related processes are outlined here.

*POLR3E* is a subunit of RNA polymerase III, important for regulating the transcription of small RNAs, such as 5S rRNA and tRNAs (Hu et al., 2002). Though, the

precise role of this subunit in relation to RNA polymerase III activity has not been well studied. RNA polymerase III is known to be critical for proper cell growth and differentiation, supporting the idea that its alteration would lead to deficits in these processes (Dumay-Odelot et al., 2010). While, depletion of *Polr3e* did not significantly alter NCC proliferation, it did effect NCC specification, suggesting that it may be important for regulating transcription of genes necessary in maintaining the identity and subsequent differentiation of NCCs. Moreover, mutations in other subunits of RNA polymerase III, *POLRIC* and *POLRID* have been associated with leukodystrophy, ataxia, and the congenital craniofacial disorder, Treacher Collins syndrome (Ghesh et al., 2019; Kadakia et al., 2014; Noack Watt et al., 2016; Papageorgiou et al., 2020). Studies suggest that loss of function of these genes results in cartilage hypoplasia and cranioskeletal anomalies due to deficient ribosome biogenesis, increases in cellular death, and deficiencies in NCC migration (Noack Watt et al., 2016). Given that *POLR3E* has been shown to interact with *POLRIC* and *POLRID*, it is plausible that it may function in a similar capacity.

Recent work in cell culture suggests that *MOSMO* acts as a negative regulator of sonic hedgehog signaling (Shh) by degrading the Frizzled class receptor, Smoothened (Pusapati et al., 2018a), and my work is the first to elucidate the *in vivo* cellular function of this gene in the context of vertebrate embryonic craniofacial development. The Shh pathway is known to be critical for craniofacial morphogenesis as upregulation or downregulation of signaling can lead to aberrant NCC patterning, development, and maintenance (Abramyan, 2019; da Costa et al., 2018; Dworkin et al., 2016; Everson et al., 2017; Grieco and Hlusko, 2016; Hammond et al., 2018; Millington et al., 2017;

Okuhara et al., 2019; Wang et al., 2019). Shh signaling coordinates the downstream intracellular activity of Gli TFs, which stimulate transcription of several target genes required for NCC induction and specification (Cerrizuela et al., 2018; Millington et al., 2017; Rogers and Nie, 2018). This aligns well with my results demonstrating that *Mosmo* can directly impact NCC specification, highlighting a new cell biological role for this gene. Additionally, Shh interacts with other morphogenic signaling pathways like BMP, Wnt, FGF, and Notch, all of which are required for NCC development. In particular, enhancement of the Shh gradient can restrict canonical Wnt signaling by promoting expression of genes encoding Wnt inhibitors, causing an increase in NCC proliferation and expansion that eventually results in craniofacial defects such as cleft lip (Hammond et al., 2018; Kurosaka et al., 2014). As *MOSMO* is a negative regulator of Shh signaling, its depletion should lead to upregulation of the pathway. Therefore, it is possible that reducing *MOSMO* dosage levels disrupts downstream target gene expression, specifically genes required for NCC specification, and perturbs Wnt signaling such that NCC development is impacted, leading to craniofacial and cartilage morphogenesis defects.

*UQCRC2* is a component of the mitochondrial respiratory chain complex III that is required for its assembly and is important for normal mitochondrial activity to produce ATP (Gaignard et al., 2017; Hammond et al., 2018; Kurosaka et al., 2014; Miyake et al., 2013). Reduced levels of *Uqcrc2* produced both craniofacial and cartilage phenotypes, potentially due to decreased NCC motility. This could be especially damaging in the context of multipotent NCCs, as metabolism is increasingly demonstrated to perform a commanding role in determination of cell fate and subsequent motility (Mathieu and Ruohola-Baker, 2017; Perestrelo et al., 2018; Sperber et al., 2015). My results also

demonstrate that depletion of *Uqcrc2* leads to an increase in PA area and length, potentially due to unchecked NCC expansion and proliferation. Studies suggest that overexpression of *UQCRC2* is correlated with tumor progression through increased cellular proliferation (Shang et al., 2018). Thus, its depletion may also upregulate cell proliferation through a feedback mechanism to compensate for lower gene dosage levels. Moreover, patients with mutations of this gene have recurrent liver failure, lactic acidosis, and hypoglycemia (Gaignard et al., 2017; Miyake et al., 2013). As *Xenopus* is an excellent model for studying the development of both liver and kidney organ systems (Blackburn et al., 2019; Blackburn and Miller, 2019), and as I have shown enrichment of *Uqcrc2* in the *Xenopus* kidney, it would be interesting to further examine how this gene mechanistically regulates development and function of these tissues.

*CDR2* is an oncogenic protein that is strongly expressed in the cerebellum and is ectopically produced by tumor cells, specifically in ovarian and breast malignancies (Hwang et al., 2016; Schubert et al., 2014; Venkatraman and Opal, 2016). Loss of immune tolerance to this protein is believed to trigger the synthesis of the autoantibody, leading to an immunological reaction causing cerebellar degeneration. *CDR2* is also believed to play multiple roles in the regulation of transcription by interacting with the TF c-Myc, sequestering it in the cytoplasm, and inhibiting its transcription of downstream target genes (O'Donovan et al., 2010; Okano et al., 1999). It is known that the expression of c-Myc is required for correct temporal and spatial development of NCCs (Bellmeyer et al., 2003), and while here, I focused on exploring how depletion of *Cdr2* affects craniofacial morphogenesis, understanding how overexpression of this gene affects NCC development warrants further study. *CDR2* mRNA can be found in almost all cell types,

however, its protein expression is limited to Purkinje neurons, some brainstem areas, and spermatogonia (Venkatraman and Opal, 2016). This could explain why depletion of this gene in *Xenopus* did not produce significant craniofacial or cartilage defects, nor affect NCC developmental processes. It is also possible that other closely related genes such as *CDR1*, *CDR3*, or *CDR2L*, can functionally compensate for the lack of *CDR2* levels. Altogether, it is clear that our current knowledge of how these genes ultimately contribute to embryonic craniofacial and cartilage morphogenesis is lacking, and further basic cell biological examination of 16p12.1-affected gene function within a developmental context is necessary for a better mechanistic understanding of the 16p12.1 deletion etiology.

Finally, it will also be essential to explore how these genes ultimately synergistically or epistatically regulate the pathology associated with the 16p12.1 deletion. To this aim, my model provides a unique advantage by being a moderate-throughput, titratable, and inexpensive system to combinatorially deplete numerous genes simultaneously. Thus, the next step will be to perform depletions in tandem to more closely reflect the genetic perturbations observed in patients with the 16p12.1 deletion and determine whether these four genes contribute to a collaborative craniofacial phenotype. Together, my current and ongoing work suggests significant roles for several 16p12.1-affected genes as potent effectors of NCC-derived tissues that regulate specific processes during their development, providing a foundation for the underlying mechanisms contributing to the craniofacial defects associated with the 16p12.1 deletion.

16p12.1 gene	Craniofacial Morph.	Cartilage Morph.	PA migration	NCC motility	NCC proliferation	NCC specification
<b>Mosmo</b>	✓ Reduced Size of facial features	✓ Reduced Size of cartilage elements	✓ Reduced Arch area, length, migration	✗ No phenotype	✗ No phenotype	✓ Reduced Expression of <i>sox9</i> and <i>twist</i>
<b>Polr3e</b>	✓ Reduced Size of facial features	✓ Reduced Size of cartilage elements	✓ Reduced Arch area, length, migration	✓ Reduced Mean NCC speed	✗ No phenotype	Reduced Expression of <i>sox9</i> and <i>twist</i>
<b>Uqrc2</b>	✓ Reduced Size of facial features	✓ Reduced Size of cartilage elements	✓ Increased Arch area, length	✓ Reduced Mean NCC speed	✗ No phenotype	✗ No phenotype
<b>Cdr2</b>	✓ Reduced Size of facial features	✗ No phenotype	✓ Increased Arch length	✓ Increased Mean NCC speed	✗ No phenotype	✗ No phenotype

**Figure 4.9 Summary table of 16p12.1-affected gene craniofacial, cartilage, and NCC phenotypes**

Partial depletion of 16p12.1-affected genes demonstrates numerous impacts on craniofacial, cartilage, and NCC development. Tissues are denoted as affected (checked box) if phenotypes were significantly different from control ( $p < 0.05$ ); see individual figures for data distribution and statistics.

#### 4.4. Materials and Methods

##### 4.4.1. *Xenopus* husbandry

Eggs obtained from female *Xenopus laevis* were fertilized in vitro, dejellied and cultured at 14-23°C in 0.X Marc's modified Ringer's (MMR) using standard methods (cite). Embryos received injections of exogenous mRNAs or antisense oligonucleotide strategies at the two or four cell stage, using four total injections performed in 0.1X MMR media containing 5% Ficoll. Embryos were staged according to Nieuwkoop and Faber (cite). All experiments were approved by the Boston College Institutional Animal Care and Use Committee and were performed according to national regulatory standards.

##### 4.4.2. Morpholino Depletion and Validation

Morpholinos (MOs) were targeted to early splice sites of *X. laevis Mosmo* (for L, 5-ACAATTGACATCCACTTACTGCCGG-3; for S, 5-CACCTTCCCTACCCCGCTACTTAC-3), *Polr3e* (for L, 5-ACTGTAAGCCTCTTTTGCCTTACCT-3), *Uqrc2* (for L, 5-

ACAGTGTCTCTAAAGCACAGATACA-3; for S, 5-CCCCTAACCCATTAAACATATACCT-3), *Cdr2* (for L and S, 5-CATCCCTCCCATACTCACCTTG-3), or standard control MO (5-cctcttacctcagttacaatttata-3); purchased from Gene Tools (Philomath, OR). In knockdown (KD) experiments, all MOs were injected at either the 2-cell or 4-cell stage with embryos receiving injections 2 or 4 times total. *Mosmo* and control MOs were injected at 12ng/embryo for 50% KD and 20ng/embryo for 80% KD; *Polr3e* and control MOs were injected at 5ng/embryo for 30% KD, 10ng/embryo for 50% KD and 20ng/embryo for 80% KD; *Uqcrc2* and control MOs were injected at 35ng/embryo for 50% KD and 50ng/embryo for 80% KD; *Cdr2* and control MOs were injected at 10ng/embryo for 50% KD. Splice site MOs were validated through a Reverse Transcriptase Polymerase Chain Reaction (RT-PCR) as previously described.

#### 4.4.3. Whole-mount *in situ* hybridization

Embryos were fixed overnight at 4°C in a solution of 4% paraformaldehyde in PBS, gradually dehydrated in ascending concentration of methanol in PBS, and stored in methanol at -20°C for a minimum of two hours, before *in situ* hybridization, performed as previously described (cite). After brief proteinase K treatment, embryos were bleached under a fluorescent light in 1.8x saline-sodium citrate, 1.5% H<sub>2</sub>O<sub>2</sub>, and 5% (vol/vol) formamide for 20 minutes to 45 minutes before prehybridization. During hybridization, probe concentration was 0.5ug/mL.

The *Xenopus twist* hybridization probe was a kind gift from Dr. Dominique Alfandari (University of Massachusetts at Amherst, MA), and the *Xenopus sox9* hybridization probe was a kind gift from Dr. Richard Harland and Dr. Helen Willsey (University of California Berkeley and University of California SF, CA). The templates

for making antisense probes for *polr3e*, *mosmo*, *uqcr2*, and *cdr2* was PCR amplified from the reverse transcribed cDNA library, using the following primer sets: *Polr3e* forward, 5' – GGATAGTCGCTCAGAACACG – 3', *Polr3e* reverse, 5' – GGGTCAGCTTTGTCTGGATC – 3', *Mosmo* forward, 5' – TCTGGATGTTTGTCTGGCTGC – 3', *Mosmo* reverse, 5' – GGGTAATTTGTAGGGTTGGCCTC – 3', *Uqcr2* forward, 5' – TCCTCTCTAGGAGGCTTTACTCTG – 3', *Uqcr2* reverse, 5' – GGGAGCCAATTCACCAATCAG – 3', *Cdr2* forward, 5' – GACAGCAACGTGGAGGAGTTC – 3', and *Cdr2* reverse, 5' – GCGCAGATCATAACAGCTCCTTC – 3'. The antisense digoxigenin-labeled hybridization probes were transcribed in vitro using the T7 MAXIscript kit. Embryos were imaged using a Zeiss AxioCam MRc attached to a Zeiss SteREO Discovery.V8 light microscope. Images were processed in ImageJ.

#### 4.4.4. Cartilage staining

At stage 42, *Xenopus* embryos were anesthetized with benzocaine and fixed in 4% paraformaldehyde in PBS overnight. Alcian blue staining of embryos was performed based on the Harland Lab protocol. Before ethanol dehydration, embryos were bleached under a fluorescent light in 1.8x saline-sodium citrate, 1.5 H<sub>2</sub>O<sub>2</sub>, and 5% (vol/vol) formamide for 30 minutes. Embryos were imaged in PBS, using a Zeiss AxioCam MRc attached to a Zeiss SteREO Discovery.V8 light microscope. Images were processed in ImageJ. Analysis of cartilage structures was performed in ImageJ utilizing the polygon, area, and line functions (cite). Measurements included the average ceratohyal area (outlined cartilage in Fig X), and the branchial arch width, which was quantified by

taking the width of the branchial arch across the widest point. Differences were analyzed by student's unpaired t-test using Graphpad (Prism).

#### **4.4.5. Half-embryo injections**

Half KDs were performed at the two-cell stage. *X. laevis* embryos were unilaterally injected two times with either control MO or 16p12.1 gene-specific MO and a GFP mRNA construct. The other blastomere was left uninjected. Embryos were raised in 0.1X MMR through neurulation, then sorted based on left/right fluorescence. For NCC specification experiments, embryos were fixed at stage 16, and for pharyngeal arch (PA) visualization, embryos were fixed between stage 25-30. Whole-mount *in situ* hybridization was then performed according to the previously described procedure. Analysis of NCC specification markers from *in situ* experiments was performed on dorsal view images in ImageJ by measuring the total area of expression using the polygon tool. Analysis of PAs from *in situ* experiments was performed on lateral view images in ImageJ. Measurements were taken to acquire: 1) arch area, the area of individual PA determined using the polygon tool, 2) arch length, the length of the distance between the top and bottom of each PA, and 3) arch migration, the ventral most part of the PA to the neural tube. All measurements were quantified by taking the ratio between the injected side versus the uninjected side for each sample, respectively. Statistical significance was determined using a student's unpaired t-test in Graphpad (Prism).

#### **4.4.6. Neural crest explants, imaging, and analysis**

Embryos at stage 17 were placed in modified DFA solution (53mM NaCl, 11.7mM  $\text{Na}_2\text{CO}_3$ , 4.25mM K Gluc, 2mM  $\text{MgSO}_4$ , 1mM  $\text{CaCl}_2$ , 17.5 mM Bicine, with 50ug/mL Gentamycin Sulfate, pH 8.3), before being stripped of vitelline membranes and imbedded in clay with the anterior dorsal regions exposed. Skin was removed above the

NCC using an eyelash knife, and NCCs were excised. Explants were rinsed, and plated on fibronectin-coated coverslips in imaging chambers filled with fresh DFA. Tissues were allowed to adhere forty-five minutes before being moved to the microscope for time-lapse imaging of NCC motility. Microscopy was performed on a Zeiss Axio Observer inverted motorized microscope with a Zeiss 20x N-Achroplan 0.45 NA Phase-contrast lens, using a Zeiss AxioCam camera controlled with Zen software. Images were collected using large tiled acquisitions to capture the entire migratory field. Eight to ten explants, from both control and experimental conditions were imaged at a six-minute interval, for six hours. Data was imported to ImageJ, background subtracted, and cropped to a uniform field size. Migration tracks of individual cells were collected manually using the Manual Tracking plug-in. Mean speed rates were imported to Graphpad (Prism), and compared between conditions using student's unpaired t-tests. Three independent experiments were performed for each condition.

For NCC proliferation, NCC tissue explants were allowed to adhere and migrate on fibronectin-coated coverslips for four hours before being fixed in 4% paraformaldehyde. Explants were permeabilized in 0.1% Triton-X 100 in PBS, blocked with a solution containing 2% bovine serum albumin, 0.1% Triton-X 100 in PBS, and incubated in Phospho-Histone H3 (Ser10) (Invitrogen, PA5-17869, polyclonal, 1:500), goat anti-rabbit Alexa Fluor<sup>488</sup> conjugate secondary antibody (Invitrogen, 1:1000), Alexa Fluor<sup>568</sup> phalloidin (Invitrogen, 1:500), and Hoechst 33342 solution (Invitrogen, 1:1000). Microscopy was performed on a Zeiss AiryScan inverted motorized microscope with a Zeiss 20X lens, using a Zeiss AxioCam camera controlled with Zen software. Images were acquired using large tiled acquisitions to capture the entire migratory field. Images

of five to seven explants, from both control and experimental conditions were imported to ImageJ, and the total number of PH3-labeled positive cells versus the total number of cells were quantified using an automated particle counter after thresholding each image. Cell counts were imported to Graphpad (Prism), and compared between conditions using student's unpaired t-test. Three independent experiments were performed for each condition.

## **CHAPTER 5**

### **Discussion**

## 5.1 Contributions to the literature

### *5.1.1 Interactions between pairs of genes within the 3q29 region underlie the potential for highly complex models of CNV pathogenicity*

Genomic and functional data have implicated multiple genes in variably-expressive CNV regions towards neuropsychiatric and neurodevelopmental phenotypes, suggesting that single causative genes cannot fully account for the phenotypic heterogeneity associated with pathogenic CNVs (Deshpande and Weiss, 2018; Girirajan et al., 2011; Jensen and Girirajan, 2017, 2019; Lauer and Gresham, 2019; Vicari et al., 2019). Therefore, more comprehensive functional analyses for each gene within CNVs and their interactions is necessary to identify convergent biological pathways responsible for neurocognitive features associated with specific affected chromosomal regions. In this regard, with my collaborators, we explored the possibility of an interaction-based model for an understudied pathogenic CNV at chromosome 3q29, in which affected genes within each region interact with each other to influence phenotypic trajectories associated with the mutation.

Although previous work has implicated the 3q29 deletion as a significant risk factor for schizophrenia and ASD, among a range of other developmental defects (Mulle, 2015; Rutkowski et al., 2019), a deeper characterization of the conserved biological mechanisms that are disrupted by this deletion was lacking. Moreover, a majority of previous studies focused on identifying singular causative genes in the 3q29 region based on their established roles in neuronal development (Humbert et al., 2003; Luo and Rubinsztein, 2009; Marlin et al., 2011; Rutkowski et al., 2019; Saiga et al., 2009; Shin et al., 2002; Walch, 2013; Wang et al., 2014; Wang et al., 2018). However, individual

haploinsufficiency of these candidate genes did not account for the wide range of phenotypes associated with the deletion, nor did they recapitulate the behavioral and developmental phenotypes observed in animal models that contain the entire 3q29 deletion region. Thus, in this work, using the *Xenopus laevis* model system (to complement my collaborator's work using *Drosophila melanogaster*), I identified novel developmental, cellular, and neuronal phenotypes for previously unexplored individual 3q29 gene homologs following their depletion, and studied the effects of their combinatorial depletion on these phenotypes to gain a better understanding of the mechanisms underlying the deletion.

One of the significant findings of my work is that my analysis of developmental phenotypes with individual knockdown of 3q29 homologs showed that a single gene within the region may not be solely responsible for the overall effects of the deletion. In particular, simultaneous depletion of *NCBP2* with other 3q29 gene homologs enhanced several developmental phenotypes in *Xenopus laevis* (and *Drosophila*), leading to significant increases in disrupted cellular organization, as well as brain and eye morphology alterations, suggesting that *NCBP2* could be a key modulator of other genes in this region. *NCBP2* does not have any identified deleterious mutations in sequencing studies of neurodevelopmental disease so far, strengthening the hypothesis that it may act as a potential modifier of other affected genes within the 3q29 region.

Additionally, the cellular and neuronal defects observed following *NCBP2* depletion were rescued with overexpression of the apoptosis inhibitor *Diap1* in flies, and *xiap* in *Xenopus*, suggesting that apoptosis is one of several potential biological mechanisms disrupted by the deletion. *NCBP2* encodes a subunit of the nuclear cap-

binding complex (CBC), which binds to the 5' end of mRNA and microRNA in the nucleus (Pabis et al., 2010). Studies have demonstrated a significant role of the CBC in post-translational regulatory mechanisms such as nonsense mediated mRNA decay, alternative splicing, and mRNA transport (Gonatopoulos-Pournatzis and Cowling, 2014; Maquat, 2004). Therefore, my collaborators and I propose that disruption of *NCBP2* could modify several cellular and molecular processes that may not be directly related to apoptosis, but instead could alter other biological events that then ultimately result in aberrant programmed cell death. Thus, my findings offer a foundation to further explore the role of *NCBP2* in the context of cell-cycle related processes, particularly apoptosis, towards modulating neuronal phenotypes associated with developmental disorders.

### ***5.1.2 16p12.1 deletion homologs independently contribute to neurodevelopmental phenotypes and are modulated by complex interactions with “second-hit” genes***

To continue my investigation from chapter 2 of functionally exploring the basis of phenotypic variability in pathogenic CNVs associated with neurodevelopmental disorders, I, along with my collaborators, analyzed neurodevelopmental phenotypes and mechanisms underlying decreased dosage of genes affected by the 16p12.1 deletion in *Xenopus laevis* and *Drosophila melanogaster*. In chapter 3, my results are the first to confirm a role for *POLR3E* and *MOSMO* during neurodevelopment, where decreased dosage of each gene caused global and specific vertebrate embryonic developmental defects.

First, we observed a global role for *POLR3E* and *MOSMO* in embryonic development, where partial depletion of these genes individually led to rough eye

phenotypes and reduced lifespan in flies, as well as alterations in brain and craniofacial development in *Xenopus laevis*. However, both of these gene homologs also exhibited other neurodevelopmental phenotypes that were gene-specific. For example, gene expression analysis showed that decreased dosage of *POLR3E* led to alteration of pathways associated with muscle contraction and developmental delay, pinpointing this gene as a candidate contributor for these phenotypes associated with the deletion. Further, partial depletion of *POLR3E* led to decreased cellular proliferation in both flies and *Xenopus laevis*, and transcriptomic analysis in this knockdown showed dysregulation of cell-cycle genes, suggesting that the phenotypes observed following *POLR3E* knockdown are caused by alterations of cellular proliferation processes.

Additionally, we found that decreased expression of *MOSMO* led to decreased complexity of dendritic arbors in flies and a reduction in axon length in *Xenopus laevis*, both of which are phenotypes recurrently associated with ASD (Castren et al., 2005; Kishi and Macklis, 2004; Kwon et al., 2006; Stuss et al., 2012). Abnormal axon and dendrite growth has been observed in hippocampal neurons in mice with altered ribosomal biogenesis (Kwon et al., 2006). Therefore, the observed decrease in dendritic arborization and axon outgrowth could potentially be related with the altered expression of genes involved in posttranscriptional modifications of ribosomal RNA, likely affecting its activation and function. Further, studies have implicated *MOSMO* as a negative regulator of Sonic hedgehog signaling (Shh) (Pusapati et al., 2018). This signaling pathway is critical for proper axon guidance during embryonic neurodevelopment, specifically impacting the correct positioning of dorsal commissural axons across the midline of the developing spinal cord (Iulianella and Stanton-Turcotte, 2019; Wu et al.,

2019; Yao et al., 2015). Thus, disruption of *MOSMO* may alter the gradient of Shh signaling such that it leads to downstream detrimental effects on axon pathfinding and growth during development of the nervous system.

In this work, I also assessed whether simultaneous depletion of “second-hit” gene homologs identified in families with the deletion, along with 16p12.1-affected genes, would contribute to a more severe neurodevelopmental phenotype in an additive or synergistic fashion. Interestingly, we found that concomitant knockdown of *MOSMO* with the “second-hit” gene, *SETD5*, worsened the eye phenotype in flies and the axon outgrowth phenotype in *X. laevis*, compared to individual partial depletion of each gene. In contrast, while simultaneous reduction of *POLR3E* with *SETD5* led to neurodevelopmental defects, these were not significantly more severe than the phenotypes observed due to individual reduction of each gene, respectively. Thus, our results indicate that *MOSMO* genetically interacts with *SETD5* in a synergistic manner, potentially functioning through a similar biological pathway to influence neurodevelopmental processes, whereas *POLR3E* and *SETD5* likely do not interact with one another and instead, lead to neurodevelopmental phenotypes associated with the deletion in an additive manner.

Thus, this work supports a pleiotropic model for haploinsufficiency of the 16p12.1 deletion genes, in which they independently sensitize, in a moderate manner, an affected individual to multiple phenotypic domains, with major defects resulting from depletion of *POLR3E* and *MOSMO*. Additionally, my results indicate that mutations of other “second-hit” genes contribute to the phenotypic variability associated with the deletion, and that the severity of an individuals’ symptoms depends on the functional

association of “second-hits” with genes in the 16p12.1 region. Together, our studies of the 16p12.1 deletion provide an example of how different genes within a pathogenic CNV contribute to multiple neurodevelopmental phenotypes and are modulated by other “second-hit” genes, offering further functional evidence of the complex oligogenic nature of neurodevelopmental disorders.

### ***5.1.3 16p12.1 deletion homologs contribute to craniofacial and cartilage phenotypes through aberrant neural crest cell development***

As discussed throughout this thesis, in addition to pronounced intellectual disability, microcephaly, seizures, and delayed growth, patients with the 16p12.1 deletion present with severe craniofacial defects. These include underdeveloped cartilaginous tissue structures in the ears and nose, jaw malformation, deep-set eyes, and facial asymmetries. As these tissues all derive from a shared embryonic precursor, the neural crest, I hypothesized that one or more of the 16p12.1-affected genes perform critical functions during NCC formation and subsequent migration. Thus, in chapter 4, I expanded upon our functional analyses of the 16p12.1-affected genes from chapter 3, and I characterized their roles during embryonic craniofacial and cartilage morphogenesis to assess whether one or more of these genes contribute to the facial phenotypes observed in patients with the deletion.

First, I found that all four *X. laevis* 16p12.1 gene homologs, *Polr3e*, *Mosmo*, *Uqrc2*, and *Cdr2*, shared tissue-specific enrichment within the neural tube, the pharyngeal arches where migratory neural crest reside, and later craniofacial structures. Moreover, I found that partial depletion of any one of these four genes was sufficient to

variably impact aspects of facial patterning, cartilage formation, and NCC development. In particular, I found that partial depletion of *Polr3e* and *Mosmo* explicitly affect *in vivo* NCC streaming into the pharyngeal arches and alter the expression of TFs that are critical for NCC specification. Additionally, reduction of *Polr3e* and *Uqcrc2* significantly impacted individual NCC migration rates *in vitro*. Thus, I have determined a model in which numerous genes within the 16p12.1 region potentially impact craniofacial and cartilage development, and that their contributions to craniofacial phenotypes associated with the 16p12.1 deletion stem from essential functions during NCC-derived tissue formation.

This model is further supported by the different established cellular functions associated with the 16p12.1-affected genes, particularly *POLR3E*, *MOSMO*, and *UQCRC2*. As stated, *POLR3E* is a subunit of RNA polymerase III, and while its role in relation to RNA polymerase III activity is not known, it may be important for regulating transcription of genes necessary in maintaining the NCC population. In relation to *MOSMO*, my work is the first to elucidate the *in vivo* function of this gene during embryonic craniofacial development. As it has been demonstrated to function in the Shh signaling pathway, which is known to be critical for NCC formation and maintenance (Dworkin et al., 2016), it is possible that *MOSMO* directly impacts NCC development through modulation of Shh signaling. Finally, *UQCRC2* likely influences NCC development through proper mitochondrial function, as metabolism has been increasingly demonstrated to perform a commanding role in cell fate determination, motility, and maintenance (Perestrelo et al., 2018).

Overall, my work is the first to propose aberrant NCC formation and migration as a potential mechanism underlying the pathology of the craniofacial defects associated with the 16p12.1 deletion. It is also the first study to uncover novel functions of multiple 16p12.1-affected genes in the context of vertebrate craniofacial and cartilage morphogenesis on a shared and easily comparable developmental model platform. Together, the studies described in chapter 4 have established the groundwork for further examination of the interplay and synergistic impacts of reduction of multiple 16p12.1-affected genes towards craniofacial patterning, and how they may contribute to unique craniofacial phenotypes of the 16p12.1 deletion that are not be fully explained by any one singular gene depletion.

## **5.2 Future directions**

A major focus of my thesis work was to identify points of functional convergence among genes that are affected by pathogenic CNVs associated with neurodevelopmental disorders. To this aim, using complementary *Drosophila* and *X. laevis* model systems, I interrogated the developmental effects, cellular mechanisms, and genetic interactions of CNV-affected gene homologs within the 3q29 and 16p12.1 chromosomal regions. My primary findings were recapitulated between both models, indicating that the embryonic functions of these genes are conserved between an invertebrate and vertebrate organism. While several themes emerged from my studies that exemplify the genetic and mechanistic complexity of these CNV-affected regions, there are further questions that remain to be answered, and the following sections will summarize these questions briefly.

### ***5.2.1 Dissecting the convergent biological mechanisms underlying CNVs associated with neurodevelopmental disorders***

The discovery of genetic mutations that lead to the dysregulation of several cellular processes, such as apoptosis and cell proliferation, have been implicated in the pathogenesis of neurodevelopmental disorders (Courchesne et al., 2011; Glantz et al., 2006; Kaushik and Zarbalis, 2016; Kreczmanski et al., 2007). For example, aberrant apoptosis in the early developing brain has been suggested as a possible mechanism for the decreased number of neurons observed in individuals with ASD or schizophrenia (Courchesne et al., 2011; Kreczmanski et al., 2007). In addition to neuropsychiatric disorders, increased neuronal apoptosis and abnormal cell proliferation have been suggested as possible mechanisms associated with microcephaly phenotypes (Poulton et al., 2011). My results provide support towards this model of functional convergence among cell-cycle related processes, as we found that multiple 3q29 and 16p12.1 gene homologs contribute to a range of deleterious phenotypes due to disruption of both apoptosis and cell proliferation in these different tissue and organ systems.

First, in chapter 2, we found that individual and simultaneous depletion of the 3q29 gene homologs, *NCBP2* and *FBXO45*, in both *Drosophila* and *X. laevis* led to altered expression of cell-cycle and apoptosis genes, morphological defects including decreased brain size and cellular disorganization, as well as increased cleaved-caspase 3 levels. We further found overexpression of the apoptosis inhibitors, *Diap1* and *xiap*, rescued the cellular and neuronal phenotypes observed with knockdown of these genes, providing important validation for the involvement of apoptosis as a mechanism underlying this deletion. Apoptosis mechanisms are well-conserved between *X. laevis*,

*Drosophila*, and humans, with key genes, such as *XIAP* (*Diap1/xiap*), sharing the same roles in programmed cell death across these organisms (Kornbluth and White, 2005; Tittel and Steller, 2000; Xu et al., 2009). Overall, my findings highlight the importance of apoptosis towards modulating neuronal phenotypes that could be responsible for developmental disorders. Although I focused on testing apoptosis phenotypes with knockdown of the 3q29 gene homologs, I note that apoptosis is potentially only one of many cellular pathways disrupted by the 3q29 deletion, as several 3q29 gene have been previously associated with other cell-cycle related functions (Bilder et al., 2000; Humbert et al., 2003; Saiga et al., 2009; Shin et al., 2002; Wang et al., 2018). Moreover, the 3q29 deletion encompasses 21 genes, many of which do not have homologs in either *Drosophila* or *X. laevis* models. Therefore, follow-up studies identifying additional conserved pathways in other model systems will be useful to overcome this limitation of testing the neurodevelopmental phenotypes and interactions of 3q29 genes without fly or *X. laevis* homologs.

Second, in chapters 3 and 4, I found that the developmental and cellular phenotypes associated with the 16p12.1 deletion were primarily caused by partial depletion of either *POLR3E* or *MOSMO*, likely due to alterations of cell proliferation and neural crest cell related processes. For example, the significant reduction in brain and eye sizes due to partial depletion of *POLR3E* correlated with decreased pH3 levels and transcriptomic analysis in this knockdown showed dysregulation of cellular proliferation genes. Further, it has been postulated that the rate of proliferation outnumbers that of apoptosis by almost 100-fold during neuronal development (Gilbert and Man, 2017), which supports a stronger consequence of reduction in proliferation processes compared

to that of apoptosis in this context. The cellular mechanisms underlying the neurodevelopmental phenotypes observed with depletion of *MOSMO* are slightly more challenging to interpret. While we observed a moderate reduction in pH3 levels in the developing fly brain when *MOSMO* was knocked down, I did not observe a similar result in *X. laevis*. This difference could potentially be explained by tissue-specific or organism-specific differences in the expression and function of the gene, or a limitation of the particular assays that were performed. Therefore, additional studies regarding the cellular functions of *MOSMO* towards neurodevelopment are necessary. Interestingly however, reduction of either *POLR3E* or *MOSMO* led to severe defects during craniofacial and cartilage morphogenesis, and these defects likely resulted from abnormal NCC specification and migration, providing evidence towards a novel convergent cellular mechanism contributing to the craniofacial phenotypes associated with this deletion.

### ***5.2.2 A multigenic model for CNV pathogenicity***

My analysis of developmental phenotypes with knockdown of either 3q29 or 16p12.1 gene homologs support a model in which a single gene within the region is not solely responsible for the effects of the deletion. In fact, my results in chapter 2 show that *NCBP2* could be a key modulator of other genes within the 3q29 region, as simultaneous depletion of this gene with other 3q29 homologs enhanced several neurodevelopmental phenotypes in both *Drosophila* and *X. laevis* models. In a similar fashion, as described in chapter 3, concomitant knockdown of the 16p12.1 gene, *MOSMO*, with the “second-hit” gene *SETD5*, also enhanced several neurodevelopmental phenotypes in both systems, suggesting a synergistic interaction between these genes. As *SETD5* is predicted to be a

histone methyltransferase (Deliu et al., 2018; Kuechler et al., 2015; Moore et al., 2019; Nakagawa et al., 2020; Osipovich et al., 2016; Szczaluba et al., 2016), it is possible that the mechanisms contributing to the neurodevelopmental phenotypes associated with concomitant reduction of *MOSMO* and *SETD5* could be due to posttranscriptional modifications and changes in chromatin remodeling, though this hypothesis requires further in-depth analyses. Overall, this genetic interaction model is in contrast to that of other syndromic CNVs where the core phenotypes can be due to a single gene (such as *RAI1* in Smith-Magenis syndrome), or a subset of individual genes in the contiguous region (as in Williams-Beuren syndrome), but rather agrees with a model in which complex interactions between genes within these deletions, acting through common pathways, determine the phenotypic severity.

While I only tested a subset of all potential interactions among the 3q29 and 16p12.1 gene homologs, my results highlight conserved mechanistic relationships between individual genes and their interactions with one another towards understanding the effects of the entire deletion. Screening for interactions among these genes and additional differentially-expressed genes in the transcriptome could be particularly useful in identifying potential therapeutic targets for these CNV deletion phenotypes. Furthermore, as these genetic interactions may vary across different species, developmental timepoints, and tissues, the role of these interactions should be more deeply explored using mouse and human cell culture models. Thus, the possibility of other genetic interactions is intriguing and warrants further study to assess whether the genes within these regions may function in similar biological pathways that affect broader neurodevelopmental processes.

### 5.3 Concluding remarks

Development of the central nervous system requires the proper function of thousands of genes in order to regulate distinct processes during neurogenesis and formation of neural connections within the brain. Understanding the mechanisms that govern various aspects of neurodevelopment is critical, as deleterious mutations of genes that are important for building a properly functioning nervous system can lead to an array of neurodevelopmental disorders including ASD, intellectual disabilities, and schizophrenia. Therefore, the aim of this thesis in that regard was to uncover points of functional convergence among understudied genes that have been recently associated with neurodevelopmental disorders.

In this thesis, I characterized novel functions of CNV-affected genes within the 3q29 and 16p12.1 regions that are linked to neurodevelopmental defects in individuals with these pathogenic deletions. I, for the first time, showed that numerous 3q29 and 16p12.1-affected genes contribute to specific neurodevelopmental phenotypes and that they likely function within shared biological pathways to influence development of the tissue and organ systems affected by these deletions. Furthermore, my results show that the 3q29 and 16p12.1 deletions are examples of how different CNV-affected genes contribute to multiple neurodevelopmental phenotypes through interactions by other developmental genes within and outside of these regions, providing functional evidence of the complex oligogenic nature of neurodevelopmental disorders.

Exploring these findings in vertebrate models, like *Xenopus laevis*, and integrating them with human functional data is necessary to provide a conserved mechanism of the pathogenicity associated with the 3q29 and 16p12.1 deletions.

Together, the work in this thesis has laid the foundation for expanding these analyses to other CNV regions associated with disease to further delineate global models of molecular pathogenesis associated with neurodevelopmental disorders.

## References

- Abrahams, B.S., Arking, D.E., Campbell, D.B., Mefford, H.C., Morrow, E.M., Weiss, L.A., Menashe, I., Wadkins, T., Banerjee-Basu, S., Packer, A., 2013. SFARI Gene 2.0: a community-driven knowledgebase for the autism spectrum disorders (ASDs). *Mol Autism* 4, 36.
- Abramyan, J., 2019. Hedgehog Signaling and Embryonic Craniofacial Disorders. *J Dev Biol* 7.
- Alonso-Gonzalez, A., Rodriguez-Fontenla, C., Carracedo, A., 2018. De novo Mutations (DNMs) in Autism Spectrum Disorder (ASD): Pathway and Network Analysis. *Front Genet* 9, 406.
- Altar, C.A., Jurata, L.W., Charles, V., Lemire, A., Liu, P., Bukhman, Y., Young, T.A., Bullard, J., Yokoe, H., Webster, M.J., Knable, M.B., Brockman, J.A., 2005. Deficient hippocampal neuron expression of proteasome, ubiquitin, and mitochondrial genes in multiple schizophrenia cohorts. *Biol Psychiatry* 58, 85-96.
- Altschul, S.F., Madden, T.L., Schaffer, A.A., Zhang, J., Zhang, Z., Miller, W., Lipman, D.J., 1997. Gapped BLAST and PSI-BLAST: a new generation of protein database search programs. *Nucleic Acids Res* 25, 3389-3402.
- Anders, S., Pyl, P.T., Huber, W., 2015. HTSeq--a Python framework to work with high-throughput sequencing data. *Bioinformatics* 31, 166-169.
- Andrews, T., Honti, F., Pfundt, R., de Leeuw, N., Hehir-Kwa, J., Vulto-van Silfhout, A., de Vries, B., Webber, C., 2015a. The clustering of functionally related genes contributes to CNV-mediated disease. *Genome research* 25, 802-813.
- Andrews, T., Meader, S., Vulto-van Silfhout, A., Taylor, A., Steinberg, J., Hehir-Kwa, J., Pfundt, R., de Leeuw, N., de Vries, B.B., Webber, C., 2015b. Gene networks underlying convergent and pleiotropic phenotypes in a large and systematically-phenotyped cohort with heterogeneous developmental disorders. *PLoS Genet* 11, e1005012.
- Antonacci, F., Kidd, J.M., Marques-Bonet, T., Teague, B., Ventura, M., Girirajan, S., Alkan, C., Campbell, C.D., Vives, L., Malig, M., Rosenfeld, J.A., Ballif, B.C., Shaffer, L.G., Graves, T.A., Wilson, R.K., Schwartz, D.C., Eichler, E.E., 2010. A large and complex structural polymorphism at 16p12.1 underlies microdeletion disease risk. *Nat Genet* 42, 745-750.
- Armstrong, J.D., Texada, M.J., Munjaal, R., Baker, D.A., Beckingham, K.M., 2006. Gravitaxis in *Drosophila melanogaster*: a forward genetic screen. *Genes Brain Behav* 5, 222-239.

- Ashitha, S.N.M., Ramachandra, N.B., 2020. Integrated Functional Analysis Implicates Syndromic and Rare Copy Number Variation Genes as Prominent Molecular Players in Pathogenesis of Autism Spectrum Disorders. *Neuroscience* 438, 25-40.
- Baba, M., Yokoyama, K., Seiriki, K., Naka, Y., Matsumura, K., Kondo, M., Yamamoto, K., Hayashida, M., Kasai, A., Ago, Y., Nagayasu, K., Hayata-Takano, A., Takahashi, A., Yamaguchi, S., Mori, D., Ozaki, N., Yamamoto, T., Takuma, K., Hashimoto, R., Hashimoto, H., Nakazawa, T., 2019. Psychiatric-disorder-related behavioral phenotypes and cortical hyperactivity in a mouse model of 3q29 deletion syndrome. *Neuropsychopharmacology* 44, 2125-2135.
- Ballif, B.C., Theisen, A., Coppinger, J., Gowans, G.C., Hersh, J.H., Madan-Khetarpal, S., Schmidt, K.R., Tervo, R., Escobar, L.F., Friedrich, C.A., McDonald, M., Campbell, L., Ming, J.E., Zackai, E.H., Bejjani, B.A., Shaffer, L.G., 2008. Expanding the clinical phenotype of the 3q29 microdeletion syndrome and characterization of the reciprocal microduplication. *Mol Cytogenet* 1, 8.
- Batalla, A., Bargallo, N., Gasso, P., Molina, O., Pareto, D., Mas, S., Roca, J.M., Bernardo, M., Lafuente, A., Parellada, E., 2015. Apoptotic markers in cultured fibroblasts correlate with brain metabolites and regional brain volume in antipsychotic-naive first-episode schizophrenia and healthy controls. *Transl Psychiatry* 5, e626.
- Battaglia, A., Carey, J.C., South, S.T., 2015. Wolf-Hirschhorn syndrome: A review and update. *Am J Med Genet C Semin Med Genet* 169, 216-223.
- Bellmeyer, A., Krase, J., Lindgren, J., LaBonne, C., 2003. The protooncogene c-myc is an essential regulator of neural crest formation in xenopus. *Dev Cell* 4, 827-839.
- Bestman, J.E., Cline, H.T., 2020. Morpholino Studies in Xenopus Brain Development. *Methods Mol Biol* 2047, 377-395.
- Bharathan, N.K., Dickinson, A.J.G., 2019. Desmoplakin is required for epidermal integrity and morphogenesis in the *Xenopus laevis* embryo. *Dev Biol* 450, 115-131.
- Bhattacharya, D., Marfo, C.A., Li, D., Lane, M., Khokha, M.K., 2015. CRISPR/Cas9: An inexpensive, efficient loss of function tool to screen human disease genes in *Xenopus*. *Dev Biol* 408, 196-204.
- Bilder, D., Li, M., Perrimon, N., 2000. Cooperative regulation of cell polarity and growth by *Drosophila* tumor suppressors. *Science* 289, 113-116.
- Blackburn, A.T.M., Bekheirnia, N., Uma, V.C., Corkins, M.E., Xu, Y., Rosenfeld, J.A., Bainbridge, M.N., Yang, Y., Liu, P., Madan-Khetarpal, S., Delgado, M.R., Hudgins, L., Krantz, I., Rodriguez-Buritica, D., Wheeler, P.G., Al-Gazali, L., Mohamed Saeed Mohamed Al Shamsi, A., Gomez-Ospina, N., Chao, H.T., Mirzaa, G.M., Scheuerle, A.E., Kukulich, M.K., Scaglia, F., Eng, C., Willsey,

- H.R., Braun, M.C., Lamb, D.J., Miller, R.K., Bekheirnia, M.R., 2019. DYRK1A-related intellectual disability: a syndrome associated with congenital anomalies of the kidney and urinary tract. *Genet Med* 21, 2755-2764.
- Blackburn, A.T.M., Miller, R.K., 2019. Modeling congenital kidney diseases in *Xenopus laevis*. *Dis Model Mech* 12.
- Blaker-Lee, A., Gupta, S., McCammon, J.M., De Rienzo, G., Sive, H., 2012. Zebrafish homologs of genes within 16p11.2, a genomic region associated with brain disorders, are active during brain development, and include two deletion dosage sensor genes. *Dis Model Mech* 5, 834-851.
- Blazjewski, S.M., Bennison, S.A., Smith, T.H., Toyo-Oka, K., 2018. Neurodevelopmental Genetic Diseases Associated With Microdeletions and Microduplications of Chromosome 17p13.3. *Front Genet* 9, 80.
- Blum, M., De Robertis, E.M., Wallingford, J.B., Niehrs, C., 2015. Morpholinos: Antisense and Sensibility. *Dev Cell* 35, 145-149.
- Blumenthal, I., Ragavendran, A., Erdin, S., Klei, L., Sugathan, A., Guide, J.R., Manavalan, P., Zhou, J.Q., Wheeler, V.C., Levin, J.Z., Ernst, C., Roeder, K., Devlin, B., Gusella, J.F., Talkowski, M.E., 2014. Transcriptional consequences of 16p11.2 deletion and duplication in mouse cortex and multiplex autism families. *Am J Hum Genet* 94, 870-883.
- Bolger, A.M., Lohse, M., Usadel, B., 2014. Trimmomatic: a flexible trimmer for Illumina sequence data. *Bioinformatics* 30, 2114-2120.
- Bolus, H., Crocker, K., Boekhoff-Falk, G., Chtarbanova, S., 2020. Modeling Neurodegenerative Disorders in *Drosophila melanogaster*. *Int J Mol Sci* 21.
- Boskovski, M.T., Yuan, S., Pedersen, N.B., Goth, C.K., Makova, S., Clausen, H., Brueckner, M., Khokha, M.K., 2013. The heterotaxy gene GALNT11 glycosylates Notch to orchestrate cilia type and laterality. *Nature* 504, 456-459.
- Branco, J., Al-Ramahi, I., Ukani, L., Perez, A.M., Fernandez-Funez, P., Rincon-Limas, D., Botas, J., 2008. Comparative analysis of genetic modifiers in *Drosophila* points to common and distinct mechanisms of pathogenesis among polyglutamine diseases. *Hum Mol Genet* 17, 376-390.
- Brand, A.H., Perrimon, N., 1993. Targeted gene expression as a means of altering cell fates and generating dominant phenotypes. *Development* 118, 401-415.
- Bronner, M.E., LeDouarin, N.M., 2012. Development and evolution of the neural crest: an overview. *Dev Biol* 366, 2-9.

- Brooks, E.R., Wallingford, J.B., 2015. In vivo investigation of cilia structure and function using *Xenopus*. *Methods Cell Biol* 127, 131-159.
- Budnik, V., Koh, Y.H., Guan, B., Hartmann, B., Hough, C., Woods, D., Gorczyca, M., 1996. Regulation of synapse structure and function by the *Drosophila* tumor suppressor gene *dlg*. *Neuron* 17, 627-640.
- Callan, M.A., Cabernard, C., Heck, J., Luois, S., Doe, C.Q., Zarnescu, D.C., 2010. Fragile X protein controls neural stem cell proliferation in the *Drosophila* brain. *Hum Mol Genet* 19, 3068-3079.
- Cerrizuela, S., Vega-Lopez, G.A., Palacio, M.B., Tribulo, C., Aybar, M.J., 2018. Gli2 is required for the induction and migration of *Xenopus laevis* neural crest. *Mech Dev* 154, 219-239.
- Chen, S.X., Tari, P.K., She, K., Haas, K., 2010. Neurexin-neurologin cell adhesion complexes contribute to synaptotropic dendritogenesis via growth stabilization mechanisms in vivo. *Neuron* 67, 967-983.
- Chen, S.Y., Huang, P.H., Cheng, H.J., 2011. Disrupted-in-Schizophrenia 1-mediated axon guidance involves TRIO-RAC-PAK small GTPase pathway signaling. *Proc Natl Acad Sci U S A* 108, 5861-5866.
- Chen, Y.C., Chang, Y.W., Huang, Y.S., 2019. Dysregulated Translation in Neurodevelopmental Disorders: An Overview of Autism-Risk Genes Involved in Translation. *Dev Neurobiol* 79, 60-74.
- Chintapalli, V.R., Wang, J., Dow, J.A., 2007. Using FlyAtlas to identify better *Drosophila melanogaster* models of human disease. *Nat Genet* 39, 715-720.
- Chirita Emandi, A., Dobrescu, A.I., Doros, G., Hyon, C., Miclea, D., Popoiu, C., Puiu, M., Arghirescu, S., 2019. A Novel 3q29 Deletion in Association With Developmental Delay and Heart Malformation-Case Report With Literature Review. *Front Pediatr* 7, 270.
- Chow, J., Jensen, M., Amini, H., Hormozdiari, F., Penn, O., Shifman, S., Girirajan, S., Hormozdiari, F., 2019. Dissecting the genetic basis of comorbid epilepsy phenotypes in neurodevelopmental disorders. *Genome Med* 11, 65.
- Coe, B.P., Stessman, H.A.F., Sulovari, A., Geisheker, M.R., Bakken, T.E., Lake, A.M., Dougherty, J.D., Lein, E.S., Hormozdiari, F., Bernier, R.A., Eichler, E.E., 2019. Neurodevelopmental disease genes implicated by de novo mutation and copy number variation morbidity. *Nat Genet* 51, 106-116.

- Corsinovi, D., Giannetti, K., Cericola, A., Naef, V., Ori, M., 2019. PDGF-B: The missing piece in the mosaic of PDGF family role in craniofacial development. *Dev Dyn* 248, 603-612.
- Courchesne, E., Mouton, P.R., Calhoun, M.E., Semendeferi, K., Ahrens-Barbeau, C., Hallet, M.J., Barnes, C.C., Pierce, K., 2011. Neuron number and size in prefrontal cortex of children with autism. *JAMA* 306, 2001-2010.
- Cousin, H., 2018. Cranial Neural Crest Transplants. *Cold Spring Harb Protoc* 2018.
- Cousin, H., Alfandari, D., 2018. Cranial Neural Crest Explants. *Cold Spring Harb Protoc* 2018.
- Cziko, A.M., McCann, C.T., Howlett, I.C., Barbee, S.A., Duncan, R.P., Luedemann, R., Zarnescu, D., Zinsmaier, K.E., Parker, R.R., Ramaswami, M., 2009. Genetic modifiers of dFMR1 encode RNA granule components in *Drosophila*. *Genetics* 182, 1051-1060.
- da Costa, M.C., Trentin, A.G., Calloni, G.W., 2018. FGF8 and Shh promote the survival and maintenance of multipotent neural crest progenitors. *Mech Dev* 154, 251-258.
- DeLay, B.D., Krneta-Stankic, V., Miller, R.K., 2016. Technique to Target Microinjection to the Developing *Xenopus* Kidney. *J Vis Exp*.
- Deniz, E., Jonas, S., Hooper, M., J, N.G., Choma, M.A., Khokha, M.K., 2017. Analysis of Craniocardiac Malformations in *Xenopus* using Optical Coherence Tomography. *Sci Rep* 7, 42506.
- Deshpande, A., Weiss, L.A., 2018. Recurrent reciprocal copy number variants: Roles and rules in neurodevelopmental disorders. *Dev Neurobiol* 78, 519-530.
- DeSimone, D.W., Davidson, L., Marsden, M., Alfandari, D., 2005. The *Xenopus* embryo as a model system for studies of cell migration. *Methods Mol Biol* 294, 235-245.
- Devotta, A., Hong, C.S., Saint-Jeannet, J.P., 2018. Dkk2 promotes neural crest specification by activating Wnt/beta-catenin signaling in a GSK3beta independent manner. *Elife* 7.
- Devotta, A., Juraver-Geslin, H., Gonzalez, J.A., Hong, C.S., Saint-Jeannet, J.P., 2016. Sf3b4-depleted *Xenopus* embryos: A model to study the pathogenesis of craniofacial defects in Nager syndrome. *Dev Biol* 415, 371-382.
- Dickinson, A., Sive, H., 2007. Positioning the extreme anterior in *Xenopus*: cement gland, primary mouth and anterior pituitary. *Semin Cell Dev Biol* 18, 525-533.
- Dickinson, A.J., 2016. Using frogs faces to dissect the mechanisms underlying human orofacial defects. *Semin Cell Dev Biol* 51, 54-63.

- Dickinson, A.J., Sive, H., 2006. Development of the primary mouth in *Xenopus laevis*. *Dev Biol* 295, 700-713.
- Dickman, D.K., Davis, G.W., 2009. The schizophrenia susceptibility gene dysbindin controls synaptic homeostasis. *Science* 326, 1127-1130.
- Dietzl, G., Chen, D., Schnorrer, F., Su, K.C., Barinova, Y., Fellner, M., Gasser, B., Kinsey, K., Oppel, S., Scheiblauer, S., Couto, A., Marra, V., Keleman, K., Dickson, B.J., 2007. A genome-wide transgenic RNAi library for conditional gene inactivation in *Drosophila*. *Nature* 448, 151-156.
- Dong, D., Zielke, H.R., Yeh, D., Yang, P., 2018. Cellular stress and apoptosis contribute to the pathogenesis of autism spectrum disorder. *Autism Res* 11, 1076-1090.
- Dubey, A., Saint-Jeannet, J.P., 2017. Modeling human craniofacial disorders in *Xenopus*. *Curr Pathobiol Rep* 5, 79-92.
- Dumay-Odelot, H., Durrieu-Gaillard, S., Da Silva, D., Roeder, R.G., Teichmann, M., 2010. Cell growth- and differentiation-dependent regulation of RNA polymerase III transcription. *Cell Cycle* 9, 3687-3699.
- Duncan, A.M., Ozawa, T., Suzuki, H., Rozen, R., 1993. Assignment of the gene for the core protein II (UQCRC2) subunit of the mitochondrial cytochrome bc1 complex to human chromosome 16p12. *Genomics* 18, 455-456.
- Duncan, A.R., Khokha, M.K., 2016. *Xenopus* as a model organism for birth defects- Congenital heart disease and heterotaxy. *Semin Cell Dev Biol* 51, 73-79.
- Dworkin, S., Boglev, Y., Owens, H., Goldie, S.J., 2016. The Role of Sonic Hedgehog in Craniofacial Patterning, Morphogenesis and Cranial Neural Crest Survival. *J Dev Biol* 4.
- Eicher, J.D., Landowski, C., Stackhouse, B., Sloan, A., Chen, W., Jensen, N., Lien, J.P., Leslie, R., Johnson, A.D., 2015. GRASP v2.0: an update on the Genome-Wide Repository of Associations between SNPs and phenotypes. *Nucleic Acids Res* 43, D799-804.
- Erdogan, B., Ebbert, P.T., Lowery, L.A., 2016. Using *Xenopus laevis* retinal and spinal neurons to study mechanisms of axon guidance in vivo and in vitro. *Semin Cell Dev Biol* 51, 64-72.
- Ernst, C., 2016. Proliferation and Differentiation Deficits are a Major Convergence Point for Neurodevelopmental Disorders. *Trends Neurosci* 39, 290-299.
- Etchevers, H.C., Dupin, E., Le Douarin, N.M., 2019. The diverse neural crest: from embryology to human pathology. *Development* 146.

- Everson, J.L., Fink, D.M., Yoon, J.W., Leslie, E.J., Kietzman, H.W., Ansen-Wilson, L.J., Chung, H.M., Walterhouse, D.O., Marazita, M.L., Lipinski, R.J., 2017. Sonic hedgehog regulation of Foxf2 promotes cranial neural crest mesenchyme proliferation and is disrupted in cleft lip morphogenesis. *Development* 144, 2082-2091.
- Faheem, M., Naseer, M.I., Rasool, M., Chaudhary, A.G., Kumosani, T.A., Ilyas, A.M., Pushparaj, P., Ahmed, F., Algahtani, H.A., Al-Qahtani, M.H., Saleh Jamal, H., 2015.
- Molecular genetics of human primary microcephaly: an overview. *BMC Med Genomics* 8 Suppl 1, S4.
- Falco, M., Amabile, S., Acquaviva, F., 2017. RAI1 gene mutations: mechanisms of Smith-Magenis syndrome. *Appl Clin Genet* 10, 85-94.
- Fenelon, K., Mukai, J., Xu, B., Hsu, P.K., Drew, L.J., Karayiorgou, M., Fischbach, G.D., Macdermott, A.B., Gogos, J.A., 2011. Deficiency of Dgcr8, a gene disrupted by the 22q11.2 microdeletion, results in altered short-term plasticity in the prefrontal cortex. *Proc Natl Acad Sci U S A* 108, 4447-4452.
- Fish, J.L., 2016. Developmental mechanisms underlying variation in craniofacial disease and evolution. *Dev Biol* 415, 188-197.
- Flach, H., Krieg, J., Hoffmeister, M., Dietmann, P., Reusch, A., Wischmann, L., Kernl, B., Riegger, R., Oess, S., Kuhl, S.J., 2018. Nosip functions during vertebrate eye and cranial cartilage development. *Dev Dyn* 247, 1070-1082.
- Gaignard, P., Eyer, D., Lebigot, E., Oliveira, C., Therond, P., Boutron, A., Slama, A., 2017. UQCRC2 mutation in a patient with mitochondrial complex III deficiency causing recurrent liver failure, lactic acidosis and hypoglycemia. *J Hum Genet* 62, 729-731.
- Garcia de la Serrana, D., Mareco, E.A., Johnston, I.A., 2014. Systematic variation in the pattern of gene paralog retention between the teleost superorders Ostariophysii and Acanthopterygii. *Genome Biol Evol* 6, 981-987.
- Garfinkel, A.M., Khokha, M.K., 2017. An interspecies heart-to-heart: Using *Xenopus* to uncover the genetic basis of congenital heart disease. *Curr Pathobiol Rep* 5, 187-196.
- Gasso, P., Mas, S., Molina, O., Lafuente, A., Bernardo, M., Parellada, E., 2014. Increased susceptibility to apoptosis in cultured fibroblasts from antipsychotic-naive first-episode schizophrenia patients. *J Psychiatr Res* 48, 94-101.

- Gatto, C.L., Broadie, K., 2011. *Drosophila* modeling of heritable neurodevelopmental disorders. *Curr Opin Neurobiol* 21, 834-841.
- Gatto, C.L., Pereira, D., Broadie, K., 2014. GABAergic circuit dysfunction in the *Drosophila* Fragile X syndrome model. *Neurobiol Dis* 65, 142-159.
- Getwan, M., Lienkamp, S.S., 2017. Toolbox in a tadpole: *Xenopus* for kidney research. *Cell Tissue Res* 369, 143-157.
- Ghaffari, M., Tahmasebi Birgani, M., Kariminejad, R., Saberi, A., 2018. Genotype-phenotype correlation and the size of microdeletion or microduplication of 7q11.23 region in patients with Williams-Beuren syndrome. *Ann Hum Genet* 82, 469-476.
- Ghesh, L., Vincent, M., Delemazure, A.S., Boyer, J., Corre, P., Perez, F., Genevieve, D., Laplanche, J.L., Collet, C., Isidor, B., 2019. Autosomal recessive Treacher Collins syndrome due to POLR1C mutations: Report of a new family and review of the literature. *Am J Med Genet A* 179, 1390-1394.
- Girirajan, S., Campbell, C.D., Eichler, E.E., 2011. Human copy number variation and complex genetic disease. *Annu Rev Genet* 45, 203-226.
- Girirajan, S., Eichler, E.E., 2010a. Phenotypic variability and genetic susceptibility to genomic disorders. *Hum Mol Genet* 19, R176-187.
- Girirajan, S., Eichler, E.E., 2010b. Phenotypic variability and genetic susceptibility to genomic disorders. *Human molecular genetics* 19, R176-R187.
- Girirajan, S., Rosenfeld, J.A., Coe, B.P., Parikh, S., Friedman, N., Goldstein, A., Filipink, R.A., McConnell, J.S., Angle, B., Meschino, W.S., 2012. Phenotypic heterogeneity of genomic disorders and rare copy-number variants. *New England Journal of Medicine* 367, 1321-1331.
- Girirajan, S., Rosenfeld, J.A., Cooper, G.M., Antonacci, F., Siswara, P., Itsara, A., Vives, L., Walsh, T., McCarthy, S.E., Baker, C., 2010a. A recurrent 16p12.1 microdeletion supports a two-hit model for severe developmental delay. *Nature genetics* 42, 203-209.
- Girirajan, S., Rosenfeld, J.A., Cooper, G.M., Antonacci, F., Siswara, P., Itsara, A., Vives, L., Walsh, T., McCarthy, S.E., Baker, C., Mefford, H.C., Kidd, J.M., Browning, S.R., Browning, B.L., Dickel, D.E., Levy, D.L., Ballif, B.C., Platky, K., Farber, D.M., Gowans, G.C., Wetherbee, J.J., Asamoah, A., Weaver, D.D., Mark, P.R., Dickerson, J., Garg, B.P., Ellingwood, S.A., Smith, R., Banks, V.C., Smith, W., McDonald, M.T., Hoo, J.J., French, B.N., Hudson, C., Johnson, J.P., Ozmore, J.R., Moeschler, J.B., Surti, U., Escobar, L.F., El-Khechen, D., Gorski, J.L., Kussmann, J., Salbert, B., Lacassie, Y., Biser, A., McDonald-McGinn, D.M., Zackai, E.H., Deardorff, M.A., Shaikh, T.H., Haan, E., Friend, K.L., Fichera, M., Romano, C., Geicz, J., DeLisi, L.E., Sebat, J., King, M.C., Shaffer, L.G., Eichler, E.E., 2010b. A

- recurrent 16p12.1 microdeletion supports a two-hit model for severe developmental delay. *Nat Genet* 42, 203-209.
- Glantz, L.A., Gilmore, J.H., Lieberman, J.A., Jarskog, L.F., 2006. Apoptotic mechanisms and the synaptic pathology of schizophrenia. *Schizophr Res* 81, 47-63.
- Glassford, M.R., Rosenfeld, J.A., Freedman, A.A., Zwick, M.E., Mulle, J.G., Unique Rare Chromosome Disorder Support, G., 2016. Novel features of 3q29 deletion syndrome: Results from the 3q29 registry. *Am J Med Genet A* 170A, 999-1006.
- Goldberg, J.L., 2003. How does an axon grow? *Genes Dev* 17, 941-958.
- Gomez-Roman, N., Grandori, C., Eisenman, R.N., White, R.J., 2003. Direct activation of RNA polymerase III transcription by c-Myc. *Nature* 421, 290-294.
- Gonatopoulos-Pournatzis, T., Cowling, V.H., 2014. Cap-binding complex (CBC). *Biochem J* 457, 231-242.
- Gonsalvez, D.G., Li-Yuen-Fong, M., Cane, K.N., Stamp, L.A., Young, H.M., Anderson, C.R., 2015. Different neural crest populations exhibit diverse proliferative behaviors. *Dev Neurobiol* 75, 287-301.
- Graveley, B.R., Brooks, A.N., Carlson, J.W., Duff, M.O., Landolin, J.M., Yang, L., Artieri, C.G., van Baren, M.J., Boley, N., Booth, B.W., Brown, J.B., Cherbas, L., Davis, C.A., Dobin, A., Li, R., Lin, W., Malone, J.H., Mattiuzzo, N.R., Miller, D., Sturgill, D., Tuch, B.B., Zaleski, C., Zhang, D., Blanchette, M., Dudoit, S., Eads, B., Green, R.E., Hammonds, A., Jiang, L., Kapranov, P., Langton, L., Perrimon, N., Sandler, J.E., Wan, K.H., Willingham, A., Zhang, Y., Zou, Y., Andrews, J., Bickel, P.J., Brenner, S.E., Brent, M.R., Cherbas, P., Gingeras, T.R., Hoskins, R.A., Kaufman, T.C., Oliver, B., Celniker, S.E., 2011. The developmental transcriptome of *Drosophila melanogaster*. *Nature* 471, 473-479.
- Greene, C.S., Krishnan, A., Wong, A.K., Ricciotti, E., Zelaya, R.A., Himmelstein, D.S., Zhang, R., Hartmann, B.M., Zaslavsky, E., Sealfon, S.C., Chasman, D.I., FitzGerald, G.A., Dolinski, K., Grosser, T., Troyanskaya, O.G., 2015. Understanding multicellular function and disease with human tissue-specific networks. *Nat Genet* 47, 569-576.
- Grice, S.J., Liu, J.L., Webber, C., 2015. Synergistic interactions between *Drosophila* orthologues of genes spanned by de novo human CNVs support multiple-hit models of autism. *PLoS Genet* 11, e1004998.
- Grieco, T.M., Hlusko, L.J., 2016. Insight from Frogs: Sonic Hedgehog Gene Expression and a Re-evaluation of the Vertebrate Odontogenic Band. *Anat Rec (Hoboken)* 299, 1099-1109.

- Griffin, J.N., Del Viso, F., Duncan, A.R., Robson, A., Hwang, W., Kulkarni, S., Liu, K.J., Khokha, M.K., 2018. RAPGEF5 Regulates Nuclear Translocation of beta-Catenin. *Dev Cell* 44, 248-260 e244.
- Gross, J.B., Hanken, J., 2008. Segmentation of the vertebrate skull: neural-crest derivation of adult cartilages in the clawed frog, *Xenopus laevis*. *Integr Comp Biol* 48, 681-696.
- Grossman, T.R., Gamliel, A., Wessells, R.J., Taghli-Lamalle, O., Jepsen, K., Ocorr, K., Korenberg, J.R., Peterson, K.L., Rosenfeld, M.G., Bodmer, R., Bier, E., 2011. Over-expression of DSCAM and COL6A2 cooperatively generates congenital heart defects. *PLoS Genet* 7, e1002344.
- Grozeva, D., Carss, K., Spasic-Boskovic, O., Parker, M.J., Archer, H., Firth, H.V., Park, S.M., Canham, N., Holder, S.E., Wilson, M., Hackett, A., Field, M., Floyd, J.A., Consortium, U.K., Hurles, M., Raymond, F.L., 2014. De novo loss-of-function mutations in SETD5, encoding a methyltransferase in a 3p25 microdeletion syndrome critical region, cause intellectual disability. *Am J Hum Genet* 94, 618-624.
- Hammond, N.L., Brookes, K.J., Dixon, M.J., 2018. Ectopic Hedgehog Signaling Causes Cleft Palate and Defective Osteogenesis. *J Dent Res* 97, 1485-1493.
- Harland, R.M., Grainger, R.M., 2011. *Xenopus* research: metamorphosed by genetics and genomics. *Trends Genet* 27, 507-515.
- Helbig, I., Mefford, H.C., Sharp, A.J., Guipponi, M., Fichera, M., Franke, A., Muhle, H., de Kovel, C., Baker, C., von Spiczak, S., Kron, K.L., Steinich, I., Kleefuss-Lie, A.A., Leu, C., Gaus, V., Schmitz, B., Klein, K.M., Reif, P.S., Rosenow, F., Weber, Y., Lerche, H., Zimprich, F., Urak, L., Fuchs, K., Feucht, M., Genton, P., Thomas, P., Visscher, F., de Haan, G.J., Moller, R.S., Hjalgrim, H., Luciano, D., Wittig, M., Nothnagel, M., Elger, C.E., Nurnberg, P., Romano, C., Malafosse, A., Koeleman, B.P., Lindhout, D., Stephani, U., Schreiber, S., Eichler, E.E., Sander, T., 2009. 15q13.3 microdeletions increase risk of idiopathic generalized epilepsy. *Nat Genet* 41, 160-162.
- Hellsten, U., Harland, R.M., Gilchrist, M.J., Hendrix, D., Jurka, J., Kapitonov, V., Ovcharenko, I., Putnam, N.H., Shu, S., Taher, L., Blitz, I.L., Blumberg, B., Dichmann, D.S., Dubchak, I., Amaya, E., Detter, J.C., Fletcher, R., Gerhard, D.S., Goodstein, D., Graves, T., Grigoriev, I.V., Grimwood, J., Kawashima, T., Lindquist, E., Lucas, S.M., Mead, P.E., Mitros, T., Ogino, H., Ohta, Y., Poliakov, A.V., Pollet, N., Robert, J., Salamov, A., Sater, A.K., Schmutz, J., Terry, A., Vize, P.D., Warren, W.C., Wells, D., Wills, A., Wilson, R.K., Zimmerman, L.B., Zorn, A.M., Grainger, R., Grammer, T., Khokha, M.K., Richardson, P.M., Rokhsar, D.S., 2010. The genome of the Western clawed frog *Xenopus tropicalis*. *Science* 328, 633-636.

- Hempel, A., Kuhl, M., 2016. A Matter of the Heart: The African Clawed Frog *Xenopus* as a Model for Studying Vertebrate Cardiogenesis and Congenital Heart Defects. *J Cardiovasc Dev Dis* 3.
- Hing, H., Xiao, J., Harden, N., Lim, L., Zipursky, S.L., 1999. Pak functions downstream of Dock to regulate photoreceptor axon guidance in *Drosophila*. *Cell* 97, 853-863.
- Hou, J., van Leeuwen, J., Andrews, B.J., Boone, C., 2018. Genetic Network Complexity Shapes Background-Dependent Phenotypic Expression. *Trends Genet* 34, 578-586.
- Hu, P., Wu, S., Sun, Y., Yuan, C.C., Kobayashi, R., Myers, M.P., Hernandez, N., 2002. Characterization of human RNA polymerase III identifies orthologues for *Saccharomyces cerevisiae* RNA polymerase III subunits. *Mol Cell Biol* 22, 8044-8055.
- Hu, Y., Flockhart, I., Vinayagam, A., Bergwitz, C., Berger, B., Perrimon, N., Mohr, S.E., 2011. An integrative approach to ortholog prediction for disease-focused and other functional studies. *BMC Bioinformatics* 12, 357.
- Huang, W.H., Guenther, C.J., Xu, J., Nguyen, T., Schwarz, L.A., Wilkinson, A.W., Gozani, O., Chang, H.Y., Shamloo, M., Luo, L., 2016. Molecular and Neural Functions of *Rai1*, the Causal Gene for Smith-Magenis Syndrome. *Neuron* 92, 392-406.
- Huizar, R.L., Lee, C., Boulgakov, A.A., Horani, A., Tu, F., Marcotte, E.M., Brody, S.L., Wallingford, J.B., 2018. A liquid-like organelle at the root of motile ciliopathy. *Elife* 7.
- Humbert, P., Russell, S., Richardson, H., 2003. *Dlg*, *Scribble* and *Lgl* in cell polarity, cell proliferation and cancer. *Bioessays* 25, 542-553.
- Hunt, P., Gulisano, M., Cook, M., Sham, M.H., Faiella, A., Wilkinson, D., Boncinelli, E., Krumlauf, R., 1991a. A distinct Hox code for the branchial region of the vertebrate head. *Nature* 353, 861-864.
- Hunt, P., Whiting, J., Muchamore, I., Marshall, H., Krumlauf, R., 1991b. Homeobox genes and models for patterning the hindbrain and branchial arches. *Dev Suppl* 1, 187-196.
- Hwang, J.Y., Lee, J., Oh, C.K., Kang, H.W., Hwang, I.Y., Um, J.W., Park, H.C., Kim, S., Shin, J.H., Park, W.Y., Darnell, R.B., Um, H.D., Chung, K.C., Kim, K., Oh, Y.J., 2016. Proteolytic degradation and potential role of onconeural protein *cdr2* in neurodegeneration. *Cell Death Dis* 7, e2240.
- Iossifov, I., Levy, D., Allen, J., Ye, K., Ronemus, M., Lee, Y.H., Yamrom, B., Wigler, M., 2015. Low load for disruptive mutations in autism genes and their biased transmission. *Proceedings of the National Academy of Sciences of the United States of America* 112, E5600-5607.

- Ishimaru, H., Kamboj, R., Ambrosini, A., Henley, J.M., Soloviev, M.M., Sudan, H., Rossier, J., Abutidze, K., Rampersad, V., Usherwood, P.N., Bateson, A.N., Barnard, E.A., 1996. A unitary non-NMDA receptor short subunit from *Xenopus*: DNA cloning and expression. *Receptors Channels* 4, 31-49.
- Iyer, J., Singh, M.D., Jensen, M., Patel, P., Pizzo, L., Huber, E., Koerselman, H., Weiner, A.T., Lepanto, P., Vadodaria, K., Kubina, A., Wang, Q., Talbert, A., Yennawar, S., Badano, J., Manak, J.R., Rolls, M.M., Krishnan, A., Girirajan, S., 2018. Pervasive genetic interactions modulate neurodevelopmental defects of the autism-associated 16p11.2 deletion in *Drosophila melanogaster*. *Nat Commun* 9, 2548.
- Iyer, J., Wang, Q., Le, T., Pizzo, L., Gronke, S., Ambegaokar, S.S., Imai, Y., Srivastava, A., Troisi, B.L., Mardon, G., Artero, R., Jackson, G.R., Isaacs, A.M., Partridge, L., Lu, B., Kumar, J.P., Girirajan, S., 2016. Quantitative Assessment of Eye Phenotypes for Functional Genetic Studies Using *Drosophila melanogaster*. *G3 (Bethesda)* 6, 1427-1437.
- James-Zorn, C., Ponferrada, V., Fisher, M.E., Burns, K., Fortriede, J., Segerdell, E., Karimi, K., Lotay, V., Wang, D.Z., Chu, S., Pells, T., Wang, Y., Vize, P.D., Zorn, A., 2018. Navigating Xenbase: An Integrated *Xenopus* Genomics and Gene Expression Database. *Methods Mol Biol* 1757, 251-305.
- Jensen, M., Girirajan, S., 2017. Mapping a shared genetic basis for neurodevelopmental disorders. *Genome Med* 9, 109.
- Jensen, M., Girirajan, S., 2019. An interaction-based model for neuropsychiatric features of copy-number variants. *PLoS Genet* 15, e1007879.
- Jensen, M., Kooy, R.F., Simon, T.J., Reyniers, E., Girirajan, S., Tassone, F., 2018. A higher rare CNV burden in the genetic background potentially contributes to intellectual disability phenotypes in 22q11.2 deletion syndrome. *Eur J Med Genet* 61, 209-212.
- Jumbo-Lucioni, P.P., Parkinson, W.M., Kopke, D.L., Broadie, K., 2016. Coordinated movement, neuromuscular synaptogenesis and trans-synaptic signaling defects in *Drosophila galactosemia* models. *Hum Mol Genet* 25, 3699-3714.
- Kadokia, S., Helman, S.N., Badhey, A.K., Saman, M., Ducic, Y., 2014. Treacher Collins Syndrome: the genetics of a craniofacial disease. *Int J Pediatr Otorhinolaryngol* 78, 893-898.
- Karayiorgou, M., Morris, M.A., Morrow, B., Shprintzen, R.J., Goldberg, R., Borrow, J., Gos, A., Nestadt, G., Wolyniec, P.S., Lasseter, V.K., et al., 1995. Schizophrenia susceptibility associated with interstitial deletions of chromosome 22q11. *Proc Natl Acad Sci U S A* 92, 7612-7616.

- Karayiorou, M., Simon, T.J., Gogos, J.A., 2010. 22q11.2 microdeletions: linking DNA structural variation to brain dysfunction and schizophrenia. *Nat Rev Neurosci* 11, 402-416.
- Karimi, K., Fortriede, J.D., Lotay, V.S., Burns, K.A., Wang, D.Z., Fisher, M.E., Pells, T.J., James-Zorn, C., Wang, Y., Ponferrada, V.G., Chu, S., Chaturvedi, P., Zorn, A.M., Vize, P.D., 2018. Xenbase: a genomic, epigenomic and transcriptomic model organism database. *Nucleic Acids Res* 46, D861-D868.
- Kasherman, M.A., Premarathne, S., Burne, T.H.J., Wood, S.A., Piper, M., 2020. The Ubiquitin System: a Regulatory Hub for Intellectual Disability and Autism Spectrum Disorder. *Mol Neurobiol*.
- Kennedy, A.E., Dickinson, A.J., 2014a. Quantification of orofacial phenotypes in *Xenopus*. *J Vis Exp*, e52062.
- Kennedy, A.E., Dickinson, A.J., 2014b. Quantitative analysis of orofacial development and median clefts in *Xenopus laevis*. *Anat Rec (Hoboken)* 297, 834-855.
- Kerney, R.R., Brittain, A.L., Hall, B.K., Buchholz, D.R., 2012. Cartilage on the move: cartilage lineage tracing during tadpole metamorphosis. *Dev Growth Differ* 54, 739-752.
- Kim, D., Pertea, G., Trapnell, C., Pimentel, H., Kelley, R., Salzberg, S.L., 2013. TopHat2: accurate alignment of transcriptomes in the presence of insertions, deletions and gene fusions. *Genome Biol* 14, R36.
- Kim, M.D., Kamiyama, D., Kolodziej, P., Hing, H., Chiba, A., 2003. Isolation of Rho GTPase effector pathways during axon development. *Dev Biol* 262, 282-293.
- Kirby, R.S., 2017. The prevalence of selected major birth defects in the United States. *Semin Perinatol* 41, 338-344.
- Kircher, M., Witten, D.M., Jain, P., O'Roak, B.J., Cooper, G.M., Shendure, J., 2014. A general framework for estimating the relative pathogenicity of human genetic variants. *Nat Genet* 46, 310-315.
- Kirov, G., Pocklington, A.J., Holmans, P., Ivanov, D., Ikeda, M., Ruderfer, D., Moran, J., Chambert, K., Toncheva, D., Georgieva, L., Grozeva, D., Fjodorova, M., Wollerton, R., Rees, E., Nikolov, I., van de Lagemaat, L.N., Bayes, A., Fernandez, E., Olason, P.I., Bottcher, Y., Komiyama, N.H., Collins, M.O., Choudhary, J., Stefansson, K., Stefansson, H., Grant, S.G., Purcell, S., Sklar, P., O'Donovan, M.C., Owen, M.J., 2012. De novo CNV analysis implicates specific abnormalities of postsynaptic signalling complexes in the pathogenesis of schizophrenia. *Mol Psychiatry* 17, 142-153.

- Kishi, N., Macklis, J.D., 2004. MECP2 is progressively expressed in post-migratory neurons and is involved in neuronal maturation rather than cell fate decisions. *Mol Cell Neurosci* 27, 306-321.
- Kornbluth, S., White, K., 2005. Apoptosis in *Drosophila*: neither fish nor fowl (nor man, nor worm). *J Cell Sci* 118, 1779-1787.
- Kreczmanski, P., Heinsen, H., Mantua, V., Woltersdorf, F., Masson, T., Ulfig, N., Schmidt-Kastner, R., Korr, H., Steinbusch, H.W., Hof, P.R., Schmitz, C., 2007. Volume, neuron density and total neuron number in five subcortical regions in schizophrenia. *Brain* 130, 678-692.
- Krishnan, A., Zhang, R., Yao, V., Theesfeld, C.L., Wong, A.K., Tadych, A., Volfovsky, N., Packer, A., Lash, A., Troyanskaya, O.G., 2016. Genome-wide prediction and functional characterization of the genetic basis of autism spectrum disorder. *Nature neuroscience* 19, 1454-1462.
- Krumm, N., Turner, T.N., Baker, C., Vives, L., Mohajeri, K., Witherspoon, K., Raja, A., Coe, B.P., Stessman, H.A., He, Z.-X., 2015. Excess of rare, inherited truncating mutations in autism. *Nature genetics* 47, 582-588.
- Kurosaka, H., Iulianella, A., Williams, T., Trainor, P.A., 2014. Disrupting hedgehog and WNT signaling interactions promotes cleft lip pathogenesis. *J Clin Invest* 124, 1660-1671.
- Kury, S., van Woerden, G.M., Besnard, T., Proietti Onori, M., Latypova, X., Towne, M.C., Cho, M.T., Prescott, T.E., Ploeg, M.A., Sanders, S., Stessman, H.A.F., Pujol, A., Distel, B., Robak, L.A., Bernstein, J.A., Denomme-Pichon, A.S., Lesca, G., Sellars, E.A., Berg, J., Carre, W., Busk, O.L., van Bon, B.W.M., Waugh, J.L., Deardorff, M., Hoganson, G.E., Bosanko, K.B., Johnson, D.S., Dabir, T., Holla, O.L., Sarkar, A., Tveten, K., de Bellescize, J., Braathen, G.J., Terhal, P.A., Grange, D.K., van Haeringen, A., Lam, C., Mirzaa, G., Burton, J., Bhoj, E.J., Douglas, J., Santani, A.B., Nesbitt, A.I., Helbig, K.L., Andrews, M.V., Begtrup, A., Tang, S., van Gassen, K.L.I., Juusola, J., Foss, K., Enns, G.M., Moog, U., Hinderhofer, K., Paramasivam, N., Lincoln, S., Kusako, B.H., Lindenbaum, P., Charpentier, E., Nowak, C.B., Cherot, E., Simonet, T., Ruivenkamp, C.A.L., Hahn, S., Brownstein, C.A., Xia, F., Schmitt, S., Deb, W., Bonneau, D., Nizon, M., Quinquis, D., Chelly, J., Rudolf, G., Sanlaville, D., Parent, P., Gilbert-Dussardier, B., Toutain, A., Sutton, V.R., Thies, J., Peart-Vissers, L., Boisseau, P., Vincent, M., Grabrucker, A.M., Dubourg, C., Undiagnosed Diseases, N., Tan, W.H., Verbeek, N.E., Granzow, M., Santen, G.W.E., Shendure, J., Isidor, B., Pasquier, L., Redon, R., Yang, Y., State, M.W., Kleefstra, T., Cogne, B., Gem, H., Deciphering Developmental Disorders, S., Petrovski, S., Retterer, K., Eichler, E.E., Rosenfeld, J.A., Agrawal, P.B., Bezieau, S., Odent, S., Elgersma, Y., Mercier, S., 2017. De Novo Mutations in Protein Kinase Genes CAMK2A and CAMK2B Cause Intellectual Disability. *Am J Hum Genet* 101, 768-788.

- Kwon, C.H., Luikart, B.W., Powell, C.M., Zhou, J., Matheny, S.A., Zhang, W., Li, Y., Baker, S.J., Parada, L.F., 2006. Pten regulates neuronal arborization and social interaction in mice. *Neuron* 50, 377-388.
- Lasser, M., Pratt, B., Monahan, C., Kim, S.W., Lowery, L.A., 2019. The Many Faces of *Xenopus*: *Xenopus laevis* as a Model System to Study Wolf-Hirschhorn Syndrome. *Front Physiol* 10, 817.
- Lasser, M., Tiber, J., Lowery, L.A., 2018. The Role of the Microtubule Cytoskeleton in Neurodevelopmental Disorders. *Front Cell Neurosci* 12, 165.
- Lauer, S., Gresham, D., 2019. An evolving view of copy number variants. *Curr Genet* 65, 1287-1295.
- Le Lievre, C.S., Le Douarin, N.M., 1975. Mesenchymal derivatives of the neural crest: analysis of chimaeric quail and chick embryos. *J Embryol Exp Morphol* 34, 125-154.
- Lee, A., Li, W., Xu, K., Bogert, B.A., Su, K., Gao, F.B., 2003. Control of dendritic development by the *Drosophila* fragile X-related gene involves the small GTPase Rac1. *Development* 130, 5543-5552.
- Lee-Liu, D., Mendez-Olivos, E.E., Munoz, R., Larrain, J., 2017. The African clawed frog *Xenopus laevis*: A model organism to study regeneration of the central nervous system. *Neurosci Lett* 652, 82-93.
- Lek, M., Karczewski, K.J., Minikel, E.V., Samocha, K.E., Banks, E., Fennell, T., O'Donnell-Luria, A.H., Ware, J.S., Hill, A.J., Cummings, B.B., Tukiainen, T., Birnbaum, D.P., Kosmicki, J.A., Duncan, L.E., Estrada, K., Zhao, F., Zou, J., Pierce-Hoffman, E., Berghout, J., Cooper, D.N., Deflaux, N., DePristo, M., Do, R., Flannick, J., Fromer, M., Gauthier, L., Goldstein, J., Gupta, N., Howrigan, D., Kiezun, A., Kurki, M.I., Moonshine, A.L., Natarajan, P., Orozco, L., Peloso, G.M., Poplin, R., Rivas, M.A., Ruano-Rubio, V., Rose, S.A., Ruderfer, D.M., Shakir, K., Stenson, P.D., Stevens, C., Thomas, B.P., Tiao, G., Tusie-Luna, M.T., Weisburd, B., Won, H.H., Yu, D., Altshuler, D.M., Ardissino, D., Boehnke, M., Danesh, J., Donnelly, S., Elosua, R., Florez, J.C., Gabriel, S.B., Getz, G., Glatt, S.J., Hultman, C.M., Kathiresan, S., Laakso, M., McCarroll, S., McCarthy, M.I., McGovern, D., McPherson, R., Neale, B.M., Palotie, A., Purcell, S.M., Saleheen, D., Scharf, J.M., Sklar, P., Sullivan, P.F., Tuomilehto, J., Tsuang, M.T., Watkins, H.C., Wilson, J.G., Daly, M.J., MacArthur, D.G., Exome Aggregation, C., 2016. Analysis of protein-coding genetic variation in 60,706 humans. *Nature* 536, 285-291.
- Lewis, B.B., Wester, M.R., Miller, L.E., Nagarkar, M.D., Johnson, M.B., Saha, M.S., 2009. Cloning and characterization of voltage-gated calcium channel alpha1 subunits in *Xenopus laevis* during development. *Dev Dyn* 238, 2891-2902.

- Li, Y., Junge, J.A., Arnesano, C., Gross, G.G., Miner, J.H., Moats, R., Roberts, R.W., Arnold, D.B., Fraser, S.E., 2018. Discs large 1 controls daughter-cell polarity after cytokinesis in vertebrate morphogenesis. *Proc Natl Acad Sci U S A* 115, E10859-E10868.
- Lichtig, H., Artamonov, A., Polevoy, H., Reid, C.D., Bielas, S.L., Frank, D., 2020. Modeling Bainbridge-Ropers Syndrome in *Xenopus laevis* Embryos. *Front Physiol* 11, 75.
- Lienkamp, S.S., 2016. Using *Xenopus* to study genetic kidney diseases. *Semin Cell Dev Biol* 51, 117-124.
- Lindsay, E.A., Vitelli, F., Su, H., Morishima, M., Huynh, T., Pramparo, T., Jurecic, V., Ogunrinu, G., Sutherland, H.F., Scambler, P.J., Bradley, A., Baldini, A., 2001. *Tbx1* haploinsufficiency in the DiGeorge syndrome region causes aortic arch defects in mice. *Nature* 410, 97-101.
- Livak, K.J., Schmittgen, T.D., 2001. Analysis of relative gene expression data using real-time quantitative PCR and the 2(-Delta Delta C(T)) Method. *Methods* 25, 402-408.
- Lowery, L.A., Faris, A.E., Stout, A., Van Vactor, D., 2012. Neural Explant Cultures from *Xenopus laevis*. *J Vis Exp*, e4232.
- Lumsden, A., Sprawson, N., Graham, A., 1991. Segmental origin and migration of neural crest cells in the hindbrain region of the chick embryo. *Development* 113, 1281-1291.
- Luo, S., Rubinsztein, D.C., 2009. Huntingtin promotes cell survival by preventing Pak2 cleavage. *J Cell Sci* 122, 875-885.
- Mackay, T.F., Stone, E.A., Ayroles, J.F., 2009. The genetics of quantitative traits: challenges and prospects. *Nat Rev Genet* 10, 565-577.
- Malhotra, D., Sebat, J., 2012. CNVs: harbingers of a rare variant revolution in psychiatric genetics. *Cell* 148, 1223-1241.
- Maquat, L.E., 2004. Nonsense-mediated mRNA decay: splicing, translation and mRNP dynamics. *Nat Rev Mol Cell Biol* 5, 89-99.
- Marlin, J.W., Chang, Y.W., Ober, M., Handy, A., Xu, W., Jakobi, R., 2011. Functional PAK-2 knockout and replacement with a caspase cleavage-deficient mutant in mice reveals differential requirements of full-length PAK-2 and caspase-activated PAK-2p34. *Mamm Genome* 22, 306-317.
- Marshak, S., Meynard, M.M., De Vries, Y.A., Kidane, A.H., Cohen-Cory, S., 2012. Cell-autonomous alterations in dendritic arbor morphology and connectivity induced by

- overexpression of MeCP2 in *Xenopus* central neurons in vivo. *PLoS One* 7, e33153.
- Mathieu, J., Ruohola-Baker, H., 2017. Metabolic remodeling during the loss and acquisition of pluripotency. *Development* 144, 541-551.
- Matthews, B.J., Kim, M.E., Flanagan, J.J., Hattori, D., Clemens, J.C., Zipursky, S.L., Grueber, W.B., 2007. Dendrite self-avoidance is controlled by Dscam. *Cell* 129, 593-604.
- Mayor, R., Theveneau, E., 2013. The neural crest. *Development* 140, 2247-2251.
- McCammon, J.M., Blaker-Lee, A., Chen, X., Sive, H., 2017. The 16p11.2 homologs *fam57ba* and *doc2a* generate certain brain and body phenotypes. *Hum Mol Genet* 26, 3699-3712.
- McCammon, J.M., Sive, H., 2015. Addressing the Genetics of Human Mental Health Disorders in Model Organisms. *Annu Rev Genomics Hum Genet* 16, 173-197.
- Melicharek, D.J., Ramirez, L.C., Singh, S., Thompson, R., Marendza, D.R., 2010. *Kismet/CHD7* regulates axon morphology, memory and locomotion in a *Drosophila* model of CHARGE syndrome. *Hum Mol Genet* 19, 4253-4264.
- Mendoza-Topaz, C., Urra, F., Barria, R., Albornoz, V., Ugalde, D., Thomas, U., Gundelfinger, E.D., Delgado, R., Kukuljan, M., Sanxaridis, P.D., Tsunoda, S., Ceriani, M.F., Budnik, V., Sierralta, J., 2008. *DLGS97/SAP97* is developmentally upregulated and is required for complex adult behaviors and synapse morphology and function. *J Neurosci* 28, 304-314.
- Merkuri, F., Fish, J.L., 2019. Developmental processes regulate craniofacial variation in disease and evolution. *Genesis* 57, e23249.
- Mi, H., Huang, X., Muruganujan, A., Tang, H., Mills, C., Kang, D., Thomas, P.D., 2017. PANTHER version 11: expanded annotation data from Gene Ontology and Reactome pathways, and data analysis tool enhancements. *Nucleic Acids Res* 45, D183-D189.
- Middleton, F.A., Mirnics, K., Pierri, J.N., Lewis, D.A., Levitt, P., 2002. Gene expression profiling reveals alterations of specific metabolic pathways in schizophrenia. *J Neurosci* 22, 2718-2729.
- Milet, C., Monsoro-Burq, A.H., 2014. Dissection of *Xenopus laevis* neural crest for in vitro explant culture or in vivo transplantation. *J Vis Exp*.
- Millington, G., Elliott, K.H., Chang, Y.T., Chang, C.F., Dlugosz, A., Brugmann, S.A., 2017. Cilia-dependent GLI processing in neural crest cells is required for tongue development. *Dev Biol* 424, 124-137.
- Mills, A., Bearce, E., Cella, R., Kim, S.W., Selig, M., Lee, S., Lowery, L.A., 2019. Wolf-Hirschhorn Syndrome-Associated Genes Are Enriched in Motile Neural Crest

Cells and Affect Craniofacial Development in *Xenopus laevis*. *Front Physiol* 10, 431.

- Miyake, N., Yano, S., Sakai, C., Hatakeyama, H., Matsushima, Y., Shiina, M., Watanabe, Y., Bartley, J., Abdenur, J.E., Wang, R.Y., Chang, R., Tsurusaki, Y., Doi, H., Nakashima, M., Saito, H., Ogata, K., Goto, Y., Matsumoto, N., 2013. Mitochondrial complex III deficiency caused by a homozygous UQCRC2 mutation presenting with neonatal-onset recurrent metabolic decompensation. *Hum Mutat* 34, 446-452.
- Moody, S.A., 2018a. Lineage Tracing and Fate Mapping in *Xenopus* Embryos. *Cold Spring Harb Protoc* 2018.
- Moody, S.A., 2018b. Microinjection of mRNAs and Oligonucleotides. *Cold Spring Harb Protoc* 2018.
- Morales, J., Hiesinger, P.R., Schroeder, A.J., Kume, K., Verstreken, P., Jackson, F.R., Nelson, D.L., Hassan, B.A., 2002. *Drosophila* fragile X protein, DFXR, regulates neuronal morphology and function in the brain. *Neuron* 34, 961-972.
- Mukai, J., Tamura, M., Fenelon, K., Rosen, A.M., Spellman, T.J., Kang, R., MacDermott, A.B., Karayiorgou, M., Gordon, J.A., Gogos, J.A., 2015. Molecular substrates of altered axonal growth and brain connectivity in a mouse model of schizophrenia. *Neuron* 86, 680-695.
- Mulle, J.G., 2015. The 3q29 deletion confers >40-fold increase in risk for schizophrenia. *Mol Psychiatry* 20, 1028-1029.
- Mulle, J.G., Dodd, A.F., McGrath, J.A., Wolyniec, P.S., Mitchell, A.A., Shetty, A.C., Sobreira, N.L., Valle, D., Rudd, M.K., Satten, G., Cutler, D.J., Pulver, A.E., Warren, S.T., 2010. Microdeletions of 3q29 confer high risk for schizophrenia. *Am J Hum Genet* 87, 229-236.
- Muller, B.M., Kistner, U., Veh, R.W., Cases-Langhoff, C., Becker, B., Gundelfinger, E.D., Garner, C.C., 1995. Molecular characterization and spatial distribution of SAP97, a novel presynaptic protein homologous to SAP90 and the *Drosophila* discs-large tumor suppressor protein. *J Neurosci* 15, 2354-2366.
- Ng, J., Luo, L., 2004. Rho GTPases regulate axon growth through convergent and divergent signaling pathways. *Neuron* 44, 779-793.
- Nieuwkoop PD, F.J., 1994. Normal table of *Xenopus laevis* (Daudin) : a systematical and chronological survey of the development from the fertilized egg till the end of metamorphosis. *Garland Pub.*, 1994.

- Noack Watt, K.E., Achilleos, A., Neben, C.L., Merrill, A.E., Trainor, P.A., 2016. The Roles of RNA Polymerase I and III Subunits Polr1c and Polr1d in Craniofacial Development and in Zebrafish Models of Treacher Collins Syndrome. *PLoS Genet* 12, e1006187.
- Nowakowska, B., 2017. Clinical interpretation of copy number variants in the human genome. *J Appl Genet* 58, 449-457.
- O'Donovan, K.J., Diedler, J., Couture, G.C., Fak, J.J., Darnell, R.B., 2010. The onconeural antigen *cdr2* is a novel APC/C target that acts in mitosis to regulate c-myc target genes in mammalian tumor cells. *PLoS One* 5, e10045.
- Okano, H.J., Park, W.Y., Corradi, J.P., Darnell, R.B., 1999. The cytoplasmic Purkinje onconeural antigen *cdr2* down-regulates c-Myc function: implications for neuronal and tumor cell survival. *Genes Dev* 13, 2087-2097.
- Okuhara, S., Birjandi, A.A., Adel Al-Lami, H., Sagai, T., Amano, T., Shiroishi, T., Xavier, G.M., Liu, K.J., Cobourne, M.T., Iseki, S., 2019. Temporospatial sonic hedgehog signalling is essential for neural crest-dependent patterning of the intrinsic tongue musculature. *Development* 146.
- Oortveld, M.A., Keerthikumar, S., Oti, M., Nijhof, B., Fernandes, A.C., Kochinke, K., Castells-Nobau, A., van Engelen, E., Ellenkamp, T., Eshuis, L., Galy, A., van Bokhoven, H., Habermann, B., Brunner, H.G., Zweier, C., Verstreken, P., Huynen, M.A., Schenck, A., 2013. Human intellectual disability genes form conserved functional modules in *Drosophila*. *PLoS Genet* 9, e1003911.
- Orr, W.C., Sohal, R.S., 1994. Extension of life-span by overexpression of superoxide dismutase and catalase in *Drosophila melanogaster*. *Science* 263, 1128-1130.
- Osipovich, A.B., Gangula, R., Vianna, P.G., Magnuson, M.A., 2016. *Setd5* is essential for mammalian development and the co-transcriptional regulation of histone acetylation. *Development* 143, 4595-4607.
- Ott, T., Kaufmann, L., Granzow, M., Hinderhofer, K., Bartram, C.R., Theiss, S., Seitz, A., Paramasivam, N., Schulz, A., Moog, U., Blum, M., Evers, C.M., 2019. The Frog *Xenopus* as a Model to Study Joubert Syndrome: The Case of a Human Patient With Compound Heterozygous Variants in *PIBF1*. *Front Physiol* 10, 134.
- Pabis, M., Neufeld, N., Shav-Tal, Y., Neugebauer, K.M., 2010. Binding properties and dynamic localization of an alternative isoform of the cap-binding complex subunit CBP20. *Nucleus* 1, 412-421.
- Papageorgiou, E., Papoulidis, I., Zavlanos, A., Papanikolaou, E., Manolakos, E., Fidani, S., 2020. A novel familial mutation associated with Treacher Collins syndrome: A case report. *Biomed Rep* 12, 285-289.

- Parker, L., Padilla, M., Du, Y., Dong, K., Tanouye, M.A., 2011. *Drosophila* as a model for epilepsy: *bss* is a gain-of-function mutation in the para sodium channel gene that leads to seizures. *Genetics* 187, 523-534.
- Parnas, D., Haghghi, A.P., Fetter, R.D., Kim, S.W., Goodman, C.S., 2001. Regulation of postsynaptic structure and protein localization by the Rho-type guanine nucleotide exchange factor dPix. *Neuron* 32, 415-424.
- Perestrelo, T., Correia, M., Ramalho-Santos, J., Wirtz, D., 2018. Metabolic and Mechanical Cues Regulating Pluripotent Stem Cell Fate. *Trends Cell Biol* 28, 1014-1029.
- Petrovski, S., Wang, Q., Heinzen, E.L., Allen, A.S., Goldstein, D.B., 2013. Genic intolerance to functional variation and the interpretation of personal genomes. *PLoS Genet* 9, e1003709.
- Pinto, D., Pagnamenta, A.T., Klei, L., Anney, R., Merico, D., Regan, R., Conroy, J., Magalhaes, T.R., Correia, C., Abrahams, B.S., Almeida, J., Bacchelli, E., Bader, G.D., Bailey, A.J., Baird, G., Battaglia, A., Berney, T., Bolshakova, N., Bolte, S., Bolton, P.F., Bourgeron, T., Brennan, S., Brian, J., Bryson, S.E., Carson, A.R., Casallo, G., Casey, J., Chung, B.H., Cochrane, L., Corsello, C., Crawford, E.L., Crossett, A., Cytrynbaum, C., Dawson, G., de Jonge, M., Delorme, R., Drmic, I., Duketis, E., Duque, F., Estes, A., Farrar, P., Fernandez, B.A., Folstein, S.E., Fombonne, E., Freitag, C.M., Gilbert, J., Gillberg, C., Glessner, J.T., Goldberg, J., Green, A., Green, J., Guter, S.J., Hakonarson, H., Heron, E.A., Hill, M., Holt, R., Howe, J.L., Hughes, G., Hus, V., Iglizzi, R., Kim, C., Klauck, S.M., Klevzon, A., Korvatska, O., Kustanovich, V., Lajonchere, C.M., Lamb, J.A., Laskawiec, M., Leboyer, M., Le Couteur, A., Leventhal, B.L., Lionel, A.C., Liu, X.Q., Lord, C., Lotspeich, L., Lund, S.C., Maestrini, E., Mahoney, W., Mantoulan, C., Marshall, C.R., McConachie, H., McDougle, C.J., McGrath, J., McMahon, W.M., Merikangas, A., Migita, O., Minshew, N.J., Mirza, G.K., Munson, J., Nelson, S.F., Noakes, C., Noor, A., Nygren, G., Oliveira, G., Papanikolaou, K., Parr, J.R., Parrini, B., Paton, T., Pickles, A., Pilorge, M., Piven, J., Ponting, C.P., Posey, D.J., Poustka, A., Poustka, F., Prasad, A., Ragoussis, J., Renshaw, K., Rickaby, J., Roberts, W., Roeder, K., Roge, B., Rutter, M.L., Bierut, L.J., Rice, J.P., Salt, J., Sansom, K., Sato, D., Segurado, R., Sequeira, A.F., Senman, L., Shah, N., Sheffield, V.C., Soorya, L., Sousa, I., Stein, O., Sykes, N., Stoppioni, V., Strawbridge, C., Tancredi, R., Tansey, K., Thiruvahindrapuram, B., Thompson, A.P., Thomson, S., Tryfon, A., Tsiantis, J., Van Engeland, H., Vincent, J.B., Volkmar, F., Wallace, S., Wang, K., Wang, Z., Wassink, T.H., Webber, C., Weksberg, R., Wing, K., Wittmeyer, K., Wood, S., Wu, J., Yaspan, B.L., Zurawiecki, D., Zwaigenbaum, L., Buxbaum, J.D., Cantor, R.M., Cook, E.H., Coon, H., Cuccaro, M.L., Devlin, B., Ennis, S., Gallagher, L., Geschwind, D.H., Gill, M., Haines, J.L., Hallmayer, J., Miller, J., Monaco, A.P., Nurnberger, J.I., Jr., Paterson, A.D., Pericak-Vance, M.A., Schellenberg, G.D., Szatmari, P., Vicente, A.M., Vieland, V.J., Wijsman, E.M., Scherer, S.W., Sutcliffe, J.S., Betancur, C.,

2010. Functional impact of global rare copy number variation in autism spectrum disorders. *Nature* 466, 368-372.

- Pizzo, L., Jensen, M., Polyak, A., Rosenfeld, J.A., Mannik, K., Krishnan, A., McCready, E., Pichon, O., Le Caignec, C., Van Dijck, A., Pope, K., Voorhoeve, E., Yoon, J., Stankiewicz, P., Cheung, S.W., Pazuchanics, D., Huber, E., Kumar, V., Kember, R.L., Mari, F., Curro, A., Castiglia, L., Galesi, O., Avola, E., Mattina, T., Fichera, M., Mandara, L., Vincent, M., Nizon, M., Mercier, S., Beneteau, C., Blesson, S., Martin-Coignard, D., Mosca-Boidron, A.L., Caberg, J.H., Bucan, M., Zeesman, S., Nowaczyk, M.J.M., Lefebvre, M., Faivre, L., Callier, P., Skinner, C., Keren, B., Perrine, C., Prontera, P., Marle, N., Renieri, A., Reymond, A., Kooy, R.F., Isidor, B., Schwartz, C., Romano, C., Sistermans, E., Amor, D.J., Andrieux, J., Girirajan, S., 2019. Rare variants in the genetic background modulate cognitive and developmental phenotypes in individuals carrying disease-associated variants. *Genet Med* 21, 816-825.
- Pla, P., Monsoro-Burq, A.H., 2018. The neural border: Induction, specification and maturation of the territory that generates neural crest cells. *Dev Biol* 444 Suppl 1, S36-S46.
- Pollak, R.M., Murphy, M.M., Epstein, M.P., Zwick, M.E., Klaiman, C., Saulnier, C.A., Emory 3q, P., Mulle, J.G., 2019. Neuropsychiatric phenotypes and a distinct constellation of ASD features in 3q29 deletion syndrome: results from the 3q29 registry. *Mol Autism* 10, 30.
- Pollak, R.M., Zinsmeister, M.C., Murphy, M.M., Zwick, M.E., Emory 3q, P., Mulle, J.G., 2020. New phenotypes associated with 3q29 duplication syndrome: Results from the 3q29 registry. *Am J Med Genet A* 182, 1152-1166.
- Popko, J., Fernandes, A., Brites, D., Lanier, L.M., 2009. Automated analysis of NeuronJ tracing data. *Cytometry A* 75, 371-376.
- Poulton, C.J., Schot, R., Kia, S.K., Jones, M., Verheijen, F.W., Venselaar, H., de Wit, M.C., de Graaff, E., Bertoli-Avella, A.M., Mancini, G.M., 2011. Microcephaly with simplified gyration, epilepsy, and infantile diabetes linked to inappropriate apoptosis of neural progenitors. *Am J Hum Genet* 89, 265-276.
- Prasad, M.S., Charney, R.M., Garcia-Castro, M.I., 2019. Specification and formation of the neural crest: Perspectives on lineage segregation. *Genesis* 57, e23276.
- Pratt, K.G., Khakhalin, A.S., 2013. Modeling human neurodevelopmental disorders in the *Xenopus* tadpole: from mechanisms to therapeutic targets. *Dis Model Mech* 6, 1057-1065.
- Pucilowska, J., Vithayathil, J., Tavares, E.J., Kelly, C., Karlo, J.C., Landreth, G.E., 2015. The 16p11.2 deletion mouse model of autism exhibits altered cortical progenitor

proliferation and brain cytoarchitecture linked to the ERK MAPK pathway. *J Neurosci* 35, 3190-3200.

- Purcell, S.M., Moran, J.L., Fromer, M., Ruderfer, D., Solovieff, N., Roussos, P., O'Dushlaine, C., Chambert, K., Bergen, S.E., Kahler, A., Duncan, L., Stahl, E., Genovese, G., Fernandez, E., Collins, M.O., Komiyama, N.H., Choudhary, J.S., Magnusson, P.K., Banks, E., Shakir, K., Garimella, K., Fennell, T., DePristo, M., Grant, S.G., Haggarty, S.J., Gabriel, S., Scolnick, E.M., Lander, E.S., Hultman, C.M., Sullivan, P.F., McCarroll, S.A., Sklar, P., 2014. A polygenic burden of rare disruptive mutations in schizophrenia. *Nature* 506, 185-190.
- Pusapati, G.V., Kong, J.H., Patel, B.B., Krishnan, A., Sagner, A., Kinnebrew, M., Briscoe, J., Aravind, L., Rohatgi, R., 2018a. CRISPR Screens Uncover Genes that Regulate Target Cell Sensitivity to the Morphogen Sonic Hedgehog. *Dev Cell* 44, 113-129 e118.
- Pusapati, G.V., Kong, J.H., Patel, B.B., Krishnan, A., Sagner, A., Kinnebrew, M., Briscoe, J., Aravind, L., Rohatgi, R., 2018b. CRISPR Screens Uncover Genes that Regulate Target Cell Sensitivity to the Morphogen Sonic Hedgehog. *Dev Cell* 44, 271.
- Qiu, Y., Arbogast, T., Lorenzo, S.M., Li, H., Tang, S.C., Richardson, E., Hong, O., Cho, S., Shanta, O., Pang, T., Corsello, C., Deutsch, C.K., Chevalier, C., Davis, E.E., Iakoucheva, L.M., Heral, Y., Katsanis, N., Messer, K., Sebat, J., 2019. Oligogenic Effects of 16p11.2 Copy-Number Variation on Craniofacial Development. *Cell Rep* 28, 3320-3328 e3324.
- Quintero-Rivera, F., Sharifi-Hannauer, P., Martinez-Agosto, J.A., 2010. Autistic and psychiatric findings associated with the 3q29 microdeletion syndrome: case report and review. *Am J Med Genet A* 152A, 2459-2467.
- Rahman, T.N., Munz, M., Kutsarova, E., Bilash, O.M., Ruthazer, E.S., 2020. Stentian structural plasticity in the developing visual system. *Proc Natl Acad Sci U S A* 117, 10636-10638.
- Rajan, S.G., Gallik, K.L., Monaghan, J.R., Uribe, R.A., Bronner, M.E., Saxena, A., 2018. Tracking neural crest cell cycle progression in vivo. *Genesis* 56, e23214.
- Reiter, L.T., Potocki, L., Chien, S., Gribskov, M., Bier, E., 2001. A systematic analysis of human disease-associated gene sequences in *Drosophila melanogaster*. *Genome Res* 11, 1114-1125.
- Ren, X., Yang, N., Wu, N., Xu, X., Chen, W., Zhang, L., Li, Y., Du, R.Q., Dong, S., Zhao, S., Chen, S., Jiang, L.P., Wang, L., Zhang, J., Wu, Z., Jin, L., Qiu, G., Lupski, J.R., Shi, J., Zhang, F., Liu, P., 2020. Increased TBX6 gene dosages induce congenital cervical vertebral malformations in humans and mice. *J Med Genet* 57, 371-379.

- Ritter, R.A., Ulrich, C.H., Brzezinska, B.N., Shah, V.V., Zamora, M.J., Kelly, L.E., El-Hodiri, H.M., Sater, A.K., 2020. miR-199 plays both positive and negative regulatory roles in *Xenopus* eye development. *Genesis* 58, e23354.
- Robinson, M.D., McCarthy, D.J., Smyth, G.K., 2010. edgeR: a Bioconductor package for differential expression analysis of digital gene expression data. *Bioinformatics* 26, 139-140.
- Rogers, C.D., Nie, S., 2018. Specifying neural crest cells: From chromatin to morphogens and factors in between. *Wiley Interdiscip Rev Dev Biol*, e322.
- Rosch, R., Burrows, D.R.W., Jones, L.B., Peters, C.H., Ruben, P., Samarut, E., 2019. Functional Genomics of Epilepsy and Associated Neurodevelopmental Disorders Using Simple Animal Models: From Genes, Molecules to Brain Networks. *Front Cell Neurosci* 13, 556.
- Rujano, M.A., Sanchez-Pulido, L., Penetier, C., le Dez, G., Basto, R., 2013. The microcephaly protein Asp regulates neuroepithelium morphogenesis by controlling the spatial distribution of myosin II. *Nat Cell Biol* 15, 1294-1306.
- Rutherford, E.L., Lowery, L.A., 2016. Exploring the developmental mechanisms underlying Wolf-Hirschhorn Syndrome: Evidence for defects in neural crest cell migration. *Dev Biol* 420, 1-10.
- Rutkowski, T.P., Purcell, R.H., Pollak, R.M., Grewenow, S.M., Gafford, G.M., Malone, T., Khan, U.A., Schroeder, J.P., Epstein, M.P., Bassell, G.J., Warren, S.T., Weinshenker, D., Caspary, T., Mulle, J.G., 2019. Behavioral changes and growth deficits in a CRISPR engineered mouse model of the schizophrenia-associated 3q29 deletion. *Mol Psychiatry*.
- Rutkowski, T.P., Schroeder, J.P., Gafford, G.M., Warren, S.T., Weinshenker, D., Caspary, T., Mulle, J.G., 2017. Unraveling the genetic architecture of copy number variants associated with schizophrenia and other neuropsychiatric disorders. *J Neurosci Res* 95, 1144-1160.
- Rylaarsdam, L., Guemez-Gamboa, A., 2019. Genetic Causes and Modifiers of Autism Spectrum Disorder. *Front Cell Neurosci* 13, 385.
- Sabin, L.R., Zhou, R., Gruber, J.J., Lukinova, N., Bambina, S., Berman, A., Lau, C.K., Thompson, C.B., Cherry, S., 2009. *Ars2* regulates both miRNA- and siRNA-dependent silencing and suppresses RNA virus infection in *Drosophila*. *Cell* 138, 340-351.
- Saiga, T., Fukuda, T., Matsumoto, M., Tada, H., Okano, H.J., Okano, H., Nakayama, K.I., 2009. *Fbxo45* forms a novel ubiquitin ligase complex and is required for neuronal development. *Mol Cell Biol* 29, 3529-3543.

- Sanchez, E., Laplace-Builhe, B., Mau-Them, F.T., Richard, E., Goldenberg, A., Toler, T.L., Guignard, T., Gatinois, V., Vincent, M., Blanchet, C., Boland, A., Bihoreau, M.T., Deleuze, J.F., Olasso, R., Nephi, W., Ludecke, H.J., Verheij, J., Moreau-Lenoir, F., Denoyelle, F., Riviere, J.B., Laplanche, J.L., Willing, M., Captier, G., Apparailly, F., Wiczorek, D., Collet, C., Djouad, F., Genevieve, D., 2020. POLR1B and neural crest cell anomalies in Treacher Collins syndrome type 4. *Genet Med* 22, 547-556.
- Sasai, N., Toriyama, M., Kondo, T., 2019. Hedgehog Signal and Genetic Disorders. *Front Genet* 10, 1103.
- Schindelin, J., Arganda-Carreras, I., Frise, E., Kaynig, V., Longair, M., Pietzsch, T., Preibisch, S., Rueden, C., Saalfeld, S., Schmid, B., Tinevez, J.Y., White, D.J., Hartenstein, V., Eliceiri, K., Tomancak, P., Cardona, A., 2012. Fiji: an open-source platform for biological-image analysis. *Nat Methods* 9, 676-682.
- Schmid, A., Hallermann, S., Kittel, R.J., Khorramshahi, O., Frolich, A.M., Quentin, C., Rasse, T.M., Mertel, S., Heckmann, M., Sigrist, S.J., 2008. Activity-dependent site-specific changes of glutamate receptor composition in vivo. *Nature neuroscience* 11, 659-666.
- Schneider, C.A., Rasband, W.S., Eliceiri, K.W., 2012. NIH Image to ImageJ: 25 years of image analysis. *Nat Methods* 9, 671-675.
- Schubert, C., 2009. The genomic basis of the Williams-Beuren syndrome. *Cell Mol Life Sci* 66, 1178-1197.
- Schubert, M., Panja, D., Haugen, M., Bramham, C.R., Vedeler, C.A., 2014. Paraneoplastic CDR2 and CDR2L antibodies affect Purkinje cell calcium homeostasis. *Acta Neuropathol* 128, 835-852.
- Schwenty-Lara, J., Nehl, D., Borchers, A., 2020. The histone methyltransferase KMT2D, mutated in Kabuki syndrome patients, is required for neural crest cell formation and migration. *Hum Mol Genet* 29, 305-319.
- Schwenty-Lara, J., Nurnberger, A., Borchers, A., 2019. Loss of function of Kmt2d, a gene mutated in Kabuki syndrome, affects heart development in *Xenopus laevis*. *Dev Dyn* 248, 465-476.
- Sears, J.C., Broadie, K., 2017. Fragile X Mental Retardation Protein Regulates Activity-Dependent Membrane Trafficking and Trans-Synaptic Signaling Mediating Synaptic Remodeling. *Front Mol Neurosci* 10, 440.
- Session, A.M., Uno, Y., Kwon, T., Chapman, J.A., Toyoda, A., Takahashi, S., Fukui, A., Hikosaka, A., Suzuki, A., Kondo, M., van Heeringen, S.J., Quigley, I., Heinz, S.,

- Ogino, H., Ochi, H., Hellsten, U., Lyons, J.B., Simakov, O., Putnam, N., Stites, J., Kuroki, Y., Tanaka, T., Michiue, T., Watanabe, M., Bogdanovic, O., Lister, R., Georgiou, G., Paranjpe, S.S., van Kruijsbergen, I., Shu, S., Carlson, J., Kinoshita, T., Ohta, Y., Mawaribuchi, S., Jenkins, J., Grimwood, J., Schmutz, J., Mitros, T., Mozaffari, S.V., Suzuki, Y., Haramoto, Y., Yamamoto, T.S., Takagi, C., Heald, R., Miller, K., Haudenschild, C., Kitzman, J., Nakayama, T., Izutsu, Y., Robert, J., Fortriede, J., Burns, K., Lotay, V., Karimi, K., Yasuoka, Y., Dichmann, D.S., Flajnik, M.F., Houston, D.W., Shendure, J., DuPasquier, L., Vize, P.D., Zorn, A.M., Ito, M., Marcotte, E.M., Wallingford, J.B., Ito, Y., Asashima, M., Ueno, N., Matsuda, Y., Veenstra, G.J., Fujiyama, A., Harland, R.M., Taira, M., Rokhsar, D.S., 2016. Genome evolution in the allotetraploid frog *Xenopus laevis*. *Nature* 538, 336-343.
- Shan, W., Li, J., Xu, W., Li, H., Zuo, Z., 2019. Critical role of UQCRC1 in embryo survival, brain ischemic tolerance and normal cognition in mice. *Cell Mol Life Sci* 76, 1381-1396.
- Shang, Y., Zhang, F., Li, D., Li, C., Li, H., Jiang, Y., Zhang, D., 2018. Overexpression of UQCRC2 is correlated with tumor progression and poor prognosis in colorectal cancer. *Pathol Res Pract* 214, 1613-1620.
- Shao, L., Shuai, Y., Wang, J., Feng, S., Lu, B., Li, Z., Zhao, Y., Wang, L., Zhong, Y., 2011. Schizophrenia susceptibility gene dysbindin regulates glutamatergic and dopaminergic functions via distinctive mechanisms in *Drosophila*. *Proc Natl Acad Sci U S A* 108, 18831-18836.
- Shin, E.Y., Shin, K.S., Lee, C.S., Woo, K.N., Quan, S.H., Soung, N.K., Kim, Y.G., Cha, C.I., Kim, S.R., Park, D., Bokoch, G.M., Kim, E.G., 2002. Phosphorylation of p85 beta PIX, a Rac/Cdc42-specific guanine nucleotide exchange factor, via the Ras/ERK/PAK2 pathway is required for basic fibroblast growth factor-induced neurite outgrowth. *J Biol Chem* 277, 44417-44430.
- Shin, J.Y., Son, J., Kim, W.S., Gwak, J., Ju, B.G., 2019. *Jmjd6a* regulates GSK3beta RNA splicing in *Xenopus laevis* eye development. *PLoS One* 14, e0219800.
- Sierra-Arregui, T., Llorente, J., Gimenez Minguez, P., Tonnesen, J., Penagarikano, O., 2020. Neurobiological Mechanisms of Autism Spectrum Disorder and Epilepsy, Insights from Animal Models. *Neuroscience*.
- Silver, D.L., Watkins-Chow, D.E., Schreck, K.C., Pierfelice, T.J., Larson, D.M., Burnett, A.J., Liaw, H.J., Myung, K., Walsh, C.A., Gaiano, N., Pavan, W.J., 2010. The exon junction complex component Magoh controls brain size by regulating neural stem cell division. *Nat Neurosci* 13, 551-558.
- Simon, R., Bergemann, A.D., 2008. Mouse models of Wolf-Hirschhorn syndrome. *Am J Med Genet C Semin Med Genet* 148C, 275-280.

- Singh, M.D., Jensen, M., Lasser, M., Huber, E., Yusuff, T., Pizzo, L., Lifschutz, B., Desai, I., Kubina, A., Yennawar, S., Kim, S., Iyer, J., Rincon-Limas, D.E., Lowery, L.A., Girirajan, S., 2020. NCBP2 modulates neurodevelopmental defects of the 3q29 deletion in *Drosophila* and *Xenopus laevis* models. *PLoS Genet* 16, e1008590.
- Sive, H.L., Grainger, R.M., Harland, R.M., 2007a. Housing and Feeding of *Xenopus laevis*. *CSH Protoc* 2007, pdb top8.
- Sive, H.L., Grainger, R.M., Harland, R.M., 2007b. *Xenopus laevis* In Vitro Fertilization and Natural Mating Methods. *CSH Protoc* 2007, pdb prot4737.
- Sive, H.L., Grainger, R.M., Harland, R.M., 2010. Microinjection of *Xenopus* embryos. *Cold Spring Harb Protoc* 2010, pdb ip81.
- Slater, P.G., Hayrapetian, L., Lowery, L.A., 2017. *Xenopus laevis* as a model system to study cytoskeletal dynamics during axon pathfinding. *Genesis* 55.
- Soba, P., Zhu, S., Emoto, K., Younger, S., Yang, S.J., Yu, H.H., Lee, T., Jan, L.Y., Jan, Y.N., 2007. *Drosophila* sensory neurons require Dscam for dendritic self-avoidance and proper dendritic field organization. *Neuron* 54, 403-416.
- Sojka, S., Amin, N.M., Gibbs, D., Christine, K.S., Charpentier, M.S., Conlon, F.L., 2014. Congenital heart disease protein 5 associates with CASZ1 to maintain myocardial tissue integrity. *Development* 141, 3040-3049.
- Sperber, H., Mathieu, J., Wang, Y., Ferreccio, A., Hesson, J., Xu, Z., Fischer, K.A., Devi, A., Detraux, D., Gu, H., Battle, S.L., Showalter, M., Valensisi, C., Bielas, J.H., Ericson, N.G., Margaretha, L., Robitaille, A.M., Margineantu, D., Fiehn, O., Hockenbery, D., Blau, C.A., Raftery, D., Margolin, A.A., Hawkins, R.D., Moon, R.T., Ware, C.B., Ruohola-Baker, H., 2015. The metabolome regulates the epigenetic landscape during naive-to-primed human embryonic stem cell transition. *Nat Cell Biol* 17, 1523-1535.
- Stefansson, H., Meyer-Lindenberg, A., Steinberg, S., Magnusdottir, B., Morgen, K., Arnarsdottir, S., Bjornsdottir, G., Walters, G.B., Jonsdottir, G.A., Doyle, O.M., 2014. CNVs conferring risk of autism or schizophrenia affect cognition in controls. *Nature* 505, 361-366.
- Strigini, M., Cohen, S.M., 1997. A Hedgehog activity gradient contributes to AP axial patterning of the *Drosophila* wing. *Development* 124, 4697-4705.
- Stuss, D.P., Boyd, J.D., Levin, D.B., Delaney, K.R., 2012. MeCP2 mutation results in compartment-specific reductions in dendritic branching and spine density in layer 5 motor cortical neurons of YFP-H mice. *PLoS One* 7, e31896.

- Sun, Y., Yolitz, J., Wang, C., Spangler, E., Zhan, M., Zou, S., 2013. Aging studies in *Drosophila melanogaster*. *Methods Mol Biol* 1048, 77-93.
- Szabo, A., Mayor, R., 2018. Mechanisms of Neural Crest Migration. *Annu Rev Genet* 52, 43-63.
- Szabo, A., Melchionda, M., Nastasi, G., Woods, M.L., Campo, S., Perris, R., Mayor, R., 2016. In vivo confinement promotes collective migration of neural crest cells. *J Cell Biol* 213, 543-555.
- Tada, H., Okano, H.J., Takagi, H., Shibata, S., Yao, I., Matsumoto, M., Saiga, T., Nakayama, K.I., Kashima, H., Takahashi, T., Setou, M., Okano, H., 2010. Fbxo45, a novel ubiquitin ligase, regulates synaptic activity. *J Biol Chem* 285, 3840-3849.
- Tahir, R., Kennedy, A., Elsea, S.H., Dickinson, A.J., 2014. Retinoic acid induced-1 (Rai1) regulates craniofacial and brain development in *Xenopus*. *Mech Dev* 133, 91-104.
- Tandon, P., Conlon, F., Furlow, J.D., Horb, M.E., 2017. Expanding the genetic toolkit in *Xenopus*: Approaches and opportunities for human disease modeling. *Dev Biol* 426, 325-335.
- Thaker, H.M., Kankel, D.R., 1992. Mosaic analysis gives an estimate of the extent of genomic involvement in the development of the visual system in *Drosophila melanogaster*. *Genetics* 131, 883-894.
- Theveneau, E., Mayor, R., 2011. Beads on the run: beads as alternative tools for chemotaxis assays. *Methods Mol Biol* 769, 449-460.
- Theveneau, E., Mayor, R., 2012. Neural crest delamination and migration: from epithelium-to-mesenchyme transition to collective cell migration. *Dev Biol* 366, 34-54.
- Thomas, B.J., Wassarman, D.A., 1999. A fly's eye view of biology. *Trends Genet* 15, 184-190.
- Thomas, P.D., Campbell, M.J., Kejariwal, A., Mi, H., Karlak, B., Daverman, R., Diemer, K., Muruganujan, A., Narechania, A., 2003. PANTHER: a library of protein families and subfamilies indexed by function. *Genome research* 13, 2129-2141.
- Thomas, U., Kim, E., Kuhlendahl, S., Koh, Y.H., Gundelfinger, E.D., Sheng, M., Garner, C.C., Budnik, V., 1997. Synaptic clustering of the cell adhesion molecule fasciclin II by discs-large and its role in the regulation of presynaptic structure. *Neuron* 19, 787-799.
- Thormann, A., Halachev, M., McLaren, W., Moore, D.J., Svinti, V., Campbell, A., Kerr, S.M., Tischkowitz, M., Hunt, S.E., Dunlop, M.G., Hurles, M.E., Wright, C.F., Firth, H.V., Cunningham, F., FitzPatrick, D.R., 2019. Flexible and scalable

- diagnostic filtering of genomic variants using G2P with Ensembl VEP. *Nat Commun* 10, 2373.
- Tickle, C., Towers, M., 2017. Sonic Hedgehog Signaling in Limb Development. *Front Cell Dev Biol* 5, 14.
- Tinevez, J.Y., Perry, N., Schindelin, J., Hoopes, G.M., Reynolds, G.D., Laplantine, E., Bednarek, S.Y., Shorte, S.L., Eliceiri, K.W., 2017. TrackMate: An open and extensible platform for single-particle tracking. *Methods* 115, 80-90.
- Tittel, J.N., Steller, H., 2000. A comparison of programmed cell death between species. *Genome Biol* 1, REVIEWS0003.
- Trainor, P.A., 2010. Craniofacial birth defects: The role of neural crest cells in the etiology and pathogenesis of Treacher Collins syndrome and the potential for prevention. *Am J Med Genet A* 152A, 2984-2994.
- Turner, T.N., Yi, Q., Krumm, N., Huddleston, J., Hoekzema, K., HA, F.S., Doebley, A.L., Bernier, R.A., Nickerson, D.A., Eichler, E.E., 2017. denovo-db: a compendium of human de novo variants. *Nucleic Acids Res* 45, D804-D811.
- Ueno, S., Kono, R., Iwao, Y., 2006. PTEN is required for the normal progression of gastrulation by repressing cell proliferation after MBT in *Xenopus* embryos. *Dev Biol* 297, 274-283.
- Ugur, B., Chen, K., Bellen, H.J., 2016. *Drosophila* tools and assays for the study of human diseases. *Dis Model Mech* 9, 235-244.
- Van Otterloo, E., Williams, T., Artinger, K.B., 2016. The old and new face of craniofacial research: How animal models inform human craniofacial genetic and clinical data. *Dev Biol* 415, 171-187.
- Vawter, M.P., Crook, J.M., Hyde, T.M., Kleinman, J.E., Weinberger, D.R., Becker, K.G., Freed, W.J., 2002. Microarray analysis of gene expression in the prefrontal cortex in schizophrenia: a preliminary study. *Schizophr Res* 58, 11-20.
- Vega-Lopez, G.A., Cerrizuela, S., Tribulo, C., Aybar, M.J., 2018. Neurocristopathies: New insights 150 years after the neural crest discovery. *Dev Biol* 444 Suppl 1, S110-S143.
- Venkatraman, A., Opal, P., 2016. Paraneoplastic cerebellar degeneration with anti-Yo antibodies - a review. *Ann Clin Transl Neurol* 3, 655-663.
- Vicari, S., Napoli, E., Cordeddu, V., Menghini, D., Alesi, V., Loddo, S., Novelli, A., Tartaglia, M., 2019. Copy number variants in autism spectrum disorders. *Prog Neuropsychopharmacol Biol Psychiatry* 92, 421-427.

- Viet, J., Reboutier, D., Hardy, S., Lachke, S.A., Paillard, L., Gautier-Courteille, C., 2020. Modeling ocular lens disease in *Xenopus*. *Dev Dyn* 249, 610-621.
- Walch, L., 2013. Emerging role of the scaffolding protein Dlg1 in vesicle trafficking. *Traffic* 14, 964-973.
- Wallmeier, J., Shiratori, H., Dougherty, G.W., Edelbusch, C., Hjeij, R., Loges, N.T., Menchen, T., Olbrich, H., Pennekamp, P., Raidt, J., Werner, C., Minegishi, K., Shinohara, K., Asai, Y., Takaoka, K., Lee, C., Griese, M., Memari, Y., Durbin, R., Kolb-Kokocinski, A., Sauer, S., Wallingford, J.B., Hamada, H., Omran, H., 2016. TTC25 Deficiency Results in Defects of the Outer Dynein Arm Docking Machinery and Primary Ciliary Dyskinesia with Left-Right Body Asymmetry Randomization. *Am J Hum Genet* 99, 460-469.
- Wang, C., Koide, T., Kimura, H., Kunimoto, S., Yoshimi, A., Nakamura, Y., Kushima, I., Banno, M., Kawano, N., Takasaki, Y., Xing, J., Noda, Y., Mouri, A., Aleksic, B., Ikeda, M., Okada, T., Iidaka, T., Inada, T., Iwata, N., Ozaki, N., 2014. Novel rare variants in F-box protein 45 (FBXO45) in schizophrenia. *Schizophr Res* 157, 149-156.
- Wang, F., Shi, Z., Cui, Y., Guo, X., Shi, Y.B., Chen, Y., 2015. Targeted gene disruption in *Xenopus laevis* using CRISPR/Cas9. *Cell Biosci* 5, 15.
- Wang, H.D., Kazemi-Esfarjani, P., Benzer, S., 2004. Multiple-stress analysis for isolation of *Drosophila* longevity genes. *Proceedings of the National Academy of Sciences of the United States of America* 101, 12610-12615.
- Wang, L., Magdaleno, S., Tabas, I., Jackowski, S., 2005. Early embryonic lethality in mice with targeted deletion of the CTP:phosphocholine cytidyltransferase alpha gene (*Pcyt1a*). *Mol Cell Biol* 25, 3357-3363.
- Wang, Q., Kurosaka, H., Kikuchi, M., Nakaya, A., Trainor, P.A., Yamashiro, T., 2019. Perturbed development of cranial neural crest cells in association with reduced sonic hedgehog signaling underlies the pathogenesis of retinoic-acid-induced cleft palate. *Dis Model Mech* 12.
- Wang, Y., Zeng, C., Li, J., Zhou, Z., Ju, X., Xia, S., Li, Y., Liu, A., Teng, H., Zhang, K., Shi, L., Bi, C., Xie, W., He, X., Jia, Z., Jiang, Y., Cai, T., Wu, J., Xia, K., Sun, Z.S., 2018. PAK2 Haploinsufficiency Results in Synaptic Cytoskeleton Impairment and Autism-Related Behavior. *Cell Rep* 24, 2029-2041.
- Wangler, M.F., Yamamoto, S., Bellen, H.J., 2015. Fruit flies in biomedical research. *Genetics* 199, 639-653.

- Weiss, L.A., Shen, Y., Korn, J.M., Arking, D.E., Miller, D.T., Fossdal, R., Saemundsen, E., Stefansson, H., Ferreira, M.A., Green, T., Platt, O.S., Ruderfer, D.M., Walsh, C.A., Altshuler, D., Chakravarti, A., Tanzi, R.E., Stefansson, K., Santangelo, S.L., Gusella, J.F., Sklar, P., Wu, B.L., Daly, M.J., Autism, C., 2008. Association between microdeletion and microduplication at 16p11.2 and autism. *N Engl J Med* 358, 667-675.
- Wilfert, A.B., Sulovari, A., Turner, T.N., Coe, B.P., Eichler, E.E., 2017. Recurrent de novo mutations in neurodevelopmental disorders: properties and clinical implications. *Genome medicine* 9, 101.
- Willatt, L., Cox, J., Barber, J., Cabanas, E.D., Collins, A., Donnai, D., FitzPatrick, D.R., Maher, E., Martin, H., Parnau, J., Pindar, L., Ramsay, J., Shaw-Smith, C., Sistermans, E.A., Tettenborn, M., Trump, D., de Vries, B.B., Walker, K., Raymond, F.L., 2005. 3q29 microdeletion syndrome: clinical and molecular characterization of a new syndrome. *Am J Hum Genet* 77, 154-160.
- Willsey, H.R., Walentek, P., Exner, C.R.T., Xu, Y., Lane, A.B., Harland, R.M., Heald, R., Santama, N., 2018. Katanin-like protein *Katnal2* is required for ciliogenesis and brain development in *Xenopus* embryos. *Dev Biol* 442, 276-287.
- Wu, Y., Bolduc, F.V., Bell, K., Tully, T., Fang, Y., Sehgal, A., Fischer, J.A., 2008. A *Drosophila* model for Angelman syndrome. *Proc Natl Acad Sci U S A* 105, 12399-12404.
- Xiao, C., Mileva-Seitz, V., Seroude, L., Robertson, R.M., 2007. Targeting HSP70 to motoneurons protects locomotor activity from hyperthermia in *Drosophila*. *Dev Neurobiol* 67, 438-455.
- Xu, D., Wang, Y., Willecke, R., Chen, Z., Ding, T., Bergmann, A., 2006. The effector caspases *drICE* and *dcp-1* have partially overlapping functions in the apoptotic pathway in *Drosophila*. *Cell Death Differ* 13, 1697-1706.
- Xu, D., Woodfield, S.E., Lee, T.V., Fan, Y., Antonio, C., Bergmann, A., 2009. Genetic control of programmed cell death (apoptosis) in *Drosophila*. *Fly (Austin)* 3, 78-90.
- Yam, P.T., Charron, F., 2013. Signaling mechanisms of non-conventional axon guidance cues: the Shh, BMP and Wnt morphogens. *Curr Opin Neurobiol* 23, 965-973.
- Yamaguchi, Y., Miura, M., 2015. Programmed cell death in neurodevelopment. *Dev Cell* 32, 478-490.
- Yan, S.J., Gu, Y., Li, W.X., Fleming, R.J., 2004. Multiple signaling pathways and a selector protein sequentially regulate *Drosophila* wing development. *Development* 131, 285-298.
- Yang, N., Wu, N., Dong, S., Zhang, L., Zhao, Y., Chen, W., Du, R., Song, C., Ren, X., Liu, J., Pehlivan, D., Liu, Z., Jia, R., Wang, C., Zhao, S., Breman, A.M., Xue, H.,

Sun, H., Shen, J., Zhang, S., Posey, J.E., Xu, H., Jin, L., Zhang, J., Liu, P., Sanna-Cherchi, S., Qiu, G., Wu, Z., Lupski, J.R., Zhang, F., 2020. Human and mouse studies establish TBX6 in Mendelian CAKUT and as a potential driver of kidney defects associated with the 16p11.2 microdeletion syndrome. *Kidney Int.*

Yates, A.D., Achuthan, P., Akanni, W., Allen, J., Allen, J., Alvarez-Jarreta, J., Amode, M.R., Armean, I.M., Azov, A.G., Bennett, R., Bhai, J., Billis, K., Boddu, S., Marugan, J.C., Cummins, C., Davidson, C., Dodiya, K., Fatima, R., Gall, A., Giron, C.G., Gil, L., Grego, T., Haggerty, L., Haskell, E., Hourlier, T., Izuogu, O.G., Janacek, S.H., Juettemann, T., Kay, M., Lavidas, I., Le, T., Lemos, D., Martinez, J.G., Maurel, T., McDowall, M., McMahon, A., Mohanan, S., Moore, B., Nuhn, M., Oheh, D.N., Parker, A., Parton, A., Patricio, M., Sakthivel, M.P., Abdul Salam, A.I., Schmitt, B.M., Schuilenburg, H., Sheppard, D., Sycheva, M., Szuba, M., Taylor, K., Thormann, A., Threadgold, G., Vullo, A., Walts, B., Winterbottom, A., Zadissa, A., Chakiachvili, M., Flint, B., Frankish, A., Hunt, S.E., G, I.I., Kostadima, M., Langridge, N., Loveland, J.E., Martin, F.J., Morales, J., Mudge, J.M., Muffato, M., Perry, E., Ruffier, M., Trevanion, S.J., Cunningham, F., Howe, K.L., Zerbino, D.R., Flicek, P., 2020. Ensembl 2020. *Nucleic Acids Res* 48, D682-D688.

Yusuff, T., Jensen, M., Yennawar, S., Pizzo, L., Karthikeyan, S., Gould, D.J., Sarker, A., Gedvilaite, E., Matsui, Y., Iyer, J., Lai, Z.-C., Girirajan, S., 2020. *Drosophila* models of pathogenic copy-number variant genes show global and non-neuronal defects during development. *bioRxiv*, 855338.

Zahn, N., Levin, M., Adams, D.S., 2017. The Zahn drawings: new illustrations of *Xenopus* embryo and tadpole stages for studies of craniofacial development. *Development* 144, 2708-2713.

Zarrei, M., MacDonald, J.R., Merico, D., Scherer, S.W., 2015. A copy number variation map of the human genome. *Nat Rev Genet* 16, 172-183.

Zufferey, F., Sherr, E.H., Beckmann, N.D., Hanson, E., Maillard, A.M., Hippolyte, L., Macé, A., Ferrari, C., Kutalik, Z., Andrieux, J., 2012. A 600 kb deletion syndrome at 16p11.2 leads to energy imbalance and neuropsychiatric disorders. *Journal of medical genetics* 49, 660-668.